2017

The seasonal cycling and physico-chemical speciation of iron on the Celtic and Hebridean shelf seas

Birchill, Antony James

http://hdl.handle.net/10026.1/10236

The seasonal cycling and physico-chemical speciation of iron in the Celtic and Hebridean shelf seas

By

Antony James Birchill

A thesis submitted to the University of Plymouth in partial fulfilment for the degree of

Doctor of Philosophy

Faculty of Science and Environment

School of Geography, Earth and Environmental Sciences

2017

II

The seasonal cycling and physico-chemical speciation of iron in the Celtic and Hebridean shelf seas

Antony James Birchill

Shelf seas represent an important source of iron (Fe) to the open ocean. Additionally, shelf seas are highly productive environments which contribute to atmospheric carbon dioxide drawdown and support large fisheries. The work presented in this thesis describes the seasonal cycle of Fe in the Celtic and Hebridean Shelf Seas, and determines the physico-chemical speciation of Fe supplied from oxic margins.

The results from repeated field surveys of the central Celtic Sea showed a nutrient type seasonal cycling of dissolved Fe (< 0.2 μm; dFe), which is surprising in a particle rich shelf system, suggesting a balance of scavenging and remineralisation processes. Coincident drawdown of dFe and nitrate (NO_3^-) was observed during the phytoplankton spring bloom. During the bloom, preferential drawdown of soluble Fe (< 0.02 μm; sFe) over colloidal Fe (0.02-0.2 μm; cFe) indicated greater bioavailability of the soluble fraction. Throughout summer stratification, it is known that NO_3^- is drawn down to < 0.02 μM in surface waters. This study revealed that both dFe and labile particulate Fe (LpFe) were also seasonally drawn down to < 0.2 nM. Consequently, it is hypothesised that the availability of Fe seasonally co-limits primary production in this region. At depth both dFe and NO_3^- concentrations increased from spring to autumn, indicating that remineralisation is an important process governing the seasonal cycling of dFe in the central Celtic Sea.

In spring, summer and autumn, distinctive intermediate nepheloid layers (INL) were observed emanating from the Celtic Sea shelf slope. The INLs were associated with elevated concentrations of dFe (up to 3.25 ± 0.16 nM) and particulate Fe (up to 315 ± 1.8 nM) indicating that they are a persistent conduit for the supply of Fe to the open ocean. Typically > 15% of particulate Fe was labile and 60-90% of dFe was in the colloidal fraction. Despite being < 50 km from the 200 m isobath, the concentration of dFe was < 0.1 nM in surface waters at several stations. Broadly, the concentration of nutrients in surface waters described an oligotrophic environment where co-limitation between multiple nutrients, including Fe, appears likely.

Over the Hebridean shelf break, residual surface NO_3^- concentrations (5.27 ± 0.79 μM) and very low concentrations of dFe (0.09 ± 0.04 nM) were observed during autumn, implying seasonal Fe limitation. The dFe:NO_3^- ratio observed is attributed to sub-optimal vertical supply of Fe relative to NO_3^- from sub-surface waters. In contrast to the shelf break, surface water in coastal regions contained elevated dFe concentrations (1.73 ± 1.16 nM) alongside low NO_3^-. Seasonal Fe limitation is known to occur in the Irminger and Iceland Basins; therefore, the Hebridean shelf break likely represents the eastern extent of sub-Arctic Atlantic seasonal Fe limitation, thus indicating that the associated weakening of the biological carbon pump exists over a wider region of the sub-Arctic Atlantic than previously recognised.

These key findings demonstrate that the availability of Fe to phytoplankton may seasonally reach limiting levels in temperate shelf waters and that oxic margins persistently supply Fe dominated by colloidal and particulate fractions to the ocean.

Author's Declaration

At no time during the registration for the degree of Ph.D. in Environmental Sciences has the author been registered for any other University award. No work submitted for this research degree will form part of any other degree at the University of Plymouth or any other establishment.

Relevant scientific seminars and conferences have been regularly attended during the course of this research and findings have been presented at conferences in the form of oral and poster presentations. Several manuscripts have been prepared for peer review publication. Manuscripts, presentations, awards and fieldwork are summarised on pages x-xiii.

Word count of main body of thesis, excluding bibliography: 36,016

Signed: Date: 07.11.2017

Acknowledgements

I will be forever grateful to my supervisors, Maeve Lohan, Angie Milne, Simon Ussher and Paul Worsfold (aka *'the trace metal dream team'*). Thank you for your continued advice and guidance, and for making this PhD so much fun.

I wish to acknowledge all the crew and scientists on-board the *RRS Discovery.* I will always look back fondly on all the friendships I made at sea. In particular, a big thank you to Dagmara, my trace metal partner in crime, I won't ever forget the phrase '*bottle or fill?*', the dangers posed by exploding Niskin bottles or the torture of sample acidification to Ed Sheeran on repeat. Also thank you to Nora for all your fantastic work in the lab, and for all the equally fantastic cakes in the office.

I am grateful for the many discussions I have had with other members of the Trace Element Analysis and Biogeochemical research groups at Plymouth, in particular for Alan and Malcom for sharing their trace metal wisdom.

Thank you to all my friends at Plymouth for all the fun times we have shared over the past 4 years, especially for all the football, cycling, hiking, squash (and the necessary post-game rehydration efforts), '*only 1*' in the JSV, '*Pasty Thursday*' and '*Cake Monday*'. (Kato, Katie 'o, Kat, Alba, Dave, Patri, Vincent, Mike, Holly, Bashdar, Matt F, Sov, Caroline, Simone, Vanessa, Mary, Pernilla, Ali, Hayley, Dan, Will, Deniz, Yann, Lucas, Maya, Marc-Andre, Neil, Paul, Anita, Fye, Rob, Andy, Madeline, Guilia, Lara, Gustavo, Christian, Matt M, Louisa, Francesa, Kieran, Rich, H, Big Phil, Maarten, Tom, plus many more....). Fran wasn't too bad either. Good luck to all for the future.

Finally, thank you to Cat and my family for supporting/tolerating my unhealthy obsession with iron in seawater. It would not have been possible without you.

Publications, Presentations, Awards and Fieldwork

Peer reviewed publications:

Birchill, A. J., A. Milne, E. M. S. Woodward, A. L. Annett, W. Giebert, S. Ussher, P. J. Worsfold, D. Rusiecka, E. P. Achterberg, C. Harris, M. Gledhill, and M. C. Lohan (2017), Seasonal iron depletion in temperate shelf seas, *Geophysical Research Letters*. 10.1002/2017GL073881

Klar, J., W. B. Homoky, P. J. Statham, **A. J. Birchill**, E. Harris, E. M. S. Woodward, B. Silburn, M. Cooper, R. H. James, and D. P. Connelly (2017), Stability of dissolved and soluble Fe (II) in shelf sediment pore waters and release to an oxic water column, *Biogeochemistry*. https://doi.org/10.1007/s10533-017-0309-x

Hopwood, M. J., **A. J. Birchill**, M. Gledhill, A. Milne, and E. P. Achterberg (2017), A 4 method comparison for the measurement of Fe(II) at nanomolar concentrations in coastal seawater, *Frontiers in Chemistry*. https://doi.org/10.3389/fmars.2017.00192

Annett, A. L., **A. J. Birchill**, J. E. Hopkins, W. B. Homoky, H. Thomas, A. Milne, D. Rusiecka, E. P. Achterberg, J. Sharples, E. M. S. Woodward, P. J. Statham, M. C. Lohan, and W. Giebert (under revision), Rapid supply of iron from continent margins to the ocean by intermediate nepheloid layers, *Nature Geoscience*.

Birchill, A. J., N. Hartner, A. Milne, S. Ussher, P. J. Worsfold, E. M. S. Woodward, C. Harris, D. Rusiecka, E. P. Achterberg and M. C. Lohan (in prep), The physico-chemical speciation of iron supplied from an oxic shelf margin, *Marine Chemistry*.

Birchill, A. J., N. Hartner, K. Kunde, D. Gonzalez-Santana, B. Siemering, A. Milne, S. C. Painter, C. J. Daniels, S. Ussher, P. J. Worsfold, and M. C. Lohan (in prep), The Hebridean

Shelf- the eastern extent of seasonal iron limitation in the Sub-Arctic North Atlantic, *Global Biogeochemical Cycles*.

Presentations:

2017   The physico-chemical speciation of iron supplied from an oxic shelf margin. Poster. *Goldschmidt meeting,* Paris.

2016   The Celtic Sea shelf system acts as a persistent source of iron to the North Atlantic. Poster, *American Geophysical Union, Ocean Sciences meeting,* New Orleans.

2016   Seasonal cycling of dissolved and colloidal iron in the Celtic Sea. Oral, *American Geophysical Union, Ocean Sciences meeting,* New Orleans.

2016   Dissolved iron acting as nutrient in the Celtic Sea. Oral (invited speaker). *POETS corner seminar series,* University of Southampton.

2016   Seasonal cycling of dissolved and colloidal iron in the Celtic Sea. Oral. *Challenger Society meeting,* University of Liverpool.

2016   Seasonal cycling of dissolved and colloidal iron in the Celtic Sea. Oral. *Advances in Marine Biogeochemistry meeting,* University of Oxford.

2015   Seasonal cycling and off-shelf transport of dissolved, soluble and colloidal iron in the Celtic Sea. Poster, *Goldschmidt meeting,* Prague.

Awards:

Grant in aid of Conference Travel, Royal Society of Chemistry, travel to Paris for attendance of Goldschmidt meeting-2017

Earth and Environmental Science Doctoral Training Centre, University of Plymouth,

travel to Prague for attendance of *Goldschmidt* meeting- 2015

Plymouth Marine Science and Education Foundation, PLYMSEFF, registration costs for

attendance of *Goldschmidt* meeting- 2015

Conferences attended:

Goldschmidt, European Association of Geochemistry meeting. 2017. Paris.

8th Annual Biogeochemistry Conference. 2016. Plymouth University.

The Challenger Society for Marine Science meeting. 2016. University of Liverpool.

Ocean Sciences, American Geophysical Union meeting. 2016. New Orleans.

Advances in Marine Biogeochemistry meeting. 2016. University of Oxford.

7th Annual Biogeochemistry Conference. 2015. Plymouth University.

Goldschmidt, European Association of Geochemistry meeting. 2015. Prague.

6th Annual Biogeochemistry Conference. 2014. Plymouth University.

The Challenger Society for Marine Science meeting. 2014. University of Plymouth.

5th Annual Biogeochemistry Conference. 2013. Plymouth University.

Courses attended:

Best Practice Workshop on Trace Element Measurements in Oceanography Laboratory;

Creative and Clear Thinking Workshop; Based Teaching Methods and Practice (ENV

5101); Keeping Laboratory Records; Introduction to applying for Research Funding

Fieldwork

May 2016- Fe(II) inter-calibration exercise, Crete

July 2015- *RRS Discovery*, DY033- Celtic Sea

April 2015- *RRS Discovery*, DY029- Celtic Sea

November 2014- *RRS Discovery*, DY018- Celtic Sea

October 2014- *RRS Discovery*, DY017- Malin shelf

Table of Contents

List of Figures

List of Tables

List of abbreviations

3-APA*	3-aminophthalate
8-HQ	8-hydroquinoline
BML	bottom mixed layer
cFe	colloidal iron
CH_3COOH	acetic acid
Chl-a	chlorophyll-a
CL	chemiluminescence
CO_2	carbon dioxide
CTD	conductivity temperature depth profiler
dFe	dissolved iron
DIC	dissolved inorganic carbon
DMG	dimethylglyoxime
ESC	European Slope Current
Fe(II)	ferrous iron
Fe(III)	ferric iron
FI	flow injection
FI-CL	flow injection-chemiluminescence
FSW	filtered seawater
GF/F	glass fiber filter
H_2O_2	hydrogen peroxide
HCl	hydrochloric acid
HNLC	high nutrient low chlorophyll
HNO_3	nitric acid
I_{cl}	intensity of chemiluminescence

ICP-MS	inter coupled plasma- mass spectrometry
IDA	iminodiacetate
INL	intermediate nepheloid layer
Kz	eddy diffusivity
LDPE	low density polyethylene
LOD	limit of detection
Na_2CO_3	sodium carbonate
NaOH	sodium hydroxide
NH_4Ac	ammonium acetate
NO_3^-	nitrate + nitrite
OTE	Ocean Test Equipment
PES	polyethersulfone
PFA	perFluoroAlkoxy
pFe	particulate iron
PMT	photo multiplier tube
PO_4^{3-}	phosphate
PVC	polyvinyl chloride
RaDeCC	Radium Delayed Coincidence Counter
RSD	relative standard deviation
SCC	Scottish Coastal Current
SCM	sub-surface chlorophyll maximum
sFe	soluble iron
Si	silicic acid
SML	surface mixed layer
TdFe	total dissolvable iron

TETA	triethylenetetramine
UHP	ultra-high purity water
α-HHP	α-hydroxy hydroperoxide

Chapter 1 - Introduction

1.0 Marine iron biogeochemistry within the Earth system

Iron (Fe) is the fourth most abundant element in the Earths' crust after oxygen, silicon and aluminium [*Wedepohl*, 1995] and an essential micronutrient used in the biological processes of photosynthesis and nitrogen fixation [*Falkowski and Raven*, 2007; *Poulton and Raiswell*, 2002]. Phytoplankton have a high Fe requirement relative to other trace elements [*Ho et al.*, 2003]. This is believed to result from the evolution of the capacity to use water as the electron source in photosynthesis, which occurred 2000-3000 Ma, in an iron rich environment [*Williams and Frausto da Silva*, 2006]. The evolution of oxygen producing photosynthetic life ultimately resulted in the oxygenation of the Ocean-Earth system, which in turn dramatically decreased the solubility of Fe in the ocean (see section 1.1). Consequently, in the modern surface and deep ocean sub-nanomolar concentrations are typical for dissolved Fe (dFe) [*Johnson et al.*, 1997], leading to the hypothesis that Fe can limit the growth of marine phytoplankton. Although reliable measurements of dFe have only been conducted in the past few decades [e.g. *Gordon et al.*, 1982], the original hypothesis of Fe limitation dates back to the 1930's [*Gran*, 1932]. In 1989 Martin and co-workers tested this hypothesis in Antarctic waters using bottle incubations where Fe was added and this resulted in an increase in phytoplankton growth [*Martin*, 1990]. This led to mesoscale *in-situ* Fe enrichment experiments which demonstrated that surface water Fe concentrations are low enough to limit algal growth in large parts of the modern Southern Ocean, Equatorial Pacific and sub-Arctic Pacific [*Boyd et al.*, 2007; *Boyd et al.*, 2000; *Coale et al.*, 2004; *Tsuda et al.*, 2003]. As well as limiting growth, Fe concentrations can influence ecosystem structure [*Landry et al.*, 2000; *Tsuda et al.*, 2003] as phytoplankton species have differing Fe requirements and/or differences in the surface/area cell ratio which can alter uptake efficiencies [*Lis et al.*, 2015; *Öztürk et al.*, 2004].

The capacity of Fe concentrations to limit primary production and affect ecosystem structure has implications for the biogeochemical cycling of major nutrients (e.g. C, Si, N, P) [*Tagliabue et al.*, 2017]. The interplay between Fe and carbon biogeochemistry has led to many studies, due to the importance of atmospheric carbon dioxide (CO_2) concentrations are a key driver of climate change [*Petit et al.*, 1999; *Watson et al.*, 2000]. In particular the *Martin* [1990] *'Iron Hypothesis'* posits that fluctuations in aeolian Fe supply to Fe limited regions, particularly to the Southern Ocean, were a driver of, or contributed to, glacial/interglacial atmospheric CO_2 change by increasing the efficiency of the 'biological carbon pump'. The international attention this received later led to the proposition that alleviation of Fe limitation could be a potential geo-engineering strategy to counteract current anthropogenically induced climate change [*Vaughan and Lenton*, 2011]. Concerns over the long term fate of the additional fixed carbon and possible side effects, including alterations to ecosystem structure and reducing the supply of macronutrients to low latitude regions, have however reduced the probability of Fe fertilization being used as a successful climate change mitigation strategy [*Buesseler et al.*, 2008; *Denman*, 2008; *Vaughan and Lenton*, 2011].

Given the essential role of Fe for primary production and hence the drawn down of atmospheric CO_2 the biogeochemical cycle of Fe is now included in climate models [e.g. *Aumont et al.*, 2015; *Dunne et al.*, 2013; *Moore et al.*, 2013b; *Tagliabue et al.*, 2015; *Yool et al.*, 2013]. However, a recent intercomparison of how the Fe cycle is represented in 13 global biogeochemical models revealed large differences in the calculated inputs of Fe to the ocean (e.g. total Fe inputs ranging from 1.4-195.4 Gmol yr^{-1}) and the rate at which dissolved Fe is lost due to scavenging, resulting in residence times varying from 5-500 years [*Tagliabue et al.*, 2015]. Therefore, a more detailed understanding of the

sources, cycling and sinks of iron in the contemporary ocean must first be achieved, including Fe transport from and cycling in highly productive continental shelf waters.

1.1 Iron species in seawater

The speciation of Fe in seawater is complex and can be investigated by physical size fractionation and analysis of the chemical speciation (Fig. 1.1). Physical separation by filtration divides Fe into operationally defined size fractions, where soluble (sFe) (< 0.02μm) and colloidal (cFe) (0.02 to 0.2 or 0.4 μm) make up the dFe fraction with the remaining Fe defined as particulate (pFe) (> 0.2 or 0.4 μm). By partitioning Fe in this manner the natural continuum of sizes present in oceanic waters is separated into distinct operational classes. Within each fraction Fe from a variety of sources, and thus different chemical species exist [*Tagliabue et al.*, 2017] (Fig. 1.1). This includes redox speciation as Fe in seawater can be found in ferric (Fe(III)) and ferrous (Fe(II)) redox states. In oxygenated seawater, Fe(III) is the predominant form as Fe(II) undergoes rapid oxidation [*Millero et al.*, 1987; *Rose and Waite*, 2002]. Although elevated Fe(II) concentrations, above those anticipated by thermodynamic theoretical calculations, have been observed due to processes such as photochemical reduction in surface waters [*Barbeau et al.*, 2001], in reducing environments such as oxygen minimum zones [*Lohan and Bruland*, 2008], anoxic sediment pore waters [*Noffke et al.*, 2012] and hydrothermal vent plumes [*Severmann et al.*, 2004].

An explanation for sub-nanomolar oceanic dFe concentrations is the inorganic chemistry of Fe, which is dominated by the hydrolysis of Fe(III) in oxygenated seawater (pH≈ 8.1). During this process the rejection of protons from surrounding hydrating water
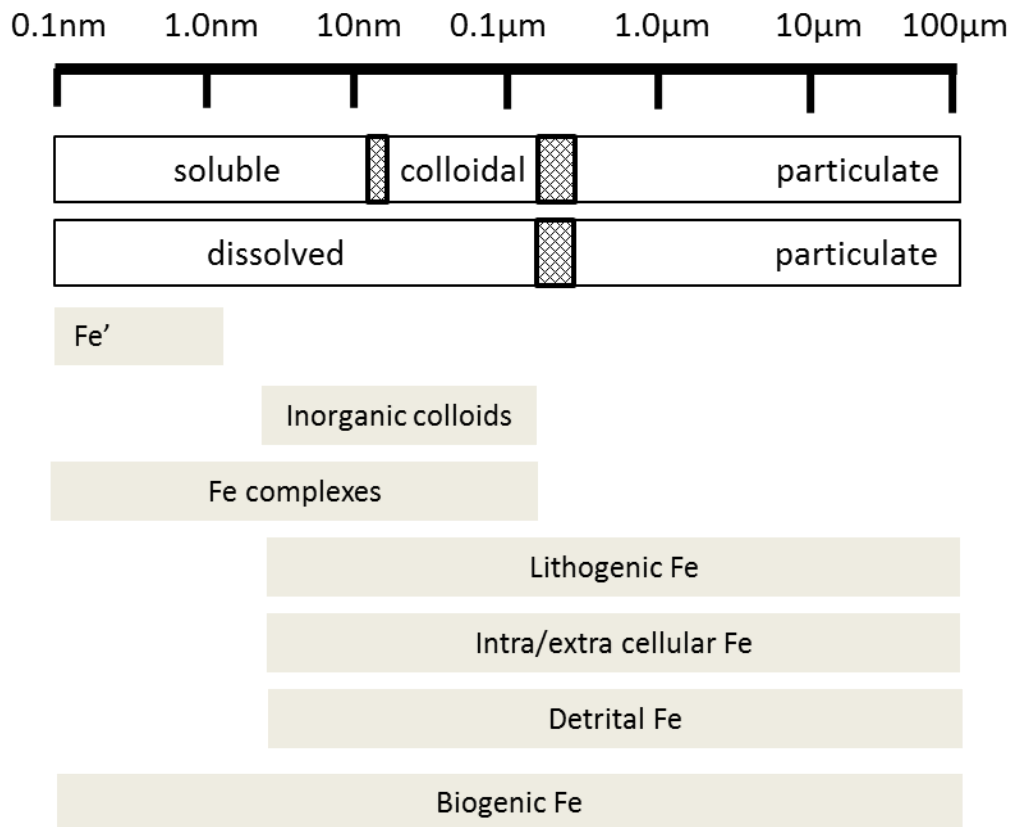
Figure 1-1- Schematic of the operational definitions used to distinguish the soluble, colloidal, dissolved and particulate fractions of Fe and the forms of iron that can exist within each phase.

molecules leads to the formation of amorphous hydrous ferric oxyhydroxides [*Byrne and Kester*, 1976]. These species are lost from solution via coagulation to form colloids and subsequently adsorbed onto particles; over time these oxyhydroxides are converted to more stable and less soluble crystalline forms, characterised by large negative Gibbs free energies of formation [*Stumm and Morgan*, 1996]. The result of this process is that the solubility of dFe in inorganic (ultra violet light digested) seawater is as low as 0.01 ± 0.002 nM [*Liu and Millero*, 2002], so that the majority of Fe is often present in the particulate form [*Wells et al.*, 2000] and results in a short residence time ($\approx$ 100-200 years in deep waters) relative to the mixing time of the ocean ($\approx$ 1000 years) [*Boyd and Ellwood*, 2010].

From solely a physico-chemical perspective, dFe oceanic profiles would be predicted to display a 'particle reactive' or 'scavenged' type profile, yet dFe profiles

typically display a 'hybrid' type profile. The concentration of dFe in deep waters across

ocean basins (≈ 0.4-0.7 nM) is consistently larger than the theoretical solubility limits

from hydrolysis alone [*Johnson et al.*, 1997] and suggests that other factors mitigate

against the loss of iron from the dissolved phase. One factor is the presence of Fe binding

organic ligands, which buffer dFe concentrations in the dissolved phase by forming

complexes with > 98% of dFe present in seawater. The conditional stability constants of

such complexes are reported to range between 10^{18} and 10^{23} and they are typically are

present in excess of dFe concentrations. Consequently, Fe binding organic ligands

maintain dFe concentrations above its inorganic solubility (0.01 ± 0.002 nM) [*Gledhill*

and van den Berg, 1994; *Ibisanmi et al.*, 2011; *Rue and Bruland*, 1995].

   In particle rich shelf systems it is also important to consider the relationship

between particulate Fe and organic complexation. In river plumes [*Buck et al.*, 2007] and

the Bering Sea shelf environment [*Buck and Bruland*, 2007], organic ligands exert a key

control on Fe solubility from particulate material. In both cases, once the organic ligand

coordination sites were saturated, no more dFe could be solubilised regardless of the
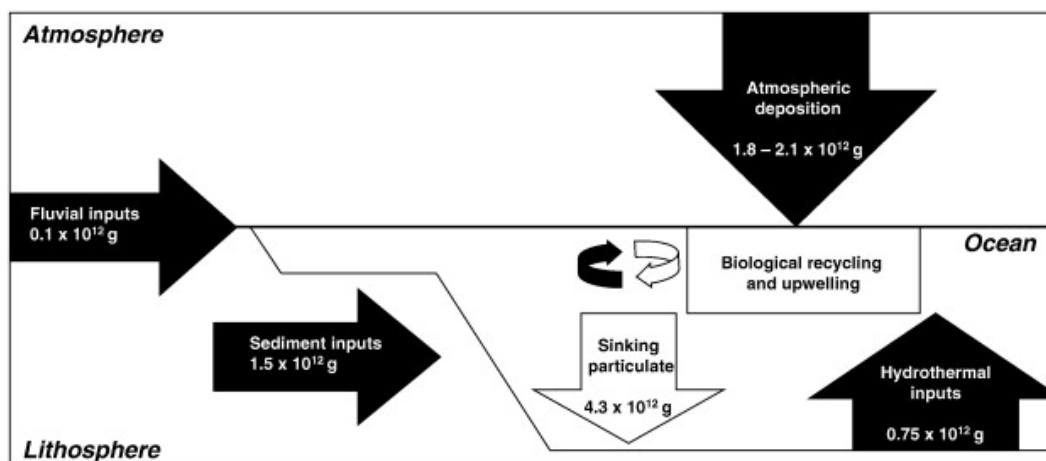
Figure 1-2- Annual fluxes of dFe to the ocean from Worsfold et al. [2014]. Original data from: Bewers and Yeats [1977]; Chester and Jickells [2012]; Stallard and Edmond [1983]; Tagliabue et al. [2014b]. Riverine flux assumes 90% estuarine removal [Boyle et al., 1977]. It should be noted that large uncertainties are currently associated with these flux estimates. See text for more details.

leachable pFe concentration present. These results indicate that strong organic ligands may influence the partitioning of Fe between the dissolved and particulate phases, a process that could be particularly important in particle rich shelf waters. Furthermore, *Rijkenberg et al.* [2008] reported a concurrent increase in dFe and decrease in the concentration of organic Fe binding ligands and conditional stability constants following a dust deposition event in the Atlantic. However, ligand-particle interaction is not a simple process; *Boyd et al.* [2010] showed the simultaneous release of dFe and Fe binding ligands from particulate material and suggested that biogenic particulates undergoing remineralisation provide excess ligands, whereas lithogenic particulates are responsible for scavenging Fe from the dissolved phase.

1.2 Sources of dissolved iron to the ocean

Iron is particle reactive and therefore seawater dFe concentrations are closely correlated with external inputs. The major sources of dFe to the ocean are from riverine input, aeolian dust, glacial inputs, hydrothermal venting, and sediments (Fig. 1.2). The contribution from each of these sources to dFe in the ocean varies geographically and temporally over seasonal to geological time scales. Additionally, mixing of Fe across the ferricline, the maximum gradient in dFe concentration between surface and subsurface waters [*Tagliabue et al.*, 2014b], can then be incorporated into and cycled within the biogenic Fe pool, termed the 'ferrous wheel' [*Strzepek et al.*, 2005], which can mediate exchange of Fe between the soluble, colloidal, dissolved and particulate phases. The major removal processes for dFe are scavenging and precipitation, leading to sedimentation and biological uptake.

At present there remains considerable uncertainty associated with these fluxes; for instance riverine data is sparse in relation to the number of rivers and is complicated by the non-conservative behaviour of dFe in estuaries due to cation induced flocculation

of organic colloids [*Boyle et al.*, 1977]. Aeolian deposition includes wet and dry atmospheric deposition. A large source of uncertainty in estimates of dry deposition is the fractional solubility of Fe in atmospheric aerosols, which ranges from < 1 to > 95% [*Sholkovitz et al.*, 2012]. Wet deposition is comparatively under sampled, but could supply 10^{10} moles of Fe per year to the surface ocean, much of which could be present as aqueous Fe(II) [*Kieber et al.*, 2001]. The estimate of hydrothermal Fe sources presented in Fig. 1.2 assumes the relationship observed over the East Pacific Rise is representative of the global input [*Resing et al.*, 2015; *Tagliabue et al.*, 2010]. Additional fluxes not displayed on Fig. 1.2 are that of sea ice and glaciers and groundwater. Sea ice and glaciers might be very significant at high latitudes [*Raiswell et al.*, 2008]. However, the fate of glacial melt water derived dFe is likely to be dependent on the physical circulation of water at the glacial terminus and the non-conservative behaviour of Fe along the salinity gradient [*Hopwood et al.*, 2015]. The flux of Fe from groundwater may represent a significant flux to coastal zones, but is very poorly characterised [*Windom et al.*, 2006]. The shelf sediment as a source of Fe is introduced in more detail below (Section 1.3.1).

1.3 Shelf seas and the marine iron cycle

Shelf seas cover < 10% of the global ocean surface area yet have a disproportionate impact on the marine carbon cycle by contributing 10-20% of global oceanic primary production [*Liu*, 2001; *Muller-Karger et al.*, 2005]. The primary production in shelf seas results in a net drawdown of atmospheric CO_2, particularly in temperate shelf seas [*Chen and Borges*, 2009], and 'fuels' fisheries, supporting 90% of the global catch [*Pauly et al.*, 2002]. Along with light and grazing pressure, nutrient availability exerts a key control on the magnitude of primary production. In coastal

regions, it has been assumed that Fe is replete due to its proximity to rivers and to sediment water exchange, in contrast to the limiting concentrations observed in the open ocean (Table 1.1). However, very few biogeochemical studies have taken place on stratified shelf systems and no seasonal studies have examined Fe cycling in stratified shelf systems, which are found globally in sub-polar regions. Therefore, an enhanced understanding of Fe in seasonally stratifying shelf seas will increase our understanding of the drivers of primary production in these important regions.

Although the Taylor-Proudman theorem puts a constraint on exchange between the shelf and the open ocean, frictional forces ensure shelf systems are not isolated from the open ocean. Transport of Fe from shelf sea sediments is an important source of Fe to the open ocean and current uncertainty in the flux estimates means that it could be larger in magnitude than the aeolian Fe flux [*Dale et al.*, 2015; *Elrod et al.*, 2004]. Moreover, shelf sediment derived Fe may have a greater impact on the global carbon cycle through the primary production it sustains than that of aeolian or hydrothermal Fe [*Tagliabue et al.*, 2014a].

To address this current gap in our understanding, this thesis examines both the role of Fe in sustaining primary production in shelf systems and the off shelf transport of Fe from shelf systems and are introduced in detail below (section 1.3.2 and 1.3.3).

Table 1-1- Comparison of dissolved (0.2 to 0.4 μm filter) iron concentrations (nM) reported for different oceanographic regimes. Surface definition varies between studies, taken here as the shallowest reported values (max 30 m depth). Data only used if verification carried out by analysis of reference/consensus material or through independent analysis of same sample/s by independent method and group. Data not included if limit of detection not reported. Data initially reported in nmol/kg converted to nM assuming 1 L seawater is equal to 1.035 kg

[a][*Bucciarelli et al.*, 2001] [b][*Measures and Vink*, 2001] [c][*Aguilar-Islas et al.*, 2007] [d][*Chever et al.*, 2010] [e][*Sarthou et al.*, 2003] [f][*Ussher et al.*, 2007] [g][*Laës et al.*, 2003] [h][*Blain et al.*, 2008] [i] [*Klunder et al.*, 2011] [j][*Klunder et al.*, 2012] [k][*Nédélec et al.*, 2007]

	Coastal Water	Continental Shelf Water	Open Ocean Influenced by Continental Shelf	Open Ocean
Southern Ocean				
Surface	8.8-12.6[a]	0.58-2.71[a]	0.46-0.71[a]	0.08-0.32[b], 0.11-0.70[d], 0.08-0.47[i]
Subsurface	18.4- 22.6[a]	1.25-1.74[a]	0.86-1.94[a]	0.15-2.2[i]
Pacific Ocean				
Surface	1.0-3.9[c]	0.5-6.3[c]	0.03-1.7[c], 0.32-1.2[h]	0.03-0.05[c],0.08-0.13[h]
Subsurface	1.0-12.6[c]	4.3-12.6[c]	1.0-2.4[c], 1.23-3.39[h]	0.06-1.34[h]
Atlantic Ocean				
Surface		0.2-1.75[f], <0.16-2.02[k]	0.15-0.5[f]	0.02-1.11[e], 0.23-0.34[g]
Subsurface	0.8-2.1[f]	0.6-2.0[f], 0.21-5.37[k]		0.5-1.19[9]
Arctic Ocean				
Surface		0.3-3.0[j]	0.1-2.8[j]	
Subsurface		0.2-11.0[j]	0.2-3.0[j]	

1.3.1 Shelf sediments as a source of iron

For both off-shelf transport and on-shelf primary production, the primary source of Fe is the continental shelf sediment. The dFe concentration in riverine water can exceed 1 µM [*Jiann et al.*, 2013] and is predominantly present in the colloidal form, yet in estuaries salt induced flocculation, and a rise in pH, can remove > 90% of riverine dFe [*Boyle et al.*, 1977] leaving the resulting pFe to settle out on the coastal and shelf sediments. However, the shelf sea environment is both physically dynamic and highly productive [*Simpson and Sharples*, 2012]. The combination of sediment resuspension [*Elrod et al.*, 2008; *Nédélec et al.*, 2007] and a diffusive flux of Fe, driven by the use of Fe(III) as the terminal electron acceptor during the respiration of organic matter, [*Dehairs et al.*, 1989; *Elrod et al.*, 2004; *Lohan and Bruland*, 2008; *Santschi et al.*, 1990; *Ussher et al.*, 2007] can lead to shelf sediments being a significant source of Fe to the overlying water column.

There are numerous factors that affect the flux of sedimentary Fe, including bottom water oxygen concentrations [*Dale et al.*, 2015; *Lohan and Bruland*, 2008; *Noffke et al.*, 2012; *Severmann et al.*, 2010], the flux of organic carbon to the sediments [*Dale et al.*, 2015; *Elrod et al.*, 2004] and the quantity of reactive Fe present in the sediments [*Chase et al.*, 2007; *Homoky et al.*, 2013; *Noffke et al.*, 2012; *Severmann et al.*, 2010]. The latter is influenced by local geology, riverine supply and regular (seasonal) oxic/anoxic periods. To highlight the present uncertainty in calculating global dFe fluxes a method of extrapolation used by *Elrod et al.* [2004] has been applied to data from other studies focusing directly on the benthic flux of dFe in order to generate comparable estimates (Fig. 1.3). The calculations involved in producing this figure have a number of caveats, for instance; not all the data used have analytical uncertainties associated with them and so errors are not propagated and the data for South Africa is

from a single station whereas the others are mean fluxes from multiple stations. Also it is noted that the Black Sea is an anoxic basin with limited connectivity with the open ocean. Nevertheless, the range of global flux estimates spans 2-4 orders of magnitude for sediments shallower than 200 m, depending on whether Black Sea data are included and 3 orders of magnitude for sediments between 200 and 1000 m depth. Moreover, most studies of shelf fluxes of dFe have concentrated on reductive dissolution of Fe, whereas *Homoky et al.* [2013] highlight the potential importance of a non-reductive pathway of Fe transport from oxic shelf margins. Although, the flux of dFe per unit area of sediment to oxic seawater is likely to be lower than the flux to oxygen deficient waters [*Elrod et al.*, 2004], oxygenated waters are typical of most shelf regions and Fe isotope measurements suggest a significant fraction of open ocean dFe is derived from oxic margin sediments [*Conway and John*, 2014; *Homoky et al.*, 2013; *Radic et al.*, 2011]. Therefore, understanding the rate and speciation of Fe fluxes from oxic shelf margins remains an important aspect of the global Fe cycle.
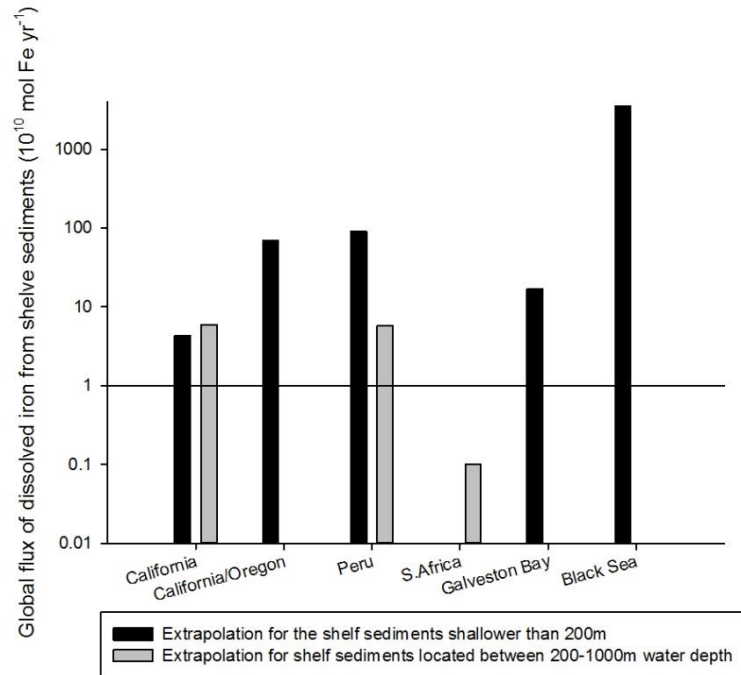
Figure 1-3- Global flux of dissolved iron from shelf sediments, based on extrapolations of observations from different locations. The method of extrapolation is the same as that used by Elrod et al. [2004], the average flux measured multiplied by the area of seafloor globally within the depth interval. The data used comes from the following sources California [*Elrod et al.*, 2004], California/Oregon [*Severmann et al.*, 2010; *Stallard and Edmond*, 1983; *Tagliabue et al.*, 2014b], Peru [*Noffke et al.*, 2012], S. Africa [*Homoky et al.*, 2013; *Stallard and Edmond*, 1983], Galveston Bay [*Warnken et al.*, 2001], Black Sea [*Friedl et al.*, 1998] and sea bed area data [*Menard and Smith*, 1966].

1.3.2 Iron and shelf primary production

Iron from shelf sediments has been identified as a potential control of primary production in shelf environments [*Johnson et al.*, 1999] but the traditional paradigm is that shelf waters are Fe replete [*Chase et al.*, 2005a]. However, Fe limitation of part or all of the phytoplankton community has been reported in the California upwelling system [*Fitzwater et al.*, 2003; *Hutchins and Bruland*, 1998; *King and Barbeau*, 2007], over the Bering Sea shelf break [*Aguilar-Islas et al.*, 2007] and in the Ross Sea once seasonal stratification has isolated surface waters from sediment derived Fe [*Arrigo et al.*, 2003; *Sedwick et al.*, 2000].

The studies detailed above suggest that (co-)limitation between multiple nutrients and light in shelf environments is complex and varies both spatially and temporally. Further evidence to support this can be found in recent studies of phytoplankton genomics. An Atlantic coastal *Synechococcus* strain retained the genetic material required to cope with variable Fe availability despite the additional nitrogen this required, whereas a strain isolated from Fe replete waters under the Saharan dust plume had not [*Mackey et al.*, 2015]. Furthermore, genetic indicators of Fe stress in coastal diatoms have been detected at elevated Fe concentrations [*Chappell et al.*, 2015]. Despite the increasing awareness that Fe may not always be replete in shelf systems, the cycling of Fe in shelf systems remains poorly constrained.

In seasonally stratifying temperate shelf seas, the seasonal changes in solar irradiance govern the degree of vertical mixing by stratifying the water column in spring. The variability in vertical mixing, in turn, determines the availability of light and nutrients to phytoplankton [*Sverdrup*, 1953]. Whilst this is well established for the macronutrients [e.g. *Hickman et al.*, 2009; *Hickman et al.*, 2012; *Pingree et al.*, 1977; *Rippeth et al.*, 2009; *Sharples et al.*, 2001], the seasonal cycling of Fe in these systems has yet to be observed.

1.3.3 Off-shelf transport of iron

The importance of Fe remobilised from the sediments will depend on its fate once in the water column. Several studies have shown that dFe concentrations decrease with distance away from the shelf [*Aguilar-Islas et al.*, 2007; *Bucciarelli et al.*, 2001; *Elrod et al.*, 2004; *Milne et al.*, 2017; *Ussher et al.*, 2010; *Ussher et al.*, 2007], indicative of offshelf transport. It has been hypothesised that shelf derived dFe drives observed patterns in oceanic primary production, including alleviation of Fe limitation in the North Pacific [*Tyrrell et al.*, 2005], fertilization of the Madagascar bloom [*Srokosz et al.*, 2015] and increased primary production downstream of islands in the Southern Ocean [*Pollard et al.*, 2009; *Van Der Merwe et al.*, 2015] and the Galapagos Island [*Martin et al.*, 1994] systems.

The region of focus in the study reported here is the North West European Shelf. The adjacent central and high latitude North Atlantic receives a similar amount of dust to that of high latitude Pacific HNLC region [*Jickells et al.*, 2005; *Measures et al.*, 2008] and dFe measurements of 0.02-0.22 nM in the Iceland and Irminger Basin surface waters confirm this is not an Fe replete region [*Martin et al.*, 1993; *Measures et al.*, 2008; *Nielsdóttir et al.*, 2009]. These results suggest a HNLC type region post spring bloom, and enrichment studies have demonstrated the potential for Fe stress/limitation in this region [*Blain et al.*, 2004; *Martin et al.*, 1993; *Moore et al.*, 2006; *Nielsdóttir et al.*, 2009; *Ryan-Keogh et al.*, 2013] which also happens to be an area of significant CO_2 draw down [*Takahashi et al.*, 2002].

Whilst it is presently understood that shelf sediments are an important source of Fe to the open ocean, less is known about the processes and physico-chemical speciation of the mobilised Fe. The physical processes include transport in intermediate nepheloid layers (INL) along isopycnals following sediment resuspension, likely a result

15

of internal tides or friction of the along-slope current [*Nédélec et al.*, 2007] and eddy transport [*Boyd et al.*, 2012; *Van Der Merwe et al.*, 2015].

Regarding chemical speciation, most studies separate dFe by filtering through 0.2-0.45 µm membrane and off-shelf transport has focused on the dFe fraction. More recently an appreciation of the pFe fraction exported from shelf systems has revealed that the transport of labile particulate Fe is pivotal to understanding the shelf sediment source of Fe [*Abadie et al.*, 2017; *Lam and Bishop*, 2008; *Lam et al.*, 2006; *Milne et al.*, 2017], particularly as much of the pFe (up to 81%) can be labile [*Hurst et al.*, 2010]. Moreover, although investigations into the partitioning of the dFe into soluble and colloidal fractions are limited, it appears that colloidal association increases near the shelf break [*Fitzsimmons et al.*, 2015a; *Hurst et al.*, 2010] which was interpreted as an input of inorganic colloidal material from sediment resuspension. However, greater variability in the relative proportions of sFe/cFe was observed in the Canary Basin, both in shelf and off shelf waters, at a time when sediment input was the dominant source of Fe to these waters [*Ussher et al.*, 2010]. Redox speciation studies show that a diffusive Fe input is also important. In hypoxic waters most of the dFe can exist as Fe(II) [*Lohan and Bruland*, 2008], whilst even in oxic waters a sedimentary Fe(II) signal is observed [*Ussher et al.*, 2007]. These studies reflect the complex processes occurring over the shelf and shelf break. These processes include diffusion of dFe, resuspension of dFe and pFe, and the subsequent interactions between the different fractions; including redox transitions, colloidal formation and particle aggregation/disaggregation.

1.4. Aims and hypotheses

This thesis investigates both the role that Fe plays in sustaining primary production in shelf systems and the role shelf systems play as a source of Fe to the open ocean. It is based around an investigation of the spatial and temporal variability in the

physio-chemical speciation of Fe in the Celtic Sea and the Malin/Hebridean Seas. This is split into 3 hypotheses with supporting objectives:

- **Hypothesis 1**: Given that seasonal stratification provides an efficient barrier to the vertical transport of macronutrients in the Celtic Sea, it is postulated that Fe will also be seasonally depleted in the surface mixed layer.

- **Hypothesis 2**: Intermediate nepheloid layers emanating from the Celtic Sea shelf slope have been observed to provide a transport mechanism of dFe to the adjacent Atlantic Ocean. In these particle rich waters, it is hypothesised that much of the dissolved iron will be present in the colloidal phase and that the particulate fraction will dominate the Fe inventory.

- **Hypothesis 3**: The seasonal cycling observed in the Celtic Sea will typify the seasonally stratifying regions of the shelf seas around the U.K and Ireland.

Chapter 2 - Analytical methodology

2.0 Introduction

Accurate and precise measurements of trace metals in seawater are essential for our understanding of their biogeochemical cycles. The major analytical challenges associated with this task are the exceptionally low trace metal concentrations (10^{-6} to 10^{-12} M) present in seawater relative to the major cation (Na, Mg, Ca, K, Sr) concentrations (10^{-1} to 10^{-4} M) and the ubiquitous nature of potential contaminants, especially aboard ship. As a result, methods of sampling and analysis used to determine trace metal concentrations need to be sensitive, selective and contamination free. Technological advances and the development of ultra-clean sample handling since the 1970's have made such sampling and analysis possible in all marine environments [*Achterberg et al.*, 2001] and attempts over the past decade to produce community wide consensus material through the IRONAGES [*Bowie et al.*, 2006], SAFe [*Bruland*, 2014] and GEOTRACES (www.geotraces.org) programmes have provided a robust way to check the accuracy of different methods for determining trace elements. The aim of the following section is to detail the methods used for the determination of Fe in this research.

2.1 Trace metal clean procedures and operationally defined fractions

2.1.1 Handling and cleaning procedures

To accurately and reliably determine trace metal concentrations in collected seawater samples, clean plastic ware and filtration equipment are required. Sample and reagent bottles (Nalgene™ low density polyethylene (LDPE)) were cleaned using the procedure outlined in Table 2.1.

Table 2-1- Cleaning procedure used for in this study, identical to that used in *Wyatt* [2013].

Step	Procedure
Stage 1. In general laboratory	
1	Rinse 3 times UHP water.
2	Immerse and cap in 3 M HCl (Fisher, Primar Plus) for 1 week.
3	Rinse 3 times with UHP water.
Stage 2. In class 100 laboratory	
1	Immerse and cap in 0.5 M HCl (Fisher, Primar Plus).
2	Rinse 3 times with UHP water.
Stage 3. Sample bottle storage	
1	Filled with UHP water acidified to 0.024M with HCl (Romil, SpA).
2	Double bagged (polyethylene) and stored in clean plastic container.

UHP= ultra-high purity water (MQ, ≥ 18.2 MΩ cm), HCl = hydrochloric acid

2.1.2 Operationally defined trace metal fractions

In this study, physio-chemical Fe speciation was defined by the filtration methods used (Table 2.2). The dissolved fraction has conventionally been defined as the fraction passing through 0.2 or 0.4 µm membrane filters. These pore sizes reflect the biological role of Fe, which makes it necessary to exclude living cells from the seawater sample to prevent alteration of the Fe pool after collection. A 0.2 µm cut off was chosen as it excludes a greater proportion of living cells, including heterotrophic bacteria in the 0.2 to 0.4 µm fraction [*Bowie and Lohan*, 2009].

The dFe fraction is further separated by filtration into soluble (sFe) and colloidal (cFe) fractions; the colloidal fraction being determined by subtraction of sFe from dFe (Table 2.2). Colloidal Fe is therefore defined as that fraction which passes through a 0.2 µm filter but not a 0.02 µm filter. A theoretical definition better elucidates why the colloidal fraction is of interest; the interior of a colloid must be chemically/physically different from its surrounding to allow the creation of an interface [*Wells*, 2002], which allows interaction with other soluble and colloidal phases through processes such as adsorption and absorption. The creation of an interface sets the lower boundary on

colloidal size with the upper limit reached when the colloid is no longer maintained in

solution by turbulent motion and gravity becomes the dominant force acting on the

particle. Colloids can therefore be theoretically defined as non-sinking particles and

colloidal Fe is Fe associated with such particles.

Table 2-2- Operationally defined size fractions of dissolved Fe species used in this study.

Fraction	Abbreviation	Filtration	Pre-Treatment
Total Dissolvable Iron	TdFe	Unfiltered	Acidification after collection (pH 1.6, HCl). Stored for > 6 months. Oxidised with H_2O_2 for 60 minutes before analysis.
Dissolved Iron	dFe	< 0.2 µm	Filtered immediately following collection. Acidification after filtration (pH 1.6, HCl). Stored for > 2 months. Oxidised with H_2O_2 for 60 minutes before analysis.
Soluble Iron	sFe	< 0.02 µm	Pre-filtered through 0.2 µm and then through 0.02 µm. Acidification after filtration (pH 1.6, HCl). Stored for > 2 months. Oxidised with H_2O_2 for 60 minutes before analysis.
Colloidal Iron	cFe	dFe-sFe	N/A
Dissolved Iron (II)	Fe(II)	< 0.2 µm	Analysed immediately after in-line filtration.

Fe(II) is produced in the oceans by the reduction of Fe(III). Processes that generate Fe(II) in UK shelf waters include photochemical reduction of Fe(III) in surface waters and the use of Fe(III) as the terminal electron acceptor during the oxidation of organic matter in reducing sediments [*Ussher et al.*, 2007]. To investigate the importance of such processes, dissolved Fe(II) concentrations were determined in selected samples.

Total dissolvable Fe (TdFe) is defined as Fe which is solubilized after at least 6 months of acidification to 0.024 M HCl.

2.2 Flow injection with chemiluminescence detection for the determination of soluble, dissolved and dissolvable iron fractions and Fe(II)

Flow injection (FI) is an analytical technique where sample is reproducibly injected into liquid phase reagent streams under laminar flow conditions. As a result the degree of sample/reagent mixing is consistent with each injection, meaning there is no requirement for equilibrium conditions to be established [*Worsfold et al.*, 2013]. FI systems benefit from a number of advantages as outlined in a review by *Worsfold et al.* [2013]. These include:

- Automated reproducible injections leading to high precision

- Closed environment and minimal sample handling reducing contamination risk

- Typically only small volumes of sample and regents required and therefore also low waste generation

- In-line sample manipulation (e.g. buffering, pre-concentration and removal of matrix interferences, filtration) which is essential for the determination of transient species such as Fe(II) in oxic seawater

- Analysis time typically of the order of minutes, leading to high sample throughput

FI manifolds can be combined with a number of different flow-through detection systems to determine a range of trace metal concentrations on-line following pre-concentration and removal of matrix interferences. Detection methods include fluorimetry [*Nowicki et al.*, 1994], atomic absorption spectroscopy [*Fang et al.*, 1984] and inductively coupled plasma mass spectrometry (ICP-MS) [*Clough et al.*, 2015; *Yin et al.*, 2005]. In this study, a photon counting head, more commonly called a photomultiplier tube (PMT) was used to measure chemiluminesence (CL), with the resulting combined system termed flow injection with chemiluminescence detection (FI-CL).

When photons enter a PMT they are converted to electrons at the photocathode due to the photoelectric effect; the ejection of electrons from a material due to it gaining energy from the interaction with electromagnetic radiation (light). Measuring a single electron is difficult as the charge is low (as low as 1.6×10^{-19} coulombs). Therefore, a series of dynodes, coated in emissive material, are each held at a positive potential relative to the next dynode. The increase in kinetic energy of the electron is proportional to the potential between the dynodes. When the electrons strike the dynode the transfer of kinetic energy causes additional electrons to be emitted, in doing so multiplying the signal, which is measured at the anode.

CL can be defined as the emission of visible light (luminescence) from a chemical reaction. For CL to occur, an excited state intermediate is formed that returns to a ground state through the release of radiation, not through vibrational conversation of energy to heat or through phosphorescence from triplet states [*Barni et al.*, 2007]. This process can either occur directly or indirectly if the molecule or atom in the excited state

is an inefficient emitter and therefore passes the energy to another species, known as a 'sensitizer'. By its definition a CL technique does not require a radiation source; radiation is produced by a reaction, so unlike spectrophotometric methods there is no need to differentiate between emitted and transmitted radiation. The result is reduced Rayleigh and Raman scattering and source noise, leading to increased sensitivity [*Barni et al.*, 2007; *Worsfold et al.*, 2013].

For analytical purposes it is generally the intensity of CL that is of interest [*Barni et al.*, 2007; *Worsfold et al.*, 2013]. The intensity of CL (I_{CL}) can be written as:

$$I_{CL} = \Phi_{CL}(dC/dt) \tag{1}$$

Where Φ_{CL} is the CL quantum yield and dC/dt is the rate of reaction (molecules reacting s^{-1}). The CL quantum yield is a function of three factors; the fraction of excited states produced, the fraction of reacting molecules following the correct chemical path and the luminescence quantum yield of the emitter. More simply it can be described as:

$$\Phi_{CL} = \frac{\text{total number of photons emitted}}{\text{number of molecules reacting}} \tag{2}$$

The rate of reaction is dependent on the reaction conditions. If the concentration of the analyte of interest determines the rate of reaction, then I_{CL} can be used to quantitatively determine the analyte concentration. However, solution CL is transient by nature and often occurs quickly (< 1 s) [*Rose and Waite*, 2002], thus creating the requirement for controlled and reproducible sample/reagent mixing if the CL is to be measured precisely [*Worsfold et al.*, 2013]. Consequently, combining a suitable CL detector with a FI manifold is an ideal method to reliably measure I_{CL}. As such, FI-CL techniques have become popular methods to determine a range of species present in seawater (e.g. Fe [*Ussher et al.*, 2007], copper (Cu) [*Coale et al.*, 1992], reactive oxygen

species [*Milne et al.*, 2009], nitrate + nitrite (hereafter NO_3^-) [*Mikuška and Večeřa*, 2003],

phosphate (PO_4^{3-}) [*Patey et al.*, 2008]).

The FI-CL systems used in this work are based on the two step oxidation of the chemiluminescent dye luminol (5-amino-2,3-dihydro-1,4-phthalazinedione) which is catalysed by a range of metal ions, including Fe(II) or Fe(III), in the presence of a suitable oxidant (either O_2 or H_2O_2). The luminol chemistry is sensitive enough to allow the determination of dFe and TdFe concentrations in all marine environments [e.g. *Bowie et al.*, 1998; *Croot and Laan*, 2002; *De Jong et al.*, 1998; *Klunder et al.*, 2011; *Lannuzel et al.*, 2006; *O'Sullivan et al.*, 1995; *Obata et al.*, 1993; *Rose and Waite*, 2001; *Ussher*, 2005; *Ussher et al.*, 2010; *Ussher et al.*, 2007; *Wyatt*, 2013]. In addition to high sensitivity, there are numerous other benefits of using luminol based FI-CL techniques that make them ideal for the detection of TdFe and Fe(II) at sea and in the laboratory [*Ussher*, 2005; *Worsfold et al.*, 2013] including:

- Elemental and redox sensitive detection

- Portable and robust in line detection unit

- Relatively inexpensive and requiring simple maintenance

- Pre-concentration of seawater followed by elution negates Schlieren effect (all reagents have densities approximating to that of UHP)

2.2.1 The oxidation of luminol

The oxidation of luminol is the key reaction leading to CL in both Fe(II) and Fe(III) systems. In alkaline solutions, luminol is deprotonated to monoanionic and dianionic forms (Fig. 2.1), with the monanionic form predominating in solutions with a pH range of 8-14. Both monoionic and dianionic forms can be oxidised to form an intermediate excited compound that can lead to CL. The excited compound produced has been

identified as 3-aminophthalate; the fluorescence spectrum of the excited intermediate 3-aminophthalate (3-APA[*]) has been shown to match the chemiluminescence spectrum of luminol [*White and Bursey*, 1964]. However, the exact mechanisms of luminol oxidation leading to the generation of 3-APA[*] are not fully characterised [*Barni et al.*, 2007; *Merényi et al.*, 1990; *Rose and Waite*, 2001; *White and Bursey*, 1964]. It is generally considered that a two-step oxidation of luminol is initiated to create the intermediate compound α-hydroxy hydroperoxide (α-HHP) which decomposes to form 3-APA[*] (Fig 2.2). However, the pathway leading to the formation of α-HHP is dependent upon the composition of the reacting system, in particular the nature of the oxidant, of which there are many that can initiate primary oxidation [*Klopf and Nieman*, 1983; *Merényi et al.*, 1990].

The chemistry used in this work to determine TdFe, dFe and sFe is based on the Fe(III)/H_2O_2/luminol FI-system first reported by *Obata et al.* [1993]. Hydrogen peroxide (H_2O_2) is the oxidant, although H_2O_2 alone is not sufficient to initiate primary oxidation [*Rose and Waite*, 2001]. The role of Fe(III) in the production of primary oxidants is not completely clear [*Barni et al.*, 2007]; it is known that Fe(III) catalyses the breakdown of H_2O_2 which would increases the rate at which suitable primary oxidants ($\cdot$OH, OH$^-$) are
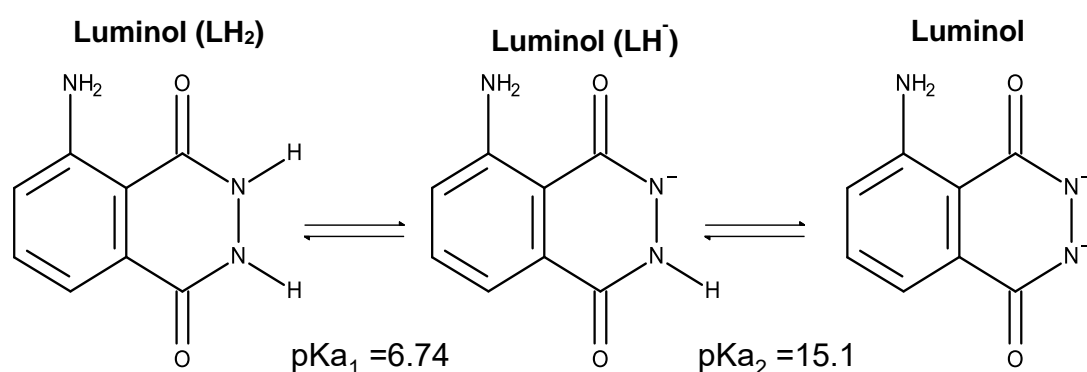
Figure 2-1- Luminol protonation. LH_2, LH^- and L_2^- represent diprotic, monoanionic and dianionic luminol forms. Adapted from Barni et al. [2007].

produced. Secondary oxidation is achieved as the luminol radical forms diazaquinone either by fast recombination of the luminol radical or through oxidation of the luminol radical by O_2, during which $O_2^{\cdot-}$ is produced [*Rose and Waite*, 2001]. The presence of excess H_2O_2 (pKa 11.7) promotes the nucleophilic attack of diazaquinone by the hydroperoxide ion (HO_2^-) relative to other nucleophiles (e.g. OH^-) and thus ensures oxidation of diazaquinone to α-HHP (Fig. 2.2. step 2). The slow generation of $O_2^{\cdot-}$ during this process also facilitates the direct oxidation of the luminol radical to α-HHP, meaning the onset of maximum I_{CL} is delayed whilst there is a build-up of $O_2^{\cdot-}$ [*Merényi et al.*, 1990; *Rose and Waite*, 2001].

The chemistry used to determine Fe(II) is based on the Fe(II)/O_2/luminol system [*Bowie et al.*, 1998; *Rose and Waite*, 2001; *Ussher*, 2005]. In this case the oxidant is molecular oxygen (O_2) which is reported to oxidise Fe(II) through the Haber-Weiss mechanism [*Haber and Weiss*, 1934]:

$$Fe(II) + O_2 \rightarrow Fe(III) + O_2^{\cdot-} \tag{3}$$

$$Fe(II) + O_2^{\cdot-} \rightarrow Fe(III) + H_2O_2 \tag{4}$$

$$Fe(II) + H_2O_2 \rightarrow Fe(III) + OH^{\cdot} + OH^- \tag{5}$$

$$Fe(II) + OH^{\cdot} \rightarrow Fe(III) + OH^- \tag{6}$$
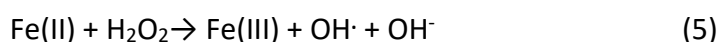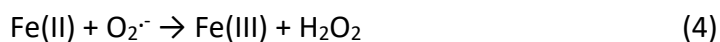
Following this mechanism, the oxidation of Fe(II) produces both $OH^{\cdot}$ and $O_2^{\cdot-}$; the former is likely to be the primary oxidiser of luminol (Fig. 2.2. step 1) as $O_2^{\cdot-}$ has been shown to be ineffective as a primary oxidant [*Merényi et al.*, 1990]. The presence of $O_2^{\cdot-}$ already in the solution does however mean that the secondary oxidation can proceed immediately via the 'fast' direct route, increasing the speed of the reaction relative to the Fe(III)/H_2O_2/luminol system [*Klopf and Nieman*, 1983; *Rose and Waite*, 2001].

The final step is dependent on the pH of the solution as only decomposition of

Luminol   **1.**   **Luminol radical (LH˙.**

Oxidant
Fe(II)/ O$_2$
Fe(III)/ H$_2$O$_2$

2.

Oxidant
(L˙ or LH˙)

Superoxide
(L˙)

Diazaquinone   **α-hydroxy- hydroperoxide (L˙OOH,**

HO$_2$⁻

Aminophthal   **3.**

+   N$_2$ +   *hv*
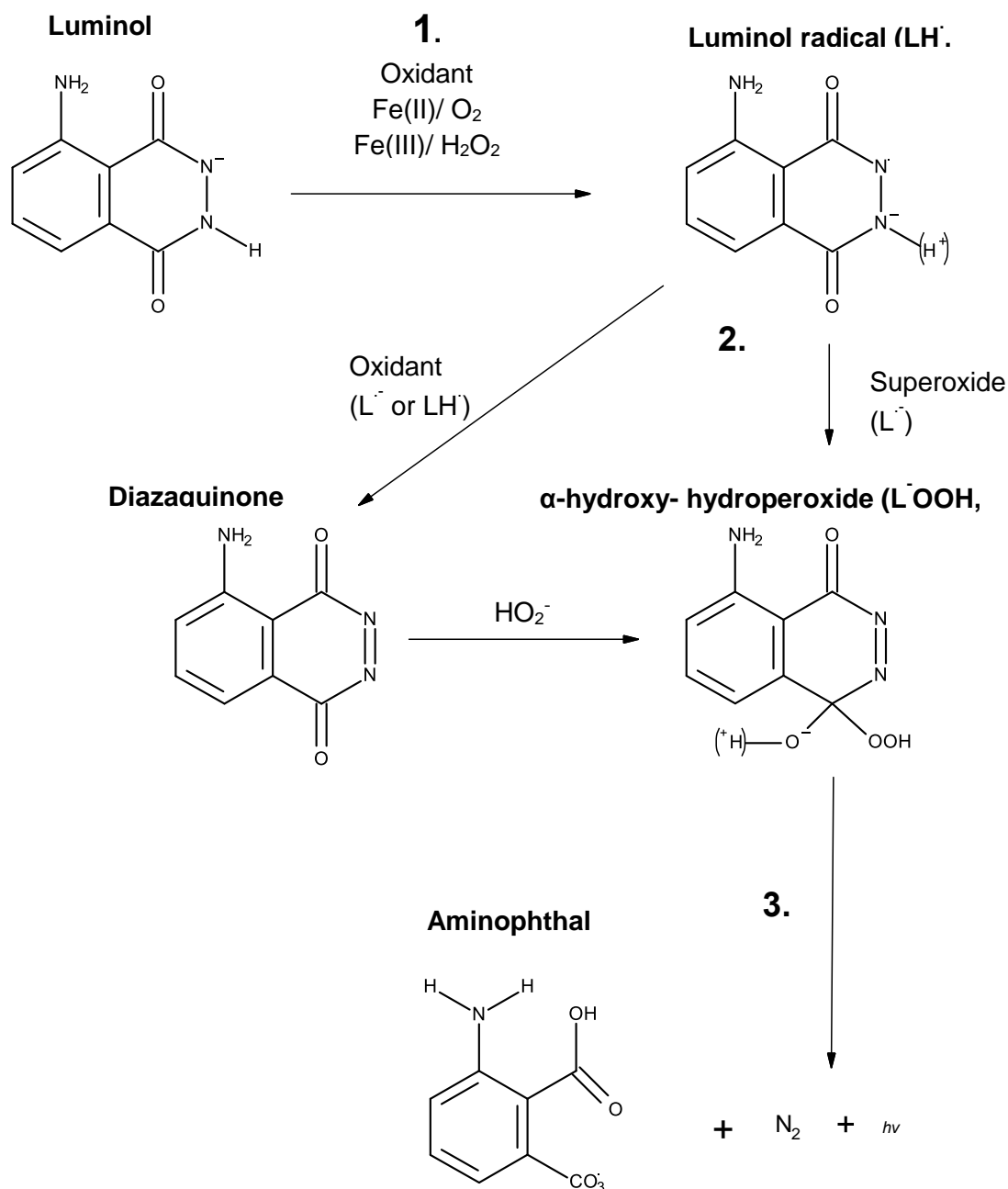
Figure 2-2- The major pathways for two step oxidation of luminol (1 & 2) and the decomposition of the intermediately compound (3). Re-drawn from Rose and Waite [2001].

the monoanion form of α-HHP will produce CL at 425 nm [*Merényi et al.*, 1990; *Rose and Waite*, 2001]. The pKa of α-HHP is 8.2; therefore, to promote dissociation the pH needs to be higher than this. The optimum reaction pH is reported to be 10.5 for the

Fe(II)/O$_2$/luminol system [*Rose and Waite*, 2001; *Ussher*, 2005] and 9.5 for the

Fe(III)/H$_2$O$_2$/luminol system [*Obata et al.*, 1993].

2.2.2 Pre-concentration and matrix removal
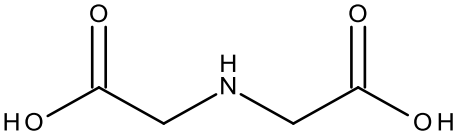
The seawater matrix is complex and major seawater ions, such as Ca^{2+} and Mg^{2+},

have been shown to supress the CL signal, whereas halide ions enhance the CL signal at

concentrations similar to those in seawater [*Bowie et al.*, 1998; *Shelley et al.*, 2010].

Furthermore, the concentration of Fe in seawater is often sub-nanomolar; therefore it

is necessary to isolate Fe from the seawater matrix to both remove interferences and

pre-concentrate the analyte. In this study, two chelating resins were used, Toyopearl®

AF-Chelate-650M (TOSOH, Sigma Aldrich), hereafter referred to as Toyopearl, and

immobilized 8-hydroquinoline (8-HQ) [*Landing et al.*, 1986].

Toyopearl (Table 2.3) was chosen for the Fe(III)/H$_2$O$_2$/luminol system. The resin

is a hydroxylated methacrylic polymer bead based resin with iminodiacetate (IDA)

functional groups. In contrast to 8-HQ, it requires no complicated laboratory synthesis

as it is commercially available. Consequently, Toyopearl has been utilized by numerous

research groups in the oceanographic community interested in determining trace metal

concentrations [e.g *Clough et al.*, 2015; *De Baar et al.*, 2008; *Klunder et al.*, 2011; *Milne

et al.*, 2010; *Warnken et al.*, 2000]. A specific advantage for the determination of Fe is

that complete retention is achieved at a loading pH of 3.5 - 5.0 on the Toyopearl resin,

making calibration and sample analysis less sensitive to small variations in loading pH

[*Clough et al.*, 2015].

8-HQ (prepared by Dr Simon Ussher) was chosen for the Fe(II)/O$_2$/ luminol

system as it has been successfully used to investigate Fe(II) concentrations in seawater

[*Bowie et al.*, 2002; *King et al.*, 1995; *Ussher et al.*, 2007].

Both Toyopearl and 8-HQ resin were packed into custom made columns (polymethyl methacrylate) and retained with acid cleaned high density polyethylene frits (BioVyon F, 0.75 mm thick, 22-57 μm pore size). These were cleaned in-line by passing 0.5 M HCl (Romil, SpA) over them at a slow pump speed (< 0.5 mL min^{-1}) for at least 3 h followed by UHP water for at least 3 h for Toyopearl and overnight for 8-HQ.

Table 2-3- Toyopearl® AF-Chelate-650M chelating resin characteristics.

Chelating group structure (iminodiacetate)	
Ion exchange capacity	25-45 μeq mL^{-1}
Pore size	0.1 μm
Particle size (mean)	65 μm

2.3 Fe(III)/H$_2$O$_2$/luminol system

2.3.1 Reagents and standards

Reagents and standards were prepared inside a class-100 laminar flow hood using UHP water.

A 50 mM luminol stock was prepared by dissolving 0.177 g luminol (Sigma-Aldrich) and 0.250 g sodium carbonate (Na$_2$CO$_3$) (Sigma-Aldrich) in 20 mL of UHP. This solution was vigorously shaken and left for 2-3 days to allow for complete dissolution. A 0.25, 0.083 or 0.025 mM working luminol solution was prepared by diluting 5, 1.5 or 0.5 mL of luminol stock and 70 μL of concentrated triethylenetetramine (TETA, Sigma-Aldrich) in 1 L UHP water. Working luminol solutions were prepared at least the day before analysis to allow the solution to stabilize [*Bowie et al.*, 1998]. TETA increases sensitivity by chelating Fe(III); the resulting TETA-Fe(III) complex increases the rate of H$_2$O$_2$ decomposition [*Wang*, 1955]. A 0.23 M HCl elution acid was prepared by dilution of 20 mL of concentrated HCl (Romil, SpA) in 1 L UHP water and a 0.012 M wash solution

was made by dilution of 1 mL of concentrated HCl in 1 L UHP water. The ammonia

(NH_4OH) solution was prepared by dilution of 40 mL of concentrated NH_4OH (Romil, SpA)

in 1 L UHP. H_2O_2 was kept refrigerated until needed, a 0.3 M working solution was

prepared by adding 30 mL of H_2O_2 (30%, Merck, Suprapur) to 1 L UHP water.

A 7 M ammonium acetate (NH_4Ac) buffer stock was prepared by the addition of

100 mL concentrated acetic acid (CH_3COOH) (Romil, SpA) to 100 mL UHP water followed

by addition of 50 mL of NH_4OH (Romil, SpA). To prepare a working buffer solution, 50

mL of stock was diluted with 950 mL UHP water (pH 4.2-4.3), and when mixed in-line

with acidified sample (pH 1.6) this gives a pH of 3.5-4.0.

In order to quantify Fe concentrations, standard additions of Fe were added to

20 mL of seawater. A serial dilution of a 17.9 mM (1000 ppm) Fe standard (Romil) was

carried out, first to an 80 μM intermediate stock which was further diluted to a working

stock. For each dilution the mass of UHP water, HCl and stock was recorded in order to

calculate the final concentration. The final working stock was acidified to 0.024 M HCl

to match the pH of the seawater to which it was added. The volume of the working

standard added was never more than 1% of the seawater volume.

2.3.2 Instrumentation and procedure

The FI manifold design used is displayed in Fig. 2.3. It consists of three peristaltic

pumps (Gilson MiniPuls 3) with two stop accu-rated™ polyvinylchloride (PVC) tubing

(Elkay), a six port injection valve and a ten port autosampler (VICI Valco Instruments), a

solenoid valve (Cole-Palmer), a photon counting head (Hamamatsu, model H8259), two

clean up columns and one pre-concentration column. Both clean-up and pre-

concentration columns contained Toyopearl. LABVIEW™ V7.1 (National Instruments)

software, laptop (Toshiba) and control module (Ruthern Instruments) were used to control pump and valves and acquire peak height data [*Bowie et al.*, 2005].

The clean-up columns were reversed every 2-3 days to prevent compaction and
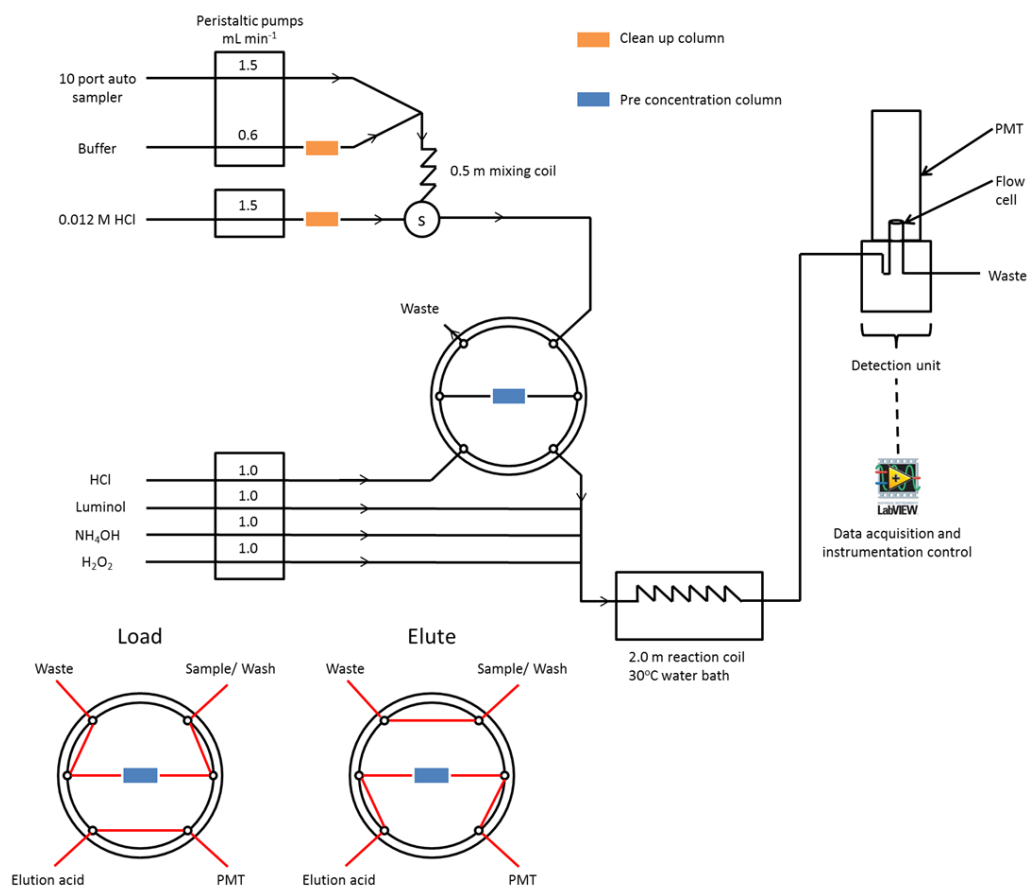
Figure 2-3- Schematic of the FI manifold design used to determine Fe(III) and load elute positions of the 6 port valve. S = solenoid valve, used to permit flow from either rinse or sample/buffer lines.

channelling. Each day, 0.5 M HCl (Romil, SpA) was passed through the system for 30-40 min and UHP water for 15 min before use. Sample and reagent lines were kept inside a class-100 laminar flow hood. Following cleaning, the reagents were run through the system to allow the baseline to settle, typically 5-10 min. UHP water was then loaded as a sample for 2-3 cycles.

To assess blank contribution the closed sample line method was used [*Bowie et al.*, 2004; *Ussher et al.*, 2010] where, the sample line was turned off and only sample buffer was loaded for typically 8-12 cycles. Following this, acidified filtered seawater

(FSW) was then loaded as sample to condition the system until a stable signal was achieved, typically 8 cycles; only then were calibrants and samples analysed.

Previous research has shown that a fraction of the Fe in acidified samples exists as Fe(II) and therefore it is necessary to oxidise this [*Lohan et al.*, 2005]. At least 1 hour before being analysed, calibrants and samples were spiked with 10 mM H_2O_2 (1 µL 10 mM H_2O_2 per 1 mL seawater) to oxidise any Fe(II) present to Fe(III).

Each analytical cycle consisted of:

1. Rinsing the pre-concentrating column for 10 s with 0.012 M HCl

2. Loading the sample/buffer mix (pH 3.5-4.0) for 20 - 120 s

3. Rinsing the pre-concentration column for 20 s with 0.012 M HCl

4. Passing the elution acid (0.23 M HCl) over the column for 60 s in the opposite direction

For steps 1 to 3, the rinse or sample/buffer mix went to waste after passing over the column; during this time the elution acid bypassed the column and mixed with reagents (pH 9.4 - 9.6). In doing so the elution acid and reagents combined to provide a baseline chemiluminescence signal when passing through the PMT. During step 3 a 0.012 M HCl rinse step was applied to the column after sample loading. This has been shown to remove > 80% more sodium from the Toyopearl resin, post seawater loading, compared with a UHP water rinse without removing Fe [*Clough et al.*, 2015].

During step 4 the elution acid passed over the column, releasing chelated Fe, before mixing with reagents and entering the flow cell. The pH of the sample/buffer mix and reagent streams was checked daily.

The analytical cycle was performed multiple times for each calibrant/sample. It was observed that the first peak generated was generally larger than the following peaks. Therefore, the first analytical cycle was always treated as a conditioning run and the peak generated was not included in any calculations. Due to the quantity of samples collected, tests were carried out to determine whether samples could reliably be analysed in duplicate using a 3 peak program (using 2nd and 3rd peaks) (Fig. 2.4). The results demonstrated excellent agreement between triplicate and duplicate analyses of the same samples and therefore samples were analysed in duplicate (i.e. using a 3 peak program and treating the first peak as a conditioning run).
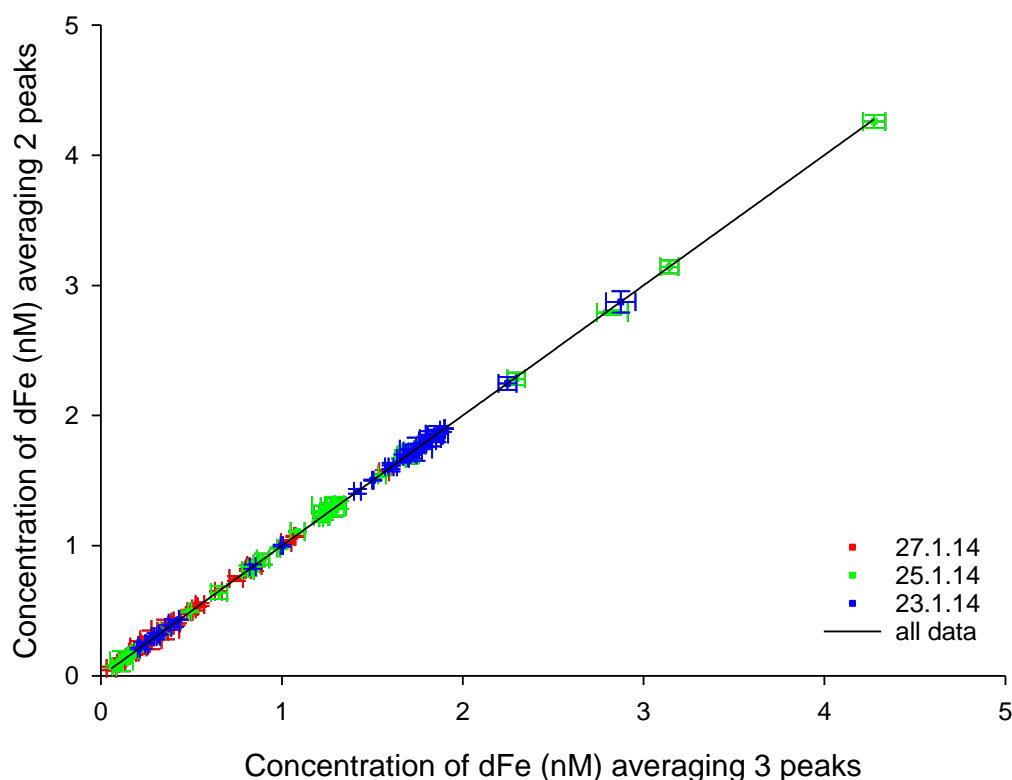
Figure 2-4- The 1:1 relationship between Celtic Sea seawater sample concentrations determined by averaging 2nd, 3rd and 4th peak and just the 2nd and 3rd peak. Horizontal error bars represent 1 standard deviation and vertical error bars represent the range of 2 values. Results from 3 separate days of analysis. y= 0.9992x − 0.0017. r^2=0.999 (*n*=119).

2.3.3 Calibration

The analytical system was calibrated by performing standard additions of Fe to low Fe (<0.2 nM) acidified (pH 1.6) seawater. Each calibration consisted of at least 5 standard additions and a zero addition as recommended by *Floor et al.* [2015] to minimise the uncertainty of this analytical technique. Sample concentrations collected during this study ranged over 6 orders of magnitude (< 0.1 to > 400 nM), thus the following approached were investigated and developed for calibration.

For low Fe concentrations (0-4 nM), an example of the peaks generated during a calibration is shown in Fig. 2.5. Standard addition curves comprising Fe additions < 10 nM were consistently described by a polynomial equation (Figs. 2.6 & 2.7) due to a non-linear response to Fe additions to low Fe seawater. The absolute concentration in each calibrant can be described as:

Absolute [dFe] = [dFe] of standard addition + starting [dFe] in SW   (7)

The concentration of Fe in the zero addition was calculated by extrapolating linearly to zero based on additions up to 1.0 nM Fe (Fig. 2.6). This concentration was then added to the calibrants to give absolute standard concentrations. These absolute concentrations were then used to plot a calibration curve that was forced through the origin and the resulting polynomial equation used to convert peak height into an Fe concentration.
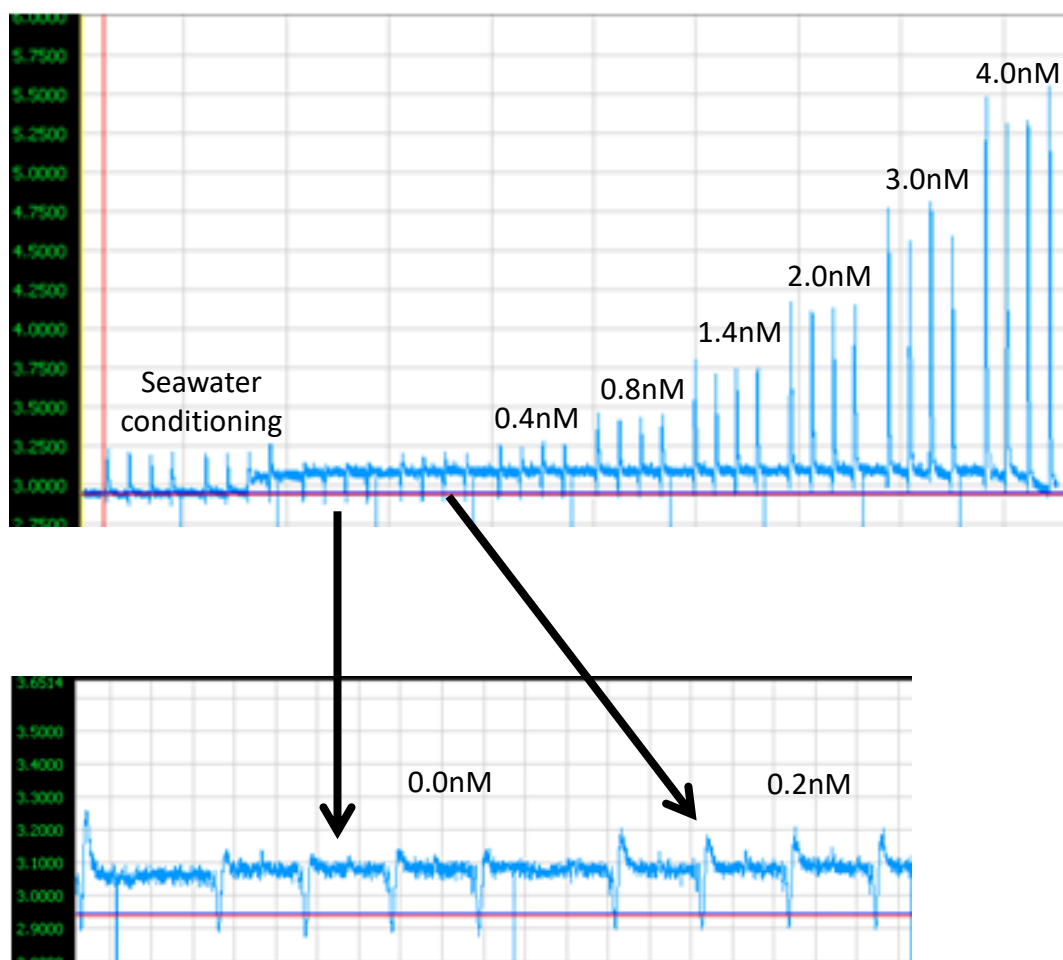
Figure 2-5- Example of the peaks generated during a calibration. Concentrations refer to the iron addition that resulted in the peaks displayed.
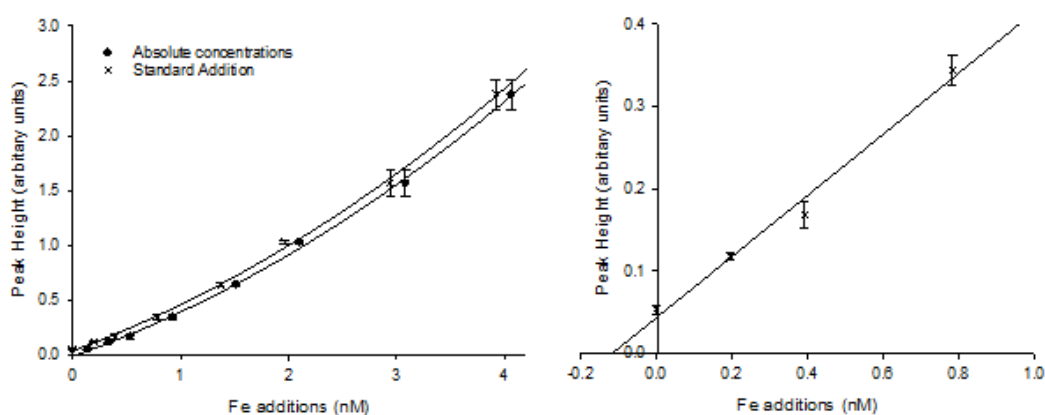
Figure 2-6- Graphical representation of peaks displayed in Figure 2.5. **Left-** Calibration plotted as standard additions (r^2=0.998) and after conversion to absolute iron concentrations (r^2=0.996). **Right-** Standard addition technique employed to estimate the concentration of iron in the calibration water (r^2=0.987). All error bars represent 1 standard deviation of triplicate injections.
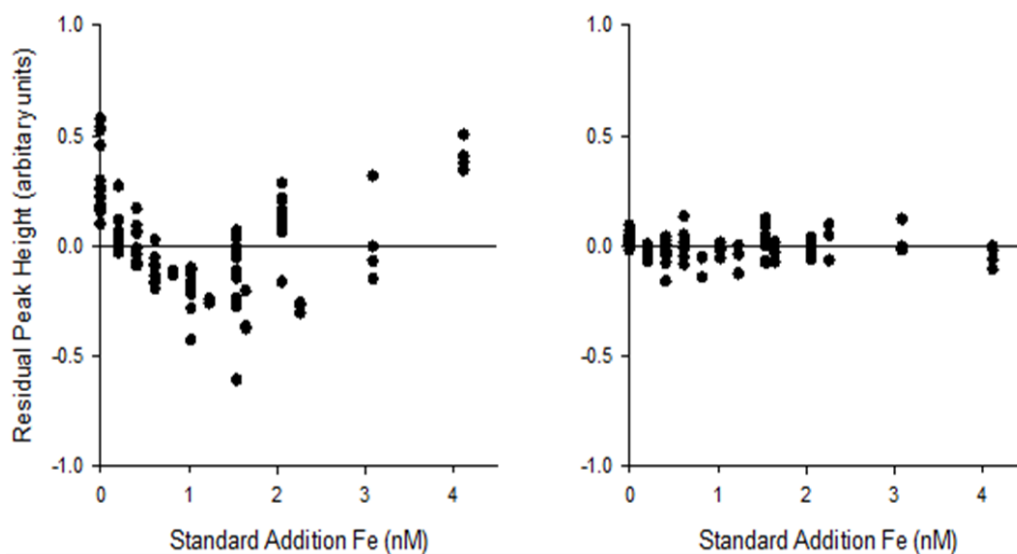
Figure 2-7-Plot of residuals from 14 independent calibrations of standard additions of Fe(III) to low Fe seawater (*n*=99). **Left**- Applying a linear regression. **Right**- Applying a polynomial equation. Polynomial equation provided the best estimation of the Fe concentrations.

For samples containing high Fe concentrations, an approach with standard additions with a calibration range >10 nM was required. A linear response was observed for concentrations from 10 - 100 nM. However, above 100 nM, a non-linear response was observed due to saturation of the detector. By reducing the concentration of luminol, from 0.25 to 0.083 mM, the sensitivity was reduced but this approximately doubled the linear range (Fig. 2.8). Despite lowering sensitivity, the precision was still typically < 5% R.S.D and this approach was adopted for concentrations between 10 and 200 nM.

An example of peaks generated and calibration plot, used to quantify Fe concentrations between 10 and 200 nM is displayed in Figs. 2.9 and 2.10. The calibration seawater was the same low Fe seawater used for low Fe (<10 nM) analysis. Due to reduced sensitivity, resulting from the lower luminol concentration and shorter loading time, the dFe concentration of the calibration seawater was below the limit of detection.

To increase confidence at the lower end of the curve the first two standard additions were analysed 6 times. As the response was known to be non-linear as the signal intensity dropped (Fig. 2.6), this curve was only used to determine Fe concentrations within the concentration range of the calibrants (i.e. not below 10 nM).
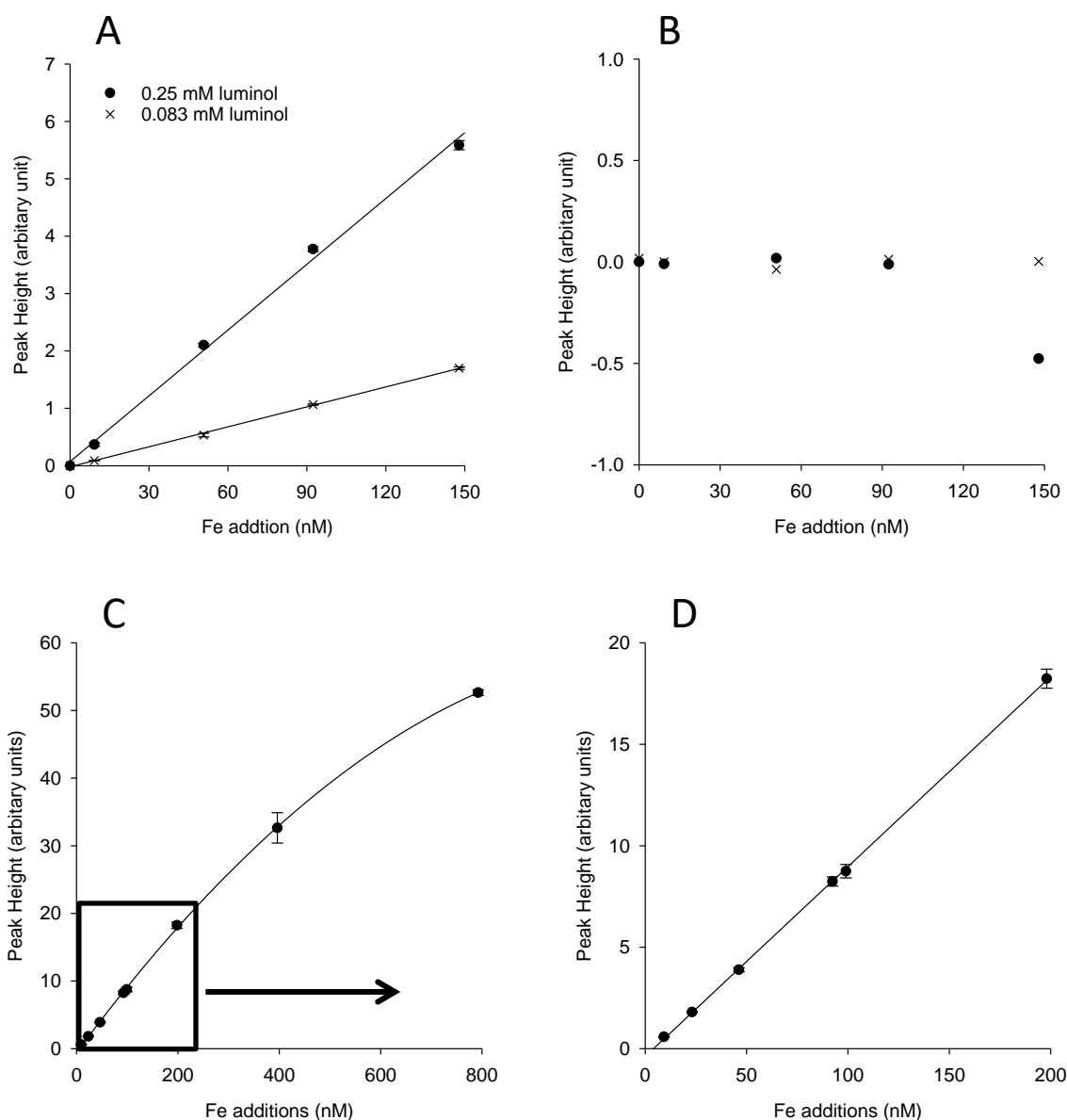
Figure 2-**8**- Extending the linear range by varying the luminol concentration. All error bars represent one standard deviation. **A**- Two standard curves obtained using same calibrants but varying luminol concentrations, with linear regression fitted to both. **B**- A plot plot of residuals from the two linear regressions; a linear regression provided a good estimation of data when using the lower luminol concentration. **C**- Determining the extent of the linear range using a luminol concentration of 0.083 mM. Standards additions of Fe of 10-800 nM, there was a loss of sensitivity evident at concentrations > 200 nM. **D**- Same curve but only showing 10-200 nM Fe additions, linear regression fitted (r^2=1.000).

Due to the dynamic concentration range employed to analyse samples, the gain (the degree of signal amplification) had to be adjusted to keep the readout within the scale of the software (Fig. 2.9). Tests were carried out to confirm that the gain adjustment resulted in a linear scaling of the signal (Fig. 2.11).
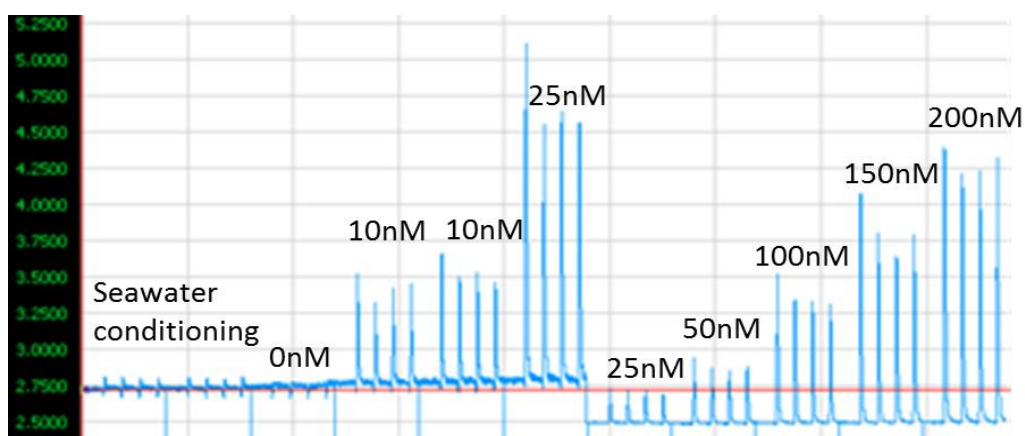
Figure 2-9- Example of the peaks generated during a calibration of iron additions ranging 10-200 nM. Concentrations refer to the iron addition that resulted in the peaks displayed. The change in gain setting causes the apparent drop in sensitivity; this is done to keep the higher concentration samples on scale. The gain adjustment is a linear adjustment to the amplitude of the signal (see Fig. 2.11); this is required to keep the signal within the limits that the software will record.
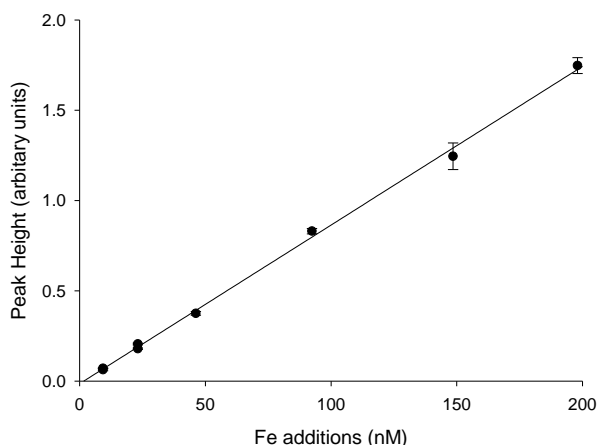
Figure 2-10- Graphical representation of peaks displayed in Figure 2.9. Standard addition technique employed to estimate the concentration of iron on the calibration water (r^2=0.998). All error bars represent 1 standard deviation of triplicate injection.
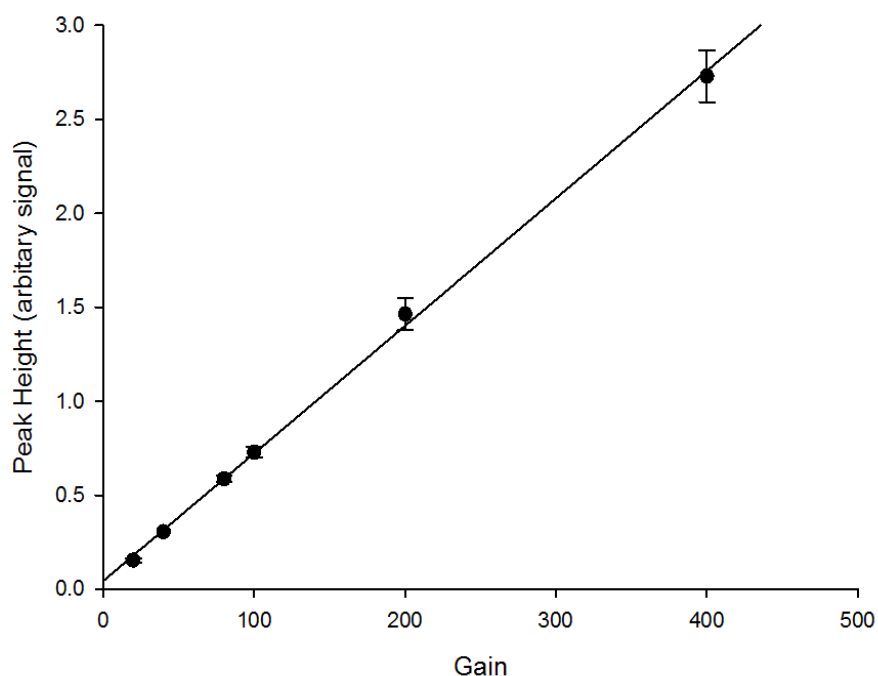
Figure 2-11- The effect of adjusting the signal gain. Acidified MQ sample spiked with 0.8 nM Fe then analysed with different gain setting, adjusting the gain results in a linear amplification of the signal (r^2=1.000).

In addition to the uncertainty of the calibration curve, the 'within sequence stability', i.e. the drift in sensitivity over hours of continuous use, is a major contributor to the analytical uncertainty of this method [*Floor et al.*, 2015]. To account for this the following procedure was developed:

1. An in-house seawater reference material was analysed after every 10 samples.

2. A 4 point calibration was analysed at the end of the day in addition to the one at the beginning. This included: a zero addition, lowest addition standard and highest standard to bracket the range of samples analysed.

3. If the difference in peak height between the start of the day and the end of day calibrations was > 5% and not within ± 1 SD then corrections were made to peak heights assuming linear drift throughout the day.

4. Drift corrected values were accepted if the drift corrected internal standard concentrations (ran as every 10th sample) were more consistent than uncorrected concentrations

On the majority of analysis days (≈ 80%) instrumental drift was not observed.

2.3.4 Figures of merit and combined uncertainty estimate

The blank associated with the reagents is included in the baseline; therefore if any blank signal was detected it would likely have been from the ammonium acetate buffer, HCl wash and/or the manifold. The closed sample line analytical blank contributions were typically below the limit of detection (LOD), defined as 3 times the standard deviation of the zero addition (Appendix A), even for calibration curves ≥ 20 nM where the average LOD was 28 ± 16 pM (1 SD, *n*=60). Analytical blanks below the LOD demonstrate that clean columns effectively removed any contribution from the

buffer and wash solutions and that the cleaning procedures maintained a trace metal

clean manifold.

Table 2-4- Validation of the analytical method, the concentration determined for consensus/reference materials in nM. Consensus values are obtained from analyses by multiple techniques (e.g. Magnesium co-precipitation, FI-CL, on and off-line pre-concentration followed by ICP-MS detection, solvent extraction followed by ICP-MS detection, voltammetry, infra-red spectroscopy).

Consensus/ Reference material	Concentration Determined (nM ± 1 SD (n))	Consensus/Reference Concentration (nM ± 1 SD)
GSP	0.15 ± 0.03 (*15*)	Not published
GSC	1.51 ± 0.08 (*14*)	Not published
SaFe D2	0.96 ± 0.10 (*14*)	0.956 ± 0.024[*]
SaFe D1	0.69 ± 0.04 (*4*)	0.69 ± 0.04[*]
SaFe S	0.12 ± 0.01 (*4*)	0.095 ± 0.008[*]
NASS-5	3.77 ± 0.03(*2*)	3.71 ± 0.63

[*]Converted to nM from nmol kg^{-1} using density of 1.025 kg L^{-1}.

Further blank contributions could be due to the manipulation of samples e.g. by

adding H_2O_2 or HCl. This can be minimised by selecting high purity reagents which was

assessed by double spiking of samples into UHP water, and has previously been shown

to be negligible [*Bowie et al.*, 2004; *Klunder et al.*, 2011].

The accuracy and reproducibility of this method was tested using SAFe and

GEOTRACES consensus materials and NASS-5 reference material. The results of these

analyses showed excellent agreement with the published values (Table 2.4); full figures

of merit can be found in Appendix A. Due to the limited quantity of these materials

available, internal quality control standards were developed and run daily to assess

reproducibility (Appendix B), both consensus material and internal quality control

standards were then used to calculate a combined uncertainty estimate.

In this work the dataset is comprised of ≈ 2 years of analyses, enabling a more

robust estimate of the analytical uncertainty than the short term repeatability

associated with replicate measurements of a single sample (typically <5% relative

standard deviations (*RSD*)). Both consensus and internal quality control standards were used to calculate a 'top down' estimate of the combined measurement uncertainty of this method using the Nordtest™ approach [*Magnusson et al.*, 2012] (Appendix C):

$$u_c = \sqrt{(u(R_w)^2 + u(bias)^2)} \qquad\qquad (8)$$

Where u_c is the combined standard uncertainty (approximates to the 68% confidence interval), $u(R_w)$ is the uncertainty estimate of within laboratory reproducibility (random effects) and $u(bias)$ is the uncertainty estimate of possible laboratory and procedural bias (systematic effects). This approach combines the uncertainties associated with day to day repeatability and possible systematic bias in the complete data set. For the Nordtest™ approach estimate carried out here, consensus material and internal quality control standards with a concentration range of 0.69 to 1.49 nM were used to estimate a relative combined uncertainty (u_c) of 9.5% (Appendix C).

The uncertainty estimate compares well with a 'bottom up' assessment where a relative combined uncertainty of 5.0 -7.5% was reported for seawater samples with Fe concentrations of 0.5 - 1.0 nM analysed using the same FI-CL technique and instrumentation [*Floor et al.*, 2015]. Further examination of the combined uncertainty estimate shows that within laboratory reproducibility contributed 65% of the analytical uncertainty, with 35% coming from possible laboratory and procedural bias (Appendix C). The work of *Floor et al.* [2015] suggests the main reason for the uncertainty contribution from the within laboratory reproducibility is likely to be associated with the calibration slope.

The contribution from possible laboratory and procedural bias includes the uncertainty of the published consensus concentrations (e.g. SAFe D2 0.956 *± 0.024* nM)

and the possible bias estimated from the difference in the published mean concentrations (e.g. SAFe D2 *0.956* ± 0.024 nM) and those determined in the course of this analyses (Appendix C). The results of the estimate carried out indicated that the uncertainty associated with the published consensus concentrations contributed 83% of the uncertainty associated with possible laboratory and procedural bias. Therefore, the results of this study are accurate and future analytical development should focus on improving within laboratory reproducibility. This could include setting more strict tolerance limits on internal standards and not analysing samples unless these criteria are met, and calibrating repeatedly during a day's analysis. However, both suggestions would inevitably increase total analysis time, thus this decision should be based on the data quality required to test a particular hypothesis.

The Fe concentration of samples analysed during this study of shelf waters spanned 6 orders of magnitude (< 0.1 to > 1000 nM) and the combined uncertainty estimated using consensus materials with a range of Fe concentrations of 0.69 - 1.49 nM was not applicable over this entire range. Due to a lack of consensus materials, it is not possible to carry out combined uncertainty estimates over the entire sample concentration range. Therefore, data are presented using the short term uncertainty associated with replicate measurements, as is common practice. An assessment of the within laboratory reproducibility can be estimated using in house quality control standards; for Fe concentrations of 4 - 16 nM this was 7%, for 49 - 70 nM this was 2% and for 0.14 - 0.24 nM this was 0.02 nM. At lower concentrations close to the LOD the relative uncertainty increases and hence absolute values were used for the 0.14 - 0.24 nM range.

2.4 Fe(II)/O₂/luminol system

2.4.1 Reagents and standards

A 2 M sodium hydroxide (NaOH) (Sigma- Aldrich) stock solution was prepared by dissolving 16 g NaOH in 200 mL UHP water. A 0.1 M stock solution of dimethylglyoxime (DMG) (Fluka, > 99%) was prepared by dissolving 0.698 g in 60 mL methanol (Acros Organics, 99.9%). A 0.04 M sulphite standard was made by dissolving 0.084 g of sodium sulphite (Sigma-Aldrich) in 60 mL of UHP water.

A 10 μM luminol working solution was prepared by dissolving 15 g of Na_2CO_3 in 500 mL UHP water, which was vigorously shaken until the Na_2CO_3 was fully dissolved (10-15 min). To this 200 μL of luminol stock (section 2.3.1), 5 ml NaOH stock and 200 μl DMG stock were added and then made up to 1 L with UHP water. Co(II) produces CL under the same reaction conditions as Fe(II) [*Klopf and Nieman*, 1983]; therefore DMG, which forms a complex with Co, was added to the luminol to mask this signal [*Ussher et al.*, 2009]. Following the method of *Bowie et al.* [1998] the luminol was then passed through a Chelex 100 column that had been previously acid cleaned with 0.5 M HCl (Fisher, Trace metal grade) for 1 h and flushed with UHP water for 2 h. Cleaning of the luminol reagent removed impurities and therefore lowered the baseline. This lowered the signal-to-noise ratio and the LOD to a usable level (< 20 pM). Working luminol solutions were prepared at least the day before analysis to allow the solution to stabilize [*Bowie et al.*, 1998].

A 0.05 M HCl elution acid was made up by diluting 4 mL of concentrated HCl in 1 L UHP water. A 2 M NH₄Ac buffer stock was prepared by adding 44 mL NH₄OH (Romil, SpA) to 29 mL CH₃COOH (Romil, SpA) to which 177 mL of UHP water was added; this was then adjusted to pH 5 using acetic acid. To make a working solution, 200 mL of this stock was diluted with UHP water to a volume of 1 L.

Fe(II) stock solutions were made up in volumetric flasks. A 0.02 M Fe(II) stock in 0.1 M HCl was prepared by adding 830 μL of concentrated HCl to ≈ 30 mL UHP water. To this 0.7841 g (exact weight recorded) of ammonium iron(II) sulphate hexahydrate (Sigma-Aldrich, 99.997%) was transferred from an acid cleaned Sterillin® vial to the solution, the vial was rinsed five times into the volumetric flask with UHP water to ensure a complete transfer. An 80 μM Fe(II) stock solution in 0.024 M HCl was prepared by adding 200 μL of concentrated HCl and 200 μL sulphite stock to 30 mL UHP. Following this 400 μL of 0.02 M Fe(II) stock was added and then the solution was made up to 100 mL with UHP water. Both 0.02 M and 80 μM stocks were prepared weekly and kept in the dark at 4 °C until use [*Bowie et al.*, 1998] .

A final 200 nM Fe(II) working stock was prepared in 0.024 M HCl by adding 100 μL of concentrated HCl to ≈30 mL UHP water in a LDPE volumetric flask. To this solution 125 μL of 80 μM Fe(II) stock was added and the solution then made up to 50 mL with UHP. This solution was made up daily and kept in dark at 4 °C until use [*Bowie et al.*, 1998].

2.4.2 Instrumentation and procedure

The manifold design for the detection of Fe(II) is displayed in Fig. 2.12. The manifold included 3 peristaltic pumps (Gilson, Minipuls 3) with 2 stop PVC accu-rated™ pump tubing (Elkay) which were changed weekly during regular use. The manifold also included a solenoid valve to control the flow of sample/buffer solution, a micro-electronically actuated 6 port, 2 position injection valve (VICI, Valco Instruments) to control loading and eluting flow and a photon counting head (Hamamatsu, Matsusada Precision) as the detection unit. There were three columns containing chelating resin included in the manifold design; two Toyopearl clean-up columns to remove reagent impurities and one 8-HQ column for pre concentrating the sample. To control the valve,

peristaltic pump timings and acquire data, a laptop (Samsung), LabVIEW v.12.0 software along with a data acquisition module (Ruthern Instruments) was used [*Bowie et al.*, 2002].

As discussed above the chemiluminescence reaction kinetics of the Fe(II)/O$_2$/luminol system are much faster than the Fe(III)/H$_2$O$_2$/luminol system and this has important implications for the manifold design. To maximise sensitivity, it was desirable to detect the maximum I_{CL} resulting from each injection, or as close to this as possible. For this to occur mixing of the eluent and luminol streams must happen as close to the flow cell as possible. This was achieved by using a T-piece in the base of the PMT, to mix the eluent stream and luminol stream and therefore minimise the time the newly combined 'emitting' stream travelled before reaching the flow cell (Fig. 2.12).

In order to maintain trace metal clean tubing, 0.5 M HCl (Romil, SpA) was passed through the manifold for 2-3 h followed by UHP for 2-3 h before a period of constant use (e.g. during an oceanographic cruise). All sample and reagent lines were kept inside a Class-100 laminar flow hood. At the start and end of the day's analyses the system was flushed with UHP water to prevent build-up of sea salt. The clean-up columns were reversed every 2-3 days to prevent compaction and channelling.

During analysis the system was operated as follows. Initially the reagent pump was continuously run to allow the reagent CL baseline settle; this process typically took 20 - 30 min. UHP water was then loaded as a sample for 3 cycles followed by assessment of the blank contribution by the closed sample line method [*Bowie et al.*, 2004; *Ussher et al.*, 2010] for typically 8 - 12 cycles. Following this aged filtered seawater was loaded and injected until a stable signal was obtained. Only then were calibrants and samples analysed. Before samples were analysed, a 0.2 µm pore size (PES membrane, Nalgene™) in-line filter was inserted into the sample line.

Each analytical cycle consisted of:

1. Loading the sample/buffer mix (pH 5.0-5.5) for 120 s

2. Rinsing the pre-concentrating column for 30 s with UHP water

3. Passing the elution acid (0.05M HCl) over the column for 80 s in the opposite direction

For steps 1 and 2, the rinse or sample/buffer mix went to waste after passing over the column; during this time the elution acid bypassed the column and mixed with reagents (pH 10.2). In doing so the elution acid and reagents combined to provide a baseline chemiluminescence signal when passing through the PMT. The pH of the sample/buffer mix and reagent streams was checked daily.

During step 3 the elution acid passed over the column, releasing chelated Fe, before mixing with reagents and entering the PMT. The analytical cycle was performed 3 times per calibrant and sample to provide triplicate measurements.
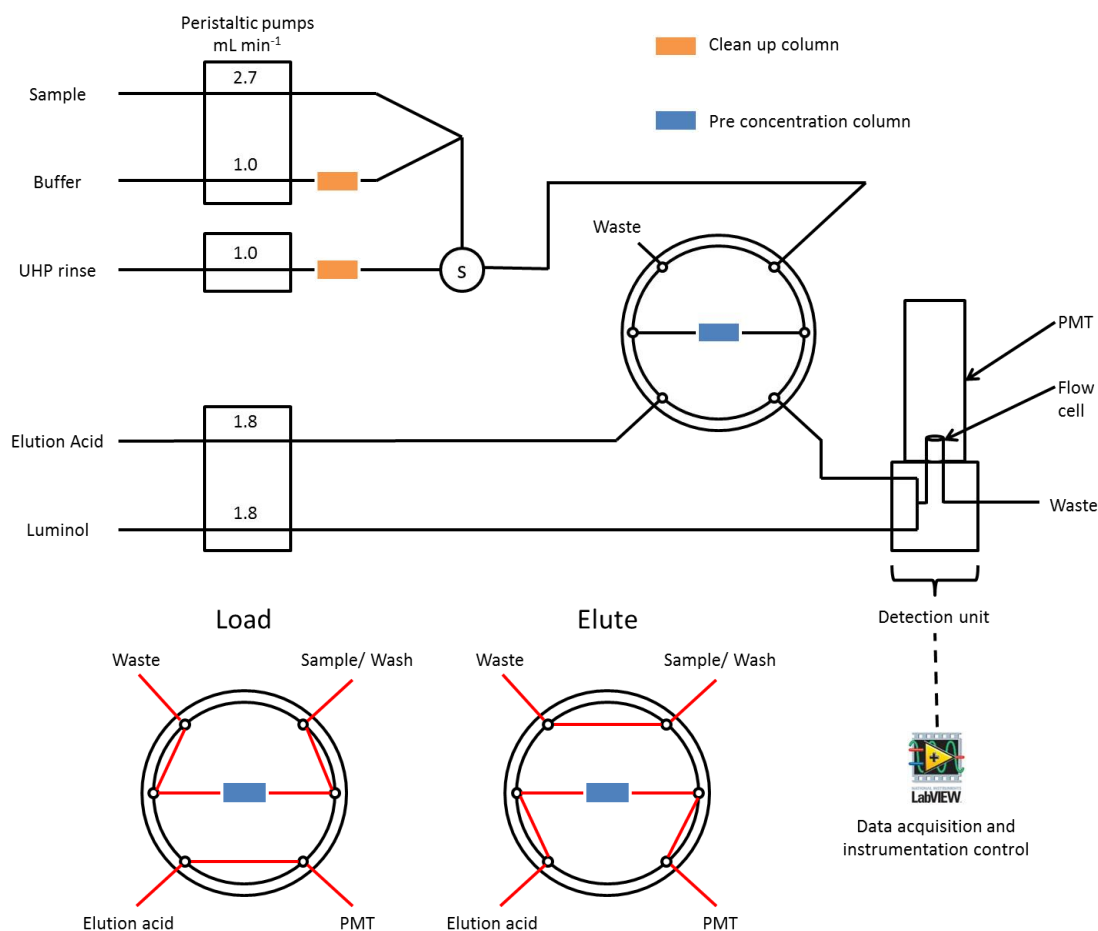
Figure 2-12- Schematic of the manifold design used to determine Fe(II) and load elute positions of the 6 port valve. S = solenoid valve, used to permit flow from either rinse or sample/buffer lines.

2.4.3 Calibration

The analytical system was calibrated by performing standard additions of Fe(II) to buffered aged filtered seawater (pH 5.0 - 5.5). Each calibration consisted of a minimum of three additions plus a zero addition. The calibration seawater was surface seawater collected from a Tow-fish underway system ($\approx$ 5 m depth) and stored in the dark for at least 24 h before use. The pH was then adjusted using 2 M NH$_4$Ac (see section 2.4.1) and again stored for 24 h before use. An example of the peaks generated are displayed in Fig. 2.13; standard additions of up to 500 pM produced a linear curve (Fig. 2.14) and this relationship was used to determine Fe(II) concentrations.
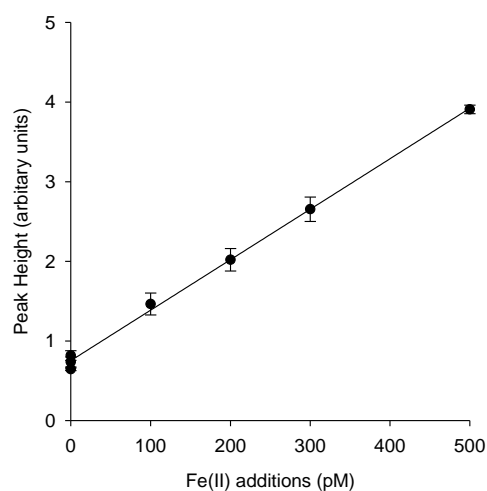
Figure 2-14- Graphical representation of peaks displayed in Figure 2.13, r^2=0.9978
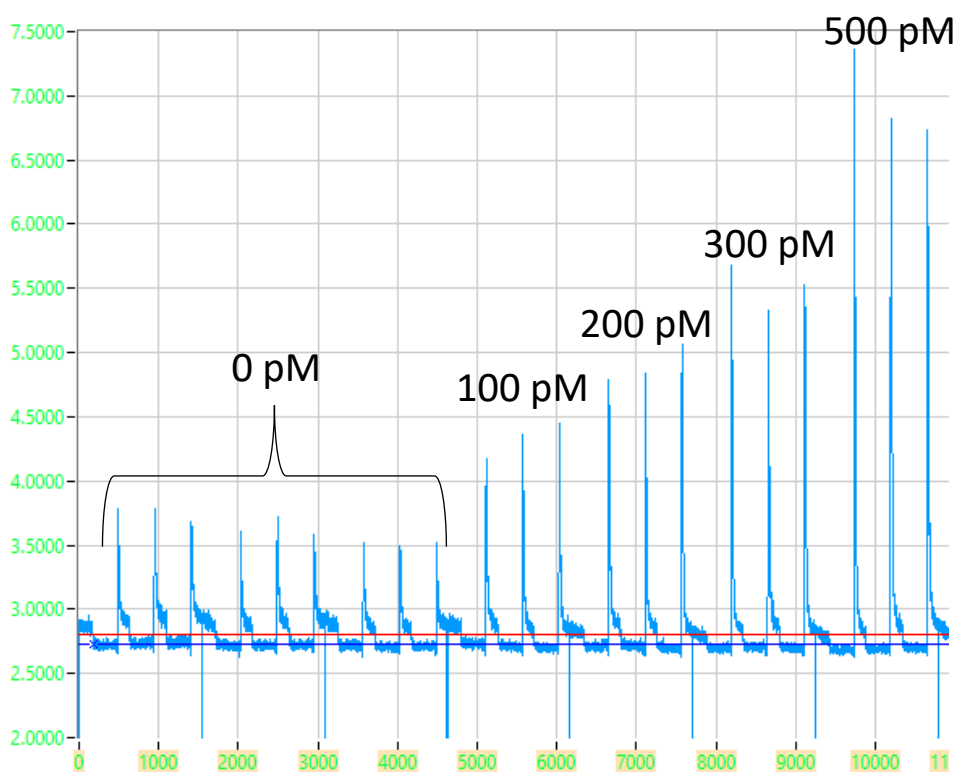
Figure 2-13- Example of the peaks generated during a calibration. Concentrations refer to the Fe(II) addition that resulted in the peaks displayed.

2.4.4 Figures of merit

The analytical figures of merit for the Fe(II)/O$_2$/luminol system are displayed in Table 2.5. The closed sample line analytical blank contributions averaged 24 ± 10 pM with an average detection limit (3 SD of blank) of 9 ± 5 pM. Due to the transient nature of Fe(II) no reference materials exist with which to validate the method and therefore Fe(II) concentrations determined have a larger associated uncertainty than dFe data. Analytical consistency was therefore evaluated by measuring the same aged filtered seawater sample during each analytical run. This approach is based on the assumption that the Fe(II) concentration had reached equilibrium in this sample. The mean concentration of the aged filtered seawater was 16 ± 5 pM (*n=7*) and these results provided reassurance that the analyses were consistent over this time period. There were two days when the sample was below the LOD; the LOD on these days were 16 and 15 pM, respectively.

Table 2-5- Analytical Figures of merit for the Fe(II)/O$_2$/luminol system. m= the gradient of calibration slope, LOD= limit of detection, Aged FSW= filtered Celtic Sea surface seawater collected in April 2015 and stored in the dark at 4°C.

Date	Calibration Range (pM)	r^2	M	LOD (pM)	Blank (pM)	Aged FSW (pM) (± 1SD)
14.7.15	LOD-500	0.9965	10.406	5	14	12 ± 1
16.7.15	LOD-500	0.9986	14.629	7	9	12 ± 3
17.7.15	LOD-500	0.9989	17.358	4	21	18 ± 4
20.7.15	LOD-500	0.9924	5.9067	15	25	<LOD
21.7.15	LDO-500	0.9961	9.6906	5	24	14 ± 9
22.7.15	LOD-500	0.9988	14.204	16	28	<LOD
25.7.15	LOD-1000	0.9996	12.087	9	26	13 ± 8
26.7.15	LOD-500	0.9966	12.196	15	46	16 ± 8
29.7.15	LOD-1000	0.9982	11.344	4	24	26 ± 2
Mean (± 1SD)				9 ± 5	24 ± 10	16 ± 5

2.5 Trouble Shooting

The following protocol is advised for trouble shooting the FI-CL systems used in this study should the system not be performing satisfactorily. In case of high baseline or suspected contamination, the system should first be cleaned by passing 0.5 M HCl through the system on a slow pump speed for several hours followed by UHP for at least the same amount of time.

1. Check all electrical equipment is switched on and responding (laptop, valves, auto sampler, PMT).

2. Check all reagents are flowing in the correct direction and with minimal pulsing. If not adjust pump tubing clamps to achieve desired flow. After approximately one week of continuous use the pump tubing will become crimped and need changing.

3. Check water bath is on and has reached desired temperature. This may take > 1 hour to become stable. It is important to make sure that the water bath is full to minimise variations in the heating cycle as this will affect sensitivity.

4. Break reagent waste line and test the reaction pH. If this is wrong then remake reagents.

5. Run sample buffer lines (for enough time that the waste line no longer contains any wash solution) and test the sample loading pH. If this is wrong check the pH of the buffer and sample.

6. Test pH of the wash solution (or in case of the Fe(II) system, refresh the MQ wash).

If after these steps the issue has not been identified then further tests should be conducted. A list of possible problems is detailed below, it is important to test these individually. The order of tests should be determined by the analyst based on his/her recent work and observations (e.g. if the luminol stock has recently been changed, start with the luminol reagent).

- Change HCl source (metals are soluble at low pH, so this is reagent is particularly susceptible to contamination).

- Change luminol source (the sensitivity and baseline can vary between stocks; it may be that the working reagent needs cleaning through a Chelex column to remove impurities, this may also reduce the observed nonlinearity and is recommended).

- Change pre-concentration or clean-up columns.

- Electronics (cables and wires can degrade and affect the signal pulse, these need changing. Change one cable at a time to identify the weak link).

- Valve degradation (the passing of acid and seawater through valves can lead to degradation of the valves. Change one at a time to identify the weak link).

- Check the Labview programme timings (particularly if this has recently been altered).

2.6 Conclusions

Two well established manifolds were used to determine total Fe and Fe(II) concentrations in seawater for this work. The Fe(III)/H_2O_2/luminol system was used to determine the different fractions of Fe (TdFe, dFe, sFe) presented in this thesis. This system was optimised so that it was sensitive (LOD 28 ± 16 pM), precise (RSD < 5%) and accurate enough to measure oceanic dFe concentrations. The FI manifold was also

successfully adapted to measure shelf sea TdFe concentrations by extending the linear range through the adjustment of the luminol reagent concentration. Additionally, an estimate of the expanded uncertainty, for $\approx$ 2 years of analysis, for the concentration range 0.69 - 1.49 nM was carried out; the expanded uncertainty (9.5%) was larger than the uncertainty associated with replicate analysis of a single sample (typically < 5%) and thus needs to be considered when interpreting the data. This increased uncertainty is likely to be present in other datasets generated via this commonly used method. It is recommended that assessment of intermediate uncertainty should be routinely conducted; this is deemed feasible as top down approaches such as Nordtest™ can be conducted with results from the daily analysis of a single quality control standard. Consequently, the value of the information obtained far outweighs the effort required to gather it.

The $Fe(II)/O_2$/luminol system was optimised so that the detection limit was appropriate for the determination of oceanic $Fe(II)$ concentrations (< 20 pM). It is not possible to validate this method but an effort to monitor day to day consistency was made by analysing the same aged filtered seawater. The results of these analyses provided confidence that the results generated were internally consistent. This relatively simple approach could be adopted by others to reduce the uncertainty associated with reported $Fe(II)$ concentrations, which is a consequence of the analytical challenge presented when measuring a transient species.

Chapter 3 - Seasonal iron depletion in a temperate shelf sea

The research presented in this chapter has been published in *Geophysical Research Letters*.

Birchill, A. J., et al. (2017), Seasonal iron depletion in temperate shelf seas, *Geophys. Res. Lett*., 44, 8987–8996, doi:10.1002/2017GL073881.

3.0 Introduction

Shelf seas cover < 10% of the global ocean surface area, yet contribute 10-20% of global oceanic primary production [*Muller-Karger et al.*, 2005]. Iron is an essential element for phytoplankton growth and hence plays a pivotal role in the functioning of marine ecosystems and the ocean carbon cycle [*Boyd and Ellwood*, 2010; *Twining and Baines*, 2013]. Shelf seas are assumed to be Fe replete due to riverine and groundwater inputs, sediment resuspension and diagenetic supplies [e.g. *Chase et al.*, 2005a; *Elrod et al.*, 2004; *Homoky et al.*, 2012; *Lohan and Bruland*, 2008; *Ussher et al.*, 2007]. However, seasonal Fe limitation has been demonstrated over narrow shelf regions of the Californian upwelling system [*Hutchins and Bruland*, 1998; *King and Barbeau*, 2007], in the Ross Sea [*Sedwick et al.*, 2011] and over the Bering Sea shelf break [*Aguilar-Islas et al.*, 2007]. Furthermore, the ability of an Atlantic coastal *Synechococcus* strain to alter its physiology in response to variable Fe availability [*Mackey et al.*, 2015], and expression of genes encoding flavodoxin in coastal diatoms [*Chappell et al.*, 2015], emphasise the importance of understanding Fe availability to phytoplankton in dynamic shelf regions.

Evidence of Fe stress at elevated dFe concentrations (0.40-1.73 nM) [*Blain et al.*, 2004; *Chappell et al.*, 2015] highlights the need to consider not just dFe concentration, but also the physico-chemical speciation of Fe, which influences bioavailability [*Lis et al.*, 2015]. In shelf systems, pFe dominates the total Fe inventory [*Hong and Kester*, 1986], where up to 81% can be in a labile particulate fraction [*Hurst et al.*, 2010]. This LpFe is considered available to phytoplankton, accessed directly from the particulate phase or indirectly following dissolution [*Chase et al.*, 2005a; *Hurst et al.*, 2010; *Rubin et al.*, 2011]. Dissolved Fe can be further quantified in terms of sFe (< 0.02 μm) and cFe (0.02-0.2 μm); with the cFe fraction found to comprise 60-80% of the dFe pool in continental shelf

waters [*Hurst et al.*, 2010]. Dissimilar bioavailability of sFe and cFe has been demonstrated in laboratory studies [*Chen et al.*, 2003; *Chen and Wang*, 2001].

3.0.1 Seasonal cycling in the Celtic Sea

The central Celtic Sea (Fig. 3.1) is characterised by weak residual currents [*Pingree and Le Cann*, 1989] with an estimated water residence time of 1-2 years [*Bailly Du Bois et al.*, 2002; *Hydes et al.*, 2004b]. As water resides in the Celtic Sea for longer than one seasonal cycle repeated vertical profiles within one year will capture the seasonality of these waters.
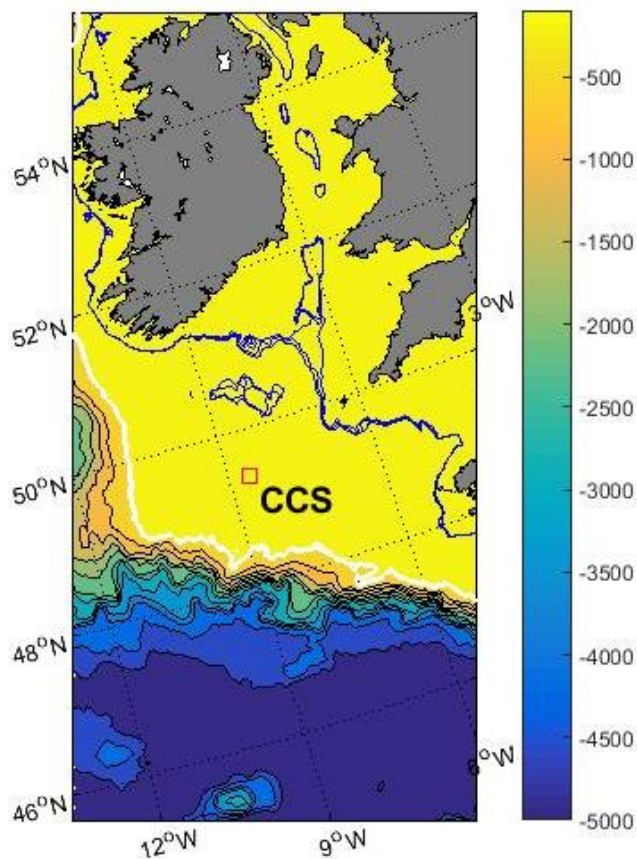
Figure 3-1- Map of Celtic Sea bathymetry (colour bar, m), the white line is the 200 m isobath and blue line is the 100 m isobath, data provided by the *National Geophysical Data Center* [1995]. The red square is the central Celtic Sea (CCS) sampling site (49° 24' N, 8° 36' W), ~150 m depth.

The Celtic Sea is a seasonally stratifying shelf sea; therefore the degree of vertical mixing principally determines the availability of light and nutrients to phytoplankton [*Pingree et al.*, 1976; *Pingree and Pennycuick*, 1975; *Sverdrup*, 1953]. Seasonal stratification occurs in April [*Fasham et al.*, 1983] as the increasing buoyancy input from solar irradiance is able to overcome dissipation due to tide and wind derived turbulence [*Pingree*, 1975; *Simpson and Bowers*, 1984; *Simpson and Hunter*, 1974]. The subsequent retention of phytoplankton in the euphotic zone facilitates a spring bloom of phytoplankton [*Fasham et al.*, 1983; *Pingree et al.*, 1976], during which ≈ 50% of annual new primary production occurs [*Hickman et al.*, 2012].

Following the spring bloom nitrate + nitrite (NO_3^-) is exhausted (< 0.02 μM) in the surface mixed layer (SML) of the stratified Celtic Sea and increases below the thermocline due to regeneration of organic material [*Hickman et al.*, 2009; *Hickman et al.*, 2012; *Pingree et al.*, 1977; *Rippeth et al.*, 2009; *Sharples et al.*, 2001]. Relatively low levels of primary production are supported in the SML by regenerated forms of nitrogen [*Pingree et al.*, 1976]. New production occurs deeper in the water column where phytoplankton biomass accumulates near the pycnocline, at lower light levels, to access the diapycnal flux of nutrients from the bottom mixed layer (BML). Consequently a subsurface chlorophyll-*a* (chl-a) maximum (SCM) is evident throughout the stably stratified central Celtic Sea [*Hickman et al.*, 2009; *Hickman et al.*, 2012]. However, the complete drawdown of NO_3^- in the SML indicates that the rate of the diapyncal NO_3^- flux is a limiting factor on new primary production [*Sharples et al.*, 2001; *Williams et al.*, 2013a; *Williams et al.*, 2013b].

At some point in late summer/autumn the net atmosphere-ocean heat flux reverses so that the sea surface progressively cools. The result is a gradual weakening of thermal stratification over several months until full winter overturning is achieved.

The weakening stratification permits increased vertical transport of nutrients that alleviates the oligotrophic conditions that prevail during the summer. The result is an autumn bloom of phytoplankton, evidenced by increased chl-*a* concentrations [*Pingree et al.*, 1976; *Pingree*, 1975].

To date research into seasonal nutrient cycling in the Celtic Sea has predominantly focussed on the availability of NO_3^- to phytoplankton. Although Fe measurements have been made previously in this region, most have sampled in March before the onset of seasonal stratification [*Boye et al.*, 2003; *De Jong et al.*, 1998; *Laes et al.*, 2007; *Ussher et al.*, 2007]. *Nédélec et al.* [2007] and *Muller et al.* [1994] both sampled in summer but were hampered by analytical problems, meaning SML dFe concentrations could not always be quantified. Consequently, the seasonal cycling of Fe in the Celtic Sea is not presently constrained. The U.K Shelf Sea Biogeochemistry programme (http://www.uk-ssb.org/) included a series of repeat cruises to the Celtic Sea and thus provided an ideal opportunity to determine the seasonal cycling of Fe. In this study, measurements of sFe and cFe which together make up dFe, TdFe, LpFe and pFe are reported for November 2014 (autumn), April 2015 (spring) and July 2015 (summer) are presented from a central Celtic Sea sampling location. It is demonstrated that all potentially available Fe sources were drawn down to limiting concentrations in the SML, implying that this system is likely co-limited by Fe and NO_3^-.

3.1 Methods

3.1.1 Sampling methods and sample storage

Sampling was conducted during three cruises (November 2014, April 2015 and July 2015) on-board the *R.R.S. Discovery* from a central Celtic Sea station (Fig. 3.1). For reference a glossary of Fe fractions determined is presented in Table 3.1. All samples

were collected following GEOTRACES protocols [*Cutter et al.*, 2010], using a titanium

conductivity, temperature, depth (CTD) rosette fitted with 24 x 10 L trace metal clean

Teflon-coated OTE (Ocean Test Equipment) bottles deployed on a Kevlar coated

conducting wire. Upon recovery, the OTE bottles were transferred into a class 1000

clean air shipboard laboratory and pressurised (1.7 bar) with compressed air filtered in

line through a 0.2 μm polytetrafluoroethylene filter capsule (Millex-FG 50, Millipore).

All water samples were collected into trace metal clean LDPE (Nalgene) bottles

(Chpt 2.1.1). Samples for dFe were filtered using 0.2 μm acetate membrane filter

cartridge filters (Sartobran-300, Sartorius) and for sFe were then filtered in-line through

0.02 μm syringe filters (Anotop, Whatman) at a flow rate of 1 ml min^{-1} [*Ussher et al.*,

2010]. Colloidal Fe (0.02-0.2 μm) was determined by calculating the difference between

the dFe and sFe concentrations. Total dissolvable Fe samples were collected unfiltered

and acidified for a minimum of 6 months before analysis. All samples were acidified to

0.024 M HCl with high purity HCl (UpA, Romil) under a class 100 flow hood.

Particulate samples were collected onto acid clean 25 mm Supor®

polyethersulfone (PES) membrane disc filters (Pall, 0.45 μm) and stored frozen (-20 °C)

until shore-based analysis.

Table 3-1- A glossary of the operationally defined iron fractions determined during this study. Concentrations of each fraction observed in surface waters are also displayed. For April 2015 the range of concentrations observed at 20 m are presented. For July 2015 the state of water column stratification was consistent and so the surface mixed layer was defined following *Hickman et al.* [2012]. In November 2014 the strength of stratification was variable and the surface mixed layer was determined by visual inspection of the profile.

Soluble Iron	sFe	< 0.02 μm	Includes all iron passing through 0.02 μm filter that is dissolved after a minimum of 2 months at pH 1.6. This includes free inorganic species and iron bound to low molecular weight organic complexes.
Colloidal Iron	cFe	dFe-sFe	Includes Fe in the size fraction 0.02-0.2 μm. Includes iron containing nanoparticles and iron bound to organic material in the colloidal phase e.g. humic substances and polysaccharides.
Total Dissolvable Iron	TdFe	Unfiltered	Includes all iron dissolved after a minimum of 6 months at pH 1.6. In this study concentrations were in excess of leachable particulate iron (see below), indicating that this treatment accessed refractory phases of particulate iron.
Leachable Particulate Iron	LpFe	> 0.45 μm	Includes readily reducible iron oxyhydroxides and intracellular iron retained on a 0.45 μm filter.
Total Particulate Iron	pFe	> 0.45 μm	Includes all iron phases (refractory + leachable particulate iron) retained on a 0.45 μm filter.

	dFe (nM)	sFe (nM)	cFe (nM)	TdFe (nM)	LpFe (nM)	pFe (nM)	NO_3^- (μM)
3rd- 26th April 2015	0.76 ± 0.009 to 0.23 ± 0.002	0.33 ± 0.000 to 0.11 ± 0.010	0.43 ± 0.010 to 0.13 ± 0.010	46.81 ± 1.267 to 6.84 ± 0.085*	5.69 ± 0.04 to 3.47 ± 0.07*	87.37 ± 0.90 to 44.82± 0.22*	6.03 to 1.15
14-31st July 2015	0.16 ± 0.071 (*n*= 15)	0.13 ± 0.069 (*n*=3)	0.07 ± 0.092 (*n*=3)	0.45 ± 0.179 (*n*=14)	0.11 ± 0.003 (*n*=1)	1.84 ± 0.010 (*n*=1)	< 0.02 μM
11th-29th November 2014	0.29 ± 0.068 (*n*= 9)	0.14 ± 0.082 (*n*=3)	0.17 ± 0.036 (*n*=3)	3.73 ± 0.583 (*n*= 6)	0.34 ± 0.024 (*n*= 2)	4.26 ± 0.251 (*n*= 2)	2.33 ± 0.037 (*n*=14)

*TDFe samples collected 12-26th April, LpFe and pFe samples collected from 3rd to 16th April

3.1.2 Determination of soluble, dissolved and total dissolvable iron in seawater

All sample and reagent handling was undertaken in an ISO 14644-1 Class 5 laminar flow hood (Bassaire, Southampton, UK) situated within an ISO 14644-1 Class 5 clean room at Plymouth University. Soluble, dissolved and total dissolvable Fe were analysed using FI-CL detection [*Floor et al.*, 2015; *Obata et al.*, 1993]. The detailed methodology is described in section 2.3.

3.1.3 Leaching and digestion of particulate samples

For leaching and digestion of filters (conducted by Dr. Angela Milne, University of Plymouth), filters were defrosted at room temperature. To assess the labile-metal fraction of the particulate material, filters were processed following a sequential leach-digestion procedure. Filter blanks for both digestion procedures were processed in the same manner as samples. All acids and bases used were of ultra-pure grade (Romil, UpA) while the H_2O_2 was supplied by Merck (Optima grade).

For the labile-metal fraction a leaching protocol similar to that described in *Berger et al.* [2008] was adopted. Filters were leached with 2 mL of 25% acetic acid and hydroxylamine hydrochloride (0.02 M, Romil) solution and heated in a drying oven for 30 min at 90 °C in LDPE vials. After a 2 h contact time, the filters were removed and placed into clean perFluoroAlkoxy (PFA) screw cap digestion vials. The leachate solution was then centrifuged at 3500 g for 15 min. Following centrifugation, 1 mL of the leachate was transferred to a separate PFA vial and taken down to dryness; the residue was quantitatively re-suspended in 2% nitic acid (HNO_3) for analysis. The remaining leachate solution was disposed of exposing any particles collected during centrifugation and each vial was rinsed with H_2O_2 and added to the digestion PFA vial containing the relevant sample filter.

A three step sequential acid addition modified from *Ohnemus et al.* [2014] was employed to fully digest the 25 mm Supor® PES membrane disc filters (Pall, 0.45 µm) and any refractory particulate material. In loosely capped vials, 0.2 mL of H_2SO_4 plus 1.0 mL H_2O_2 were heated at 200 °C until the PES filter dissolved. Secondly, a 4 M mix of hydrochloric acid /HCl/HNO_3 (2 mL) was added and heated overnight at 135 °C in tightly capped vials. Finally, 1 mL of a HNO_3/H_2O_2 mix (50%/15% v/v) was heated at 130 °C for ≈ 1 hr. After each stage the sample was heated to dryness. After the final evaporation stage, the samples were quantitatively re-suspended in 2% HNO_3.

3.1.4 Leachate and digest analysis

Analyses of all particulate leachate and digest samples (conducted by Dr. Angela Milne, University of Plymouth) were conducted using ICP-MS (Thermo Fisher X Series 2). Potential interferences (e.g. $^{40}Ar^{16}O$ on ^{56}Fe) were minimized through the use of a collision/reaction cell utilizing 7% H in He. Evaluation of the leach and digestion efficiencies was made using four CRMs with the results showing good agreement (Table 3.2).

Table 3-2- Results from the digestion and analysis of certified reference material for the determination of Fe. The measured values are the mean of 3 replicate analyses. All values are in mg kg^{-1}.

Reference material	BCR-414	SO-2	LKSD-4	IAEA-433
Certified	1850 ± 190*	55600 ± 1600	28000	40800 ± 1900
Measured	2030 ± 24	57100 ± 758	27800 ± 236	46200 ± 226
% Recovery	*110*	*103*	*99*	*113*

Uncertainties are ± 1 S.D. (*n*=3).
*Indicative value.

3.1.5 Sampling and analysis of radium

Sampling and analysis of radium was conducted by Dr. Amber Annett, Rutgers University. Radium samples were collected from 20 L Niskin bottles deployed on a stainless steel frame. Water from multiple bottles closed at a single depth were passed slowly (<750 mL min^{-1}) over 20 g of manganese-dioxide impregnated acrylic fiber, which has been shown to quantitatively extract Ra from these volumes of seawater at flow rates <1 L min^{-1} [Moore 2008]. Fibers were rinsed with ultra-high purity water (Millipore systems), and dried to a moisture ratio of 0.4 – 1.1 g:g H_2O:fiber to optimize emanation of the radon daughter [*Sun and Torgersen*, 1998]. Fibers were then counted immediately using a Radium Delayed Coincidence Counter [RaDeCC; *Moore*, 2008; *Moore and Arnold*, 1996]. Counts were repeated after intervals of ~30 and ~90 days to determine the activity of parent isotopes of ^{224}Ra and ^{223}Ra, respectively, which are also retained on the manganese fiber. Uncertainty calculations follow the methods of *Garcia-Solsona et al.* [2008], and RaDeCC systems were calibrated using standards prepared from actinium-227 and thorium-232 stocks obtained from the International Atomic Energy Agency in Monaco and previously reported in *Annett et al.* [2013].

3.1.6 Nutrients, temperature, salinity, oxygen, chlorophyll-*a* and turbidity

Dissolved NO_3^- (determined as nitrate + nitrite) was determined on-board (conducted by Malcolm Woodward and Carolyn Harris, Plymouth Marine Laboratory) and measurements were made from all OTE bottles that were sampled for dissolved and particulate Fe. Unfiltered samples were collected for nutrient analysis from every OTE bottle sampled, these were taken into 'aged' high density polyethylene bottles that had been 10% HCl acid washed and rinsed with UHP water prior to taking the samples. The

bottles were rinsed with sample water in triplicate prior to final sampling. Sample handling and processing was according to the GO-SHIP nutrient manual [*Hydes et al.*, 2010], and 'nutrient free ' gloves were used at all occasions. All analysis was carried out within a couple hours of sampling, and NO_3^- was analysed using a Bran and Luebbe 5 channel segmented flow autoanalyser, with high resolution colorimeters. The analytical method used was *Brewer and Riley* [1965]. Certified reference materials (Kanso, http://www.kanso.co.jp/eng/production/) were run as part of the daily analytical protocols to ensure good quality control and reproducibility of the results. The accuracy is to within 2% or better of the stated values of the reference materials. By adopting analytical methods and techniques according to GO-SHIP protocols, improvements and checks are made to ensure and check the analytical accuracy of the analyses. Precision is at or better than 2% when this is determined along with the regular sample analysis.

Salinity, temperature, and depth were measured using a CTD system (Seabird 911+) equipped with optical backscatter (WET Labs, ECO BB), dissolved oxygen (O_2; Seabird SBE 43 O_2 sensor) and a fluorimeter. Salinity was calibrated on-board using discrete samples using an Autosal 8400B salinometer (Guildline). Daily O_2 calibrations were conducted using a photometric automated Winkler titration system [*Carritt and Carpenter*, 1966]. Daily samples for chl-*a* analysis were filtered through 0.7 μm glass microfiber filters (Whatman GF/F) and extracted in 90% acetone overnight [*Holm-Hansen et al.*, 1965]. The chl-*a* extract was measured on a precalibrated (spinach chlorophyll-a standard, Sigma) fluorimeter (Turner Designs Trilogy).

3.2 Results and discussion

The central Celtic Sea is characterised by weak residual currents [*Pingree and Le Cann*, 1989] with a water residence time of 1-2 years [*Bailly Du Bois et al.*, 2002].

Consequently, by sampling over autumn (November), spring (April) and summer (July) it was possible to capture the seasonality of these waters.

3.2.1 Conditions following winter mixing

At the onset of seasonal stratification (3rd April), the vertical distributions of dFe (0.82 ± 0.04 nM, *n*=6) and NO$_3^-$ (6.68 ± 0.37 µM, *n*=14) were relatively uniform, with only minor evidence of surface drawdown, and thus reflecting winter mixing conditions and concentrations before the spring bloom (Fig. 3.2a,b). At this time, cFe comprised 59-81% of dFe (Fig. 3.2e,f), similar to the contributions observed near the North West Atlantic continental margin [*Fitzsimmons et al.*, 2015a] and shelf regions of the Bering Sea [*Hurst et al.*, 2010], though less variable than in the Canary basin [*Ussher et al.*, 2010]. The cFe fraction was greater than the ≈50:50 partitioning observed in deep oceanic waters [*Fitzsimmons et al.*, 2015a; *Ussher et al.*, 2010]. Therefore, this suggests either enhanced input of colloidal material from sediment resuspension and/or from break up of organic material, which particle reactive metals such as Fe associate with.

3.2.2 Iron and nitrate uptake during the spring phytoplankton bloom

During the phytoplankton spring bloom (3rd-26th April), both dFe and NO$_3^-$ were removed from the SML, where a depletion of 4.93 µM of NO$_3^-$ at 20 m was observed (Fig 3.2b,g), consistent with published NO$_3^-$ data [*Fasham et al.*, 1983]. Here a 0.53 nM depletion of dFe was observed as part of the first seasonal Fe data set for this region (Fig. 3.2a,g). If all the dFe drawdown was a result of biological uptake this would equate to a phytoplankton Fe:N (nM:µM) ratio of 0.11, this assumes no loss of dFe through scavenging, and so represents a maximum value. Our uptake ratio is lower than the average phytoplankton ratio reported for coastal (Fe:N (nM:µM) 0.58, *n*=6) and oceanic (Fe:N (nM:µM) 0.32, *n*=4) phytoplankton [*Ho et al.*, 2003]. The medium in which these

phytoplankton were cultured was designed to minimise extracellular Fe precipitation (< 30% of digested Fe), whilst maintaining near optimal (85%) growth rates. Therefore, our observation suggest that the dFe drawdown may have been driven by phytoplankton growing at a sub-optimal Fe:N, or those with a tolerance for lower Fe:N ratios than observed by *Ho et al.* [2003]. However, the concentration of the LpFe fraction, which is considered a bioavailable source of Fe [*Chase et al.*, 2005a; *Hurst et al.*, 2010; *Milne et al.*, 2017], was 3.96 ± 1.16 nM (*n*=4) at 20 m in April (Fig. 3.3c) and decreased by ≈ 2 nM from 3rd-16th April, and therefore sufficient to meet the Fe requirement necessary for NO_3^- drawdown. Additionally, when considering this calculation it should also be noted that phytoplankton Fe quotas are highly variable [*Twining and Baines*, 2013], and that other N species (e.g. organic nitrogen) may also contribute to the bioavailable N pool.

Distinct temporal trends in the different size fractions of dFe were observed during the spring bloom. At the start of the bloom (5th-12th April), sFe decreased from 0.33 ± 0.00 to 0.16 ± 0.01 nM (*n*=4; Fig. 3.2g). In contrast, the cFe concentration remained constant at 0.42 ± 0.03 nM (*n=4;* Fig. 3.2g). These results suggest that phytoplankton preferentially utilized sFe during the initial stages of the bloom, consistent with laboratory culture studies [*Chen et al.*, 2003; *Chen and Wang*, 2001]. A decrease in cFe concentration from 0.40 ± 0.03 to 0.13 ± 0.01 nM (Fig. 3.2g) occurred once the bloom had established (16th-26th April). Biological uptake of cFe by phytoplankton can occur, either directly [*Nodwell and Price*, 2001; *Rubin et al.*, 2011] or indirectly, following dissolution to the soluble phase by ligand/light interaction [*Borer et al.*, 2005; *Sulzberger et al.*, 1989] or grazing [*Schmidt et al.*, 2016]. Given the scarcity of sFe (< 0.16 nM), and elevated primary production, at this time, it is probable that biological uptake contributed to the depletion of cFe in the SML. Preferential removal of sFe appears to contrast with observations in the open ocean, where preferential cFe

uptake is hypothesised to be the cause of cFe minima in the deep chlorophyll maximum [*Fitzsimmons et al.*, 2015a]. Our spring bloom time-series in a shelf environment allows us to suggest that sFe is the more bioavailable fraction as sFe uptake precedes the removal of cFe, and therefore the observed cFe minima represents the net effect of sFe and cFe removal processes.

The observed timescale of cFe removal from the SML ($\approx$ 10 days), is consistent with the typically short residence times of colloidal thorium, which is in the order of hours to days in shelf waters [*Baskaran et al.*, 1992; *Moran and Buesseler*, 1993]. This suggests that the decreasing cFe concentration reflected a change in the balance between sources and sinks of colloids over these timescales. In addition to biological uptake, both adsorption and coagulation of cFe lead to particle formation [*Honeyman and Santschi*, 1991] and export from the SML. Using profiles of excess radium activity (Ra_{XS}) ($^{224}Ra_{XS}$ half-live= 3.66 days, $^{223}Ra_{XS}$ half-live= 11.4 days) as a tracer of vertical mixing (Fig. 3.4), it is shown that increasing stratification progressively restricted vertical exchange with cFe rich bottom waters, simultaneously reducing the supply of cFe to the SML.

Figure 3-2- The seasonal time series of dFe at the Central Celtic Sea (CCS), November 2014 to July 2015. Top row relates dFe (a) to the oceanographic setting at the time of sampling, including the concentration of NO$_3^-$ (limit of detection 0.02 µM) (b), the state of stratification (c), indicated by sigma-theta, and biomass (d), indicated by the chlorophyll-a concentration. Sigma-theta plots are identified by the month of sampling only (red= November 14', green= April 15', blue= July 15'), except the short dashed green line which represents the 3.4.15, from which point the surface density continuously decreased throughout April to the 26.4.15, represented by the large dashed green line. Chlorophyll-*a* plots are identified by month of sampling (same colour scheme as sigma-theta) except peak spring bloom chl-*a* concentrations on 16.4.15 (short dashed line) and 21.4.15 (long dashed line). The bottom row includes the temporal evolution of sFe (e) and cFe (f), which together make up dFe, shows the drawdown of sFe, cFe and NO$_3^-$at 20 m depth during the spring bloom in April 2015 (g) and the concentration of dFe and NO$_3^-$ in the pycnocline during July 2015 (h), in relation to the subsurface chlorophyll-*a* maximum. The pycnocline region determined following *Hickman et al.* [2012]**.**
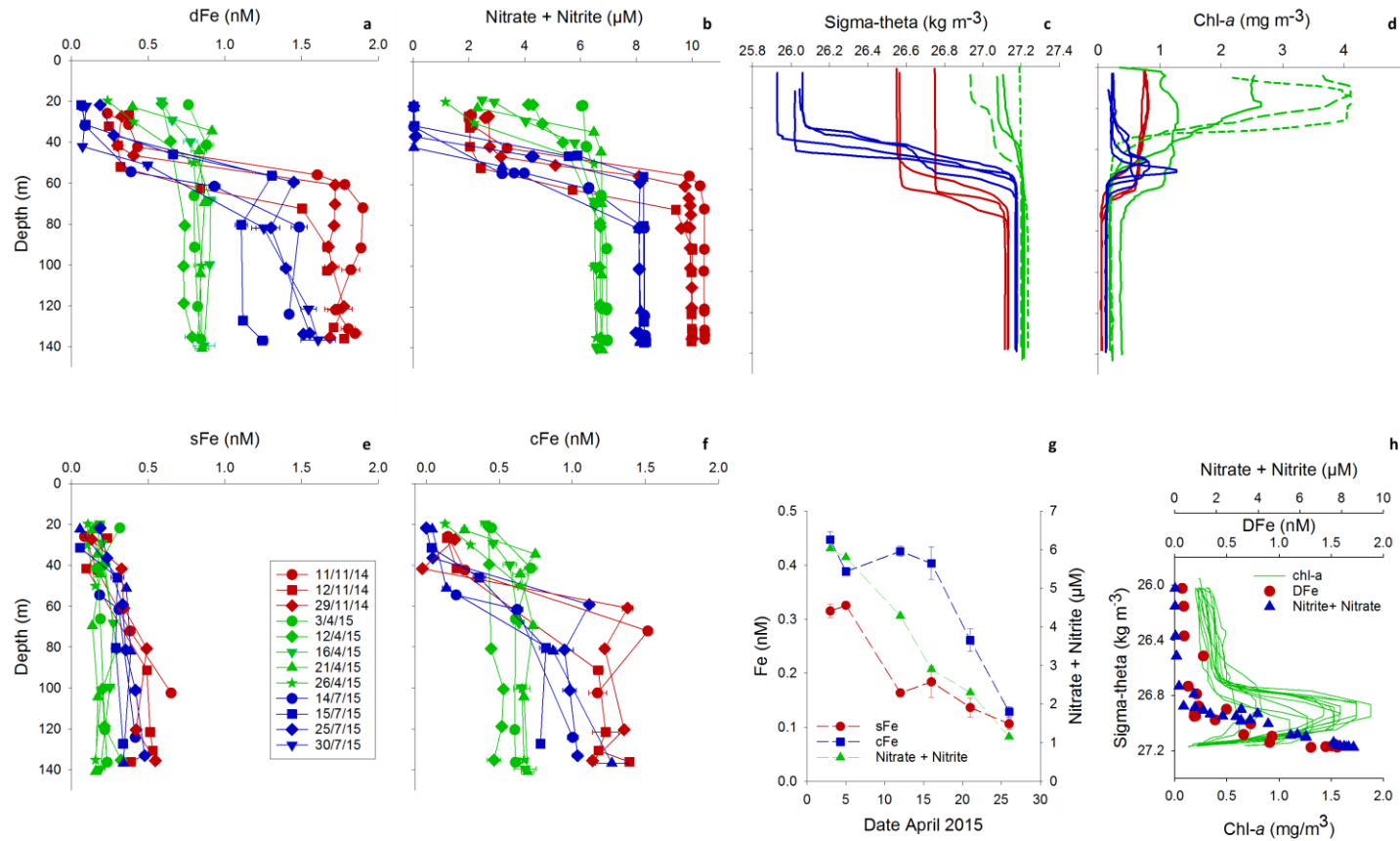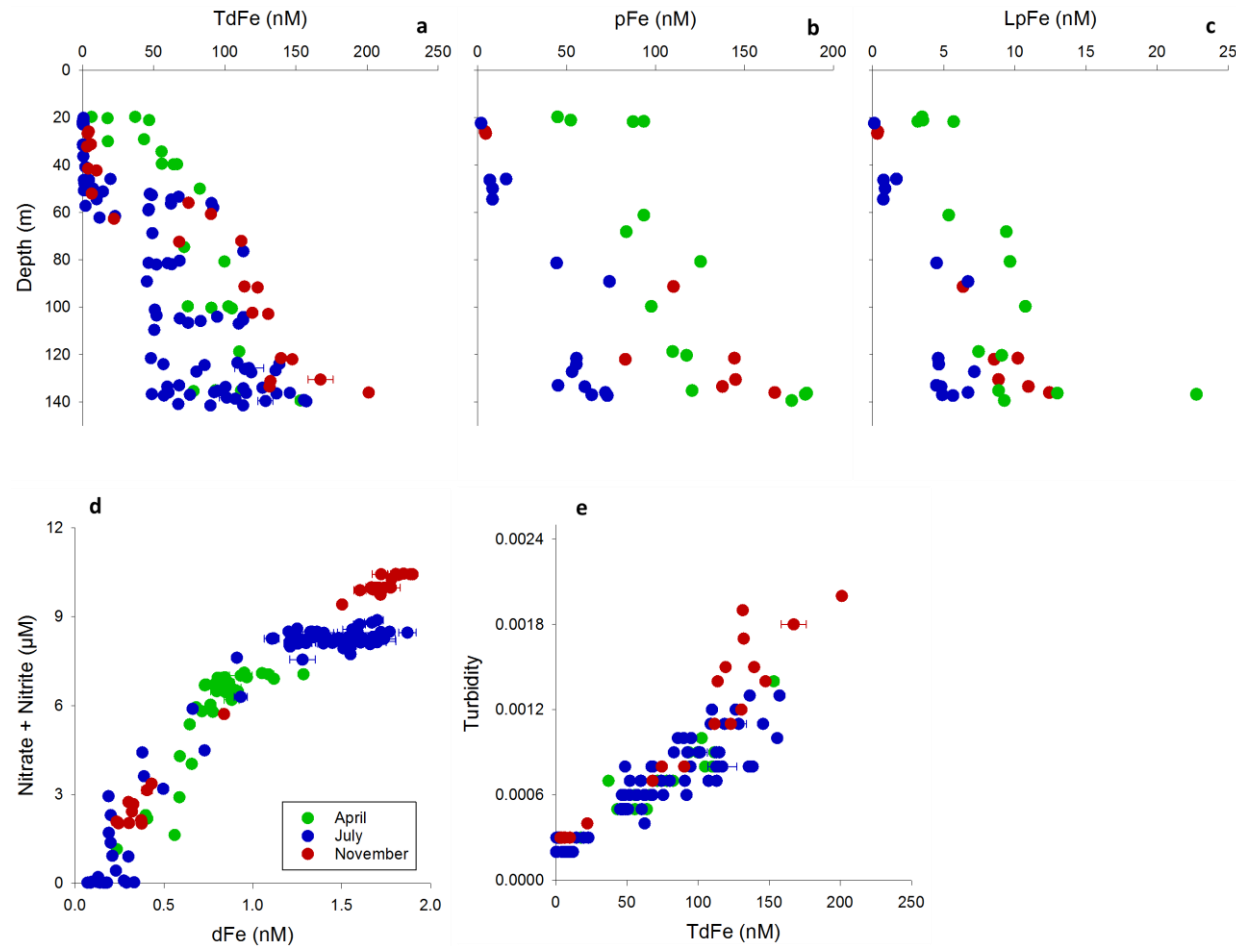
Figure 3-3- The seasonal time series of particulate iron in the central Celtic Sea, November 2014 to July 2015. Depth profiles of TdFe (a), pFe (b), LpFe (c). Bottom row displays close coupling between dFe and NO_3^- (d) (r^2=0.94, y=3.2924Ln(x) + 6.8389) compared to the coupling between TdFe and particle load, as indicated by turbidity (e) (April r^2= 0.87, y=0.000007x + 0.0002, July r^2= 0.86, y=0.000006x + 0.0002, and November r^2=0.92, y=0.000009x + 0.0002).
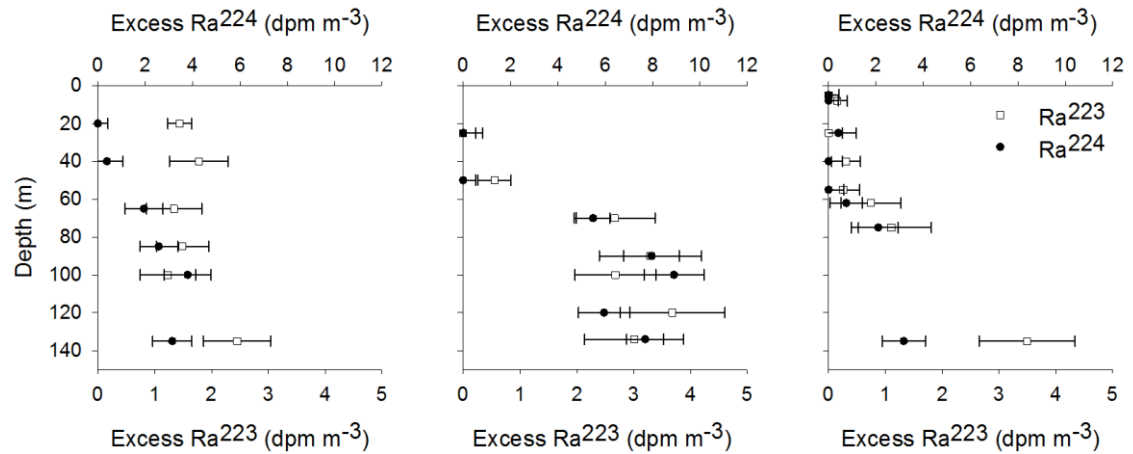
Figure 3-4- The seasonality of Radium in the central Celtic sea. Left- 3rd April 2015. Middle- 11th November 2014. Right- 22nd November 2014.

3.2.3 Iron and nitrate availability during summer stratification

During summer stratification (July), the SML was depleted of both dFe (0.16 ± 0.07 nM, *n*= 15) and NO_3^- (typically <0.02 µM) (Table 1; Fig. 3.2a,b,c). As particulate Fe fractions were also quantified (Fig. 3.3a,b,c), all potentially bioavailable Fe sources can be considered. All particulate Fe fractions were lowest in the SML during summer (Table 3.1), including LpFe which was 0.11 ± 0.00 nM. The removal of LpFe, as well as dFe, indicated that all potentially bioavailable Fe sources were depleted in the SML of the central Celtic Sea and raises the question of whether primary production in the SML was seasonally co-limited by Fe and NO_3^- availability.

Analogous Fe cycling occurs in seasonally Fe-limited shelf regions of the southern Ross Sea. In these waters, winter convective overturning supplies both dFe and particulate Fe to surface waters. Subsequent biological uptake and export coupled with a reduction in vertical exchange, leads to these waters becoming Fe limited in late spring/summer [*Marsay et al.*, 2014; *McGillicuddy et al.*, 2015; *Sedwick et al.*, 2011]. In contrast, the stratified central shelf waters of the Bering Sea maintain average summer SML LpFe concentrations of 6 nM, an important reservoir of bioavailable Fe for phytoplankton [*Hurst et al.*, 2010]. The central Celtic Sea represents an intermediate Fe

cycle between these two environments. Unlike in the southern Ross Sea, complete NO_3^- drawdown is observed during summer (Fig. 3.2b), yet our SML bioavailable Fe concentrations (dFe and LpFe; Figs. 3.2a, 3.3c) were similar, and much lower than observed in the central Bering Sea. It is hypothesized that the Celtic Sea ecosystem exists in a fine balance of Fe and NO_3^- availability. Therefore, the structure of the summer ecosystem would be sensitive to changes in the availability of both nutrients. In the central Celtic Sea smaller species (< 20 μm) dominate the summer phytoplankton community, with *Synechococcus* most abundant [*Sharples et al.*, 2007; *Tarran et al.*, in prep]. Small phytoplankton have a competitive advantage over larger phytoplankton in Fe deplete waters [*Lis et al.*, 2015]. Moreover, *Synechococcus* species has been shown to dominate in Fe-limited Southern Californian stratified coastal waters, where upon the addition of Fe the ecosystem shifted in favour of diatom growth [*Hopkinson and Barbeau*, 2008].

The dFe pool in the SML during July 2015 represents the Fe fuelling regenerative production [*Strzepek et al.*, 2005] in these nutrient poor waters. On average, the concentration of sFe (0.13 ± 0.07 nM *n*=3) was in excess of the colloidal fraction (0.07 ± 0.09 nM, *n*=3) (Fig. 3.2e,f). Interestingly, these shelf concentrations were comparable to those seen in central oligotrophic gyres such as those observed at station ALOHA where sFe ranged from 0.05 - 0.1 nM in the upper 150 m, whereas cFe was depleted in the chlorophyll maximum [*Fitzsimmons et al.*, 2015b]. Although the concentration of sFe was low in both systems, it exceeded the solubility of the hydrolysis species [*Liu and Millero*, 2002]. Siderophores are low molecular weight complexes with high affinity and specificity for Fe(III) that are produced by marine bacterioplankton [*Gledhill et al.*, 2004], which may maintain the low, but persistent, sFe concentration in oligotrophic surface waters.

During summer months, the biomass maximum in the central Celtic Sea is observed below the SML, as a sub-surface chlorophyll maximum located in the pycnocline (Fig. 3.2c,d). This is an important region of new production as phytoplankton are able to access the diapycnal flux of nutrients from the BML [*Hickman et al.*, 2012]. Within the pycnocline, zonation of phytoplankton species is driven by vertical gradients in light and NO_3^- [*Hickman et al.*, 2009]. Here a vertical gradient in dFe, NO_3^- was observed (Fig. 3.2h) and photosynthetically available radiation of 16.4-0.11 W m^{-2} (during daytime casts). Photoacclimation at these light levels leads to increased cellular Fe quotas [*Strzepek and Price*, 2000; *Sunda and Huntsman*, 1997]. Where the flux of Fe across the pycnocline is insufficient to meet requirements, Fe and light co-limitation influences phytoplankton species composition in the sub-surface chlorophyll maximum [*Hopkinson and Barbeau*, 2008; *Johnson et al.*, 2010].

An estimate of the diffusive flux of dFe and NO_3^- to the pycnocline can be made using the following:

Diffusive flux of N= -Kz(ΔN/Δz)   (1)

where N is the dissolved nutrient of interest, Kz is the eddy diffusivity (m^2 s^{-1}), ΔN is the change in concentration (mol m^{-3}) of nutrient N through the pycnocline and Δz is the thickness of the pycnocline in meters. The pycnocline can be described as a thermocline, as temperature primarily drives seasonal stratification in the Celtic Sea. The thermocline was typically a shallow region (≈ 20 m thickness); consequently only 1 to 3 samples within the pycnocline were collected from a given profile. To establish a relationship for dFe and NO_3^- through the pycnocline, data from all profiles were compiled (Fig. 3.5). Therefore the flux through the pycnocline can be calculated as follows:
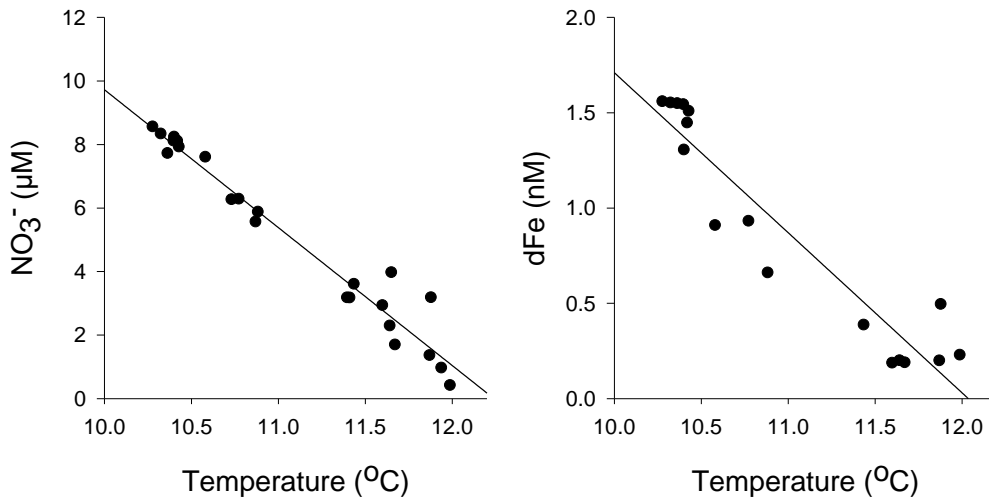
Figure 3-5- Collated data from the base of the pycnocline region (defined as 10.2-12 °C, based on visual observation of profiles) from July 2015, the difference in density is primarily driven by a temperature gradient (thermocline). Left- the relationship between NO_3^- and temperature (r^2=0.96). Right- the relationship between dFe and temperature (r^2=0.90).

$$\text{Diffusive flux of N= -Kz}((\Delta N/\Delta temp)x(\Delta temp/\Delta z)) \qquad (2)$$

where ΔN/Δtemp is the complied nutrient/temperature relationship (Fig. 3.5) and Δtemp/Δz is the temperature gradient through the thermocline for a given profile. Daily averaged values for eddy diffusivity were obtained from the Ocean Microstructure Glider that was present at the sampling site for the duration of the July 2015 cruise [pers.comm *Palmer*, 2016]. The results of this calculation are presented in Table 3.3. By using the compiled the nutrient concentration/temperature relationship and daily mean eddy diffusivity values, results in the estimate only representing a first order approximation. However, confidence in the approach is obtained by comparing estimated NO_3^- fluxes with previous studies were a typical value of 2 mmol NO_3^- m^{-2} d^{-1} is observed for the central Celtic Sea [*Sharples et al.*, 2009], similar to 1.86 ± 0.63 mmol NO_3^- m^{-2} d^{-1} reported here (Table 3.3). The estimated diffusive flux of dFe and NO_3^- through the thermocline indicated a dFe:NO_3^- molar ratio of new production of 0.19 nM:µM (Table 3.3). This is similar to the uptake ratio (0.11 nM:µM) observed during the

spring bloom, and would suggest a sub-optimal Fe supply relative to the phytoplankton

Fe:N ratios reported by _Ho et al._ [2003]. Therefore, the species distribution in the

pycnocline may be regulated by Fe and light co-limitation in the subsurface chlorophyll

maximum of the central Celtic Sea.

Table 3-3- Diffusive flux estimates of dFe and NO_3^- through the thermocline in the central Celtic Sea. The eddy diffusivity ranged from 1.09×10^{-5} to 2.64×10^{-5} m^2 s^{-1}.

Date	flux dFe (μmol m^{-2} d^{-2})	flux NO_3^- ($mmol$ m^{-2} d^{-2})
14.7.15	0.19	0.98
15.7.15	0.14	0.73
25.7.15	0.12	0.64
29.7.15	0.39	2.00
30.7.15	0.37	1.92
31.7.15	0.42	2.14
31.7.15	0.42	2.18
31.7.15	0.43	2.24
31.7.15	0.53	2.76
31.7.15	0.40	2.05
31.7.15	0.41	2.12
31.7.15	0.47	2.45
31.7.15	0.38	1.99
31.7.15	0.37	1.89
Mean	**0.36**	**1.86**
1 SD	**0.12**	**0.63**

3.2.4 Iron and nitrate availability during the autumn phytoplankton bloom

Water column stratification was also observed in autumn (November) (Fig. 3.2c),

and was reflected in the profiles of dFe, NO_3^- and all particulate Fe fractions (Fig. 3.2 a,b;

Fig. 3.3a,b,c). Radium activity profiles also showed complete depletion in the SML in

November 2014 (Fig. 3.4). The short half-lives of [223]Ra and [224]Ra indicate that rapid

vertical exchange was still largely limited by the persistence of the seasonal pycnocline

into November. Although still stratified, a net heat flux to the atmosphere meant

stratification was progressively weakening relative to summer conditions [*Wihsgott et al.*, in prep] (Fig. 3.2c). The relative increase in vertical exchange resulted in higher SML concentrations of bioavailable Fe and NO_3^-, than observed during the summer stratified period (Table 3.1; Fig. 3.2a,b; Fig. 3.3c). The increased supply nutrients (including Fe) fuelled an autumn bloom [*Wihsgott et al.*, in prep]; observed here as elevated chl-*a* concentrations of ≈ 0.7 mg m^{-3} (Fig. 3.2d).

3.2.5 Seasonal cycling in the bottom mixed layer

A seasonal build-up of dFe and NO_3^- in the BML (Fig. 3.2a,b) occurred alongside an increase in dissolved inorganic carbon (DIC) [*Humphreys. et al.*, in prep] and a decrease in dissolved oxygen (O_2) [*Williams et al.*, in prep]. The seasonal redistribution of NO_3^-, DIC and O_2 was consistent with previous findings suggesting NO_3^- cycling was driven by uptake in the SML and subsequent remineralisation in the BML [*Hickman et al.*, 2012; *Sharples et al.*, 2001]. When dFe concentrations (SML + BML, all seasons) are compared with corresponding NO_3^- concentrations a statistically significant relationship is noted ($r^2= 0.94$, $p< 0.001$, *n*= 163; Fig. 3.3d), suggesting that similar processes drive the observed seasonality of dFe with a limited net removal of dFe through particle formation. Moreover, an estimated 95% of the organic carbon present in Celtic Sea surface sediments is remineralised in repeated resuspension cycles rather than preserved [*de Haas et al.*, 2002]. Our results suggest a similar process is occurring for the Fe associated with the organic matter. Additionally, no clear increase of dFe towards the seabed is observed in our profiles (Fig. 3.2a) to suggest a significant diffusive sedimentary input of dFe. This is in contrast to a localised area in the north-eastern Celtic Sea where weaker current and wave activity permit the deposition of fine, organic-rich

sediment [*de Haas et al.*, 2002; *McCave*, 1971], and a significant benthic source of dFe to the overlying water column was observed at the time of our study [*Klar et al.*, 2017].

The majority (> 98%) of dFe present in seawater is associated with organic complexes [*Gledhill and Buck*, 2012] which enhance the solubility of dFe in seawater above that of inorganic species [*Liu and Millero*, 2002]. Moreover, the concentration of organic-Fe chelators has been shown to control the solubility of Fe in particle rich coastal and shelf waters [*Buck and Bruland*, 2007; *Buck et al.*, 2007]; in the BML the LpFe fraction (Fig. 3.3c) was always in excess of dFe (Fig. 3.2a). Partial remineralisation of organic matter releases both dFe and organic Fe binding complexes [*Boyd et al.*, 2010], which provides a potential mechanism for the seasonal increase in dFe concentrations. Although temperature and pH also affect the solubility of Fe in seawater [*Liu and Millero*, 2002] and the binding strength of organic Fe-binding complexes [*Avendaño et al.*, 2016; *Gledhill et al.*, 2015], the seasonal changes of temperature (≈ 2 °C) and pH (≈ 0.1 pH; *Humphreys. et al.* [in prep]) in the BML are insufficient to account for the seasonal build-up of dFe.

In contrast to dFe, the concentration of TdFe in the BML correlated with turbidity (Fig. 3.3e), indicating that short-term resuspension events were the primary cause of high particulate Fe concentrations. Sediment resuspension events are driven by processes occurring on shorter timescales than seasonal changes (e.g. semi-diurnal tides, internal tides, and storm events) and result in high particle loads in the BML of shelf systems relative to open ocean waters. Furthermore, the observed pFe:pAl molar ratio was seasonally invariant and ranged from 0.22-0.28, similar to the upper crustal ratio [0.19-0.23; *McLennan*, 2001; *Rudnick and Gao*, 2003; *Wedepohl*, 1995], and consistent with the majority of pFe being supplied from a lithogenic source. Our results indicate that a large proportion of particulate Fe (≈ 80%) is refractory (Fig. 3.3b,c) and cycles

independently of dFe. This is consistent with the majority of the Celtic Sea surface sediments being relict deposits from the Pleistocene and early Holocene, consisting of reworked, fine and coarse sands [*de Haas et al.*, 2002].

3.3 Conclusions

Our results show a seasonal, nutrient-type cycling of dFe in a temperate shelf sea. During summer, stratification isolates surface waters from Fe rich bottom waters and provides a mechanism whereby temperate and high latitude shelf sea ecosystems can become sensitive to Fe availability. The strength of seasonal stratification in North West European shelf seas is predicted to increase by ≈ 20% by the end of the 21st century as a result of climate change [*Holt et al.*, 2010]. Under these conditions the magnitude of the diapycnal nutrient flux, including dFe, will decrease, exacerbating the summer oligotrophic conditions. When assessing the effect this will have upon shelf sea primary production it is suggested that it is necessary to consider the role of Fe as potentially co-limiting nutrient.

Chapter 4 - The physico-chemical speciation of iron over an oxic shelf margin

The research presented in this chapter is being prepared for publication in *Marine Chemistry*.

4.0 Introduction

Due to the extremely low solubility of Fe in oxic seawater, [*Liu and Millero*, 2002] concentrations of dFe are typically in the sub-nanomolar range in the ocean [*Johnson et al.*, 1997]. Consequently, Fe availability regulates phytoplankton growth in over 20-40% of the world's ocean [*Boyd et al.*, 2007; *Boyd and Ellwood*, 2010; *Martin*, 1990; *Martin and Fitzwater*, 1988]. In order to alleviate Fe limitation, new external sources of Fe are required. A combination of sediment resuspension and a diffusive flux of Fe, driven by the use of Fe(III) as a terminal electron acceptor during the oxidation of organic matter, can lead to sediments being a significant source of dFe to the overlying water column [*Berelson et al.*, 2003; *Elrod et al.*, 2004; *Klar et al.*, 2017; *Lohan and Bruland*, 2008; *Santschi et al.*, 1990; *Severmann et al.*, 2010; *Ussher et al.*, 2007]. A recent revised estimate of the global sedimentary dFe flux suggests that the flux from shelf slope sediments (200-2000 m) is 37 x 10^9 mol dFe yr^{-1} [*Dale et al.*, 2015], ≈ 3-4 times larger than the global atmospheric aerosol flux of dissolvable Fe [*Jickells et al.*, 2005; *Mahowald et al.*, 2005]. Furthermore, modelling of the Southern Ocean iron/carbon cycles suggests sedimentary Fe sources are more readily connected to surface waters than hydrothermal sources. Consequently, atmospheric CO_2 concentrations are 7-15 times more sensitive to fluctuation in the strength of sedimentary Fe sources to the Southern Ocean than that of dust or hydrothermal inputs [*Tagliabue et al.*, 2014a].

Indeed, Fe from continental shelf sediments is reported to be an important source of Fe for phytoplankton growth in highly productive shelf environments [*Aguilar-Islas et al.*, 2007; *Chase et al.*, 2005b; *Chase et al.*, 2007; *Hurst et al.*, 2010; *Hutchins and Bruland*, 1998; *Johnson et al.*, 1999] and shown most clearly downstream of the Crozet [*Pollard et al.*, 2009], Kerguelen [*Van Der Merwe et al.*, 2015] and Galapogos [*Martin et*

al., 1994] island systems in Fe limited waters. Moreover, observed decreases in dFe concentration with distance from shelf slopes [*Aguilar-Islas et al.*, 2007; *Boye et al.*, 2003; *Bucciarelli et al.*, 2001; *Elrod et al.*, 2004; *Milne et al.*, 2017; *Nishioka et al.*, 2007; *Ussher et al.*, 2010], Fe(II) rich particles with a shelf origin in the central North Pacific [*Lam and Bishop*, 2008; *Lam et al.*, 2006] and Fe isotope studies [*Conway and John*, 2014; *John et al.*, 2012] indicate that the impact of sedimentary derived Fe is not restricted to coastal zones, but that Fe is transported 100-1000's km from the continental margins into the open ocean.

Large sedimentary Fe fluxes have been reported in anoxic/hypoxic waters [*Dale et al.*, 2015; *Elrod et al.*, 2004; *Homoky et al.*, 2012; *Hong and Kester*, 1986; *Lohan and Bruland*, 2008; *Severmann et al.*, 2010] where low oxygen concentrations retard the oxidation rate of Fe(II) [*Millero et al.*, 1987] and dissimilartory Fe reduction result in isotopically lighter dFe signatures (δ^{56}dFe ≈ -3.0 ‰) [*Homoky et al.*, 2013]. Additionally, observations of istopically heavier dFe (δ^{56}dFe ≈ 0.2 ‰) have been attributed to a non-reductive disolution pathway for Fe in oxic margin sediments [*Homoky et al.*, 2013; *Radic et al.*, 2011], a process which *Conway and John* [2014] estimate contributes up to 100% of the dFe inventory in upper Labrador Seawater in the North West Atlantic. Though it should be noted that uncertaunties remain regarding the effect of water column processes on the δ^{56}dFe signature [*Abadie et al.*, 2017; *Staubwasser et al.*, 2013]. Whilst a picture is emerging that transport of Fe from oxic margins is an important aspect of the marine Fe cycle, less is currently known about the physico-chemical speciation, and longevity, of Fe derived from these regions. Particulate Fe dominates the Fe inventory over shelf slopes [*Hong and Kester*, 1986; *Laes et al.*, 2007]. This particulate Fe remobilised from shelf sediments contains a readily exchangeable fraction [*Hurst and Bruland*, 2007], the

transport of which may represent an important source of bioavailable Fe [*Hurst et al.*, 2010; *Lam and Bishop*, 2008; *Lam et al.*, 2006; *Wells and Mayer*, 1991b] and act to buffer dFe concentrations [*Abadie et al.*, 2017; *Milne et al.*, 2017].

The physico-chemical speciation of dFe can be further separated into sFe and cFe fractions; the limited available data points towards cFe contributing 60-80% of the dFe supplied from oxic margins [*Fitzsimmons et al.*, 2015a; *Hurst et al.*, 2010]. If so this may have implications for the bioavailability of Fe derived from oxic margins as laboratory culture studies indicate that colloidal mineral Fe phases can be utilized by certain species [*Nodwell and Price*, 2001; *Rubin et al.*, 2011]. However, the bioavailability of cFe decreases with ageing [*Yoshida et al.*, 2006]. When cFe and sFe bioassay experiments are compared, phytoplankton growth rates are faster under sFe additions [*Chen et al.*, 2003; *Chen and Wang*, 2001], consistent with preferential drawdown of sFe during the Celtic Sea spring bloom [*Birchill et al.*, 2017]. Moreover, an inert fraction of cFe has been shown not to be exchangeable with ligands in the soluble phase [*Cullen et al.*, 2006], potentially limiting the exchange between these size fractions.

The area of interest in this study was the Celtic Sea shelf slope, an oxic shelf margin of the NE Atlantic where elevated dFe concentrations have been observed in intermediate nepheloid layers (INLs) [*Nédélec et al.*, 2007]. Intermediate nepheloid layers are the result of a detachment of the benthic nepheloid layer (BNL). The BNL is maintained by persistent sediment resuspension events over the steep (mean gradient of 11°) Celtic Sea shelf slope [*McCave et al.*, 2001], which includes localised areas of very steep, even vertical, gradients along canyon walls which incise the shelf break [*Cunningham et al.*, 2005]. Interaction between the steep topography and the overlying water column creates a physically dynamic environment over the shelf break, including

large tidal currents (> 50 cm s⁻¹), which generate large internal tides during the stratified

period (displacements up to 150 m), and an along-slope poleward current of ≈ 5 cm s⁻¹

centred at ≈500 m [*Huthnance et al.*, 2001; *Pingree and New*, 1989; *Pingree and Le Cann*,

1989; *Sharples et al.*, 2009; *van Weering et al.*, 1998]. Detachment of the BNL results

from enhanced near sea bed currents, due to processes such as intensification of the

internal tide [*Bourgault et al.*, 2014], which may result from localised changes in

stratification [*Dickson and McCave*, 1986]. Additionally, extreme events lasting days to

weeks, and driving a ≈ 20 fold increase in lithogenic particle concentration, have been

observed over the Celtic Sea shelf slope [*Antia et al.*, 1999]. This suggests that there are

multiple mechanisms of sediment resuspension, which along the steep Celtic Sea slope

may include mass flows along canyons initiated by faulting and/or slope failure of

canyon walls [*Cunningham et al.*, 2005; *Zaragosi et al.*, 2000].

As a consequence of this dynamic environment, lateral transport of particulate

material in INLs, which spread along isopycnals, are common features over the Celtic

Sea shelf slope [*Antia et al.*, 1999; *Dickson and McCave*, 1986; *McCave et al.*, 2001]. In

this study the distribution of sFe, cFe, dFe, Fe(II), TdFe and LpFe concentrations are

reported for 3 cross slope transects sampled in November 2014, April 2015 and July

2015 as part of the Shelf Sea Biogeochemistry programme (http://www.uk-ssb.org/).

During each sampling period we observed INLs with elevated TdFe and dFe

concentrations indicating that these are persistent modes of Fe transport from the Celtic

Sea shelf slope.

4.1 Methods

4.1.1 Sampling methods

Seawater samples from vertical depth profiles were collected from repeat stations during three research cruises on the *R.R.S.* Discovery to the Celtic Sea shelf slope (Fig. 4.1) during November (autumn) 2014, April (spring) and July (summer) 2015. Three transects were sampled with stations at bottom depths of 2500, 2000, 1500, 1000, 750, 500 and 250 m; transects 1 and 3 followed canyons that incised the shelf slope whereas transect 2 sampled over a spur. As the slope was steepest over the spur, the length of the spur transect (T2) was shorter (15.8 km) than the canyon transects (T1 = 50.0 km, T3 = 33.0 km). Water and particulate sample collection for the determination of dFe, sFe, TdFe and LpFe fractions followed the procedure outlined in section 3.2.1. Samples for the determination of Fe(II) were collected unfiltered, immediately upon recovery in acid clean 60 mL LDPE bottles, that were stored in UHP water between use. Sample bottles were rinsed 3 times with sample then filled and capped with no headspace. In order to minimise Fe(II) oxidation, samples were stored in the dark at 4 °C prior to analysis, which was typically within 1 hour of collection.

4.1.2 Soluble, dissolved and total dissolvable iron analysis

All sample and reagent handling was undertaken in an ISO 14644-1 Class 5 laminar flow hood (Bassaire, Southampton, UK) situated within an ISO 14644-1 Class 5 clean room at Plymouth University. Soluble, dissolved and total dissolvable Fe were analysed using FI-CL detection [*Floor et al.*, 2015; *Obata et al.*, 1993]. The detailed methodology is described in section 2.3.

1
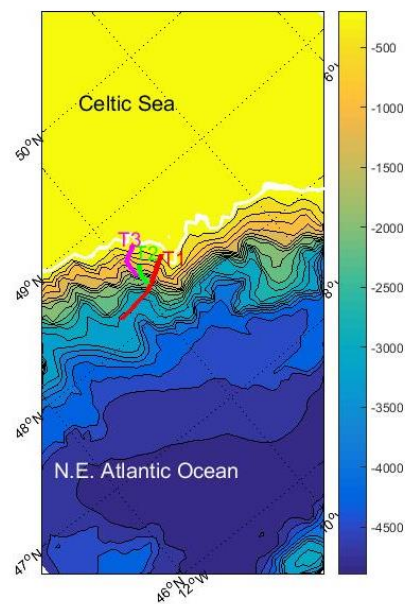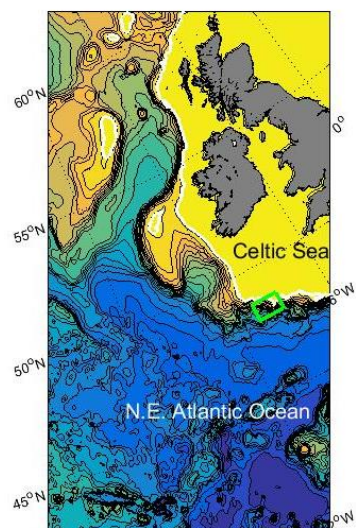
Figure 4-1- Station locations sampled during this study. Solid white line represents the 200 m isobath. Data provided by the _National Geophysical Data Center_ [1995].
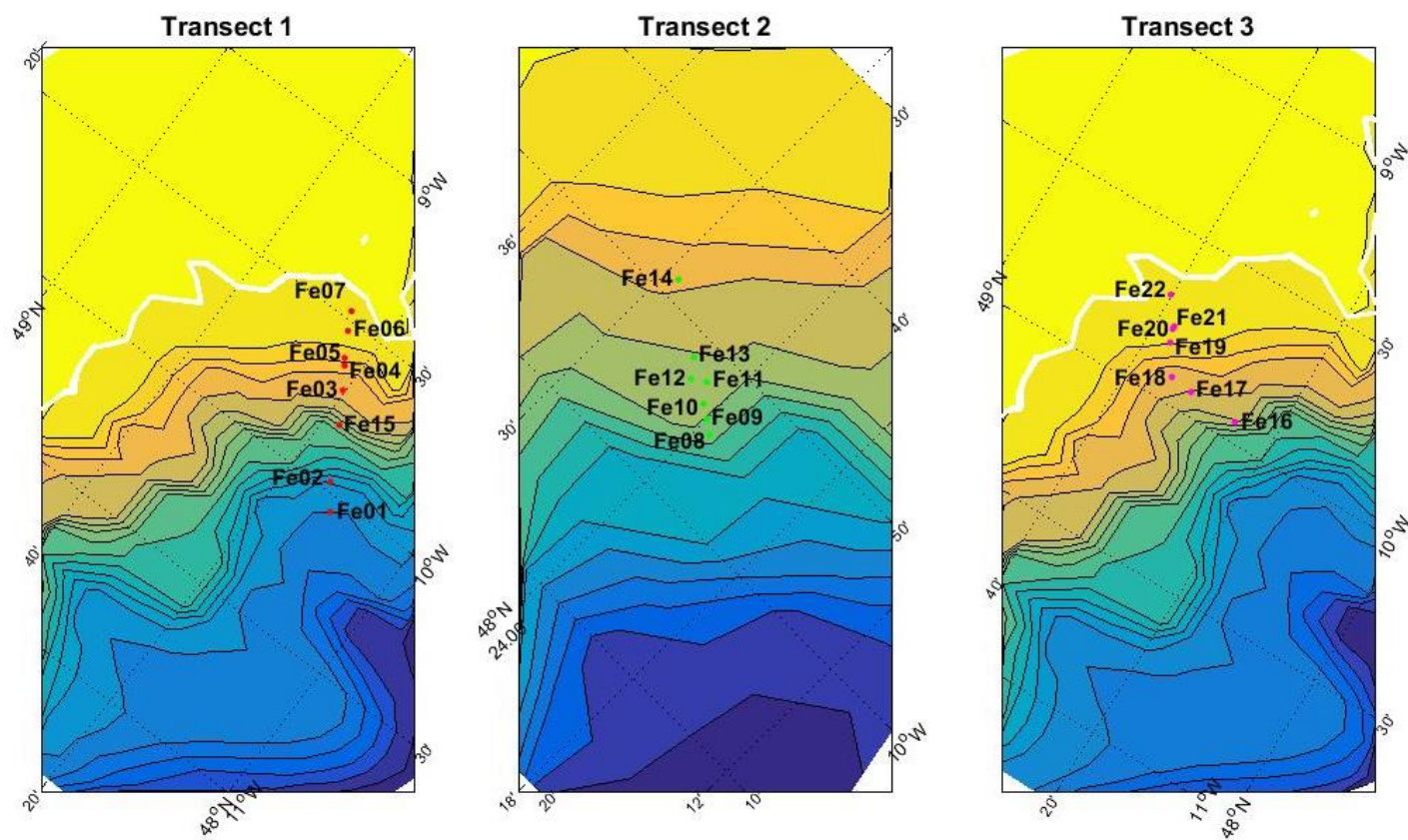
4.1.3 Fe(II) determination

The fraction of dFe determined as Fe(II) is dependent on the analytical method used and is therefore operationally defined [*Hopwood et al.*, 2017]. Here dissolved Fe(II) was determined by flow injection with in line filtration and pre-concentration, followed by chemiluminesence detection, modified after [*Bowie et al.*, 2002; *Bowie et al.*, 2005]. The detailed methodology is described in section 2.4.

4.1.4 Leaching and analysis of particulate samples

The leaching of filters (conducted by Dr. Angela Milne, University of Plymouth) followed the procedure outlined in sections 3.1.3 and 3.1.4.

4.1.5 Nutrients, temperature, salinity, oxygen, chlorophyll-*a* and turbidity

The collection and analysis of nutrients (conducted by Malcolm Woodward and Carolyn Harris, Plymouth Marine Laboratory) and measurements of temperature, salinity, oxygen, chlorophyll-*a* and turbidity were conducted following the procedures outlined in section 3.1.6.

4.2 Results and discussion

4.2.1 A note on the fraction of particulate Fe accessed by long term sample acidification

Particulate Fe concentrations were defined as TdFe-dFe; this better helps to display the surface waters where dFe and TdFe concentrations were typically low (< 0.5 nM). It is interesting to note that concentration of LpFe equated to 20 ± 14 % (mean ± SD, *n*= 105) of the concentration of TdFe-dFe at depths below 100 m (Fig. 4.2). In surface waters, this was more variable 39 ± 25 % (mean ± SD, *n*= 39) and included higher values, presumably due to biological processing maintaining particulate Fe in more soluble phases. Indeed the most elevated surface values were observed during summer (July,

2015) when biological recycling would be most intense. These proportions are

consistent with the assumption that long term sample acidification accesses most of the

particulate iron sampled [*Sedwick et al.*, 2008]. Importantly therefore, assuming that

long term sample acidification provides a measure of the 'labile' particulate fraction may

be incorrect [e.g. *Chever et al.*, 2010; *Loscher et al.*, 1997]. If so, this would result in a

large overestimation of the concentration of Fe in the particulate fraction that can

exchange with the dissolved fraction over relatively short (hours to days) timescales

[*Hurst and Bruland*, 2007]. The degree to which long term sample acidification accesses

refractory components of the particulate phase will be affected by the leaching pH, with

some studies acidifying to 0.024 M HCl and others to 0.01 M HCl. Clearly, correctly

identifying the fraction(s) of Fe accessed by different leaching procedures has important

implications for environmental interpretation of the data, and thus more work is

required in this area.
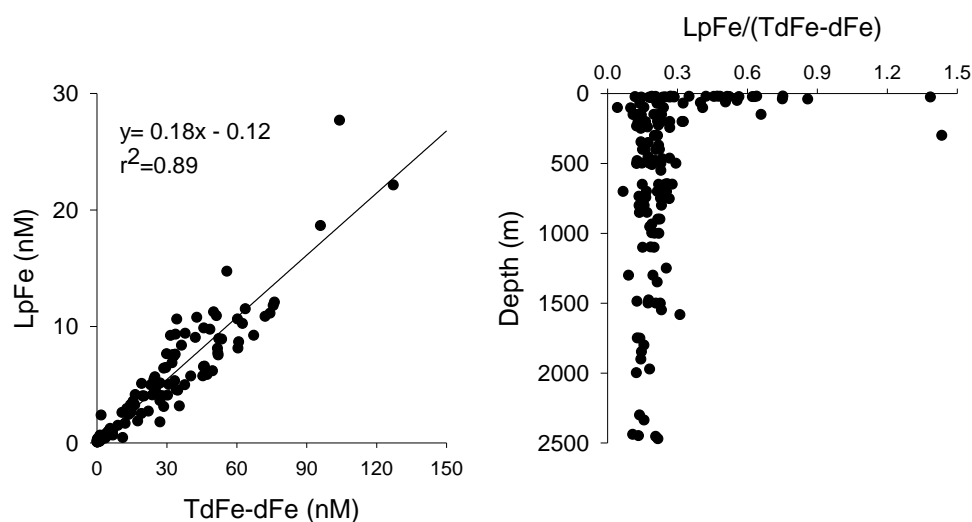
Figure 4-2 - Left- Scatter plot of TdFe-dFe and LpFe concentration. **Right**- Depth profile of LpFe/(TdFe-dFe). Plots include all data from November 2014 and April and July 2015.

4.2.2 Hydrography over the Celtic Sea shelf slope

The water masses identified over the Celtic Sea shelf break (Fig. 4.3) are consistent with previous observations in this region [*Dickson and McCave*, 1986; *Huthnance et al.*, 2001; *Laës et al.*, 2003; *Pingree*, 1973]. Station Fe01 was the deepest and most westerly (off-shelf) station and encompassed the full range of the water masses present. In all sampling months a pronounced salinity minimum at ≈ 2000 m (Fig. 4.3) is indicative of Labrador Sea Water (LSW) [*Pingree*, 1973]. The salinity at this depth was ≈ 34.98, which is higher than the estimated salinity at the formation of LSW (34.890) [*van Aken*, 2000], reflecting vertical mixing with more saline Mediterranean Outflow Water (MOW) that overlies LSW in this region [*Pingree*, 1973]. In all seasons, the presence of MOW was evidenced as a warm (9.12-9.44 °C) salinity maximum present at ≈ 850 to 1000 m (Fig. 4.3). The salinity of the MOW core was higher in November 2014 (35.749) and July 2015 (35.753) relative to April 2014 (35.659) (Fig. 4.3), indicating that prevalence of MOW over the shelf break can vary over monthly timescales. Below LSW, at ≈ 2150 m the potential temperature dropped below, the estimated potential temperature of LSW at formation [3.428 °C; *van Aken*, 2000], and therefore indicates the influence of colder North Atlantic Deep Water (NADW) (Fig. 4.3).

The upper water column (i.e. base of the seasonal thermocline to ≈ 700 m) was comprised solely of East North Atlantic Central Water (ENACW). Winter overturning means that the physical characteristics of ENACW are primarily determined by atmosphere-ocean heat and water exchange and thus reported values of temperature (8-18 °C) and salinity (35.2-36.7) are highly variable [*Emery and Meincke*, 1986]. The measurements from this study fall within this range (Fig. 4.3). In surface waters, seasonal stratification is driven by the yearly cycle of solar irradiance, with the onset of seasonal

stratification occurring in April [*Fasham et al.*, 1983]. Accordingly, surface waters sampled in spring (April 2015) were only weakly stratified, with strongest stratification during summer (July 2015; surface temperature of 17.5 °C). In autumn (November 2014) a net heat flux to the atmosphere cooled surface waters to 14.6 °C reducing the strength of stratification.

At station Fe03, the water depth of ca. 1500 m meant that the cold NADW was not present. The effect of LSW was present but the salinity minimum was not as prominent as at Fe01 due to the shallower water column (Fig. 4.3). Both MOW and ENACW cores were still evident but were not as prominent as at station Fe01 (Fig. 4.3), reflecting enhanced vertical mixing over the shelf break [*Pingree*, 1973]. Enhanced vertical mixing in the upper water column, attributed to breaking of internal tides [*Pingree et al.*, 1986; *Sharples et al.*, 2009], is evidenced by reduced surface temperatures (16.7 °C) relative to station Fe01 (17.5 °C) during July 2015. The effect of seasonal stratification was again evident in surface waters as a seasonal thermocline in July and November.

At station Fe06, (water depth of ca. 500 m) there was no significant variation in salinity to indicate the presence of different water masses (Fig. 4.3). The uniform temperature in April indicated that winter mixing, driven by heat loss to the atmosphere, had fully overturned the water column, this is consistent with previous findings of a winter mixing depth of ≈ 500 m over the Goban Spur [*Huthnance et al.*, 2001]. The increased temperature of the entire water column and the presence of a seasonal thermocline, in July and November indicated that the physical structure of the water column is primarily determined by the seasonal cycle of solar irradiance.

1
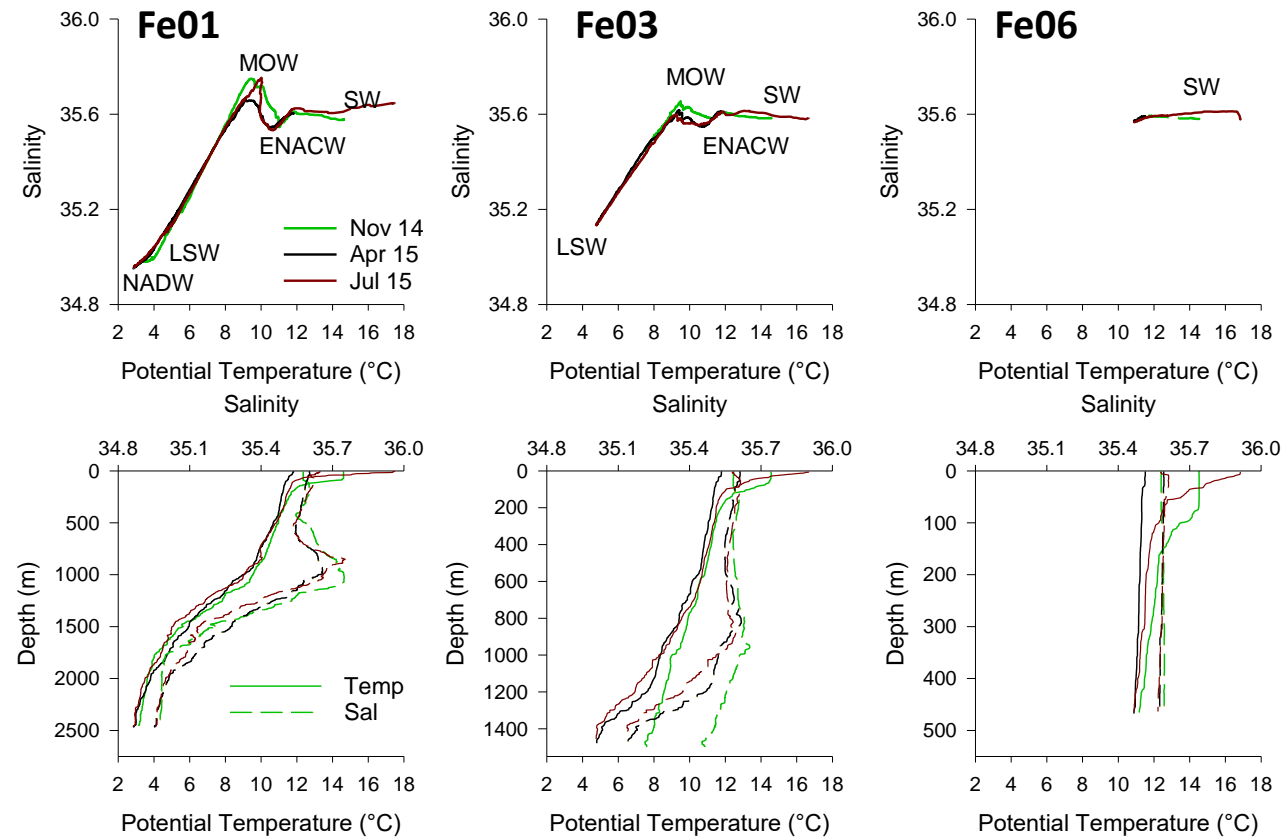
Figure 4-3- The water masses present over the Celtic Sea shelf break. NADW= North Atlantic Deep Water, LSW= Labrador Sea Water, MOW= Mediterranean Outflow Water, ENACW= East North Atlantic Central Water and SW= surface water. **Left**- station Fe01. **Middle**- Station Fe03. **Right**- Station Fe06. Note change in depth scales. See Figure 4.1 for station locations.

4.2.3 Distribution of dFe and particulate Fe over the Celtic Sea shelf slope

The distribution of dFe and TdFe-dFe over the Celtic Sea shelf slope in November 2014, April and July 2015 is displayed in Figs. 4.4, 4.5, 4.6. In nearby North East Atlantic waters, 'background' dFe concentrations of 0.23-0.93 nM have been reported [*Laës et al.*, 2003]. Over the Celtic Sea shelf slope, dFe concentrations in excess of this were a common feature throughout all seasons. The range of dFe concentrations observed for all seasons was 0.03 to 4.09 nM, which is broadly consistent with previous observations over the Celtic Sea [*Nédélec et al.*, 2007] and Bay of Biscay [*Laes et al.*, 2007; *Ussher et al.*, 2007] shelf slopes. Notably, the dFe concentrations observed in this study during summer (July 2015) surface mixed layer (SML) include the lowest reported dFe concentrations (< 0.1 nM) for waters overlying the Celtic Sea or Bay of Biscay shelf slope.
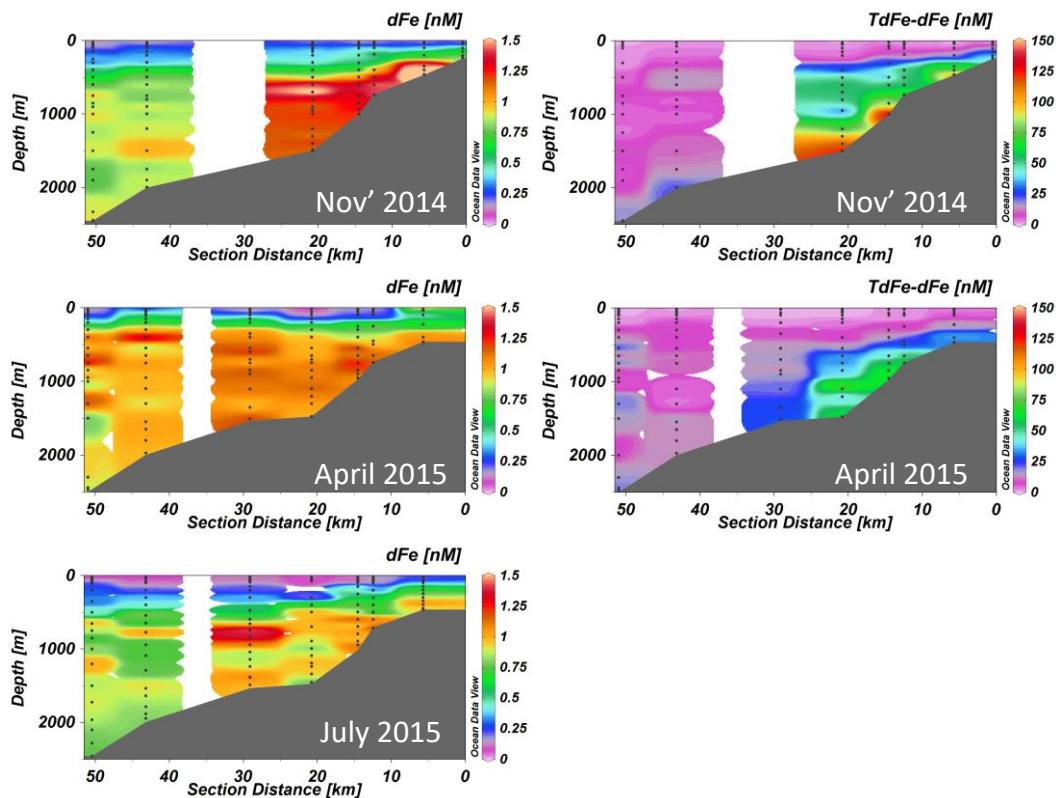
Figure 4-4- Shelf break (transect 1) sections of dissolved and total dissolvable-dissolved iron for autumn (November), spring (April) and summer (July). Total dissolvable iron samples for July 2015 yet to be analysed.
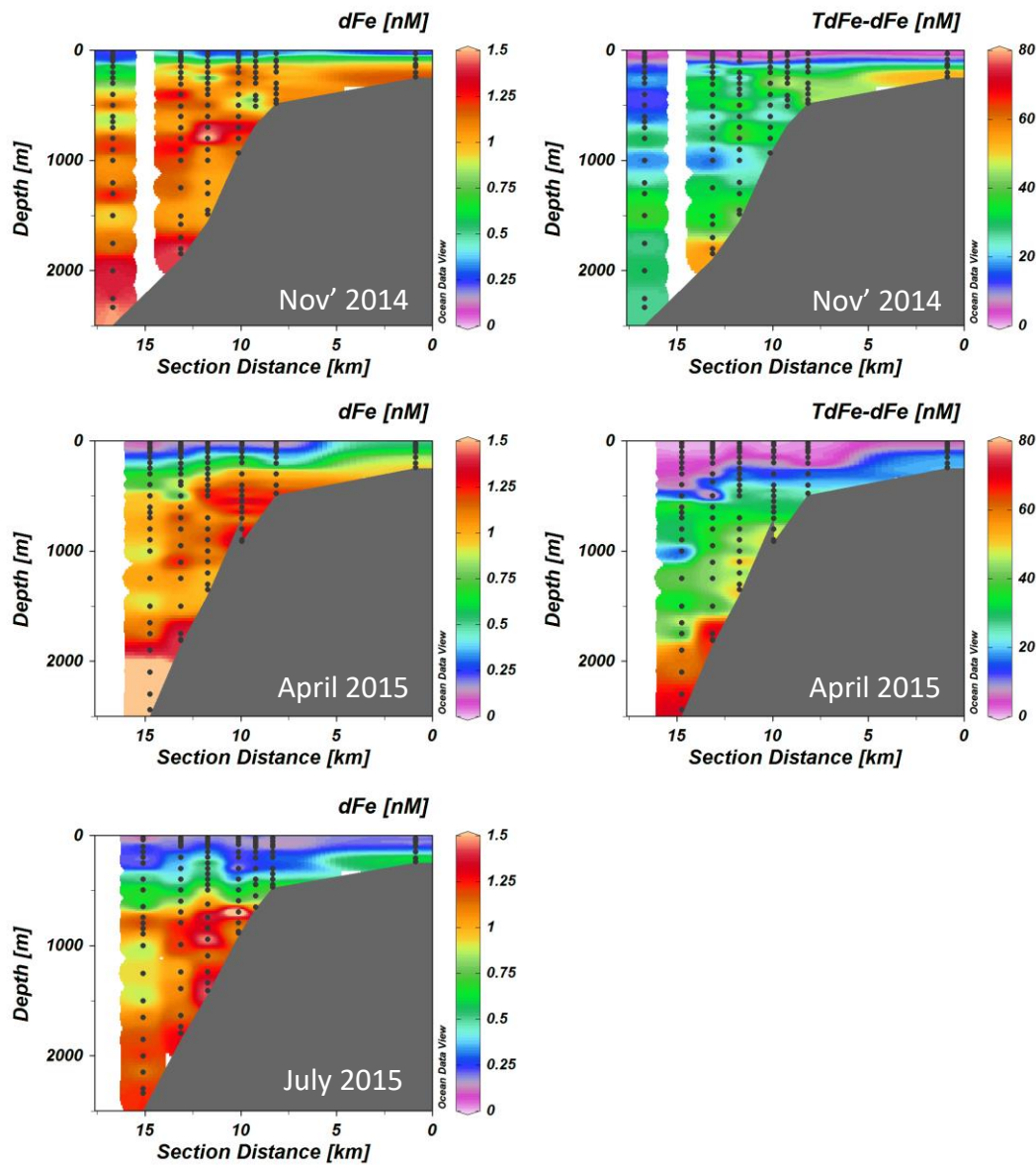
Figure 4-6- Shelf break (transect 2) sections of dissolved and total dissolvable-dissolved iron for autumn (November), spring (April) and summer (July). Total dissolvable iron samples for July 2015 yet to be analysed.
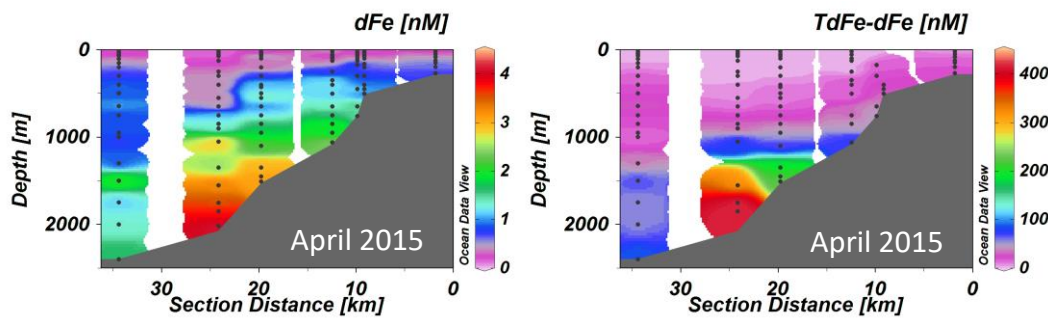
Figure 4-5 Shelf break (transect 3) sections of dissolved and total dissolvable iron for spring (April). Transect only sampled in April 2015.

The range of TdFe-dFe concentrations observed in the whole dataset was 0.17 to 423 nM which generally decreased with distance from the shelf slope and particularly in surface waters, similar to observations over the Bay of Biscay shelf slope [*Laes et al.*, 2007]. However, the concentrations presented here are generally in excess of those described by *Laes et al.* [2007] who reported a maximum TdFe concentration of 24.6 nM. The shelf slope over the Celtic Sea is steeper and more heavily incised with canyons relative to Bay of Biscay shelf slope [*Harris et al.*, 2014], which may promote greater sediment resuspension. Alternatively, the difference may result from differing operational definitions where, *Laes et al.* [2007] acidified their TdFe samples to 0.01 M HCl for > 6 months whereas in this work samples were acidified to 0.024 M HCl for > 6 months. The TdFe-dFe concentrations reported here are comparable with those observed over the seasonally anoxic Californian shelf slope, where a maximum of 427 nM was reported over the shelf slope using a similar operating definition as here [*Chase et al.*, 2005a].

Near the sea floor, the BNL was evident as an increase TdFe-dFe concentration (Figs. 4.4, 4.5, 4.6). In particular, remarkably high TdFe-dFe (> 400 nM) concentrations were observed in the BNL of Transect 3 during April 2015, and were associated with elevated dFe concentrations (> 4 nM; Fig. 4.6), suggesting a large and/or recent sediment resuspension event(s). Even outside of the BNL, TdFe-dFe concentrations were typically at least one order of magnitude higher than dFe concentrations (Figs. 4.4, 4.5, 4.6), with the exceptions of stations Fe01 and Fe02, which are furthest from the shelf slope, and the SML. At intermediate depths the lateral flux of particulate material emanating from the Celtic Sea shelf slope dominated transport by a factor of 2.7 over the vertical flux from the SML [*Antia et al.*, 1999]. Therefore, the source of elevated

TdFe-dFe concentration is interpreted as slope derived particulate material that 'escaped' from the BNL.

Within a given profile, dFe and TdFe-dFe generally exhibited similar distributions, implying a common sediment source (Fig. 4.7). Moreover, statistically significant Spearman's rho correlations indicated that increasing TdFe-dFe concentration was associated with increased dFe concentration (Fig. 4.8). However, it is also evident that the relationship between dFe and TdFe-dFe was asymptotic. A linear relationship was observed between TdFe-dFe and LpFe up to concentrations of 140 nM TdFe-dFe, indicating that in sub surface waters typically 20 ± 14 % of TdFe-dFe was persistently present as an exchangeable labile fraction (Fig. 4.2). Therefore, the asymptotic relationship between dFe and particulate iron (Fig. 4.8) was not the result of changes in the lability of Fe in particulate material. Instead, it suggests that dFe removal processes become more important at increased TdFe-dFe concentrations. This is likely due to an increased rate of scavenging in turbid waters [*Baskaran et al.*, 1992; *Moran and Buesseler*, 1993] and saturation of the ambient dissolved Fe-binding ligand pool which act to stabilise against scavenging [*Buck and Bruland*, 2007; *Buck et al.*, 2007; *Moore and Braucher*, 2008; *Noble et al.*, 2012], which are present in both the soluble and colloidal pools [*Cullen et al.*, 2006]. Moreover, a complexing capacity of 0.84-2.10 nM for dFe has been reported for this region [*Boye et al.,* 2003].
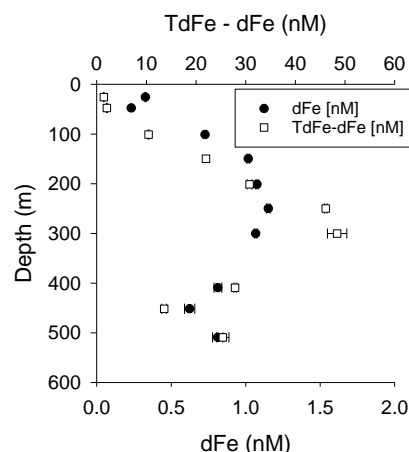
Figure 4-8- Example depth profile showing similarity between dFe and TdFe-dFe distributions. Station Fe12, November 2014.
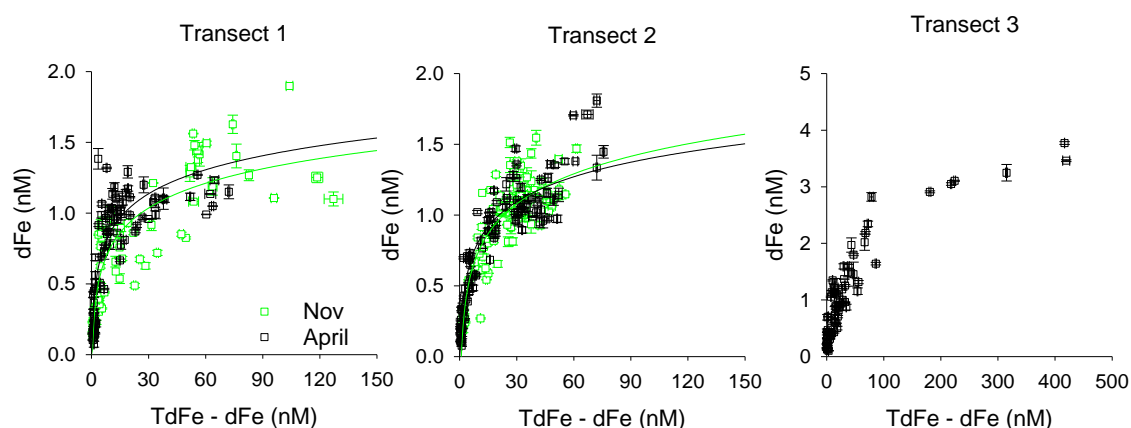
Figure 4-7- Relationships between dFe and TdFe-dFe. Transect, 1 November 2014 r_s=0.88, p <0.0001, n= 72, April 2015 r_s=0.78, p <0.0001, n= 87. Transect 2, November 2014 r_s=0.77, p <0.0001, n= 101, April 2015 r_s=0.91, p <0.0001, n= 103. Transect 3, April 2015 r_s=0.87, p <0.0001, n= 78. The relationship identified in transects 1 and 2 described by a logarithmic curve. The relationship is transect 3 did not.

4.2.4 Distribution of sFe and cFe over the Celtic Sea shelf slope

The physico-chemical speciation of dFe was further broken down into soluble and colloidal fractions. When sFe and cFe concentrations are plotted against dFe concentration it is evident that dFe was largely present in the colloidal fraction (Fig. 4.9; dFe/cFe regression slopes of 0.80 to 0.86), which is consistent with previous observations near and over oxic continental margin sediments [*Fitzsimmons et al.*, 2015a; *Hurst et al.*, 2010]. The large proportion of Fe in the colloidal fraction indicates

input of cFe from sediments and sediment pore waters [*Homoky et al.*, 2011], and/or

rapid association of pore water sFe [*Klar et al.*, 2017] with colloidal material in the water

column [*Honeyman and Santschi*, 1991; *Hurst and Bruland*, 2007]. Here the

concentration of sFe also increased with dFe concentration (Fig. 4.9), consistent with

dFe concentrations being controlled by a dynamic equilibrium between soluble and

colloidal fractions [*Fitzsimmons and Boyle*, 2014; *Fitzsimmons et al.*, 2015b; *Ussher et al.*,

2010], though the increase in sFe concentration here could be driven by input of

nanoparticles with a diameter < 30 nm that have been observed in seawater [*Wells and*

Goldberg, 1994]. In deep open ocean waters, an approximation is that dFe reaches a

50:50 steady state equilibrium between sFe and cFe [*Fitzsimmons et al.*, 2015a; *Ussher*

et al., 2010]. Over the Celtic Sea shelf break there is clearly a greater excess of cFe. The
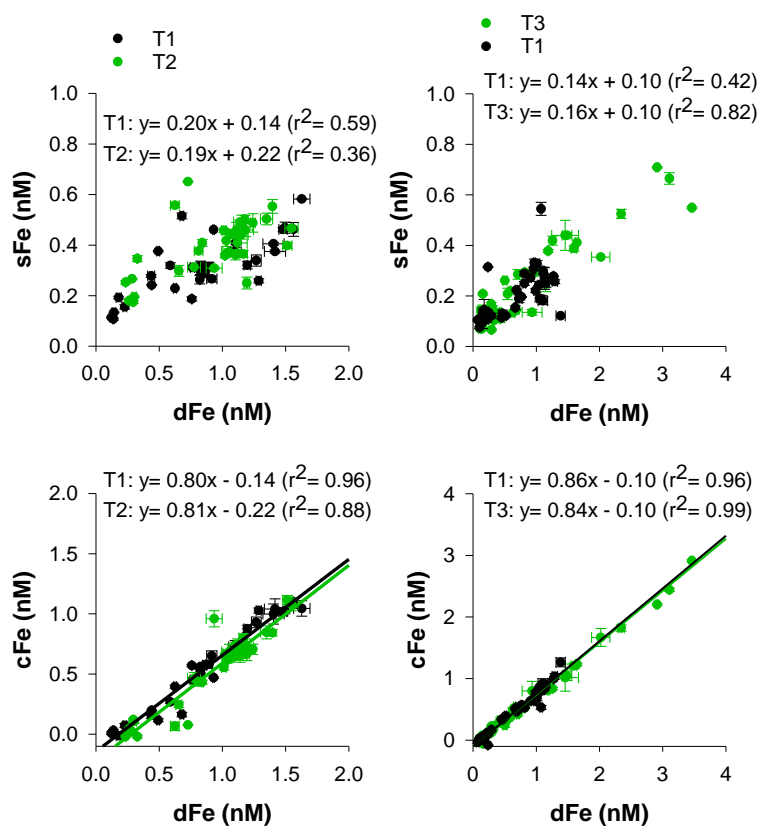
Figure 4-9- Scatter plots of dissolved iron against soluble
and colloidal iron. Left- November 2014. Right- April 2015.
Note change of scaling.

lability of the cFe will determine whether equilibrium with the soluble phase can be achieved. If the cFe is not readily exchangeable with the sFe fraction, as has been shown for some fraction of the cFe pool [*Cullen et al.*, 2006], then the fate of cFe will be inexorably tied to that of the colloidal material.

The number of marine colloids increases logarithmically with decreasing size, creating a continuum linking sub-micron material to larger particulates [*Wells and Goldberg*, 1993]. This colloidal size spectrum indicates that the removal pathway of colloids is aggregation to larger particles, whereby shear and gravity become the dominant forces acting upon the particle, and hence gravitational settling can occur. Therefore, aggregation to the particulate phase provides a mechanism to remove excess cFe from the dissolved phase; this process has been demonstrated for metals (including Fe) associated with colloidal material [*Baskaran et al.*, 1992; *Honeyman and Santschi*, 1991; *Hurst and Bruland*, 2007; *Moran and Buesseler*, 1993]. As discussed above, removal processes of dFe are important at elevated particulate concentrations, thus it is likely that scavenging of Fe proceeds via 'colloidal pumping' pathway for dFe supplied from oxic shelf margins, leading to an asymptotic relationship between dFe and TdFe-dFe (Fig. 4.8).

4.2.5 Seasonal iron depletion in the surface mixed layer

In surface waters, dFe is predominantly in the soluble phase as indicated by the negative y-axis intercept of the dFe/cFe plot (-0.10 to -0.22 nM; Fig. 4.9). Transition from cFe dominated bottom waters to sFe dominated surface waters is consistent with observations in shelf waters of the central Celtic Sea [*Birchill et al.*, 2017] and stratified Bering Sea [*Hurst et al.*, 2010]. In addition to removal of cFe through particle formation,
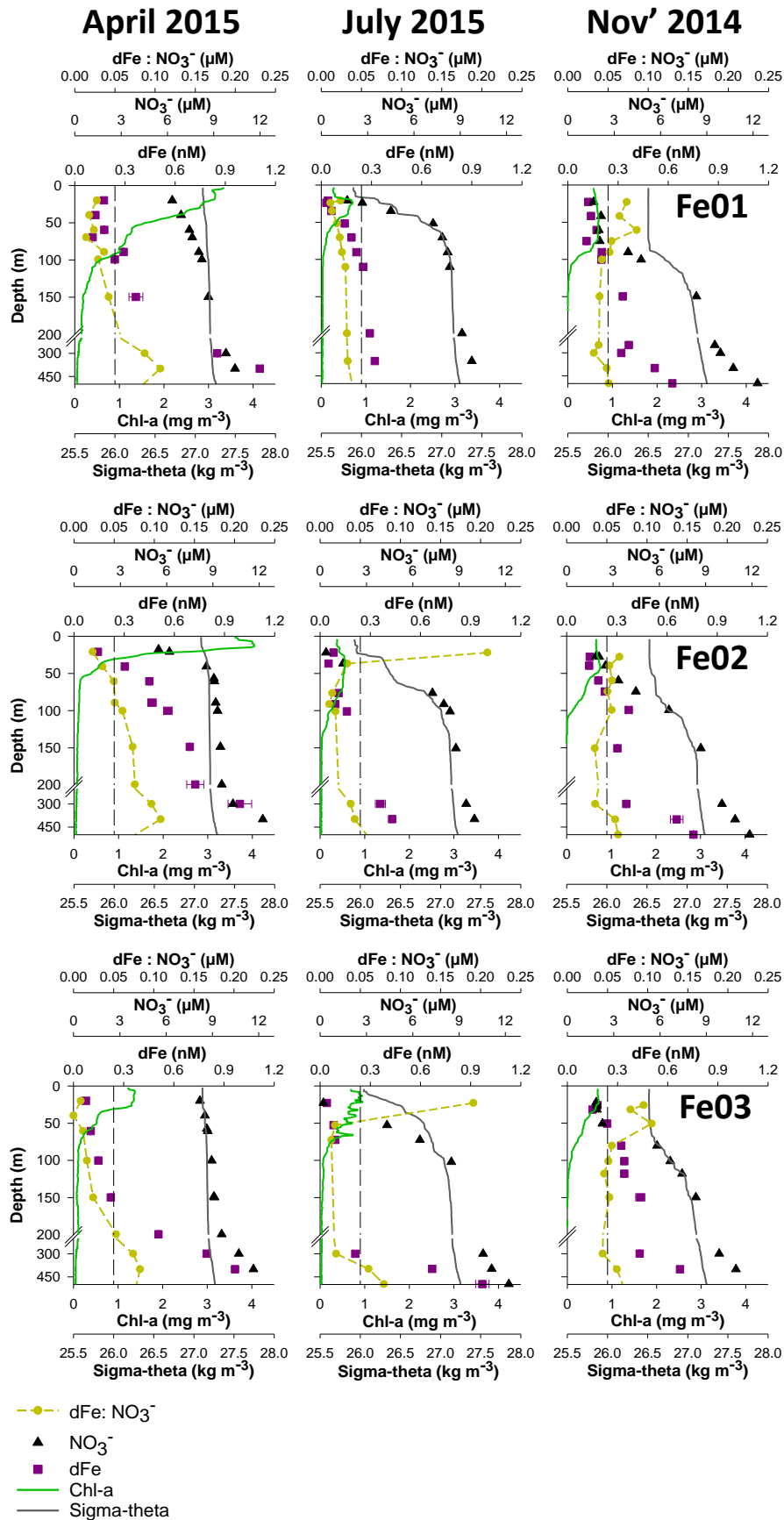
Figure 4-10- Seasonal cycling in surface waters of stations Fe01 (**top**) Fe02 (**middle**) and Fe03 (**bottom**). Black dashed line denotes 0.05 dFe:NO₃⁻, the lower limit observed in cultured phytoplankton [*Ho et al.*, 2003; *Sunda and Huntsman*, 1995].

numerous processes have been identified to facilitate the dissolution of cFe, and hence production of sFe, in surface waters. These include grazing [*Barbeau and Moffett*, 2000; *Barbeau et al.*, 1996; *Schmidt et al.*, 2016], light/ligand interaction [*Barbeau et al.*, 2001; *Borer et al.*, 2005; *Sulzberger et al.*, 1989; *Wells et al.*, 1991] and slower thermal dissolution [*Rich and Morel*, 1990]. It is also noted that direct biological uptake of colloidal/particulate Fe has been demonstrated for some phytoplankton species [*Chen et al.*, 2003; *Chen and Wang*, 2001; *Nodwell and Price*, 2001; *Rubin et al.*, 2011]. The maintenance of sFe in surface waters through processes such as grazing, light ligand interaction and uptake of colloidal material is broadly consistent with biology influencing the nutritional state of Fe retained in the SML [*Strzepek et al.*, 2005; *Wells and Mayer*, 1991b].

By sampling during spring, summer and autumn it was possible to capture the seasonality of the physico-chemical speciation of Fe in these temperate surface waters. Here the focus is on stations Fe01-03 (Fig. 4.10), the furthest stations from the shelf slope, but still within 50 km of the 200 m isobath. At these stations remarkably low summer surface SML dFe concentrations were observed. In April 2015, the onset of stratification triggered a large spring phytoplankton bloom. At the time of sampling, the bloom was more developed at stations Fe01 and Fe02, as evidenced by the high chl-*a* concentrations > 3.4 mg m^{-3} and nutrient depletion in surface waters (20 m) NO_3^- (5.47-6.31 μM), compared with station Fe03 where 0.7 mg m^{-3} chl-*a* and 8.12 μM NO_3^- were observed. Dissolved Fe concentrations in the upper 50 m of these stations ranged from 0.07 - 0.30 nM, resulting in dFe:NO_3^- ratios < 0.05 (nM:μM), the lower limit observed in phytoplankton cultured in nutrient replete environments [*Ho et al.*, 2003; *Sunda and Huntsman*, 1995]. This suggests that dFe availability can impact the phytoplankton

community structure during the spring bloom. Despite the apparently unfavourable dFe:NO_3^- ratios observed during April 2015, complete NO_3^- draw down occurred in surface waters by July 2015; samples collected from the ship's underway supply ($\approx$ 5 m) contained undetectable (< 0.02 µM) NO_3^- concentrations. Explanations for this include luxury uptake of dFe by phytoplankton during the spring bloom [*Sunda and Huntsman*, 1995], enhanced Fe over N recycling by zooplankton [*Giering et al.*, 2012] and access to the labile particulate fraction [*Chase et al.*, 2005a; *Hurst et al.*, 2010; *Milne et al.*, 2017]. The concentration of LpFe at stations Fe01-03 (including Fe15) at 20 m was 0.53 ± 0.11 nM in April 2015, which decreased to 0.07-0.18 nM in July 2015.

During summer stratification, the majority of new production occurs at the sub surface chl-*a* maximum (SCM), where phytoplankton accesses a diapycnal flux of NO_3^-. At the SCM, concentrations of dFe and NO_3^- were 0.03-0.16 nM and 0.2-8.4 µM respectively (Table 4.1), resulting in very low dFe:NO_3^- ratios (minimum 0.01 nM: µM). At low light intensities, typical of the SCM, the Fe demand of phytoplankton increases to facilitate the production of photosynthetic iron based redox proteins [*Sunda and Huntsman*, 1997]. Accordingly, dFe and light co-limitation has been observed at the SCM over the shelf slope in the Californian Bight, whereby addition of dFe enhanced diatom growth [*Hopkinson and Barbeau*, 2008]. The concentrations of dFe observed at the SCM in the Celtic Sea were generally lower than observed in the Californian Bight, with NO_3^- concentrations being comparable (Table 4.1). Particulate Fe was unlikely to represent a large additional source of Fe to phytoplankton as LpFe concentrations at the SCM were also drawn down to < 0.2 nM in July 2015 (Table 4.1).

The minimum concentration of Si at the SCM was noticeably different over the Celtic Sea shelf slope relative to the Californian Bight (Table 4.1). In the Celtic Sea, a

vertical gradient in Si concentrations was observed (Fig. 4.11), that included

concentrations < 2 µM in the SCM, the concentration that is considered a threshold for

diatom growth [*Egge and Aksnes*, 1992]. Additionally, previous work has shown a similar

surface depletion of other trace metals (Cu, Pb, Cd, Ni) in the SML over the Celtic Sea

shelf slope during summer months [*Cotté-Krief et al.*, 2002]. Phosphate was also

seasonally drawn down in surface waters, however summer N:P ratios were far below

(minimum 0.9) Redfield values (15 - 16) [*Redfield*, 1958]. Therefore, the nutrient

(including Fe) concentrations measured in the upper water column described an

oligotrophic environment during summer stratification. Consequently, it is postulated

that the phytoplankton community structure was seasonally sensitive to changes in the

availability of NO_3^-, Si, Fe, other micronutrients and light, with the potential for Fe stress

being greatest at the SCM. Broadly, smaller phytoplankton would be expected to have

a competitive advantage under such conditions due to increased surface area to volume

ratio aiding uptake of nutrients [*Lis et al.*, 2015; *Moore et al.*, 2013a]. Indeed, at station

Fe01-03 in July 2015, 98.38 ± 0.01 % (mean ± SD) of cells counted by flow cytometry

were either S*ynechococcus* or picoeukaryotes [*Tarran et al.*, in prep].

Table 4-1- The range of concentrations observed at the summer sub surface chlorophyll
maximum. The depth range was decided upon based on the chlorophyll-*a* profile. CB=
Californian Bight, data from *Hopkinson and Barbeau* [2008].

Station	Depth (m)	dFe (nM)	TdFe-dFe (nM)	NO_3^- (µM)	LpFe (nM)	Si (µM)
Fe01	21-51	0.03-0.14	0.14-0.29	1.7-7.2	0.10 ± 0.01	0.6-2.2
Fe02	23-101	0.05-0.16	0.13-0.20	0.4-8.4	0.13 ± 0.00	0.3-2.8
Fe03	22-73	0.04-0.09	0.28-0.84	0.2-6.6	0.17 ± 0.00	0.3-1.9
CB	45-78	0.11-0.27	nd	0.7-6.3	nd	2.3-5.2

nd= not determined
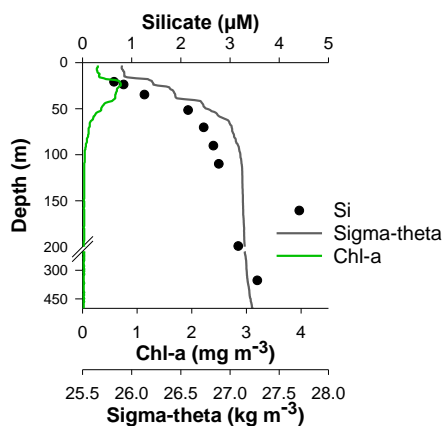
Figure 4-12- Example of silicate profile for the upper 500 m. Station Fe01, July 2015.
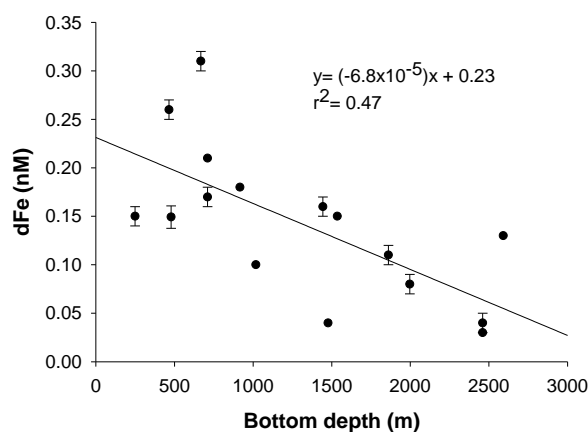
Figure 4-11- Near surface (< 28 m) dissolved concentrations plotted against station bottom depth. July 2015.

During stratified periods, internal tides enhance the vertical supply of NO_3^- to a narrow band of water overlying the Celtic Sea shelf break resulting in increased primary productivity and promoting the growth of larger (> 10 µm) eukaryotic phytoplankton [*Holligan and Groom*, 1986; *Sharples et al.*, 2007]. Here, a decrease in near surface dFe concentration with station bottom depth was observed in July 2015 (Fig. 4.12), which is attributed to enhanced vertical mixing over the shelf break. Therefore, the assertion is that the increase in productivity and associated change in community structure

observed over the shelf break is also driven by enhanced vertical supply of dFe to surface waters. Conversely, the degree of seasonal Fe stress likely increases as the strength of vertical mixing decreases with distance from the shelf break.

Seasonal stratification persisted to November (2014) (Fig. 4.10), but, convective overturning had deepened the SML relative to summer conditions. Entrainment of nutrients increased dFe and NO_3^- concentrations in the SML, similar to what has been observed in the central Celtic Sea [*Birchill et al.*, 2017; *Wihsgott et al.*, in prep]. Under the conditions of a deepening mixed layer it is likely that light was the limiting factor regulating phytoplankton growth at this point of the season.

4.2.6 Remineralisation controls the distribution of dFe in East North Atlantic Central Water over the outer shelf

Apparent oxygen utilisation (AOU) represents the oxygen consumed during the respiration of organic matter since the water was last in contact with the atmosphere, assuming isolation of a water mass from the atmosphere and that the water mass was saturated with oxygen when last in contact with the atmosphere. In contrast, the dFe concentration represents the net result of preformed dFe plus dFe supplied from remineralisation and other external sources (e.g. sediment resuspension, atmospheric) minus any loss to the particulate phase due to scavenging and oxidative removal [*Tagliabue et al.*, 2017] and is described by the following equation:

$$Fe_{total} = Fe_{preformed} + Fe_{regenerated} + Fe_{external\ inputs} - Fe_{scavenged}$$

Hence, observed dFe:AOU relationships have been used to infer the net rate of dFe input due to remineralisation in the North Atlantic, where the intercept indicates the preformed dFe concentration [*Hatta et al.*, 2015; *Rijkenberg et al.*, 2014; *Ussher et al.*, 2013]. Here strong and significant dFe:AOU relationships were identified in sub-surface

(upper 600m) ENACW at stations furthest from the shelf break (Fe01-03) in November 2014 (Table 4.2). This indicated that unlike near slope waters, remineralisation of organic material exerted a primary control over dFe concentrations in these waters. Previous work, indicates that the flux of particulate material is dominated (80-100%) by biogenic material at 600 m over the mid to outer Celtic Sea shelf slope ($\geq$ 1440 m bottom depth) [*Antia et al.*, 1999] and that partial remineralisation of particulate organic matter is known to release dFe and Fe binding ligands to the water column [*Boyd et al.*, 2010]. Moreover, light Fe isotope signals between 200-1300 m in the Southern Ocean are considered to result from remineralisation dominating the dFe inventory at intermediate depths [*Abadie et al.*, 2017].

Table 4-2- The linear relationship between dFe and apparent oxygen utilisation (AOU) identified in the upper water column in Nov' 2014 over the outer shelf slope of transect 1. Depth range is the distance over which the regression was calculated, determined as the shallowest sampling depth below the surface mixed layer to the depth that the linear relationship remained apparent. Pearson's correlation used to determine p value.

Station	Bottom depth (m)	Depth range (m)	dFe (nM) / O_2 (μM)	dFe (nM) range	dFe (nM) preformed	r^2	p	*n*
Fe01	2455	90-600	0.012	0.20-0.75	0.067	0.95	<0.001	8
Fe02	2003	59-599	0.014	0.29-0.87	0.073	0.87	<0.001	9
Fe03	1500	51-501	0.017	0.24-0.82	0.032	0.88	<0.001	9
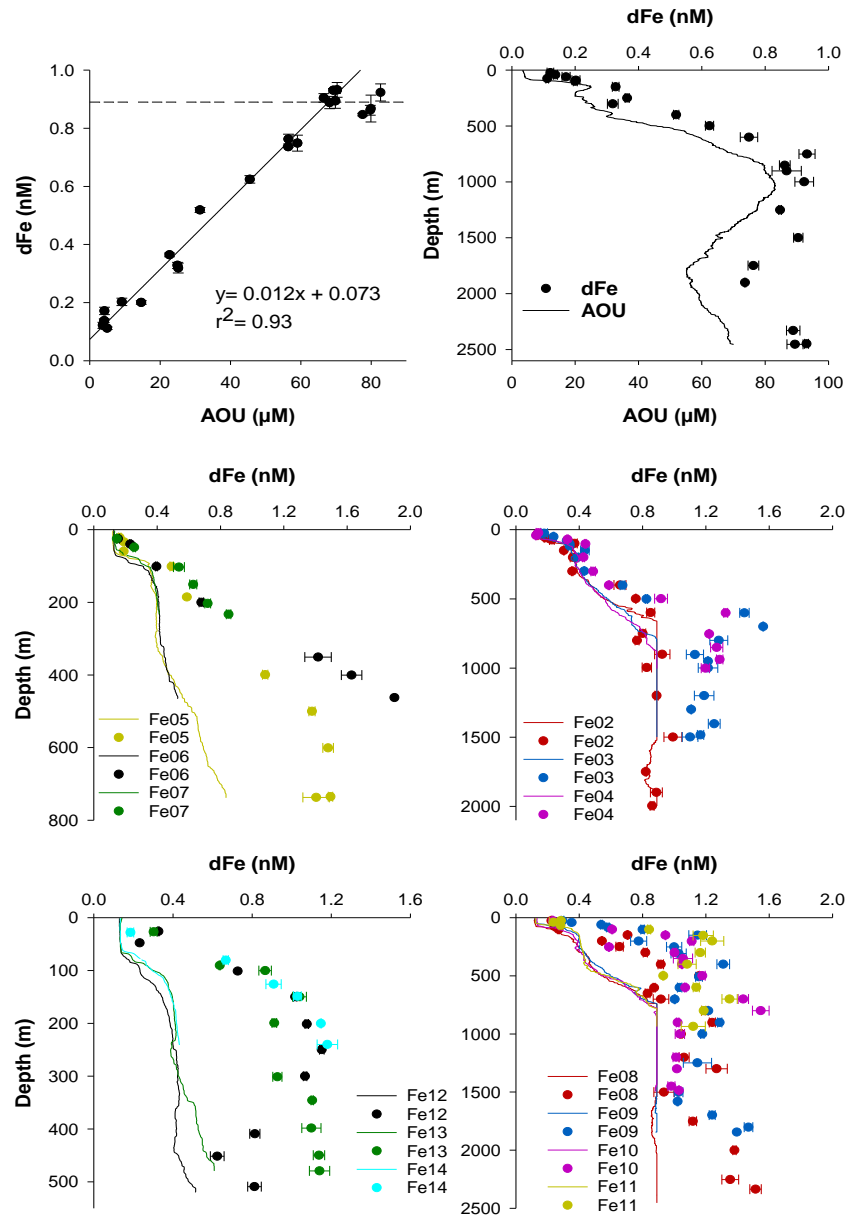
Figure 4-13- Estimating the contribution of 'remineralised dFe' compared to the observed dFe concentration. This was achieved by using the relationship between dFe and AOU observed at station Fe01 in Nov' 2014 (top), a linear relationship was evident up to 67 µM AOU, >67 µM dFe plateaued at 0.89 ± 0.05 nM. Middle- Transect 1 upper shelf stations (left) and outer shelf stations (right). Bottom-Transect 2 upper shelf stations (left) and outer shelf stations (right). AOU converted to 'remineralised dFe' is indicated by solid lines. Dots represent the measured dFe concentrations. Plots include Nov' 2014 data only.

The preformed dFe concentration reported here for ENACW (0.06 ± 0.02 nM dFe;

Table 4.2) is lower than that reported by *Hatta et al.* [2015] for North Atlantic Central

Water (0.17 ± 0.02 nM dFe). This difference is driven by a dFe:AOU gradient that is ≈3 times steeper over the Celtic Sea shelf slope than observed in the open Atlantic Ocean [*Hatta et al.*, 2015; *Ussher et al.*, 2013]. The steeper gradient could be interpreted as an increased Fe content of organic matter formed in waters overlying the shelf break, or a slower scavenging rate of remineralised dFe. However, this would assume a closed one dimensional system, thus precluding any additional input of dFe or oxygen that would act to steepen the dFe:AOU gradient.

In November 2014, the dFe profile at station Fe01 displayed typical open ocean characteristics, with depletion in surface waters and sub-nanomolar concentrations (≤ 0.93 nM) at depth (Fig. 4.13). This is typical of corresponding water masses in the adjacent North East Atlantic waters not affected by the shelf slope [0.23 - 0.93 nM; *Laës et al.*, 2003]. Moreover, the concentration of TdFe-dFe throughout the water column profile, with the exception of the bottom two samples in the benthic boundary layer, contained TdFe-dFe concentrations of 4.5 ± 2.8 nM (*n*=12) (Fig. 4.4). This is slightly elevated, but of the same order of magnitude as values reported for the open Atlantic Ocean away from margin influences [*Milne et al.*, 2017; *Revels et al.*, 2015; *Wu and Luther*, 1994].

The linear dFe:AOU gradient at Fe01 in November 2014 persisted to a dFe concentration of 0.90 ± 0.015 nM and AOU of 67 μM (Fig. 4.13). The extended dFe:AOU relationship incorporates MOW at ≈ 1800 m depth; thus it may be fortuitous that the preformed dFe signal and AOU of MOW fit the ENACW linear relationship. Between AOU values of 67 - 83 μM, dFe concentrations plateaued at 0.89 ± 0.03 nM (*n*= 8) (Fig. 4.13) suggesting that a solubility limit and/or that other processes determine the dFe concentration at depth, such as interaction with the particulate phase [*Abadie et al.*,

2017; *Milne et al.*, 2017]. By using Fe01 as a background/oceanic station for November 2014, the relationship between dFe and AOU is used to estimate the amount of 'remineralised dFe' at other stations over the shelf slope (Fig. 4.13). At station Fe02 94 ± 15 % of the dFe is accounted for by 'remineralised dFe', whilst at station Fe03 nearer the shelf slope this drops to 70 ± 12 % at depths below ENACW. At all other stations closer to the shelf, the significance of shelf sediments as an external source of dFe increases, such that as little as 28% of dFe can be accounted for by 'remineralisation'.

4.2.7 Transport of dFe and TdFe-dFe in intermediate nepheloid layers

The waters over the shelf slope are generally elevated in dFe and TdFe-dFe (Fig. 4.4, 4.5, 4.6). As discussed above, waters overlying the shelf break are expected to be regions of high scavenging. Therefore, for efficient transport of dFe and LpFe to occur from these regions, a strong physical transport mechanism is required [*Croot and Hunter*, 1998; *Hong and Kester*, 1986], combined with slow sinking particles. Over the Celtic Sea shelf slope distinctive INLs enriched in cFe, dFe and TdFe-dFe were observed in all seasons, providing an ever present conduit to the adjacent ocean. The two most Fe enriched INLs were found in transect 3 at stations Fe16 and Fe17 in April 2015 (Fig. 4.14a). It should be noted that the high beam attenuation values in surface waters are driven by enhanced particle formation due to primary production and not sediment input. A deeper (σ_T= 27.78 - 27.29 kg m^{-3}, 1500 m) INL was identified at both Fe16 and Fe17. The distance between stations Fe17 and Fe16 is 12.3 km; over this distance the concentration of TdFe-dFe decreased from 315 ± 1.8 to 66.4 ± 0.5 nM, corresponding with a decrease in dFe of 3.25 ± 0.16 to 2.02 ± 0.14 nM. A shallower (σ_T= 27.589 kg m^{-3}, 1051 m) INL was identified only at Fe17, with a concentration of dFe and TdFe-dFe of 2.82 ± 0.007 and 78.5 ± 3.1 nM respectively. Similarly, in November 2014, elevated beam

attenuation and TdFe-dFe concentrations (56.2 ± 1.1 nM, *n*=3) were observed between

σ_T = 27.283 - 27.355 kg m^{-3} at stations Fe03 and Fe04 (Transect 1) in November 2014

(Fig. 4.14b). This was associated with elevated dFe concentrations (1.44 ± 0.12 nM, *n*=3).
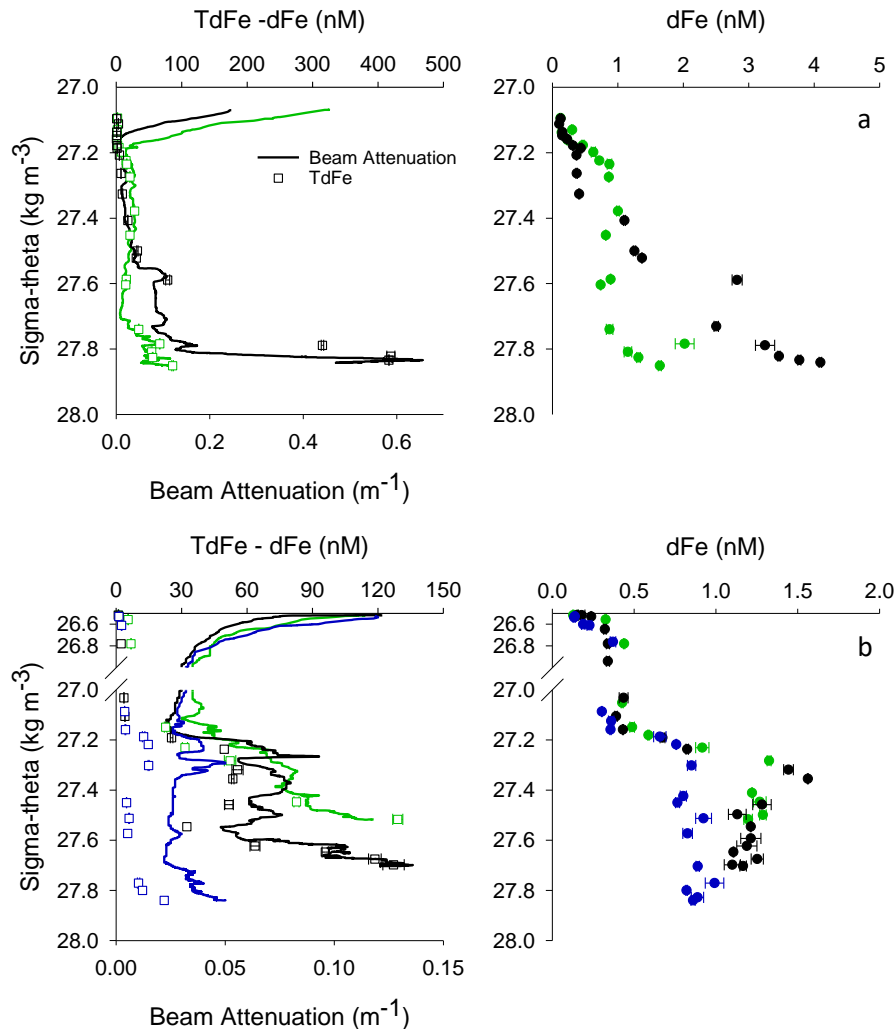
Figure 4-14- -Examples of iron enriched intermediate nepheloid layers .

a- INLs observed at stations Fe16 (black, bottom depth 2500 m) and Fe17 (green, bottom depth 2000 m) sampled in April 2015. INL at σ_T= 27.589 (Fe17) at 1051 m, INL at σ_T= 27.789 (Fe17) at 1552 m and at σ_T= 27.784 (Fe16) at 1500 m.

b- INL observed at stations Fe02 (blue, bottom depth 2000 m), Fe03 (black, bottom depth 1500 m) and Fe04 (green, bottom depth 1000 m) sampled in November 2014. INL at σ_T= 27.302 at 599 m (Fe02), INL at σ_T= 27.319 and 27.355 at 601 and 700 m (Fe03) and INL at σ_T= 27.283 at 601 m (Fe04). Note change in scale of dFe and TdFe-dFe.

At station Fe02 (22.9-29.0 km from Fe03 and Fe04) at σ_T = 27.302 kg m^{-3} the concentration of TdFe-dFe was significantly reduced, but remained elevated above background at 15.7 ± 0.3 nM, indicating that lateral transport of particulate material had occurred, which was also evident in the beam attenuation profile. The corresponding dFe concentration was also reduced to 0.85 ± 0.025 nM, equivalent to typical oceanic concentrations for the North East Atlantic [*Laës et al.*, 2003].

Broadly, in the INLs observed the concentration of particulate and dissolved Fe declined over relatively short distances (10's km) from the shelf slope to near
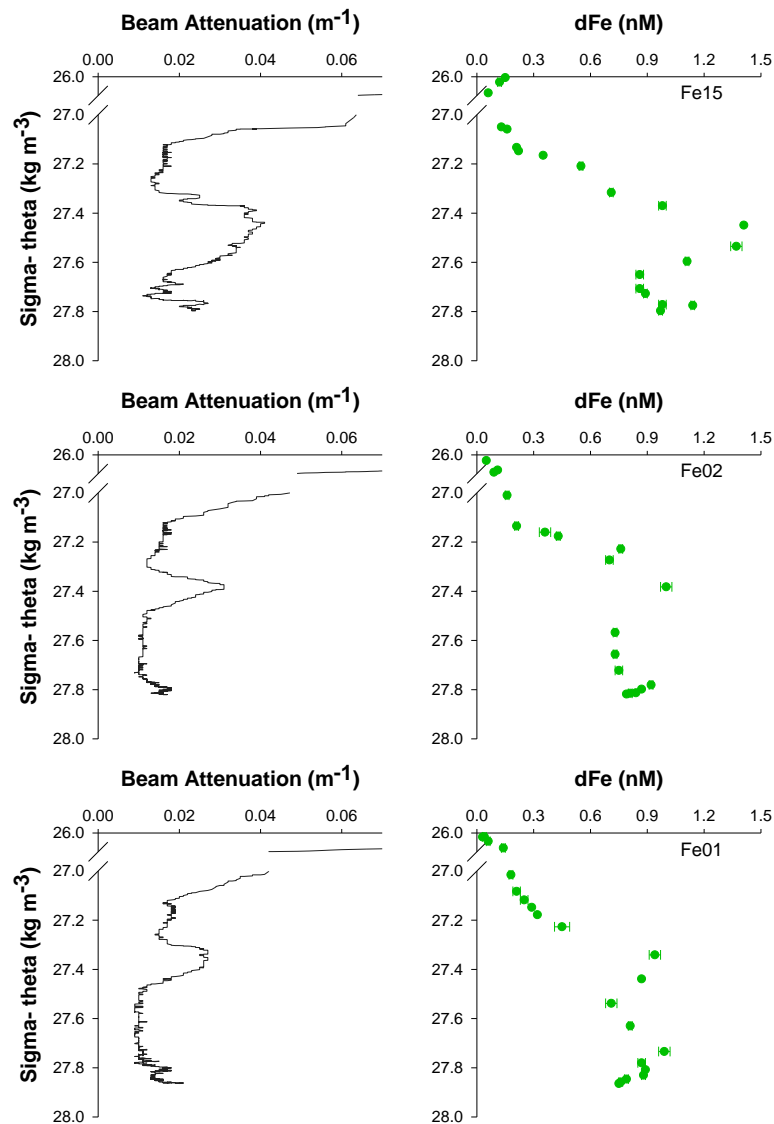
Figure 4-15- A distinctive intermediate nepheloid layer observed at station Fe15, 02, and 01 in July 2015.

background levels. This suggests that the spatial extent of lateral transport from the Celtic Sea shelf slope is limited to 10's of km, rather than 100-1000's km as observed elsewhere where the dominant direction of lateral advection is offshelf [e.g. *Lam and Bishop*, 2008; *Noble et al.*, 2012]. However, there was evidence of elevated dFe and TdFe-dFe concentrations at station Fe01, the most oceanic station located ≈ 50 km from the 200 m isobath in April 2015 (max dFe 1.29 ± 0.043 nM; max TdFe 21.1 ± 0.5 nM; Fig. 4.4). This may be related to seasonal changes in the strength of the along slope current, which weakens and reverses direction from February to April [*Pingree and Le Cann*, 1990] and therefore may allow greater lateral transport. Additionally, in July 2015, a distinctive INL was observed over the outer slope (≥ 1500 m bottom depth) that had emanated from the shelf slope. Maximum dFe concentrations of 1.31-1.41 nM were observed at station Fe15; in comparison at station Fe01 this was 0.87 – 0.94 nM (Fig. 4.15). Moreover, as there is a significant along slope current over the shelf slope the possibility of northwards transport cannot be excluded, though this would occur in particle rich water where the scavenging rate is likely high. Therefore, this study supports the view that sediment derived Fe is important in the wider marine Fe cycle, but that for sedimentary derived Fe to influence the open ocean, both a sediment source and a strong physical transport mechanism, such as INLs, are required. Additionally, given that 20 ± 14 % of TdFe-dFe was typically labile, the transport of LpFe likely dominates the supply of bioavailable Fe from shelf slope sediments [*Milne et al.*, 2017].

4.2.8 Redox cycling over the Celtic Sea shelf slope

Iron in seawater is present as Fe(III) and Fe(II) redox species, with Fe(II) more soluble but thermodynamically unstable in oxic seawater [*Millero and Sotolongo*, 1989; *Millero et al.*, 1987]. Oxidation half-lives of Fe(II) in oxic seawater range from minutes to days [*Klar et al.*, 2017; *Santana-Casiano et al.*, 2005; *Sarthou et al.*, 2011; *Ussher et al.*, 2007], resulting in Fe(III) being the dominant oxidation state. The bioavailability of iron is related to its physico-chemical speciation. As a reductive Fe uptake strategy has been shown to be utilised by eukaryotic and prokaryotic phytoplankton [*Shaked and Lis*, 2012], Fe(II) is considered to be more bioavailable [*Sunda et al.*, 2001]. Moreover, reduction processes will act to maintain Fe in more labile phases as under oxic conditions inorganic Fe(III) phases progressively hydrolyse and crystallise into forms with ever decreasing Gibbs free energies of formation [*Ussher et al.*, 2004; *Wells and Mayer*, 1991a].
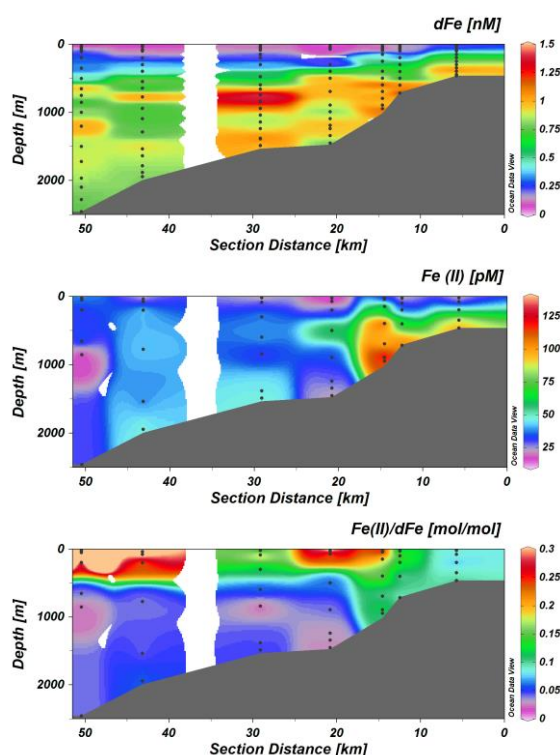
Figure 4-16- Shelf break (transect 1) sections of dissolved iron, dissolved Fe(II) and dFe(II)/dFe (as labelled) for July 2015.

The use of Fe(III) as the terminal electron acceptor during the respiration of organic matter by bacteria leads to a build-up of Fe(II) in interstitial pore waters [*Froelich et al.*, 1979]. This can be fluxed to the overlying water column by diffusion and sediment resuspension. In oxygenated waters, oxidation to Fe(III) and subsequent scavenging/precipitation at the sediment water interface limit the magnitude of this flux [*Dale et al.*, 2015], though indirect evidence suggests that the efficiency of the 'oxidative trap' may be reduced by the stabilising effect of Fe(II) binding ligands [*Klar et al.*, 2017; *Ussher et al.*, 2007]. Here increased Fe(II) concentrations (maximum 134 pM) were observed at near bottom waters over the upper shelf sediments ($\leq$ 1017 m bottom depth) that contributed 9-16% of dFe in July 2015 (Fig. 4.16). At deeper stations concentrations of up to 49 pM were observed over shelf sediments contributing < 6% of the total dFe pool (Fig. 16). The distribution of Fe(II), and the proportions of dFe present as Fe(II) observed are similar to previous measurements over the Bay of Biscay shelf slope [*Ussher et al.*, 2007].

Both the concentration of Fe(II) and the proportion of Fe(II) as dFe present over the outer slope, is consistent with background values measured in sub-surface North Atlantic waters using similar sampling and analytical approaches [*Sedwick et al.*, 2015], suggesting dFe input resulting from dissimilatory Fe(III) reduction is weaker/negligible over the outer shelf. This assertion is strengthened by combining the proposed causal relationship for oxic water column conditions, between benthic carbon oxidation rates and sedimentary diffusive dFe fluxes [*Elrod et al.*, 2004], with benthic carbon oxidation rates for Celtic Sea shelf slope sediments [*Lohse et al.*, 1998]. The resulting estimate suggests a relatively modest net diffusive dFe flux of 0.5 − 2.5 µmol dFe m^{-2} d^{-1} that decreases with water column depth (200 - 1440 m). At deeper stations (> 1440 m)

respiration of organic carbon was almost entirely (97-99%) aerobic [*Lohse et al.*, 1998].

The decrease in anaerobic respiration is linked to productivity in overlying waters. Over

the upper slope enhanced productivity is supported by large vertical nutrient fluxes,

[*Holligan and Groom*, 1986; *Huthnance et al.*, 2001; *Pingree*, 1984; *Sharples et al.*, 2009],

which, coupled with a shallower water column, supplies organic carbon to the benthos

at a greater rate than over the outer shelf slope [*van Weering et al.*, 1998].

As discussed above evidence of sediment and pore water resuspension events

resulting in elevated dFe are seen to depths of 2500 m (max depth of sampling) (Fig. 4.3,

4.4, 4.5). It is advocated that resuspension of sediments and pore waters from the upper

shelf slope are likely to contain more labile, and potentially bioavailable, Fe phases as a

result of recent redox processing. The leachable particulate fraction accesses both

readily reducible hydroxide phases and intra-cellular Fe [*Berger et al.*, 2008] and thus

the LpFe/LpAl ratio is always in excess of the crustal abundance ratio. However, a

systematic increase in the Fe:Al ratio of the leachable fraction was observed in bottom

waters at stations shallower than 1500 m (Table 4.3), consistent with sediments

resuspended from upper slope sediments containing more labile phases. Moreover, in

shelf sediments underlying regions of high productivity, dissimilatory Fe reduction

results in pore water dFe being almost entirely aqueous Fe(II) [*Klar et al.*, 2017], which

when resuspended into seawater will rapidly attach to, or form, colloids [*Honeyman and*

Santschi, 1991]. In contrast, where the organic carbon flux is smaller, resulting in

oxygenated near surface pore waters, non-reductive dissolution is thought to produce

colloidal mineral phases such as goethite [*Homoky et al.*, 2011]. The bioavailability of

mineral colloidal iron phases decreases with ageing [*Yoshida et al.*, 2006]. Therefore, it

is likely that nepheloid layers resulting from resuspension of upper shelf sediments

result in freshly formed colloidal Fe that is subsequently more bioavailable. Importantly, as the winter mixing depth is around 500 m, there is potential for Fe in the INL from the upper water column to reach surface waters fuel primary production. In contrast, deeper INL will be subject to longer term ocean circulation pathways and thus Fe would need to be stabilised for decades or more to reach surface waters. This ageing would reduce the bioavailable/leachable fraction.

Table 4-3- The LpFe/LpAl ratio of bottom water samples. nd= not determined.

Sampling period	Station	LpFe (nM)	LpFe/LpAl	Bottom depth (m)
November 2014	Fe01	3.20 ± 0.02	1.68	2500
	Fe02	2.73 ± 0.01	1.48	2000
	Fe03	22.14 ± 0.16	2.28	1500
	Fe04	10.74 ± 0.11	2.21	1000
	Fe05	12.08 ± 0.05	2.32	750
	Fe06	27.70 ± 0.09	2.38	500
	Fe07	5.88 ± 0.01	2.08	250
April 2015	Fe01	4.99 ± 0.04	1.58	2500
	Fe02	2.44 ± 0.02	1.52	2000
	Fe15	6.42 ± 0.05	2.14	1500
	Fe03	10.64 ± 0.04	2.16	1500
	Fe04	11.51 ± 0.22	2.26	1000
	Fe05	10.26 ± 0.03	2.62	750
	Fe06	7.57 ± 0.02	2.15	500
July 2015	Fe01	2.06 ± 0.01	1.27	2500
	Fe02	2.14 ± 0.01	1.27	2000
	Fe15	2.59 ± 0.01	1.54	1500
	Fe03	5.53 ± 0.01	1.65	1500
	Fe04	7.62 ± 0.00	1.74	1000
	Fe05	6.83 ± 0.04	1.86	750
	Fe06	nd	nd	500

In surface waters, the proportion of dFe present as Fe(II) increased (Fig. 4.16); in some instances dFe was entirely present as Fe(II). However, the exact percentage should be interpreted with caution as the concentrations of dFe and Fe(II) were as low as 30 pM and therefore approaching the limit of detection of both analytical systems.

Nevertheless, photochemical reduction of Fe(III) bound to organic ligands is known to occur is seawater, providing a mechanism for the production of Fe(II) in surface waters [*Barbeau*, 2006], and it is consistent with biological processing maintaining dFe in the soluble phase in the SML.

4.3 Conclusions

In surface waters of the Celtic Sea shelf slope dFe was maintained predominantly in the soluble fraction, consistent with biological processing influencing the physico-chemical speciation of iron retained in the SML, and loss of colloids via 'colloidal pumping'. Despite their proximity to the continental shelf slope, surface waters within 50 km of the 200 m isobath are seasonally deplete in bioavailable Fe, including dFe concentrations as low as 30 pM during summer. During the summer stratification, restricted vertical mixing resulted in nutrient conditions in the SML described an oligotrophic environment and evidence is given that co-limitation between availability of Fe and other macronutrients shapes the phytoplankton community structure. In particular, conditions at the SCM are comparable with previous studies where Fe/light co-limitation has been observed; suggesting the degree of Fe limitation may increase below surface waters. As discussed in section 3.2.2, a more rigorous assessment of nutrient stoichiometry should be made by including all available N sources (e.g. organic nitrogen).

Below the SML on the shelf slope, both the vertical flux of remineralising particulate material from the SML and lateral advection of shelf slope particulate material contribute to the Fe inventory. The remineralisation signal was generally masked by the much larger lateral flux of Fe from the shelf slope, except at the stations furthest (50 km) from the shelf slope. Despite the flux from the shelf slope, the

concentrations of dissolved and particulate Fe were both attenuated over relatively short distances (10's km) from the shelf break, indicating that effective physical transport mechanisms are required to deliver shelf sediment derived Fe far out to the open ocean.

In this study, lateral transport of Fe from the shelf slope occurred in distinct INLs during all sampling seasons (spring, summer, autumn), and thus provided a persistent conduit for the transport of Fe to the adjacent N.E. Atlantic. Determination of the physico-chemical speciation of Fe supplied from oxic margin sediments revealed that the concentration TdFe-dFe>>>LpFe>>cFe>sFe. As dFe was predominantly (60-90%) present in the colloidal form, 'colloidal pumping' likely represents an important removal pathway of dFe to the particulate phase and further investigation into scavenging processes are needed. The majority of Fe export from oxic margins occurs as LpFe, which, if advected, may act to buffer the deep ocean dFe inventory [*Abadie et al.*, 2017; *Milne et al.*, 2017]. Additionally, it is postulated that dFe supplied from upper shelf sediment and pore waters is in a more bioavailable/labile form due to recent 'redox processing' and recycling.

Chapter 5 - The Hebridean Shelf- the eastern extent of seasonal iron limitation in the sub-Arctic North Atlantic

The research presented in this chapter is being prepared for submission to *Nature Communications,* with additional total dissolvable iron and phytoplankton count data to be incorporated.

5.0 Introduction

It is well established that the availability of Fe regulates the growth of phytoplankton in the high nutrient low chlorophyll (HNLC) regions of the Southern Ocean, Eastern Equatorial Pacific and Sub-Arctic North Pacific [*Boyd et al.*, 2007]. Despite the Sub-Arctic North Atlantic receiving a similar amount of dust to that of Sub-Arctic Pacific [*Jickells et al.*, 2005; *Measures et al.*, 2008], it is not considered a classical HNLC region as there is enough Fe available to sustain a productive spring bloom [*Martin et al.*, 1993; *Ryan-Keogh et al.*, 2013]. However, repeated observations of residual NO_3^- in high latitude North Atlantic surface waters, post spring bloom, indicate a restriction on the efficiency of the biological carbon pump [*Nielsdóttir et al.*, 2009; *Ryan-Keogh et al.*, 2013; *Sanders et al.*, 2005].

Dissolved Fe measurements of 0.02-0.22 nM in high latitude North Atlantic surface waters indicate that this is not an Fe replete region [*Martin et al.*, 1993; *Measures et al.*, 2008; *Nielsdóttir et al.*, 2009; *Painter et al.*, 2014]. Winter vertical mixing in the Iceland Basin is estimated to supply enough dFe to surface waters to facilitate drawdown of available silicate (Si), but not NO_3^- [*Forryan et al.*, 2012; *Painter et al.*, 2014]. Therefore, Si limitation is expected to limit the extent of diatom growth during the spring bloom [*Henson et al.*, 2006; *Sieracki et al.*, 1993] and community wide Fe limitation to prevail post bloom. This is consistent with observations that phytoplankton become increasingly Fe stressed as the spring bloom progresses [*Ryan-Keogh et al.*, 2013]. During summer, Fe bioassay experiments [*Nielsdóttir et al.*, 2009] and responses to volcanic Fe inputs [*Achterberg et al.*, 2013], indicate that Fe availability limits not just diatom growth but also the wider summer phytoplankton community. Though process

studies have been conducted the spatial extent of this seasonal Fe limitation has not been ascertained.

In this study the nutrient stoichiometry (dFe:NO_3^-:Si:PO_4^{3-}) of waters on, and adjacent to, the Hebridean and Malin shelf (hereafter Hebridean shelf) were determined during Autumn 2014. Despite the proximity to shelf sediments, which represent a large source of Fe to the overlying water column [e.g. *Dale et al.*, 2015; *Elrod et al.*, 2004; *Klar et al.*, 2017], the results show that the conditions leading to seasonal Fe limitation observed in the Iceland and Irminger Basins of the high latitude North Atlantic persist up to, and in some instances beyond, the Hebridean shelf break.

5.0.1 Oceanographic setting

A map of the sampling area and major currents is displayed in Fig. 5.1. Adjacent to the Hebridean shelf is the Rockall Trough, which is separated from the Iceland Basin to the west by the Rockall Plateau and Hatton Bank, and the Nordic Seas to the north by the Wyville Thomson Ridge (500m). Surface water (upper 700m) in the Rockall Trough predominantly originates from the south in the Bay of Biscay, and to a lesser extent the northwest, of the basin [*Holliday et al.*, 2000; *Johnson et al.*, 2013]. The depth of winter convective overturning shoals with decreasing latitude, reducing the replenishment of surface water nutrients associated from mixing with intermediate water masses [*Louanchi and Najjar*, 2000]. Consequently, waters originating from south of the Rockall Trough bring less nutrients than waters from the northwest, which are modified by interaction with nutrient rich subpolar waters in the Iceland Basin [*Johnson et al.*, 2013].
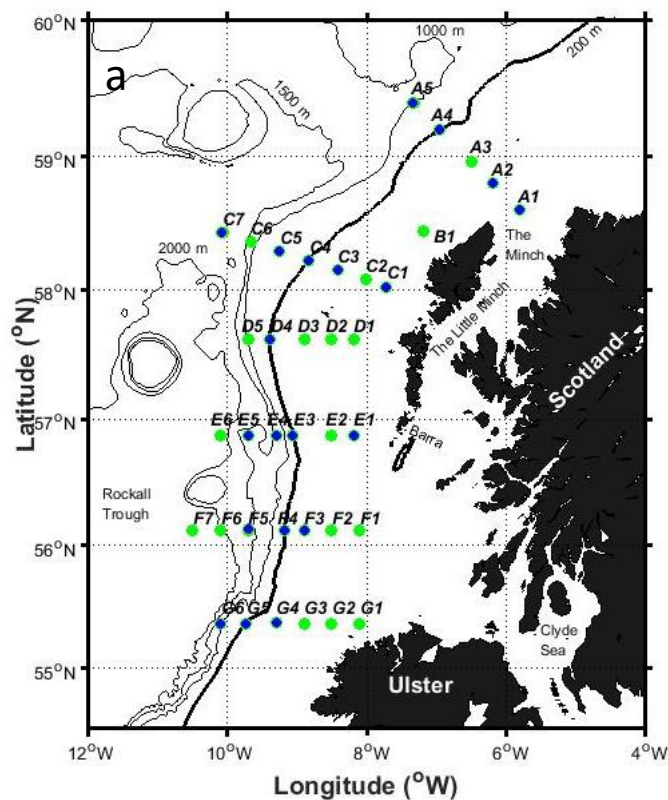
Figure 5-1- **A**- Map of survey area denoting CTD sampling stations. Samples where the determination of dissolved iron occurred are indicated by stations with blue fill. **B**- Map detailing the major currents and their approximate paths (ESC= European Slope Current, SCC= Scottish Coastal Current).
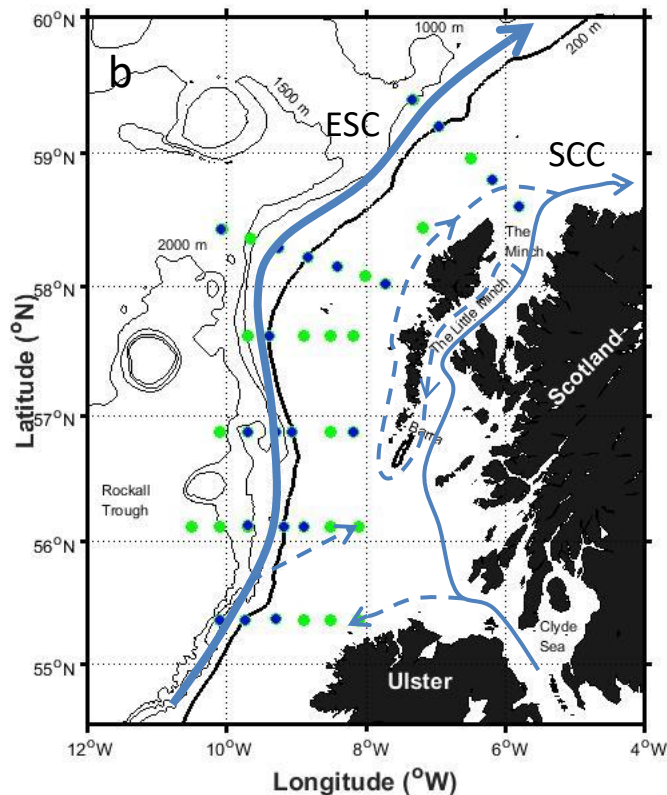
The relative influence of either the southerly or sub-polar modified surface water masses in the Rockall Trough is thought to be determined by the strength of the

Sub-polar Gyre. A strengthening Sub-polar Gyre expands southwards and enters the Iceland Basin and Rockall Trough, resulting in cooler and fresher surface waters with elevated nutrient concentrations [*Holliday*, 2003; *Johnson et al.*, 2013]. At depth, the shoaling topography to the north of the Rockall Trough restricts northwards flow of water below 1200 m, forcing an anticyclonic recirculation within the basin [*Holliday et al.*, 2000].

Separating the Hebridean shelf sea from the Rockall Trough is a region of steep topography, where the water column deepens from 200 to 1000 m over a distance of ≈ 30 km [*Souza et al.*, 2001]. Steep topography combined with geostrophic forcing, results in a bathymetric steering of flow. Along the Hebridean shelf slope this is observed as the European slope current (ESC; Fig. 5.1b), which is considered to be a persistent northwards current flowing from the Goban Spur to the Shetland Islands, with seasonal reversals in flow along the Bay of Biscay and Celtic Sea [*Booth and Ellett*, 1983; *Pingree et al.*, 1999; *Souza et al.*, 2001]. At ≈ 56° N the ESC is predominantly a barotropic flow of ≈20 cm s^{-1} parallel to the shelf break, with a characteristic high salinity (35.35-35.40) core at ≈ 200-300m [*Souza et al.*, 2001]. The result of near geostrophic conditions is a restriction on cross shelf exchange. However, wind driven surface exchange drives on-shelf flow in surface waters, while frictional forces resulting from the ESC drives a compensating off-shelf downwelling circulation ('Ekman Drain') [*Holt et al.*, 2009; *Huthnance et al.*, 2009; *Painter et al.*, 2016; *Simpson and McCandliss*, 2013].

The on-shelf circulation of the Hebridean shelf sea is well studied. Near to the coast, the Scottish Coastal Current carries low salinity water originating from the Clyde and Irish Seas around western Scotland and ultimately into the North Sea (Fig. 5.1b). Flowing northwards, at a mean velocity of ≈ 2-5 cm s^{-1} and volume transport of ≈ 0.1 Sv,

the current interacts with the Hebridean islands. The majority (≈ 80%) of flow continues northwards inshore of the Outer Hebridean Islands, the remaining flow returns south through the Minches before flowing northwards along the east coast of the Outer Hebridean Islands [*Inall et al.*, 2009; *McCubbin et al.*, 2002; *McKay et al.*, 1986; *Simpson and Hill*, 1986]. Measurements of Caesium-137 originating from Sellafield, Cumbria indicate that some outflow from the Irish Sea also occurs westerly along the north coast of Ulster [*Jefferies et al.*, 1973], and that a residual northward flow occurs over the wider Hebridean shelf [*McKay et al.*, 1986]. West of the Scottish Coastal Current, increased salinity (> 35) indicates that the shelf water is of Atlantic origin [*Inall et al.*, 2009; *Simpson and Hill*, 1986]. A tongue of high salinity (> 35.2) water has been observed penetrating south of the Isle of Barra [*Simpson and Hill*, 1986], though observations at the same location [*Ellett and Edwards*, 1983] show that the shoreward extent to which high salinity waters penetrate is interannually variable [*Inall et al.*, 2009].

5.1 Methods

5.1.2 Sampling methods and sample storage

Sampling was conducted in October 2014 on-board the *R.R.S. Discovery* in the Hebridean shelf sea and adjacent NE Atlantic Ocean (Fig. 5.1). Samples for the determination of dFe were collected following protocols outlined in section 3.1.1. Additionally, surface seawater was pumped into the trace metal clean laboratory using a Teflon diaphragm pump (Almatec A-15, Germany) connected by acid-washed braided PVC tubing to a towed "fish" positioned at approximately 2–3 m depth using a davit on the port side of the ship. Underway samples for the determination of dFe were filtered in-line through 0.2 µm pore size, acetate membrane filter capsules (Sartobran-P size 7, Sartorius).

5.1.2 Determination of dissolved iron in seawater

All sample and reagent handling was undertaken in an ISO 14644-1 Class 5 laminar flow hood (Bassaire, Southampton, UK) situated within an ISO 14644-1 Class 5 clean room at Plymouth University. Dissolved Fe was determined using an automated FI-CL system [*Floor et al.*, 2015; *Obata et al.*, 1993]. The detailed methodology is described in section 2.3. The majority of data presented in this chapter results from dFe analyses carried out by Nora Hartner; a European Union Erasmus funded master's student from the University of Ulm, working under the supervision of Antony Birchill. To ensure reproducibility of analyses between operators, a rigorous assessment of the quality of data generated by Nora Hartner was conducted (Appendix D).

5.1.3 Nutrients, temperature and salinity

Macronutrient analysis was carried on-board by Dr Christopher Daniels (National Oceanography Centre, Southampton). The concentrations of nitrate + nitrite (hereafter NO_3^-), phosphate (PO_4^{3-}) and silicic acid ($Si(OH)_4$; hereafter silicate) were determined on a Skalar Sanplus continuous flow analyser using common methodologies [*Hydes et al.*, 2010; *Kirkwood*, 1996]. Macronutrient measurements were made from all trace metal clean OTE bottles that were sampled for dFe, as well as from additional depth profiles sampled using a stainless steel rosette.

Salinity, temperature, and depth were measured using a CTD system (Seabird 911+) equipped with optical backscatter (WET Labs, ECO BB), dissolved oxygen (O_2; Seabird SBE 43 O_2 sensor) and a fluorimeter. Salinity was calibrated on-board using discrete samples using an Autosal 8400B salinometer (Guildline). Daily O_2 calibrations were conducted using a photometric automated Winkler titration system [*Carritt and Carpenter*, 1966]. Daily samples for chl-*a* analysis were filtered through 0.7 μm glass microfibre filters (Whatman GF/F) and extracted in 90% acetone overnight [*Holm-*

Hansen et al., 1965]. The chl-*a* extract was measured on a pre-calibrated (spinach chlorophyll-a standard, Sigma) fluorimeter (Turner Designs Trilogy).

5.2 Results and discussion

5.2.1 Surface fields

A large range of dFe concentrations (0.03-3.51 nM) was observed in surface waters during this study (Fig. 5.2). The western (oceanic) extent of the survey area was characterised by elevated salinities (> 35.2) and uniformly low dFe concentrations (typically < 0.15 nM) (Fig. 5.2), comparable to concentrations observed in Fe limited regions [*Boyd and Ellwood*, 2010]. Coinciding with low dFe concentrations were elevated NO_3^- (3.22-6.90 μM) and PO_4^{3-} (0.27-0.44 μM) concentrations, resulting in a surface water dFe:NO_3^- ratio far less than the uptake ratio of phytoplankton grown under nutrient replete environments [Fe:N of 0.05 - 0.9 nM μM; *Ho et al.*, 2003; *Sunda and Huntsman*, 1995]. The concentration of NO_3^- and PO_4^{3-} was higher in the northwest than the southwest of the survey area, with the increase in concentration associated with cooler surface waters (indicated by the 11.9 °C isotherm; Fig. 5.2).   Silicate concentrations were lower in the southwest than the northwest of the survey area, but in both regions remained below the 2 μM concentration considered a threshold value for diatom growth [*Egge and Aksnes*, 1992]. The north-south gradient in macronutrient distribution over the western (oceanic) extent of the survey area is consistent with surface waters originating from the south of the Rockall Trough being relatively nutrient poor in comparison to those entering from the north-west after passage through the Iceland Basin [*Johnson et al.*, 2013]. No north-south gradient in dFe was observed over the western extent of the survey area as dFe concentrations were < 0.15 nM.

Broadly, the salinity of shelf waters decreased and dFe concentration increased towards the coast (Fig. 5.2), but a number of distinctive features are evident in on-shelf surface waters. A tongue of high salinity (> 35.2) Atlantic water penetrated onto the shelf at 56.1° N, consistent with previous observations [*Simpson and Hill*, 1986]. This surface water was associated with lower concentrations of dFe (0.21-0.23 nM). A salinity minimum (34.7) was observed northeast of the Outer Hebridean Islands, in the path of the Scottish Coastal Current. This was associated with elevated dFe (3.51 nM) and Si (2.55 µM) concentrations. North of the coast of Ulster, a distinctive tongue of warmer (> 13°C) and fresher (35.1) water was present, likely outflow from Irish Sea [*Jefferies et al.*, 1973]. The Irish Sea outflow was characterised by lowest observed concentrations of NO_3^- (≈ 2 µM) and PO_4^{3-} (0.25 µM), whereas the concentration of dFe was 0.75 nM.

1
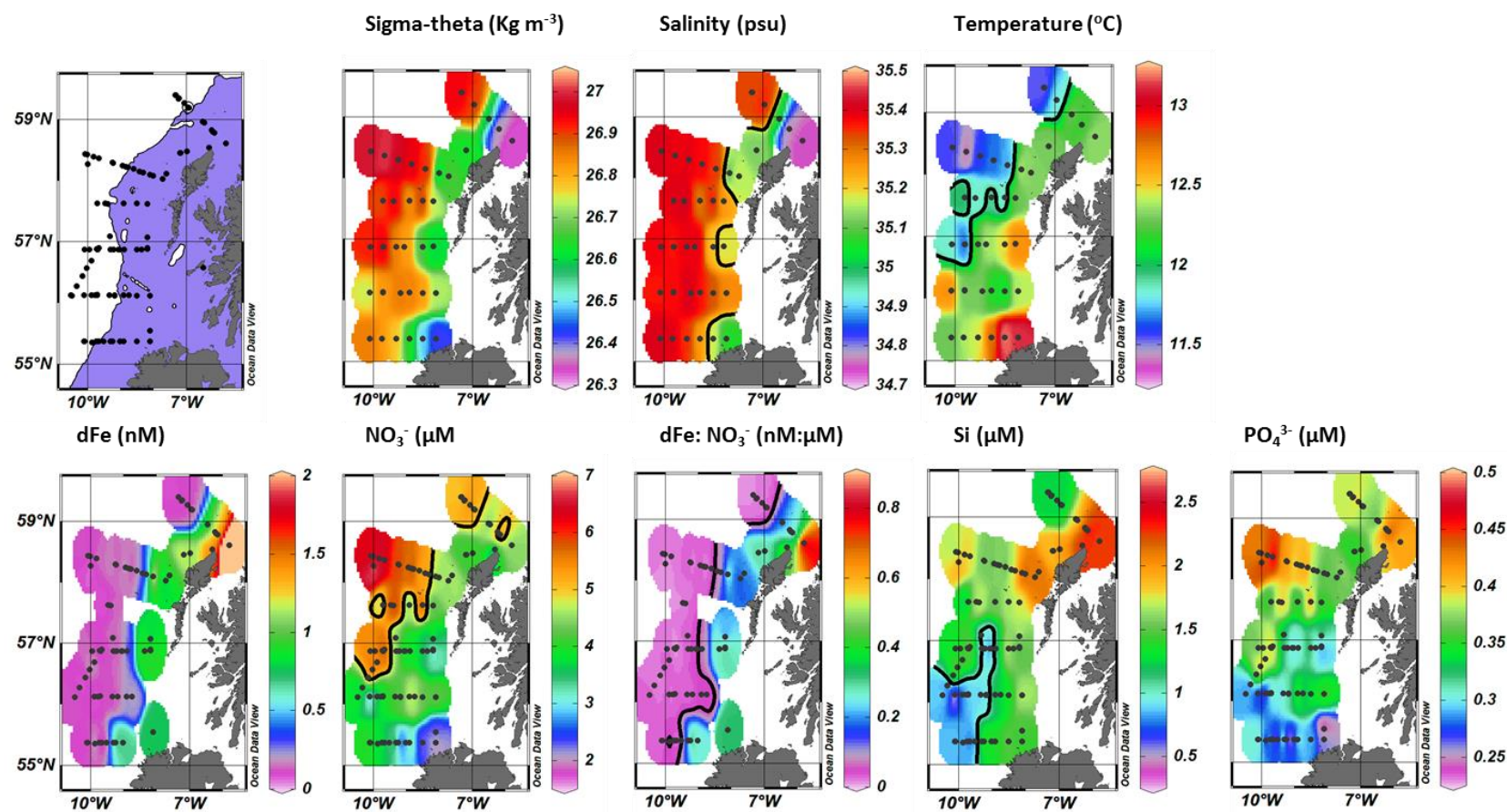
Figure 5-2- Contoured surface maps (as labelled) showing regional gradients in hydrography and nutrient distributions. Blue shaded area on the map indicates bottom depth < 200 m. Solid black lines indicate contours of 35.2 (salinity), 11.9 °C, 0.05 dFe:NO_3^- , 5 µM NO_3^- and 1 µM Si. Physical data collected from CTD sampling. Nutrient data collected from CTD cast (≈ 20 m) and Tow-fish sampling.

5.2.2 Cross shelf sections

The surface distributions reveal differing distributions of macronutrients and dFe. Due to the non-conservative nature of dFe in oxic seawater, the concentration of dFe is closely coupled to sources. Here the main external sources of dFe are coastal waters and shelf sediments. To indicate their influence on dFe concentrations, cross-shelf sections of dFe, turbidity, temperature and salinity are plotted in Fig. 5.3. At the shoreward
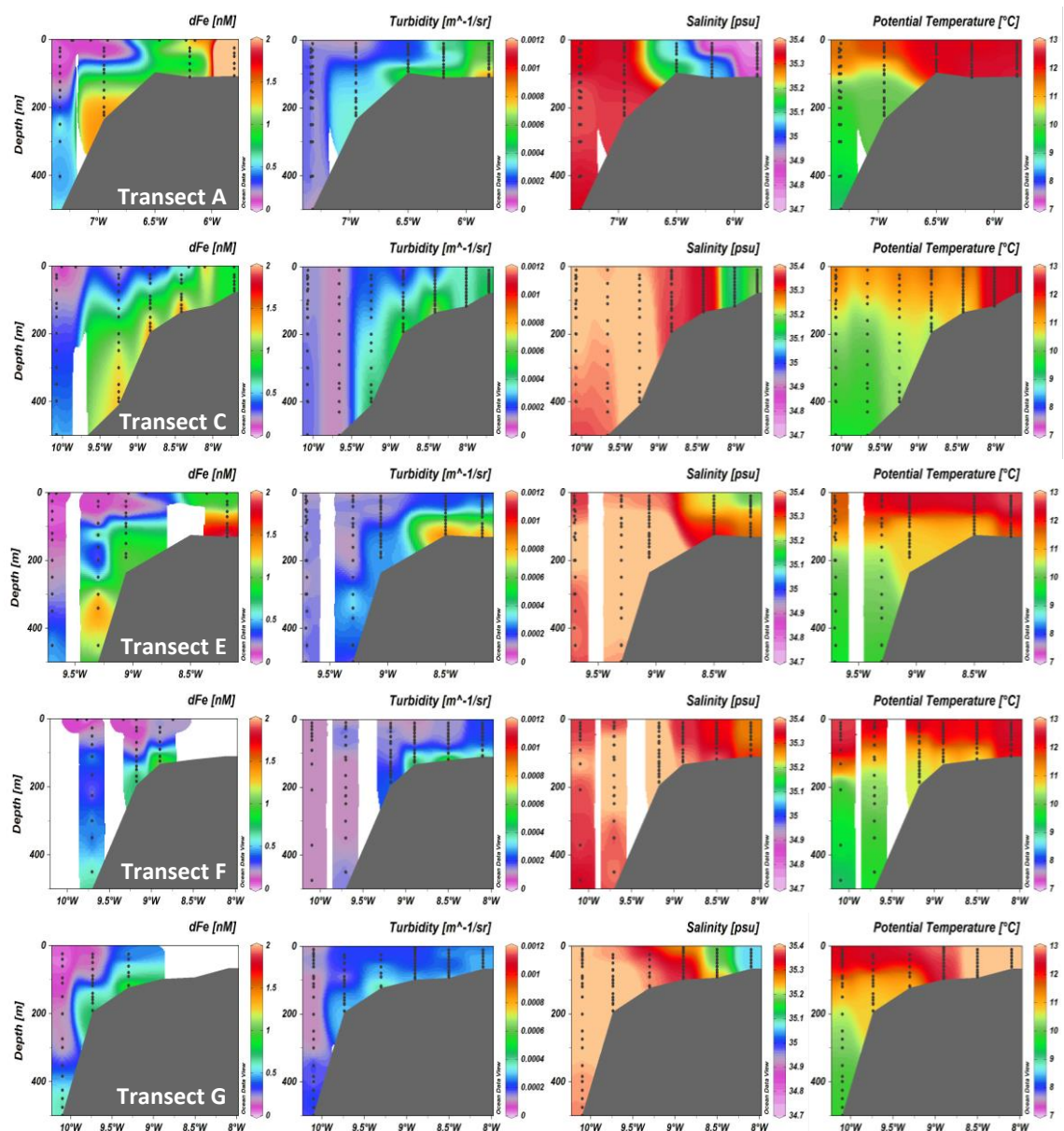
Figure 5-3- Contoured section plots for the upper 500 m of transects A, C, E, F and G of dFe, turbidity, salinity and potential temperature. Within each transect station number increases from right to left.

extent of transect A, the influence the Scottish Coastal Current is evidenced by low salinity (< 34.8) water, with increased particle loading and dFe concentrations > 3 nM. However, water with salinities < 35.2 was restricted to shallow (< 131 m) stations at the eastern (coastal) extent of the cross-shelf sections (Fig. 5.3). Westward of coastal waters, salinities > 35.2 indicated shelf water with an Atlantic source.

Elevated turbidity was observed over the shelf sediments, which typically coincided with increased concentrations of dFe (Fig. 5.3), indicating a sedimentary source of dFe [*Ussher et al.*, 2007]. At on-shelf stations, vertical transport of sedimentary derived dFe to surface waters was restricted by the presence of the seasonal thermocline, except at the well mixed coastal stations. At the western (oceanic) extent of the survey area, waters with the lowest turbidity and lowest dFe concentrations (0.03-0.69 nM) were observed, indicating that lateral transport of dFe from shelf sediments to the upper 500 m of these stations was limited. This is consistent with the dominant direction of passage for surface waters being either northward in the ESC, or on-shelf resulting from wind driven transport [*Huthnance et al.*, 2009]. An exception to this was observed at station E4 where an intermediate nepheloid layer was observed at ≈ 300-450 m containing dFe concentrations of 1.17-1.47 nM (Fig. 5.3). However, this was not observed westward at station E5, indicating that this was a localised feature.

For comparison, cross-shelf sections of macronutrients are displayed in Fig. 5.4.
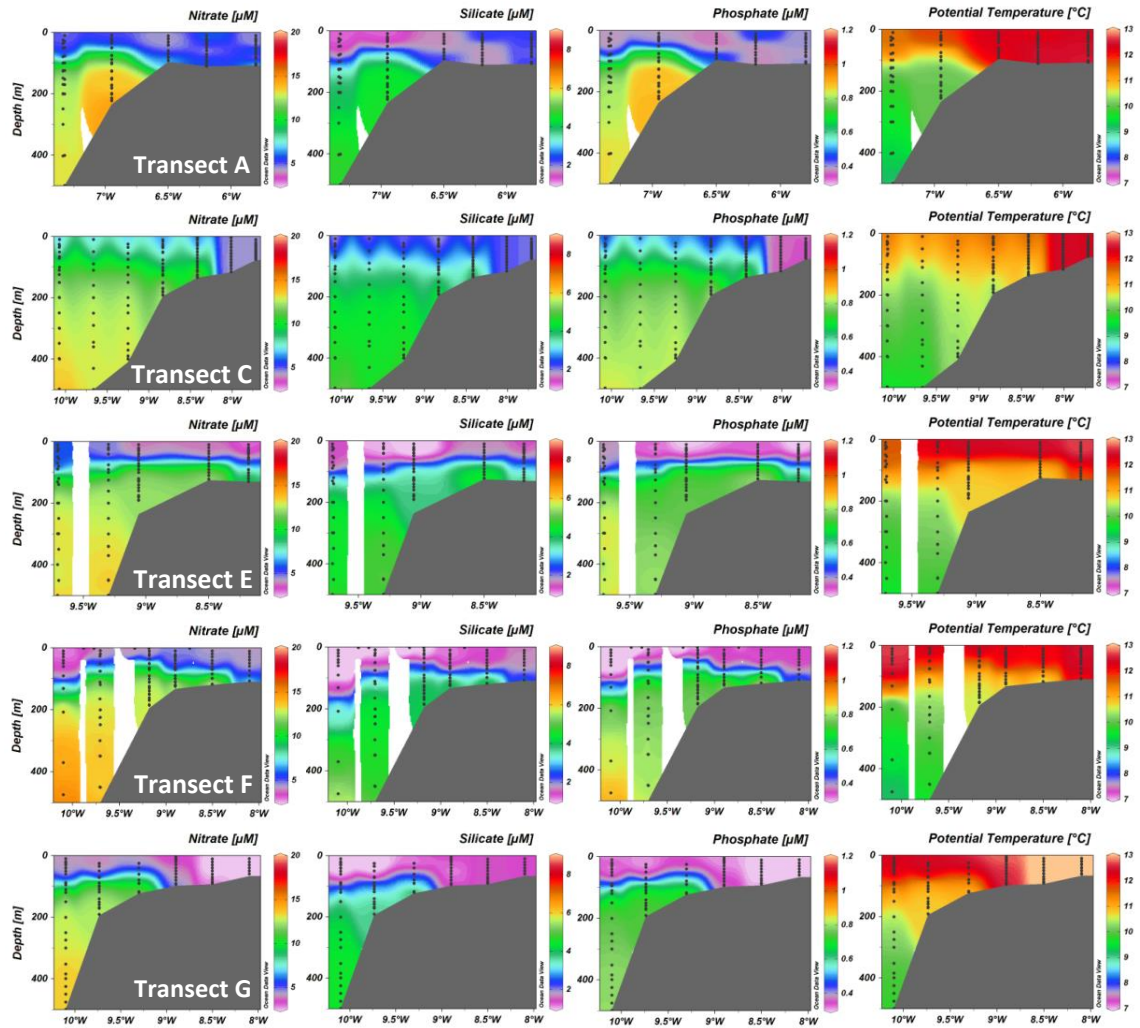
Figure 5-4- Contoured section plots for the upper 500m of transects A, C, E, F and G of, NO_3^-, Si , PO_4^{3-} and potential temperature. Within each transect station number increases from right to left.

At well mixed stations the patterns observed in surface waters are also observed in the vertical distributions. For instance, at the shoreward extent of transect G, warmer water (> 13°C) indicative of Irish Sea Outflow is associated with reduced NO_3^- (≈ 2 µM) and PO_4^{3-} (≈ 0.26 µM) throughout the water column. At stratified stations macronutrient concentrations were lower in surface waters and increased at depth (NO_3^- ≈ 12-14 µM, Si ≈ 3.5-5.0 µM, PO_4^{3-} ≈ 0.7-0.9 µM). Unlike dFe concentrations, the increase with depth in the upper 500 m was typically smooth, reflecting remineralising organic matter as the

primary source of macronutrients, uncomplicated by non-conservative behaviour or sediment inputs.

In order to further examine the different oceanographic regimes observed, trace metal sampling stations were classified into 3 groups based on their temperature-salinity signature. A summary of station classifications is presented in Table 5.1. Furthest offshore 'oceanic' stations had water column depths of 1013-1865 m, sufficient to observe intermediate water masses (Fig. 5.5; box 3). At all of these stations salinity increased to > 35.40 in the upper 500 m, indicative of the ESC [*Souza et al.*, 2001]. Stations with a similar T-S signature (T= 10.00-12.40 °C, S= 35.35-35.50; Fig. 5.5; box 2) were termed 'shelf break' and had water column depths of 120-410 m. The remaining stations, with water depths of 76-130 m, were classified as 'shelf' stations (Fig. 5.5; box 1). Shelf stations were fresher than at shelf break stations and oceanic surface waters;
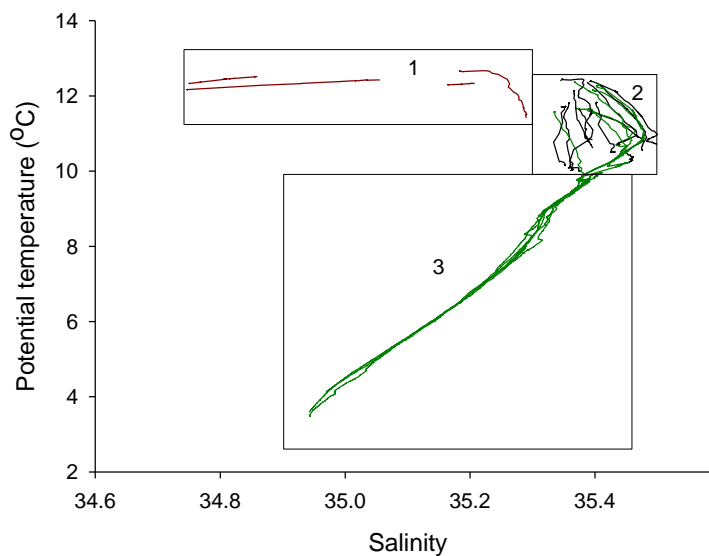
Figure 5-5- Temperature and salinity plot of stations observed in this study. 1. Shelf stations. 2. Surface waters of oceanic stations (green) and stations over the shelf and shelf break (termed shelf influenced) with a corresponding T-S signature (black). 3. Intermediate water masses observed at oceanic stations.

however, as discussed above, shelf stations exhibited a wide range of salinities (34.74-35.29), due to a patchwork of water masses present due to variations in freshwater input [*Hydes et al.*, 2004a] and influence of the Scottish Coastal Current. The potential temperature at shelf stations ranged from 11.42-12.67 °C.

Table 5-1- Trace metal sampling stations classified into 3 different domains; Shelf, Shelf Break and Oceanic.

Station	Latitude (°)	Longitude (°)	Bottom depth (m)	Domain
A1	-5.803	58.602	110	Shelf
A2	-6.195	58.801	112	Shelf
C1	-7.716	58.023	76	Shelf
E1	-8.183	56.875	130	Shelf
A4	-6.949	59.196	225	Shelf break
C3	-6.418	58.149	136	Shelf break
C4	-8.832	58.223	193	Shelf break
C5	-9.248	58.289	401	Shelf break
D4	-9.391	57.62	191	Shelf break
E3	-9.059	56.88	191	Shelf break
F3	-8.898	56.122	128	Shelf break
F4	-9.177	56.119	187	Shelf break
G4	-9.302	55.371	120	Shelf break
G5	-9.736	55.369	191	Shelf break
A5	-7.339	59.398	1013	Oceanic
C7	-10.077	58.433	1865	Oceanic
E4	-9.299	56.87	1399	Oceanic
E5	-9.696	56.869	1851	Oceanic
F5	-9.704	56.128	1612	Oceanic
G6	-10.101	55.367	1130	Oceanic

The mean concentration of dFe and macronutrients in the SML of each sub-region is displayed in Table 5.2. The concentrations of NO_3^- and Si in the SML of shelf stations have been shown to be significantly different from those observed at shelf break or oceanic stations [*Siemering et al.*, 2016]. Results presented here indicate that the dFe concentration in shelf waters are also significantly elevated relative to shelf break and oceanic stations. Therefore, shelf stations were chemically distinct with a greater mean dFe (1.73 ± 1.16 nM, ± 1 SD) and Si (1.98 ± 0.36 µM), and lower NO_3^- (4.18

± 0.88 µM) concentration. At shelf stations, a mixed phytoplankton community was observed that was significantly different from shelf break and oceanic communities. The shelf community included species of the diatom genus *Pseudo-nitzchia,* which were absent elsewhere, contributing 2.5-37% of counts [*Siemering et al., 2016*]. It was concluded that phytoplankton growth at shallow shelf stations was likely to be light limited due to the resuspension of sediments. The increased diatom abundance was attributed to a better adaptation to turbulent environments and lower light availability, providing that there were sufficient nutrients [*Jones and Gowen*, 1990; *Siemering et al.*, 2016]. Silicate concentrations were at the 2 µM threshold for diatom growth, and the N:Si ratio was the lowest (≈ 2:1) observed and thus most favourable for diatom growth [*Brzezinski*, 1985; *Davidson et al.*, 2012]. As the dFe concentration was elevated, Fe availability was unlikely to increase diatom Si demand as has been demonstrated under Fe limited conditions [*Hutchins and Bruland*, 1998; *Takeda*, 1998].

Table 5-2- The observed mean (± 1 standard deviation) nutrient concentrations in the surface mixed layer in October 2014. Surface mixed layer defined as near surface density plus 0.03 kg m^{-3}. At shelf stations A1 and C1 were well mixed.

Domain	dFe (nM)	NO$_3^-$ (µM)	Si (µM)	PO$_4^{3-}$ (µM)
Shelf (*n*= 19)	1.73 ± 1.16	4.18 ± 0.88	1.98 ± 0.36	0.36 ± 0.06
Shelf Break (*n*= 37)	0.22 ± 0.16	5.36 ± 1.36	1.47 ± 0.47	0.38 ± 0.07
Oceanic (*n*= 19)	0.09 ± 0.04	5.27 ± 0.79	1.32 ± 0.29	0.38 ± 0.05

Shelf break and oceanic stations were chemically similar in terms of macronutrients [*Siemering et al.*, 2016], reflecting the common source of these waters (Fig. 5.5). The concentration of dFe did differ between oceanic and shelf break stations, which although low at shelf break stations (0.22 ± 0.16 nM) was remarkably low at oceanic stations (0.09 ± 0.04 nM) (Table 5.2). The phytoplankton community was similar at shelf break and oceanic stations, and both were distinct from shelf stations. Phytoplankton counts at shelf break and oceanic stations consisted almost entirely

(>97%) of dinoflagellates from the genus *Tripos* [*Siemering et al., 2016*]. The shift in species composition relative to shelf waters was attributed to different nutrient concentrations and ratios, with the N:Si ratio in particular being less favourable for diatom growth. The dFe concentrations observed at shelf break, and particularly oceanic, stations are comparable to those observed in Fe limited regions. Therefore, it is likely that the unfavourable N:Si ratio would have been exacerbated by sub-optimal Fe availability, increasing rates of silicification [*Hutchins and Bruland*, 1998; *Takeda*, 1998]. Though to fully assess whether the N:Si ratio does reflect Fe stress a seasonal time series of N:Si would be needed so that it can be linked to preformed ratios. Interestingly, the concentrations of dFe (< 0.010 - 0.218 nM), NO_3^- (2-5 µM) and chl-*a* (0.2-0.4 µg L^{-1}) observed during summer in surface waters of the central Iceland basin [*Nielsdóttir et al.*, 2009] were almost identical to the autumn concentrations observed at oceanic and shelf break stations in this study (Table 5.2). Addition of Fe to the Icelandic waters resulted in an increase in diatom and coccolithophore abundance and a decrease in NO_3^- concentration. Therefore, the results strongly suggest that the condition for Fe limitation of both diatom growth and the wider phytoplankton community, appear to occur at the Hebridean shelf break.

A caveat is that the nutrient concentrations observed in October 2014 may not represent the summer minimum due to recent vertical mixing caused by stormy conditions prior to and during sampling. However, > 1 µM of NO_3^- has been observed in shelf break surface waters during summer (August) [*Gowen et al.*, 1998], strengthening the assertion that seasonal Fe limitation is present in waters over the Hebridean shelf break. Moreover, even if recent vertical mixing had elevated macronutrients concentrations in surface waters, it had not significantly elevated dFe concentrations (Table 5.2).

5.2.3 Vertical supply of nutrients and dFe by winter mixing

As sinking organic matter is remineralised it releases macronutrients and dFe back to the water column. This happens at different rates, in the order of $PO_4^{3-} > NO_3^- >$ Si [*Tett et al.*, 2003b], with Fe remineralisation thought to be slower than NO_3^- [*Bowie et al.*, 2009]. Additionally, dFe can be lost to particle formation/scavenging, and in shelf waters NO_3^- is lost via denitrification eventually becoming dinitrogen [*Hydes et al.*, 2004a; *Tett et al.*, 2003b]. These processes shape the vertical profiles of these elements, influencing the stoichiometric ratio at which they are returned to surface waters by vertical mixing/diffusion processes [*Painter et al.*, 2014; *Tagliabue et al.*, 2014b]. The stoichiometry of supplied nutrients will determine whether complete utilisation by phytoplankton can occur. The depth profiles of dFe:NO_3^- are displayed for shelf, shelf break and oceanic stations and the central Iceland basin in Fig. 5.6. In accordance with profiles from the seasonally Fe limited Iceland and Irminger Basins [*Nielsdóttir et al.*, 2009; *Painter et al.*, 2014], the dFe:NO_3^- ratio at oceanic stations is typically less than the uptake ratio of phytoplankton grown under nutrient replete environments [Fe:N of 0.05-0.9 nM:μM; *Ho et al.*, 2003; *Sunda and Huntsman*, 1995] to depths of at least 1800 m (maximum depth of sampling).
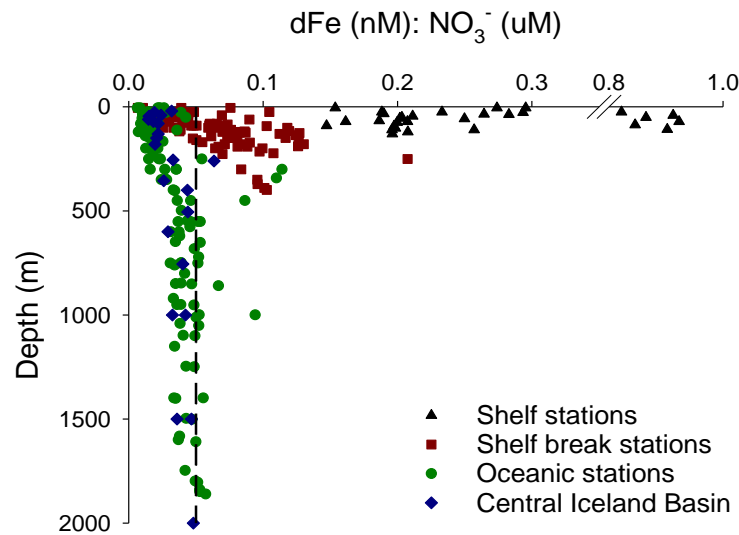
Figure 5-6- Depth profile of dFe:NO$_3^-$ stoichiometry for each sub-region in this study and for the central Iceland Basin (60.0-60.8 N, 20.0-21.7 W) [*Painter et al.*, 2014]. Dashed line denotes 0.05 dFe:NO$_3^-$ (nM:µM), the lower limit observed in cultured phytoplankton [*Ho et al.*, 2003; *Sunda and Huntsman*, 1995]. All samples to right of break in the x axis were from station A1 in the path of the Scottish Coastal Current.

Winter mixing homogenises the upper water column, replenishing surface waters with nutrients. This process determines the concentration of nutrients available for the spring bloom and sets a quasi-limit on annual primary production [*Hydes et al.*, 2004a]. During winter (February) the upper 500 m of the water column overlying the Hebridean shelf slope has been shown to be homogenous [*Souza et al.*, 2001]. Assuming this to represent the depth of winter mixing it is possible to estimate the surface winter nutrient concentrations by integrating over the upper 500 m, or entire water column if this is < 500 m (Table 5.3). A winter mixing depth of 500 m is consistent that reported over the Bay of Biscay and Goban Spur, but it can reach depths of 750-900 m in this region [*Huthnance et al.*, 2001]. Estimating winter nutrient concentrations in this

manner assumes a closed 2-dimensional system; uncertainties in this approach include advective processes and any input or removal of macronutrients or dFe from within the system. The validity of this calculation is first considered by comparing estimated concentrations with previous observations. *Hydes et al.* [2004a] carried out a detailed assessment of winter (February) macronutrient concentrations for North-West European shelf seas. Similar to results presented here, their values for NO_3^-, PO_4^{3-} and Si all decrease from oceanic to shelf break environments (Table 5.3). A noticeable difference is the estimated Si concentrations, which for this study are ≈ 1 µM lower than observed in winter (Table 5.3). *Painter et al.* [submitted] interpreted this as a loss of Si to the adjacent ocean and/or the organic nutrient pool. As biogenic silica remineralises more slowly than organic nitrogen and phosphorus, a significant fraction of the biogenic silica may not have returned to the water column as orthosilicate by October 2014. Alternatively, this may reflect spatial and temporal variability; a range of 3.1-4.7 µM of Si has been reported for the Iceland Basin in March [*Daniels et al.*, 2015]. Previous dFe measurements are less numerous. The dFe concentrations estimated here are slightly in excess of dFe concentrations (0.16-0.64 nM) reported in an early May surface transect [*Achterberg et al.*, 2013], by which time some dFe would have been consumed in the spring bloom. Thus, this approach is considered a reasonable first order estimate of winter surface concentrations of dFe, NO_3^- and PO_4^{3-}, with Si concentrations subject to greater uncertainty.

Table 5-3 Top- The predicted winter surface mean nutrient concentration (± 1 standard deviation). Estimate carried out by integrating concentrations observed in October 2014 from surface waters to a maximum depth of 500 m, and dividing through by the depth of integration. **Bottom-** Reported winter concentrations for Malin shelf and adjacent NE Atlantic Ocean.

Domain	dFe (nM)	NO_3^- (µM)	Si (µM)	PO_4^{3-} (µM)	dFe:NO_3^- (nM:µM)	N:Si	N:P
Shelf (*n*= 4)	1.59 (1.19)	4.59 (0.92)	2.01 (0.29)	0.38 (0.05)	0.37 (0.34)	2.3 (0.4)	12.1 (1.6)
Shelf Break (*n*= 9)	0.62 (0.16)	9.06 (1.47)	2.81 (0.58)	0.59 (0.09)	0.07 (0.02)	3.3 (0.3)	15.5 (0.5)
Oceanic (*n*= 6)	0.37 (0.18)[1]	11.37 (0.39)	3.78 (0.12)	0.72 (0.04)	0.03 (0.02)	3.0 (0.1)	16.1 (0.7)
Malin Shelf break[2]	nd	10.3	4.25	0.65		2.4	15.8
Malin Oceanic[2]	nd	11	4.75	0.68		2.3	16.2

[1]median of estimated surface dFe 0.33 nM
[2] *Hydes et al.* [2004a]- Sampled February 2000 (nd= not determined)

The estimated winter concentrations display some clear trends; from oceanic to shelf stations dFe increases and NO_3^- and PO_4^{3-} decrease. The increase in dFe concentration is attributed to shelf inputs and more efficient annual recycling due to the shallow sea bed. At oceanic stations the N:P ratio (16.1 ± 0.8) was very close to Redfield values (15-16) [*Redfield*, 1958], indicating nutrient concentrations were primarily controlled by remineralising organic matter. The N:P ratio progressively diminishes on shelf to 12.9 ± 0.3 at shelf stations, consistent with *Hydes et al.* [2004a] observations. This is likely driven by a loss of NO_3^- through denitrification, which is a ubiquitous process on the North West European shelf [*Hydes et al.*, 2004a], and NO_3^- poor inputs from coastal waters. The Clyde Sea (S ≈ 31-34), is a nearby semi-enclosed basin which receives large amounts of fresh water input [*Rippeth and Jones*, 1997]. Nutrient ratios observed in the Clyde Sea have been shown to be NO_3^- poor (N:P ≈ 10 & N:Si ≈ 1) [*Grantham and Tett*, 1993; *Tett et al.*, 2003a] relative to values reported here for more saline waters. The result of these processes is a shelf-wide gradient in dFe:NO_3^- (Table 5.3; Fig 5.6).

The predicted winter concentration (Table 5.3) minus autumn observations (Table 5.2), imply a seasonal drawdown of 0.28 nM of dFe at oceanic stations. By assuming a net seasonal phytoplankton uptake ratio of 0.05 dFe:NO_3^- (nM:μM), a predicted residual NO_3^- concentration of ≈ 5.9 μM was estimated. This is within the range observed during autumn 2014 (5.27 ± 0.79; Table 5.2). Applying this calculation to the shelf break stations would result in a residual NO_3^- concentration of ≈ 0.86 μM. This is much lower than observed in autumn (5.36 ± 1.36; Table 5.2) and is attributed to persistent wind driven on shelf transport of dFe deplete oceanic surface water during summer months.
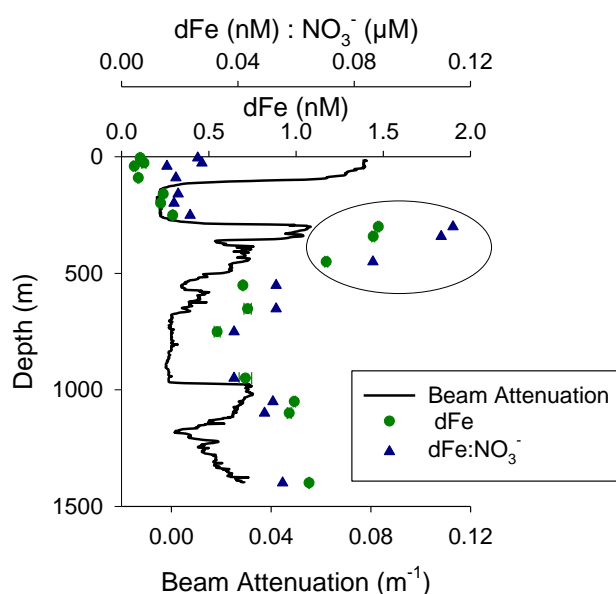
Figure 5-7- The impact of nepheloid layers on the depth profile of dFe, dFe: NO_3^- and beam attenuation at station E4. Oval encompasses samples collected from shallow nepheloid layers.

Whilst these estimates of surface winter concentrations represent a reasonable first order approximation, additional levels of complexity can be included if lateral transport of dFe from shelf sediments and variable ferricline depths are considered. The estimated winter surface concentrations of dFe at oceanic stations ranged from 0.20-

0.70 nM (*n*= 4), with a median value of 0.33 nM. A higher value of 0.70 nM was calculated

for station E4; the elevation was caused by a dFe rich (> 1.5 nM) intermediate nepheloid

layer(s) at ≈ 300-500 m (Fig. 5.7). Shallow INLs were not observed at other oceanic

stations indicating a spatially variability in the occurrence and/or extent of INLs

originating from the Hebridean shelf slope. Therefore, the irregular distribution of INLs

is likely to cause a 'patchwork' of winter surface dFe conditions over the shelf break. It

is hypothesised that the resulting variation in dFe availability due to lateral transport

may affect the productivity of the spring bloom, in a similar manner to that which

episodic aeolian supply of Fe is hypothesised to affect spring bloom productivity in the

central Atlantic [*Moore et al.*, 2006]. The ferricline, the depth of maximal increase in dFe

concentration [*Tagliabue et al.*, 2014b], shoaled towards the north of the survey area.

At the most south-westerly oceanic stations, E5 and G6, dFe concentrations remained <

0.2 nM to depths of 300 and 350 m (Fig. 5.3), resulting in estimated winter surface

concentrations of 0.20 and 0.25 nM. In contrast, at the north-westerly stations, A5 and

C7, concentrations were < 0.2 nM to restricted depths of 170 and 100 m (Fig. 5.3),

resulting in estimated winter surface concentrations of 0.39 and 0.30 nM respectively.

Winter mixing is considered the dominant source of nutrients to surface waters

in this region [*Hydes et al.*, 2004a; *Painter et al.*, 2014], but diapycnal diffusion also

provides a mechanism to resupply remineralised nutrients to surface waters. Diapycnal

diffusion through the seasonal pycnocline can be described as:

Diffusive flux of N= Kz (ΔN/Δz)

where N is the dissolved nutrient of interest, Kz is the eddy diffusivity ($m^2\,s^{-1}$), ΔN is the

change in concentration of nutrient N through the pycnocline and Δz is the thickness of

the pycnocline. As measurements of Kz are not available, the flux was not calculated,

but the stoichiometry of supply will reflect the ratio of nutrient concentrations above

and below the pycnocline. At oceanic stations there was often no distinctive gradient in the $dFe:NO_3^-$ above and below the pycnocline to drive a diffusive flux of dFe to surface waters (Fig. 5.3; 5.6). Shallow, even negative, gradients in dFe concentrations down through the seasonal pycnocline resulted in negligible diffusive fluxes of dFe in the Iceland and Irminger Basin. Consequently, the annual dFe flux to surface waters from winter mixing was 29-52 times greater than that of the diffusive flux [*Painter et al.*, 2014]. In contrast, the increasing $dFe:NO_3^-$ below the seasonal pycnocline ($\approx$ 60-100 m) at shelf break stations (Fig. 5.6) means the diffusive flux may provide an important source of dFe rich water, though evidently not enough to allow dFe to proliferate in shelf break surface waters (Table 5.2).

5.2.4 The spatial extent of sub-Arctic Atlantic seasonal iron limitation

The results presented indicate that the conditions for seasonal Fe limitation occur over the Hebridean shelf break. It is therefore suggested that the Hebridean shelf represents part of the eastern boundary of sub-Arctic Atlantic seasonal Fe limitation. This interpretation is strengthened when summer surface climatology of NO_3^- for the sub-Artic Atlantic is plotted (Fig. 5.8). Residual NO_3^- in excess of 1 µM is observed near the Hebridean shelf. Maximum summer surface NO_3^- concentrations (8-10 µM) are in the Iceland and Irminger Basins, suggesting that the degree of seasonal Fe limitation is greater in these regions. Interestingly, the western extent of seasonal Fe limitation may extend into the southern Labrador Sea and northern extent potentially north of Iceland. Consequently the spatial extent of seasonal Fe limitation may be much greater than previously considered.

Summer surface nitrate [μM]
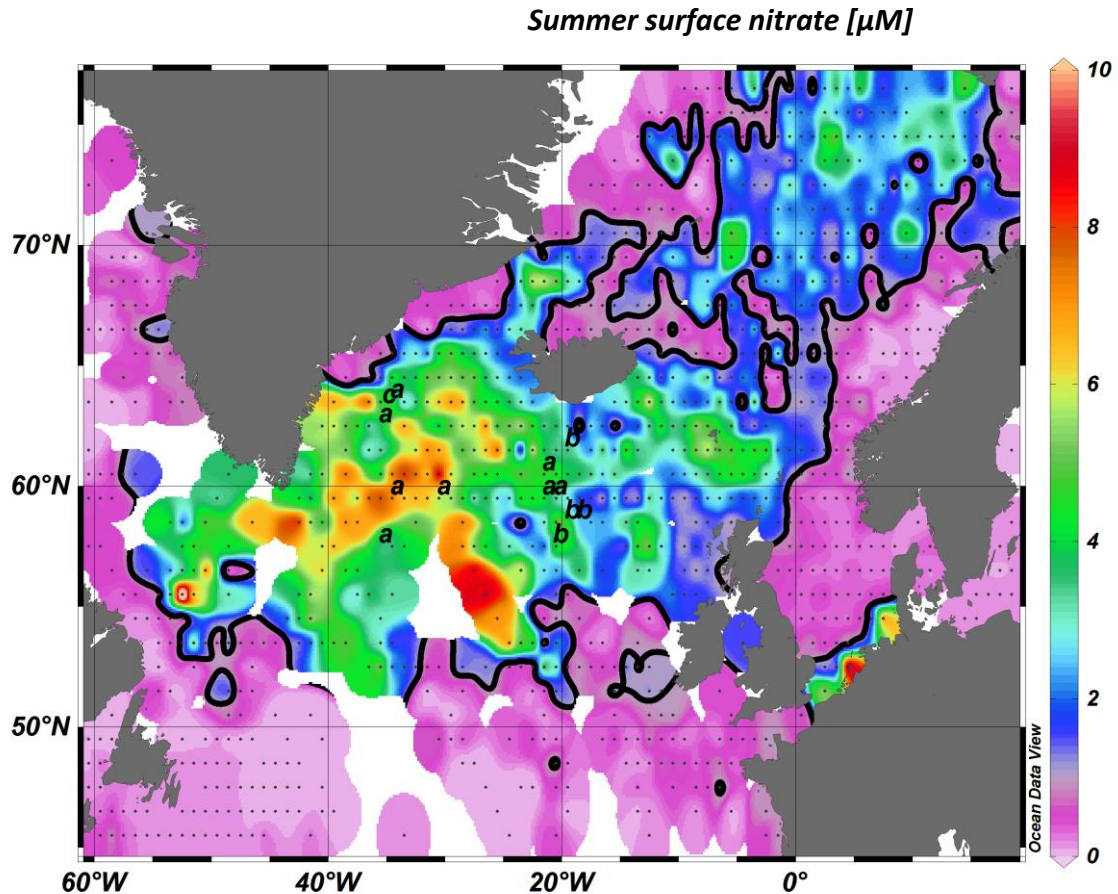
Figure 5-8- Climatology of summer surface nitrate concentrations in the sub-Arctic Atlantic from the World Ocean Atlas [*Garcia et al.*, 2014]. Solid line indicates the 1 μM contour. Letters mark locations where seasonal iron limitation has been observed a) *Ryan-Keogh et al.* [2013] b) *Nielsdóttir et al.* [2009] c) *Achterberg et al.* [2013].

5.3 Conclusions

The oceanic water close to, and over, the Hebridean shelf break was observed to be nutrient deficient with respect to dFe, with coastal waters being dFe replete. Vanishingly low dFe concentrations and the presence of residual macronutrients suggest that the seasonal Fe limitation and associated weakening of the biological carbon pump observed in the Sub-Arctic Atlantic extends further eastward than previously recognised. The vertical profile of dFe suggests that this results from sub optimal supply of Fe from vertical mixing, as is observed in the Iceland and Irminger basins. On-shelf, low salinity water of the Scottish Coastal current transports dFe northwards around the coast of Scotland, the fate of this dFe is unknown. The northwest European shelf exports carbon

141

to the Atlantic via a downwelling circulation of bottom waters over the continental shelf slope ('Ekman Drain') [*Painter et al.*, 2016; *Thomas et al.*, 2004]. Therefore, incomplete use of macronutrients in the region, and restriction of large phytoplankton growth over the shelf slope will restrict the build-up organic carbon in the bottom layer, and hence the efficiency of the continental shelf carbon pump.

Chapter 6 - Conclusions and future works

6.0 Introduction

The availability of Fe is known regulate primary production over large parts of the ocean. The GEOTRACES co-ordinated sampling campaign has vastly increased our knowledge of Fe distribution in the major ocean basins, yet process studies in highly productive shelf systems remain scarce. The research in this thesis is a GEOTRACES process study of the seasonal cycling and transport of Fe in the North-West European shelf sea and has contributed to our knowledge of Fe cycling in this region and the wider North Atlantic. A schematic of processes occurring in the marine Fe is displayed in Fig. 6.2. This schematic highlights the complexity of the Fe cycle in relation the operationally defined definitions used during this study and it is used to help structure the following conclusions and future work. Initially the three hypotheses (section 1.4) which are described below and are revisited in light of the data presented in this thesis.
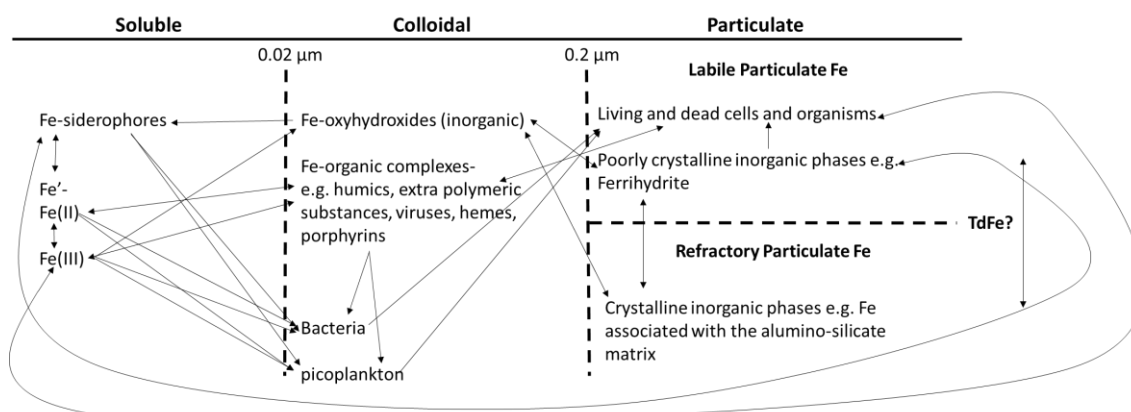
Figure 6-1- A schematic of the marine iron cycle in relation to the operational definitions used in this study. This is not meant to be an exhaustive description of the marine Fe cycle, but instead to highlight the complexity of the system. Many of the processes are subject to uncertainty, for instance there is no current consensus on whether Fe(II) is organically complexed in seawater.

6.0.1 Hypothesis 1:

> *As seasonal stratification provides an effective barrier to the vertical transport of macronutrients in the Celtic Sea, it is postulated that Fe will also be seasonally depleted in the surface mixed layer.*

Previous studies of macronutrient distributions in the Celtic Sea have primarily focussed on the availability of NO_3^- to phytoplankton [*Hickman et al.*, 2009; *Hickman et al.*, 2012; *Pingree et al.*, 1977; *Rippeth et al.*, 2009; *Sharples et al.*, 2001]. In the central Celtic Sea, the seasonal cycling of dFe mirrored that of NO_3^-. Briefly, winter mixing resulted in homogenous distributions of dFe (0.82 ± 0.041 nM). During the spring bloom, preferential removal of sFe over cFe was observed, suggesting that sFe represents a more bioavailable fraction. Though it should be noted that dynamic exchange likely occurred between the soluble and colloidal fractions, thus whether the uptake occurred directly from the soluble phase or via the colloidal phase (or *vice versa*) cannot be confirmed (Fig. 6.1).

During summer, uptake and removal, coupled with reduced vertical mixing, resulted in a depletion of dFe (0.16 ± 0.071 nM, *n*= 15) and LpFe (0.11 ± 0.003 nM) in the SML. Given the particle rich nature of shelf water, it was a somewhat surprising result that below the seasonal pycnocline, dFe increased from spring to autumn, similar to NO_3^- and DIC [*Humphreys. et al.*, in prep] and thus consistent with seasonal remineralisation. This implies that a mechanism exists whereby dissolved Fe is seasonally stabilised against scavenging to the particulate phase (Fig. 6.1). This mechanism is hypothesised to be the seasonal build-up of organic Fe binding ligands derived from remineralising organic matter. It is possible that when the water column

overturns in the autumn, exposure to surface U.V irradiation may act to break down

organic Fe binding ligands, thus completing the seasonal cycle, though at present this is

conjecture.

The observed seasonal cycling observed provides a mechanism whereby Fe can

be removed from the SML of temperate shelf waters. Even lower concentrations of dFe

(< 0.1 nM) were observed during summer stratification over the Celtic and Hebridean

shelf breaks, indicating that seasonal Fe depletion to potentially growth limiting levels

is typical of seasonally stratifying regions in the North West European shelf sea. By also

measuring particulate fractions, all potentially bioavailable Fe fractions were accounted

for (Fig. 6.1), rather than just dFe as is typical, and thus the corresponding depletion of

particulate fractions adds weight to this conclusion. Depletion of available nutrients

(including Fe) exerts a bottom up control on the ecosystem structure, resulting in a

dominance of pico and nano phytoplankton [*Azam et al.*, 1983; *Boyd et al.*, 2012; *Lis et

al.*, 2015]. The dominance of smaller plankton increases the importance of energy

transfer through the microbial loop (Fig 6.2), thus reducing the efficiency of energy

transfer to higher trophic levels. Significantly, the large fisheries in shelf regions are

supported by efficient transfer of energy through trophic levels driven by blooms of

larger phytoplankton [*Cushing*, 1989]. Over the coming century, the strength of seasonal

stratification in North West European shelf seas is predicted to increase by ≈ 20% as a

result of climate change [*Holt et al.*, 2010]. The increasing strength of stratification is

expected to exacerbate oligotrophic conditions and reduce secondary production,

therefore increasing stress on fish and marine mammal populations [*Richardson and

Schoeman*, 2004]. The results presented in this thesis indicated that Fe seasonally

reached concentrations shown to be growth limiting elsewhere [e.g. *Blain et al.*, 2004].

Consequently, future studies aiming to understand bottom up controls of the ecosystem structure in highly productive temperate shelf seas should incorporate the seasonal cycling of Fe.
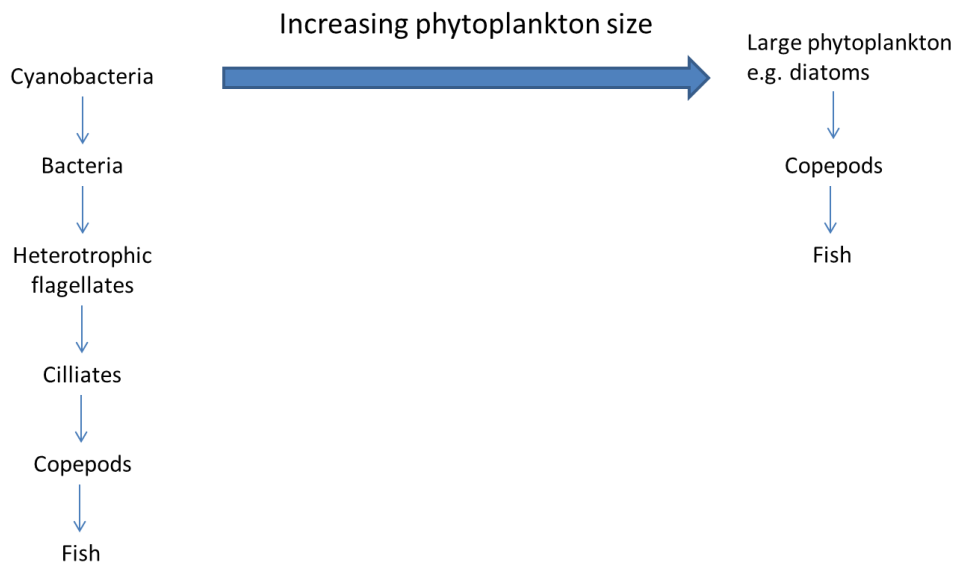
Figure 6-2- The effect of phytoplankton size on the structure of the food chain, modified from *Azam et al.* [1983]. At each trophic level, energy is lost from the food chain.

6.0.2 Hypothesis 2:

Intermediate nepheloid layers emanating from the Celtic Sea shelf slope have been observed to provide a transport mechanism of dFe to the adjacent Atlantic Ocean. In these particle rich waters, it is hypothesised that much of the dFe will be present in the colloidal phase and that the particulate fraction will dominate the Fe inventory.

The supply of Fe from oxic margin sediments is recognised as an important source of Fe to the ocean [*Conway and John*, 2014; *Homoky et al.*, 2013; *Radic et al.*, 2011]. The results of repeated shelf break transects revealed that the concentration of

dissolved and particulate Fe generally decreased over relatively short distances (10's km) from the Celtic Sea shelf break, indicating that an effective physical transport mechanism is required to deliver Fe to the ocean interior. Intermediate nepheloid layers, enriched in Fe, were present throughout all sampling seasons (spring, summer, autumn) over the Celtic Sea shelf slope and thus were a persistent conduit for the transport of Fe to the adjacent N.E Atlantic Ocean. The generation of INLs result from interaction between steep and irregular topography and strong currents. The Celtic Sea shelf slope is steep and incised with many canyons, likely enhancing the generation of INLs. Globally, 11.2% of the shelf slope area is incised with canyons; consequently transport of Fe by INLs from shelf slopes to the ocean interior is postulated to be a widespread phenomenon. Interestingly, 15.1% of Antarctic shelf slope area is incised with canyons [*Harris et al.*, 2014], therefore INLs may be an important mechanism for the transport of Fe to the most Fe starved region of the global ocean.

Determination of the physico-chemical speciation of Fe revealed that the concentration of TdFe-dFe>>>LpFe>>cFe>sFe. The majority of Fe over the Celtic Sea shelf slope was present in the particulate fraction, 20 ± 14 % of which was labile, therefore if particulate material is advected it may act to buffer the deep ocean dFe inventory (Fig. 6.1) [*Abadie et al.*, 2017; *Milne et al.*, 2017]. Consequently, effort should be made to calculate the flux of exchangeable particulate Fe from shelf margins, rather than the flux of dFe alone.

The dissolved fraction was dominated (60-90%) by cFe. This has important implications for our understanding of Fe cycling over oxic margins as cFe can be removed from solution via a 'colloidal pumping' mechanism (Fig. 6.1) [*Honeyman and Santschi*, 1991]. Additionally, the bioavailability of cFe decreases with ageing [*Yoshida et al.*, 2006],

cFe resuspended in deeper INLs will be subject to longer term ocean circulation pathways and thus would take decades or more to reach surface waters. In contrast, Fe remobilised from shallower INLs are connected to surface waters annually by winter mixing. Moreover, elevated near bottom Fe(II) concentrations (max 134 pM) over the upper shelf indicated redox processing of Fe in the upper slope sediments. Therefore, shallower INLs resulting from the resuspension of upper slope sediments are not only more readily connected to surface waters but also likely contain more labile, freshly formed cFe. Shelf sediment derived Fe is known to sustain highly productive shelf break ecosystems [*Aguilar-Islas et al.*, 2016], a comprehensive knowledge of the physico-chemical speciation and mechanisms of transport is an important aspect of these systems will aid our understanding of these systems.

Broadly, this study highlights the important role that colloidal Fe has in INLs and shelf waters. In Figure 6.1, it is shown that the colloidal fraction is comprised of both organic and inorganic components, which at present are poorly characterised. Additionally, it is shown the cFe can exchange with various phases within the soluble and particulate fractions (Fig. 6.1). A better understanding of both the composition of the colloidal fraction, and relative importance of the processes occurring between the colloidal and soluble and particulate fractions (the relative importance of the processes will likely be influenced by the colloidal composition) will improve our mechanistic understanding of the Fe cycling within INLs and shelf systems. In turn this will facilitate a more robust assessment of the function of shelf systems in the wider marine Fe cycle (e.g. the longevity of Fe rich INLs).

6.0.3 Hypothesis 3:

> *The seasonal cycling observed in the Celtic Sea will typify seasonally*
>
> *stratifying regions of the shelf seas around the U.K and Ireland.*

The results from an autumn field survey of the Hebridean shelf sea demonstrated that seasonal stratification impacted upon the distribution of dFe. In well mixed coastal waters, eutrophic conditions were observed including elevated concentrations of dFe (1.73 ± 1.16nM). In contrast, in stratified oceanic waters overlying the shelf break, Fe deplete (0.09 ± 0.04 nM) conditions were observed. The autumnal distribution of dFe in stratifying regions of the Hebridean Sea suggests the seasonal cycling of dFe is comparable to that observed in the Celtic Sea. However, unlike the Celtic Sea, the nutrient stoichiometry of the Hebridean Sea suggests that waters over the Hebridean shelf break system are seasonally Fe stressed to the degree that incomplete use of macronutrients occurs. This results from vertical mixing of water with a sub-optimal Fe:NO_3^- ratio. The distribution of dFe and macronutrients is consistent with observations in the Iceland and Irminger Basins, where seasonal Fe limitation prevents the complete use of available NO_3^- [*Achterberg et al.*, 2013; *Forryan et al.*, 2012; *Nielsdóttir et al.*, 2009; *Painter et al.*, 2014; *Ryan-Keogh et al.*, 2013]. It is therefore suggested that the Hebridean shelf represents part of the eastern boundary of sub-Arctic Atlantic seasonal Fe limitation, and that the associated weakening of the biological carbon pump occurs over a larger spatial area than previously recognised. Importantly, the northwest European shelf exports carbon to the Atlantic via downwelling circulation of bottom waters over the continental shelf slope ('Ekman Drain') [*Painter et al.*, 2016; *Thomas et al.*, 2004]. Incomplete use of macronutrients and

restriction of large phytoplankton growth over the shelf slope will restrict the build-up

of organic carbon in the bottom layer, and hence reduce the efficiency of the continental

shelf carbon pump.

6.1 Is the seasonal cycling of Fe in the Celtic and Hebridean Seas typical of temperate shelf systems?

Temperate shelf seas are present around all continental land masses with the

exception of Antarctica (Fig. 6.3). Below the major temperate shelf seas are briefly

summarised, with a comment on the likelihood that similar seasonal Fe cycling occurs

to that observed in the Celtic and Hebridean shelf seas. This discussion does not include

the temperate shelf regions within the major upwelling regions of the Americas as the

Fe cycling is already well described in the literature [e.g. *Chase et al.*, 2005a; *Hong and*
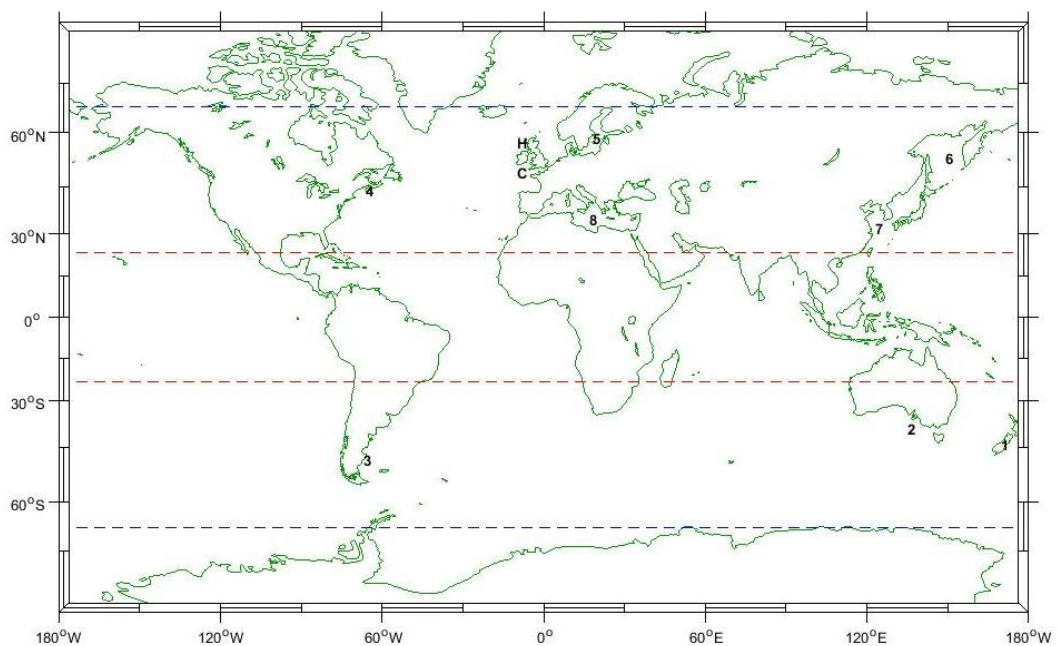
Figure 6-3- The location of major temperate shelf seas, this does not include the upwelling regions on the west coast of the Americas. Blue dashed lines mark the Arctic and Antarctic Circles. Red dashed lines mark the Tropics of Cancer (North) and Capricorn (south). C and H mark the Celtic and Hebridean Seas. 1. New Zealand 2. South Australia 3. Patagonia 4. New England 5. Baltic 6. Sea of Okhotsk 7. Yellow Sea 8. Mediterranean

Kester, 1986; *Hutchins and Bruland*, 1998; *King and Barbeau*, 2007; *Lohan and Bruland*,

2008; *Severmann et al.*, 2010].

1. New Zealand shelf-

The location of the sub-tropical convergence zone occurs near to the south-east

of New Zealand, separating warm nutrient poor waters to the north from cool nutrient

rich waters to the south. The macronutrient concentrations in New Zealand shelf waters

reflect the varying influence of sub-Antarctic and sub-Arctic waters. South East of New

Zealand, shelf waters contain elevated macronutrients associated with the mixing of

sub-Antarctic water, with sub-tropical influenced shelf waters to the north containing

lower macronutrient concentrations [*Butler et al.*, 1992]. Seasonal changes in the

availability of Fe/Si/light have been shown to limit the growth of diatoms in nearby

oceanic sub-Antarctic waters [*Boyd et al.*, 1999]. It is postulated here, that similar to the

Hebridean shelf, the conditions for Fe/Si co-limitation persist near to or over the south-

eastern shelf break of New Zealand. Over the inner shelf, coastal inputs of both Fe and

Si are predicated to alleviate these conditions. This hypothesis is supported by previous

work reporting a strong shelf wide gradient in Fe concentrations over the south-east

New Zealand shelf, with lateral exchange of Fe-rich neritic waters restricted by currents

flowing parallel to the shelf break [*Croot and Hunter*, 1998]. However, the distribution

of Fe limited waters is likely to be irregular as cross-shelf Fe transport in eddies is

important in this region [*Boyd et al.*, 2012].

In northern and westerly regions of the New Zealand shelf, comparable seasonal

cycling to the Celtic Sea has been reported. Seasonal stratification and associated

primary production results in drawdown of NO_3^- during late summer and shift in species

composition to smaller phytoplankton species [*Chang et al.*, 2003; *Hadfield and Sharples*,

1996]. It is likely that seasonal Fe draw down occurs in the SML, though the extent to which this may occur is unknown.

2. South Australian shelf-

The temperate shelf region south of Australia is a relatively narrow band of shelf sea stretching westwards from Tasmania to Perth. In the west, surface properties are dominated by the transport of nutrient poor sub-tropical water by the Leeuwin Current, which is a permanent feature resulting in little seasonality in surface waters. Concentrations of NO_3^- are permanently deplete (< 0.5 μM; N:P ≈ 4) indicating persistent NO_3^- limitation [*Lourey et al.*, 2006]. Therefore, a similar seasonal cycle of Fe to that observed in the Celtic or Hebridean Seas is unlikely. However, the lack of seasonality does not imply that Fe is replete, for instance Fe limitation of diazotrophs in coastal eddies has been suggested [*Holl et al.*, 2007]. East of Cape Leeuwin, seasonal coastal upwelling brings nutrient rich water to the surface, which stimulates increased primary productivity [*Kämpf et al.*, 2004]. Therefore, Fe cycling is more likely to mirror that observed in California upwelling system rather than the Celtic or Hebridean Seas. Consequently, the narrow south Australian shelf might not permit enough contact with sediments to provide sufficient Fe to fully utilise the nutrients in upwelled waters [*Chase et al.*, 2005b; *Chase et al.*, 2007]. Given the proximity to the semi-arid Australian continent, any investigation into Fe cycling in temperate Australian shelf systems will need to consider atmospheric deposition of Fe [*Mahowald et al.*, 2005].

3. Patagonian shelf-

The Patagonian shelf can be split into 3 zones, the coastal zone which remains well mixed year round, seasonally stratifying sub-Antarctic shelf waters and the Malvinas current system over the shelf break. Seasonally stratifying regions present

similar characteristics to the central Celtic Sea; water column depths > 100 m and during summer, a ≈ 10 °C difference between surface and bottom temperatures and NO_3^- depletion in surface waters [*Carreto et al.*, 1995]. Therefore, it is postulated that dFe will follow a similar seasonal distribution to that of NO_3^-. Comparison can also be made with the Hebridean Sea, the sub-Antarctic source water for the Patagonian shelf is the Malvinas current system, this has been shown to be Fe deplete with respect to macronutrients [*Rijkenberg et al.*, 2014]. Consequently, it is hypothesised that a shelf wide gradient in Fe availability exists, whereby coastal waters are Fe replete and shelf break waters are Fe limited with shelf waters representing the transition zone.

Highly productive frontal features exist in this region [*Garcia et al.*, 2008; *Romero et al.*, 2006], the role of Fe in sustaining this productivity is currently unknown. It is possible that the mixing of Fe limited sub-Antarctic water with NO_3^- limited sub-tropical waters creates these fertile frontal zones. Analogy can be made with the 'Green Belt' in the Bering Sea where Fe rich shelf water mixes with NO_3^- rich oceanic water stimulating a belt of increased productivity [*Aguilar-Islas et al.*, 2007].

Given the proximity to semi-arid south American terrain stretching from Peru to the Patagonian coast coupled with the presence of southern hemisphere westerlies, any investigation into Fe cycling in the Patagonian shelf systems will need to consider atmospheric deposition of Fe [*Gaiero et al.*, 2003; *Mahowald et al.*, 2005].

4. New England continental shelf-

The New England shelf contains regions that seasonally stratify, resulting in an 8-10 °C difference between surface and bottom waters during summer [*Lentz et al.*, 2003]. Similar to the Celtic Sea, the annual cycle of primary production is dominated by the spring and autumn blooms and the drawdown of NO_3^- to limiting levels during

summer stratification [*Townsend and Pettigrew*, 1997]. A noticeable difference between New England shelf waters and those of the Celtic and Hebridean Seas is the salinity. Salinities over the mid to outer New England shelf remain at ≈ 32-34 indicating a greater influence of freshwater [*Lentz et al.*, 2003]. Coastal waters in the Hebridean Sea had increased dFe concentrations. Therefore, although a similar seasonal cycle to that observed in the Celtic/Hebridean Sea is likely, over the New England shelf the initial inventory of Fe may be greater and prevent drawdown to potentially limiting levels. However, a New England shelf strain of *Synechococcus* retained the proteins required to uptake Fe at low concentrations despite the additional nitrogen needed to synthesise such proteins. In contrast, a strain from the permanently Fe replete and nitrogen deplete Sargasso Sea did not [*Mackey et al.*, 2015]. Therefore, Fe may not be permanently replete year round over the New England shelf, if so it is likely that Fe stress is greatest during summer stratification.

5. Baltic Sea-

The Baltic Sea is a semi-enclosed brackish basin which towards the north is fresher and seasonally covered in sea ice. Poor ventilation results in anoxic bottom waters with elevated (10-100's nM) dFe concentrations, which provide a large flux of dFe (annual mean= 12,400 nmol m^{-2} d^{-1}) to surface waters. Consequently, The concentration of iron in oxic surface waters ranges ≈ 2-15 nM and is lowest during summer when uptake and export, coupled with increased stratification reduces surface concentrations [*Breitbarth et al.*, 2009]. This system is clearly not comparable to the Celtic or Hebridean shelf seas and it would be reasonable to suggest that it is Fe replete given the Fe concentrations reported. However, the Baltic Sea has a very low (< 10) N:P ratio due to denitrification in anoxic bottom waters coupled with sedimentary PO_4^{4-}

input, which is exacerbated by N poor anthropogenic inputs [*Bonsdorff et al.*, 1997; *Bonsdorff et al.*, 2002]. Consequently, following uptake of the dissolved inorganic nitrogen by eukaryotic phytoplankton species in spring, diazotrophs bloom during summer. The nitrogen fixed by diazotrophs during this period accounts for 20-40% of N input to the Baltic [*Larsson et al.*, 2001]. The limiting nutrient(s) controlling the growth of Baltic Sea diazotrophs is currently not clear, with one bioassay study surprisingly suggesting that Fe availability may restrict their growth [*Lucas et al.*, 1999].

6. Sea of Okhotsk-

Despite its temperate latitude, the Sea of Okhotsk is ice free for only 4 months of the year [*Parkinson and Gratz*, 1983], and thus is not comparable to the Celtic or Hebridean shelf seas. Although sea ice is a source of Fe to the water column [*Sedwick and DiTullio*, 1997] and that water emanating from the Sea of Okhotsk contains elevated dFe concentrations [*Nishioka et al.*, 2007], a modelling study suggests that seasonal release of Fe from melting sea ice relieves Fe stress in the Sea of Okhotsk allowing the growth of diatoms [*Wang et al.*, 2014]. Thus, seasonal availability of Fe may influence the growth of phytoplankton in this region.

7. Yellow Sea-

The Yellow Sea is a shallow semi-enclosed shelf sea with an average depth of 44 m. Input of fresh water results in salinities < 32 towards the north and more oceanic values of 35 to the south [*Liu et al.*, 2003]. Macronutrient distributions are affected by seasonal stratification [*Liu et al.*, 2003], and thus seasonal Fe drawdown may also occur. However, given the coastal salinities, proximity to sediments and atmospheric Fe input from Asian dust [*Gao et al.*, 2001; *Mahowald et al.*, 2005], it is likely that this is an Fe replete region.

8. Mediterranean shelf seas-

The Mediterranean Sea is situated immediately north of the Saharan desert, a major source of Fe to oceanic surface waters via atmospheric deposition [*Ussher et al.*, 2013]. The concentration of dFe in surface waters of the Cretan Sea is higher (1.4-2.0 nM) in both spring and autumn that at depth ($\approx$ 0.5 nM), reflecting the dominance of atmospheric deposition of Fe [*Statham and Hart*, 2005]. Consequently, seasonality of Fe cycling in Mediterranean shelf waters is likely masked by atmospheric Fe inputs, which also make it likely that shelf seas in this region are Fe replete.

Summary

Of the temperate shelf regions considered, the New Zealand, Patagonian and New England shelf systems are most likely to exhibit a similar seasonal cycling. Therefore, these regions may also be subject to seasonal Fe (co-)limitation, thus the conclusions drawn regarding bottom up control of the ecosystem structure and reduction in the efficiency of atmospheric carbon draw down may also apply to these shelf systems. Although other temperate shelf systems exhibit different Fe cycling due to physical regimes, sea ice cover and atmospheric inputs, the availability of Fe may still influence the phytoplankton community structure. For instance, Fe availability may limit the growth of diazotrophs in the South Australian shelf system and surprisingly in the Baltic Sea, with seasonal release of Fe from sea ice potentially relieving Fe stress in the Sea of Okhotsk.

6.2 Future work

6.2.1 Confirming the degree and extent of Fe stress/limitation in Celtic and Hebridean Seas

The studies presented in this thesis combine geochemical measurements of Fe and macronutrients, with physical and biological parameters. These are combined with a wider knowledge of biogeochemical cycling to postulate that Fe seasonally co-limits primary production in the regions studied. The data presented from the Hebridean shelf are currently being combined with phytoplankton cell count data to identify correlations between the dFe distribution and the phytoplankton community composition [*Birchill et al.*, in prep]. In doing so, this will provide further insight into how the structure of the phytoplankton community is affect by Fe availability. Additionally, future sampling campaigns could use bioassay experiments as diagnostic tools to confirm Fe (co-)limitation and examine spatial variability, such as Fe stress at the subsurface chlorophyll maximum in comparison to surface waters [e.g. *Blain et al.*, 2004; *Hopkinson and Barbeau*, 2008]. Diagnostic bioassay experiments could also be combined with measurements of the expression of proteins associated with Fe stress [e.g. *Mackey et al.*, 2015]. This is particularly important as the stoichiometric ratios used in this study assume that dFe represents bioavailable Fe. However, the speciation of Fe within the dissolved fraction is complex (Fig. 6.1), thus assuming a uniform bioavailability of dFe is more than likely an over simplification. Moreover, addition bioavailable Fe may come from the particulate fraction (Fig. 6.1). By conducting bioassay experiments, the issue of identifying what represents bioavailable Fe would be left to biological community, who are clearly the best judge.

In addition, improving the parametrisation of Fe in the European Regional Seas Ecosystem Model would allow investigations into the spatial extent of Fe limitation on the shelf. For instance, localised regions of enhanced vertical mixing, such as over Jones Bank [*Palmer et al.*, 2013], and the spring-neap adjustment of tidal mixing fronts [*Sharples et al.*, 2007] might increase Fe supply to surface waters during summer stratification. The results of such a modelling study could be used to inform future sampling campaigns and test the hypothesis that the predicted increase in stratification over the coming century will further exacerbate Fe stress.

6.2.2 Transport of Fe from oxic shelf margins

The results presented in this thesis demonstrate that INLs represent a persistent conduit for the supply of Fe to the ocean interior from the Celtic Sea shelf slope. A key piece of information missing at this time is the rate of Fe transport in INLs. By combining the physico-chemical speciation of Fe observations from this work, with radium isotope measurements, estimates of the Fe flux from the Celtic Sea shelf slope are underway [*Annett et al.*, in prep]. A better understanding of rates of Fe supply to the ocean is needed, as evidenced by residence time estimates varying from 5-500 years in a recent global biogeochemical model inter-comparison [*Tagliabue et al.*, 2015].

6.2.3 Seasonal Fe cycling in other shelf margins

The results presented in this thesis demonstrate that despite proximity to shelf sediments, Fe reached growth limiting concentrations in temperate shelf waters during summer stratification. Targeted summer field surveys of New Zealand, Patagonian and New England shelf waters would test the hypothesis that similar seasonal cycling also occurs in these shelf systems. Temperate shelf systems are reported to be regions of atmospheric CO_2 drawdown [*Chen and Borges*, 2009], seasonal Fe (co-)limitation may

be a feature of many temperate shelf systems, and the effect this may have on carbon cycling is currently unclear. As evidenced in Fig. 6.1, the marine Fe cycle is complex, thus for a full understanding of temperate shelf sea Fe cycling, future studies should make comprehensive measurements of the physico-chemical speciation of Fe.

6.2.4 Analytical recommendations for the determination of particulate Fe fractions

In section 4.2.1 it was demonstrated that long term acidification of unfiltered samples (TdFe) accessed more Fe than particulate material subjected to a weak acid leach (with a reducing agent; LpFe). Therefore, it was demonstrated that long term acidification of unfiltered water samples accessed refractory particulate Fe phases. Previous studies have been inconsistent in their treatment of the TdFe fraction, with some viewing it as a labile fraction [e.g. *Chever et al.*, 2010; *Loscher et al.*, 1997] and others as a refractory fraction [*Sedwick et al.*, 2008]. Correctly or incorrectly defining this fraction has clear implications for our environmental interpretation (Fig. 6.1), thus this should be an area of future work.

The collection and analysis of unfiltered water samples is simpler than that of particulate material and thus it is tempting to just collect unfiltered water samples. However, it is recommended that future studies simultaneously collect a representative set of particulate samples for leaching so that the fraction accessed by long term acidification can be assessed by comparison. It is suggested that this is conducted by all future studies as the assessment carried out in this study is unlikely to be representative of all environments (e.g. open ocean, hydrothermal systems) and particulate leaching [see *Lam et al.*, 2015] and water sample acidification (0.024 or 0.01 M) procedures.

References

Abadie, C., F. Lacan, A. Radic, C. Pradoux, and F. Poitrasson (2017), Iron isotopes reveal distinct dissolved iron sources and pathways in the intermediate versus deep Southern Ocean, *Proceedings of the National Academy of Sciences*, *114*(5), 858-863, doi:10.1073/pnas.1603107114.

Achterberg, E. P., T. W. Holland, A. R. Bowie, R. F. C. Mantoura, and P. J. Worsfold (2001), Determination of iron in seawater, *Analytica Chimica Acta*, *442*(1), 1-14, doi:http://dx.doi.org/10.1016/S0003-2670(01)01091-1.

Achterberg, E. P., M. C. Moore, S. A. Henson, S. Steigenberger, A. Stohl, S. Eckhardt, L. C. Avendano, M. Cassidy, D. Hembury, and J. K. Klar (2013), Natural iron fertilization by the Eyjafjallajökull volcanic eruption, *Geophysical Research Letters*, *40*(5), 921-926, doi:10.1002/grl.50221.

Aguilar-Islas, A. M., M. P. Hurst, K. N. Buck, B. Sohst, G. J. Smith, M. C. Lohan, and K. W. Bruland (2007), Micro-and macronutrients in the southeastern Bering Sea: Insight into iron-replete and iron-depleted regimes, *Progress in Oceanography*, *73*(2), 99-126, doi:https://doi.org/10.1016/j.pocean.2006.12.002.

Aguilar-Islas, A. M., M. J. M. Séguret, R. Rember, K. N. Buck, P. Proctor, C. W. Mordy, and N. B. Kachel (2016), Temporal variability of reactive iron over the Gulf of Alaska shelf, *Deep Sea Research Part II: Topical Studies in Oceanography*, *132*, 90-106, doi:http://dx.doi.org/10.1016/j.dsr2.2015.05.004.

References

Annett, A. L., A. J. Birchill, J. E. Hopkins, W. B. Homoky, H. Thomas, A. Milne, D. Rusiecka, E. P. Achterberg, J. Sharples, E. M. S. Woodward, P. J. Statham, M. C. Lohan, and W. Giebert (in prep), Rapid supply of iron from continent margins to the ocean by intermediate nepheloid layers, *Nature Geoscience*.

Annett, A. L., S. F. Henley, P. Van Beek, M. Souhaut, R. Ganeshram, H. J. Venables, M. P. Meredith, and W. Geibert (2013), Use of radium isotopes to estimate mixing rates and trace sediment inputs to surface waters in northern Marguerite Bay, Antarctic Peninsula, *Antarctic Science*, *25*(03), 445-456, doi:https://doi.org/10.1017/S0954102012000892.

Antia, A. N., B. von Bodungen, and R. Peinert (1999), Particle flux across the mid-European continental margin, *Deep Sea Research Part I: Oceanographic Research Papers*, *46*(12), doi:https://doi.org/10.1016/S0967-0637(99)00041-2.

Arrigo, K. R., D. L. Worthen, and D. H. Robinson (2003), A coupled ocean-ecosystem model of the Ross Sea: 2. Iron regulation of phytoplankton taxonomic variability and primary production, *Journal of Geophysical Research: Oceans*, *108*(C7), doi:10.1029/2001JC000856.

Aumont, O., C. Ethé, A. Tagliabue, L. Bopp, and M. Gehlen (2015), PISCES-v2: an ocean biogeochemical model for carbon and ecosystem studies, *Geoscientific Model Development*, *8*(8), 2465-2513.

Avendaño, L., M. Gledhill, E. P. Achterberg, V. M. C. Rérolle, and C. Schlosser (2016), Influence of ocean acidification on the organic complexation of iron and copper in

Northwest European shelf seas; a combined observational and model study, *Frontiers in Marine Science*, *3*, doi:10.3389/fmars.2016.00058.

Azam, F., T. Fenchel, J. Field, J. Gray, L. Meyer-Reil, and F. Thingstad (1983), The ecological role of water-column microbes in the sea, *Marine ecology progress series. Oldendorf*, *10*(3), 257-263.

Bailly Du Bois, P., P. Germain, M. Rozet, and L. Solier (2002), Water masses circulation and residence time in the Celtic Sea and English Channel approaches, characterisation based on radionuclides labelling from industrial releases, in *International Conference on Radioactivity in Environment*, edited by P. Borretzen, T. Jolle and P. Strand, pp. 395-399, Monaco.

Barbeau, K. (2006), Photochemistry of Organic Iron(III) Complexing Ligands in Oceanic Systems, *Photochemistry and Photobiology*, *82*(6), 1505-1516, doi:10.1562/2006-06-16-IR-935.

Barbeau, K., and J. W. Moffett (2000), Laboratory and field studies of colloidal iron oxide dissolution as mediated by phagotrophy and photolysis, *Limnology and Oceanography*, *45*(4), 827-835, doi:10.4319/lo.2000.45.4.0827.

Barbeau, K., J. W. Moffett, D. A. Caron, P. L. Croot, and D. L. Erdner (1996), Role of protozoan grazing in relieving iron limitation of phytoplankton, *Nature, 380*(6569), 61, doi:doi:10.1038/380061a0.

References

Barbeau, K., E. Rue, K. Bruland, and A. Butler (2001), Photochemical cycling of iron in the surface ocean mediated by microbial iron (III)-binding ligands, *Nature*, *413*(6854), 409-413, doi:doi:10.1038/35096545.

Barni, F., S. W. Lewis, A. Berti, G. M. Miskelly, and G. Lago (2007), Forensic application of the luminol reaction as a presumptive test for latent blood detection, *Talanta*, *72*(3), 896-913, doi:https://doi.org/10.1016/j.talanta.2006.12.045.

Baskaran, M., P. H. Santschi, G. Benoit, and B. Honeyman (1992), Scavenging of thorium isotopes by colloids in seawater of the Gulf of Mexico, *Geochimica et cosmochimica Acta*, *56*(9), 3375-3388, doi:https://doi.org/10.1016/0016-7037(92)90385-V.

Berelson, W., J. McManus, K. Coale, K. Johnson, D. Burdige, T. Kilgore, D. Colodner, F. Chavez, R. Kudela, and J. Boucher (2003), A time series of benthic flux measurements from Monterey Bay, CA, *Continental Shelf Research*, *23*(5), 457-481, doi:http://dx.doi.org/10.1016/S0278-4343(03)00009-8.

Berger, C. J., S. M. Lippiatt, M. G. Lawrence, and K. W. Bruland (2008), Application of a chemical leach technique for estimating labile particulate aluminum, iron, and manganese in the Columbia River plume and coastal waters off Oregon and Washington, *Journal of Geophysical Research*, *113*(C2), doi:10.1029/2007JC004703.

Birchill, A. J., N. Hartner, K. Kunder, D. Gonzalez-Santana, B. Siemering, A. Milne, S. C. Painter, C. J. Daniels, S. Ussher, P. J. Worsfold, and M. C. Lohan (in prep), The Hebridean Shelf- the eastern extent of seasonal iron limitation in the Sub-Arctic North Atlantic, *Global Biogeochemical Cycles*.

References

Birchill, A. J., A. Milne, E. M. S. Woodward, A. L. Annett, W. Giebert, S. Ussher, P. J. Worsfold, D. Rusiecka, E. P. Achterberg, C. Harris, M. Gledhill, and M. C. Lohan (2017), Seasonal iron depletion in temperate shelf seas, *Geophysical Research Letters*.

Blain, S., S. Bonnet, and C. Guieu (2008), Dissolved iron distribution in the tropical and sub tropical South Eastern Pacific, *Biogeosciences*, *5*(1), 269-280, doi:10.5194/bg-5-269-2008.

Blain, S., C. Guieu, H. Claustre, K. Leblanc, T. Moutin, B. Quèguiner, J. Ras, and G. Sarthou (2004), Availability of iron and major nutrients for phytoplankton in the northeast Atlantic Ocean, *Limnology and Oceanography*, *49*(6), 2095-2104, doi:10.4319/lo.2004.49.6.2095.

Bonsdorff, E., E. M. Blomqvist, J. Mattila, and A. Norkko (1997), Coastal eutrophication: Causes, consequences and perspectives in the Archipelago areas of the northern Baltic Sea, *Estuarine, Coastal and Shelf Science*, *44*, 63-72, doi:http://dx.doi.org/10.1016/S0272-7714(97)80008-X.

Bonsdorff, E., C. Rönnberg, and K. Aarnio (2002), Some ecological properties in relation to eutrophication in the Baltic Sea, in *Nutrients and Eutrophication in Estuaries and Coastal Waters: Proceedings of the 31st Symposium of the Estuarine and Coastal Sciences Association (ECSA), held in Bilbao, Spain, 3–7 July 2000*, edited by E. Orive, M. Elliott and V. N. de Jonge, pp. 371-377, Springer Netherlands, Dordrecht, doi:10.1007/978-94-017-2464-7_27.

Booth, D. A., and D. J. Ellett (1983), The Scottish continental slope current, *Continental Shelf Research*, *2*(2), 127-146, doi:http://dx.doi.org/10.1016/0278-4343(83)90012-2.

References

Borer, P. M., B. Sulzberger, P. Reichard, and S. M. Kraemer (2005), Effect of siderophores on the light-induced dissolution of colloidal iron(III) (hydr)oxides, *Marine Chemistry*, *93*(2–4), 179-193, doi:http://dx.doi.org/10.1016/j.marchem.2004.08.006.

Bourgault, D., M. Morsilli, C. Richards, U. Neumeier, and D. E. Kelley (2014), Sediment resuspension and nepheloid layers induced by long internal solitary waves shoaling orthogonally on uniform slopes, *Continental Shelf Research*, *72*, 21-33, doi:http://dx.doi.org/10.1016/j.csr.2013.10.019.

Bowie, A., and M. Lohan (2009), Determination of iron in seawater, in *Practical Guidelines for the Analysis of Seawater* edited by O. Wurl, Taylor & Francis Group, Florida.

Bowie, A. R., E. P. Achterberg, P. L. Croot, H. J. W. de Baar, P. Laan, J. W. Moffett, S. Ussher, and P. J. Worsfold (2006), A community-wide intercomparison exercise for the determination of dissolved iron in seawater, *Marine Chemistry*, *98*(1), 81-99, doi:http://dx.doi.org/10.1016/j.marchem.2005.07.002.

Bowie, A. R., E. P. Achterberg, R. F. C. Mantoura, and P. J. Worsfold (1998), Determination of sub-nanomolar levels of iron in seawater using flow injection with chemiluminescence detection, *Analytica Chimica Acta*, *361*(3), 189-200, doi:https://doi.org/10.1016/S0003-2670(98)00015-4.

Bowie, A. R., E. P. Achterberg, P. N. Sedwick, S. Ussher, and P. J. Worsfold (2002), Real-time monitoring of picomolar concentrations of iron (II) in marine waters using automated flow injection-chemiluminescence instrumentation, *Environmental science & technology*, *36*(21), 4600-4607, doi:10.1021/es020045v.

References

Bowie, A. R., E. P. Achterberg, S. Ussher, and P. J. Worsfold (2005), Design of an automated flow injection-chemiluminescence instrument incorporating a miniature photomultiplier tube for monitoring picomolar concentrations of iron in seawater, *Journal of Analytical Methods in Chemistry*, *2005*(2), 37-43, doi:10.1155/JAMMC.2005.37.

Bowie, A. R., D. Lannuzel, T. A. Remenyi, T. Wagener, P. J. Lam, P. W. Boyd, C. Guieu, A. T. Townsend, and T. W. Trull (2009), Biogeochemical iron budgets of the Southern Ocean south of Australia: Decoupling of iron and nutrient cycles in the subantarctic zone by the summertime supply, *Global Biogeochemical Cycles*, *23*(4), doi:10.1029/2009GB003500.

Bowie, A. R., P. N. Sedwick, and P. J. Worsfold (2004), Analytical intercomparison between flow injection-chemiluminescence and flow injection-spectrophotometry for the determination of picomolar concentrations of iron in seawater, *Limnology and Oceanography: Methods*, *2*(2), 42-54, doi:10.4319/lom.2004.2.42.

Boyd, P., E. Ibisanmi, S. Sander, K. Hunter, and G. Jackson (2010), Remineralization of upper ocean particles: Implications for iron biogeochemistry, *Limnology and Oceanography*, *55*(3), 1271, doi:10.4319/lo.2010.55.3.1271.

Boyd, P., T. Jickells, C. Law, S. Blain, E. Boyle, K. Buesseler, K. Coale, J. Cullen, H. De Baar, and M. Follows (2007), Mesoscale iron enrichment experiments 1993-2005: Synthesis and future directions, *science*, *315*(5812), 612-617, doi:10.1126/science.1131669.

References

Boyd, P., J. LaRoche, M. Gall, R. Frew, and R. M. L. McKay (1999), Role of iron, light, and silicate in controlling algal biomass in subantarctic waters SE of New Zealand, *Journal of Geophysical Research: Oceans*, *104*(C6), 13395-13408, doi:10.1029/1999JC900009.

Boyd, P., A. J. Watson, C. S. Law, E. R. Abraham, T. Trull, R. Murdoch, D. C. E. Bakker, A. R. Bowie, K. O. Buesseler, H. Chang, M. Charette, P. Croot, K. Downing, R. Frew, M. Gall, M. Hadfield, J. Hall, M. Harvey, G. Jameson, J. LaRoche, M. Liddicoat, R. Ling, M. T. Maldonado, R. M. McKay, S. Nodder, S. Pickmere, R. Pridmore, S. Rintoul, K. Safi, P. Sutton, R. Strzepek, K. Tanneberger, S. Turner, A. Waite, and J. Zeldis (2000), A mesoscale phytoplankton bloom in the polar Southern Ocean stimulated by iron fertilization, *Nature*, *407*(6805), 695-702, doi: doi:10.1038/35037500.

Boyd, P. W., and M. J. Ellwood (2010), The biogeochemical cycle of iron in the ocean, *Nature Geoscience*, *3*(10), 675-682, doi:doi:10.1038/ngeo964.

Boyd, P. W., R. Strzepek, S. Chiswell, H. Chang, J. M. DeBruyn, M. Ellwood, S. Keenan, A. L. King, E. W. Maas, S. Nodder, S. G. Sander, P. Sutton, B. S. Twining, S. W. Wilhelm, and D. A. Hutchins (2012), Microbial control of diatom bloom dynamics in the open ocean, *Geophysical Research Letters*, *39*(18), n/a-n/a, doi:10.1029/2012GL053448.

Boye, M., A. P. Aldrich, C. M. G. van den Berg, J. T. M. de Jong, M. Veldhuis, and H. J. W. de Baar (2003), Horizontal gradient of the chemical speciation of iron in surface waters of the northeast Atlantic Ocean, *Marine Chemistry*, *80*(2–3), 129-143, doi:http://dx.doi.org/10.1016/S0304-4203(02)00102-0.

References

Boyle, E. A., J. M. Edmond, and E. R. Sholkovitz (1977), The mechanism of iron removal in estuaries, *Geochimica et Cosmochimica Acta*, *41*(9), 1313-1324, doi:http://dx.doi.org/10.1016/0016-7037(77)90075-8.

Breitbarth, E., J. Gelting, J. Walve, L. J. Hoffmann, D. R. Turner, M. Hassellöv, and J. Ingri (2009), Dissolved iron (II) in the Baltic Sea surface water and implications for cyanobacterial bloom development, *Biogeosciences*, *6*(11), 2397-2420, doi:10.5194/bg-6-2397-2009.

Brewer, P., and J. Riley (1965), The automatic determination of nitrate in sea water, paper presented at Deep Sea Research and Oceanographic Abstracts, Elsevier.

Bruland, K. W. (2014), Dissolved Iron – values in nmol/kg Consensus values (± 1 std. dev.) for SAFe Reference Samples as of May 2013, edited, doi:https://websites.pmc.ucsc.edu/~kbruland/GeotracesSaFe/2012GeotracesSAFeValues/SAFe_Ref_Fe.pdf.

Brzezinski, M. A. (1985), The Si: C: N ratio of marine diatoms: interspecific variability and the effect of some environmental variables, *Journal of Phycology*, *21*(3), 347-357, doi:10.1111/j.0022-3646.1985.00347.x.

Bucciarelli, E., S. Blain, and P. Tréguer (2001), Iron and manganese in the wake of the Kerguelen Islands (Southern Ocean), *Marine Chemistry*, *73*(1), 21-36, doi:http://dx.doi.org/10.1016/S0304-4203(00)00070-0.

References

Buck, K. N., and K. W. Bruland (2007), The physicochemical speciation of dissolved iron in the Bering Sea, Alaska, *Limnology and Oceanography*, *52*(5), 1800, doi:10.4319/lo.2007.52.5.1800.

Buck, K. N., M. C. Lohan, C. J. Berger, and K. W. Bruland (2007), Dissolved iron speciation in two distinct river plumes and an estuary: Implications for riverine iron supply, *Limnology and Oceanography*, *52*(2), 843-855, doi:10.4319/lo.2007.52.2.0843.

Buesseler, K. O., S. C. Doney, D. M. Karl, P. Boyd, K. Caldeira, F. Chai, K. H. Coale, H. J. W. de Baar, P. G. Falkowski, K. S. Johnson, R. S. Lampitt, A. F. Michaels, S. W. A. Naqvi, V. Smetacek, S. Takeda, and A. J. Watson (2008), Ocean Iron Fertilization--Moving Forward in a Sea of Uncertainty, *Science*, *319*(5860), 162-162, doi:10.1126/science.1154305.

Butler, E., J. Butt, E. Lindstrom, P. Teldesley, S. Pickmere, and W. Vincent (1992), Oceanography of the subtropical convergence zone around southern New Zealand, *New Zealand Journal of Marine and Freshwater Research*, *26*(2), 131-154, doi:http://dx.doi.org/10.1080/00288330.1992.9516509.

Byrne, R. H., and D. R. Kester (1976), A potentiometric study of ferric ion complexes in synthetic media and seawater, *Marine Chemistry*, *4*(3), 275-287, doi:https://doi.org/10.1016/0304-4203(76)90013-X.

Carreto, J., V. A. Lutz, M. O. Carignan, A. D. Cucchi Colleoni, and S. G. De Marco (1995), Hydrography and chlorophyll a in a transect from the coast to the shelf-break in the Argentinian Sea, *Continental Shelf Research*, *15*(2), 315-336, doi:http://dx.doi.org/10.1016/0278-4343(94)E0001-3.

<u>*References*</u>

Carritt, D., E, and J. Carpenter, H (1966), Comparison and evaluation of currently employed modifications of the Winkler method for determining dissolved oxygen in seawater; a NASCO report, *Journal of Marine Reseaidi*, *24*, 286-318.

Chang, F. H., J. Zeldis, M. Gall, and J. Hall (2003), Seasonal and spatial variation of phytoplankton assemblages, biomass and cell size from spring to summer across the north-eastern New Zealand continental shelf, *Journal of Plankton Research*, *25*(7), 737-758, doi:10.1093/plankt/25.7.737.

Chappell, P. D., L. P. Whitney, J. R. Wallace, A. I. Darer, S. Jean-Charles, and B. D. Jenkins (2015), Genetic indicators of iron limitation in wild populations of Thalassiosira oceanica from the northeast Pacific Ocean, *ISME J*, *9*(3), 592-602, doi:10.1038/ismej.2014.171.

Chase, Z., B. Hales, T. Cowles, R. Schwartz, and A. van Geen (2005a), Distribution and variability of iron input to Oregon coastal waters during the upwelling season, *Journal of Geophysical Research: Oceans*, *110*(C10), n/a-n/a, doi:10.1029/2004JC002590.

Chase, Z., K. S. Johnson, V. A. Elrod, J. N. Plant, S. E. Fitzwater, L. Pickell, and C. M. Sakamoto (2005b), Manganese and iron distributions off central California influenced by upwelling and shelf width, *Marine Chemistry*, *95*(3), 235-254.

Chase, Z., P. G. Strutton, and B. Hales (2007), Iron links river runoff and shelf width to phytoplankton biomass along the US West Coast, *Geophysical Research Letters*, *34*(4), doi:10.1029/2006GL028069.

References

Chen, C.-T. A., and A. V. Borges (2009), Reconciling opposing views on carbon cycling in the coastal ocean: continental shelves as sinks and near-shore ecosystems as sources of atmospheric CO 2, *Deep Sea Research Part II: Topical Studies in Oceanography*, *56*(8), 578-590.

Chen, M., R. C. H. Dei, W.-X. Wang, and L. Guo (2003), Marine diatom uptake of iron bound with natural colloids of different origins, *Marine Chemistry*, *81*(3–4), 177-189, doi:http://dx.doi.org/10.1016/S0304-4203(03)00032-X.

Chen, M., and W.-X. Wang (2001), Bioavailability of natural colloid-bound iron to marine plankton: Influences of colloidal size and aging, *Limnology and oceanography*, *46*(8), 1956-1967.

Chever, F., E. Bucciarelli, G. Sarthou, S. Speich, M. Arhan, P. Penven, and A. Tagliabue (2010), Physical speciation of iron in the Atlantic sector of the Southern Ocean along a transect from the subtropical domain to the Weddell Sea Gyre, *Journal of Geophysical Research: Oceans*, *115*(C10), doi:10.1029/2009JC005880.

Clough, R., H. Sela, A. Milne, M. C. Lohan, S. Tokalioglu, and P. J. Worsfold (2015), Uncertainty contributions to the measurement of dissolved Co, Fe, Pb and V in seawater using flow injection with solid phase preconcentration and detection by collision cell - quadrupole ICP-MS, *Talanta*, doi:http://dx.doi.org/10.1016/j.talanta.2014.08.045.

Coale, K. H., K. S. Johnson, F. P. Chavez, K. O. Buesseler, R. T. Barber, M. A. Brzezinski, W. P. Cochlan, F. J. Millero, P. G. Falkowski, J. E. Bauer, R. H. Wanninkhof, R. M. Kudela, M. A. Altabet, B. E. Hales, T. Takahashi, M. R. Landry, R. R. Bidigare, X. Wang, Z. Chase,

References

P. G. Strutton, G. E. Friederich, M. Y. Gorbunov, V. P. Lance, A. K. Hilting, M. R. Hiscock, M. Demarest, W. T. Hiscock, K. F. Sullivan, S. J. Tanner, R. M. Gordon, C. N. Hunter, V. A. Elrod, S. E. Fitzwater, J. L. Jones, S. Tozzi, M. Koblizek, A. E. Roberts, J. Herndon, J. Brewster, N. Ladizinsky, G. Smith, D. Cooper, D. Timothy, S. L. Brown, K. E. Selph, C. C. Sheridan, B. S. Twining, and Z. I. Johnson (2004), Southern Ocean Iron Enrichment Experiment: Carbon Cycling in High- and Low-Si Waters, *Science*, *304*(5669), 408-414, doi:10.1126/science.1089778.

Coale, K. H., K. S. Johnson, P. M. Stout, and C. M. Sakamoto (1992), Determination of copper in sea water using a flow-injection method with chemiluminescence detection, *Analytica chimica acta*, *266*(2), 345-351.

Conway, T. M., and S. G. John (2014), Quantification of dissolved iron sources to the North Atlantic Ocean, *Nature*, *511*(7508), 212-215.

Cotté-Krief, M.-H., A. J. Thomas, and J.-M. Martin (2002), Trace metal (Cd, Cu, Ni and Pb) cycling in the upper water column near the shelf edge of the European continental margin (Celtic Sea), *Marine Chemistry*, *79*(1), 1-26, doi:https://doi.org/10.1016/S0304-4203(02)00013-0.

Croot, P. L., and K. A. Hunter (1998), Trace metal distributions across the continental shelf near Otago Peninsula, New Zealand, *Marine Chemistry*, *62*(3–4), 185-201, doi:http://dx.doi.org/10.1016/S0304-4203(98)00036-X.

Croot, P. L., and P. Laan (2002), Continuous shipboard determination of Fe (II) in polar waters using flow injection analysis with chemiluminescence detection, *Analytica Chimica Acta*, *466*(2), 261-273.

References

Cullen, J. T., B. A. Bergquist, and J. W. Moffett (2006), Thermodynamic characterization of the partitioning of iron between soluble and colloidal species in the Atlantic Ocean, *Marine Chemistry*, *98*(2), 295-303.

Cunningham, M. J., S. Hodgson, D. G. Masson, and L. M. Parson (2005), An evaluation of along- and down-slope sediment transport processes between Goban Spur and Brenot Spur on the Celtic Margin of the Bay of Biscay, *Sedimentary Geology*, *179*(1–2), 99-116, doi:http://dx.doi.org/10.1016/j.sedgeo.2005.04.014.

Cushing, D. H. (1989), A difference in structure between ecosystems in strongly stratified waters and in those that are only weakly stratified, *Journal of Plankton Research*, *11*(1), 1-13, doi:10.1093/plankt/11.1.1.

Cutter, G., P. Andersson, L. Codispoti, P. Croot, R. Francois, M. Lohan, H. Obata, and M. Rutgers vd Loeff (2010), Sampling and sample-handling protocols for GEOTRACES Cruises, edited, doi:10013/epic.42722.

Dale, A. W., L. Nickelsen, F. Scholz, C. Hensen, A. Oschlies, and K. Wallmann (2015), A revised global estimate of dissolved iron fluxes from marine sediments, *Global Biogeochemical Cycles*, *29*(5), 691-707.

Daniels, C. J., A. J. Poulton, M. Esposito, M. L. Paulsen, R. Bellerby, M. St. John, and A. P. Martin (2015), Phytoplankton dynamics in contrasting early stage North Atlantic spring blooms: composition, succession, and potential drivers, *Biogeosciences Discussions*, *12*, 93-133.

References

Davidson, K., R. J. Gowen, P. Tett, E. Bresnan, P. J. Harrison, A. McKinney, S. Milligan, D. K. Mills, J. Silke, and A.-M. Crooks (2012), Harmful algal blooms: How strong is the evidence that nutrient ratios and forms influence their occurrence?, *Estuarine, Coastal and Shelf Science*, *115*, 399-413.

De Baar, H. J. W., K. R. Timmermans, P. Laan, H. H. De Porto, S. Ober, J. J. Blom, M. C. Bakker, J. Schilling, G. Sarthou, M. G. Smit, and M. Klunder (2008), Titan: A new facility for ultraclean sampling of trace elements and isotopes in the deep oceans in the international Geotraces program, *Marine Chemistry*, *111*(1–2), 4-21, doi:http://dx.doi.org/10.1016/j.marchem.2007.07.009.

de Haas, H., T. C. E. van Weering, and H. de Stigter (2002), Organic carbon in shelf seas: sinks or sources, processes and products, *Continental Shelf Research*, *22*(5), 691-717, doi:http://dx.doi.org/10.1016/S0278-4343(01)00093-0.

De Jong, J., J. Den Das, U. Bathmann, M. Stoll, G. Kattner, R. Nolting, and H. De Baar (1998), Dissolved iron at subnanomolar levels in the Southern Ocean as determined by ship-board analysis, *Analytica Chimica Acta*, *377*(2), 113-124.

Dehairs, F., W. Baeyens, and D. Van Gansbeke (1989), Tight coupling between enrichment of iron and manganese in North Sea suspended matter and sedimentary redox processes: evidence for seasonal variability, *Estuarine, Coastal and Shelf Science*, *29*(5), 457-471.

Denman, K. L. (2008), Climate change, ocean processes and ocean iron fertilization, *Marine Ecology Progress Series*, *364*, 219-225.

References

Dickson, R. R., and I. N. McCave (1986), Nepheloid layers on the continental slope west of Porcupine Bank, *Deep Sea Research Part A. Oceanographic Research Papers*, *33*(6), 791-818, doi:http://dx.doi.org/10.1016/0198-0149(86)90089-0.

Dunne, J. P., J. G. John, E. Shevliakova, R. J. Stouffer, J. P. Krasting, S. L. Malyshev, P. Milly, L. T. Sentman, A. J. Adcroft, and W. Cooke (2013), GFDL's ESM2 global coupled climate–Carbon Earth System Models. Part II: Carbon system formulation and baseline simulation characteristics, *Journal of Climate*, *26*(7), 2247-2267.

Egge, J., and D. Aksnes (1992), Silicate as regulating nutrient in phytoplankton competition, *Marine ecology progress series. Oldendorf*, *83*(2), 281-289.

Ellett, D., and A. Edwards (1983), Oceanography and inshore hydrography of the Inner Hebrides, *Proceedings of the Royal Society of Edinburgh, Section B: Biological Sciences*, *83*, 144-160.

Elrod, V., K. Johnson, S. Fitzwater, and J. Plant (2008), A long term, high resolution record of surface water iron concentrations in the upwelling‐driven central California region, *Journal of Geophysical Research: Oceans*, *113*(C11).

Elrod, V. A., W. M. Berelson, K. H. Coale, and K. S. Johnson (2004), The flux of iron from continental shelf sediments: A missing source for global budgets, *Geophysical Research Letters*, *31*(12).

Emery, W., and J. Meincke (1986), Global water masses-summary and review, *Oceanologica acta*, *9*(4), 383-391.

References

Falkowski, P. G., and J. A. Raven (2007), *Aquatic photosynthesis*, Princeton University Press, Oxford.

Fang, Z., J. Růžička, and E. H. Hansen (1984), An efficient flow-injection system with on-line ion-exchange preconcentration for the determination of trace amounts of heavy metals by atomic absorption spectrometry, *Analytica Chimica Acta*, *164*(0), 23-39, doi:http://dx.doi.org/10.1016/S0003-2670(00)85614-7.

Fasham, M. J. R., P. M. Holligan, and P. R. Pugh (1983), The spatial and temporal development of the spring phytoplankton bloom in the Celtic Sea, April 1979, *Progress in Oceanography*, *12*(1), 87-145, doi:http://dx.doi.org/10.1016/0079-6611(83)90007-1.

Fitzsimmons, J. N., and E. A. Boyle (2014), Both soluble and colloidal iron phases control dissolved iron variability in the tropical North Atlantic Ocean, *Geochimica et Cosmochimica Acta*, *125*, 539-550, doi:http://dx.doi.org/10.1016/j.gca.2013.10.032.

Fitzsimmons, J. N., G. G. Carrasco, J. Wu, S. Roshan, M. Hatta, C. I. Measures, T. M. Conway, S. G. John, and E. A. Boyle (2015a), Partitioning of dissolved iron and iron isotopes into soluble and colloidal phases along the GA03 GEOTRACES North Atlantic Transect, *Deep Sea Research Part II: Topical Studies in Oceanography*, *116*, 130-151, doi:http://dx.doi.org/10.1016/j.dsr2.2014.11.014.

Fitzsimmons, J. N., C. T. Hayes, S. N. Al-Subiai, R. Zhang, P. L. Morton, R. E. Weisend, F. Ascani, and E. A. Boyle (2015b), Daily to decadal variability of size-fractionated iron and iron-binding ligands at the Hawaii Ocean Time-series Station ALOHA, *Geochimica et Cosmochimica Acta*, *171*, 303-324.

References

Fitzwater, S. E., K. S. Johnson, V. A. Elrod, J. P. Ryan, L. J. Coletti, S. J. Tanner, R. M. Gordon, and F. P. Chavez (2003), Iron, nutrient and phytoplankton biomass relationships in upwelled waters of the California coastal system, *Continental Shelf Research*, *23*(16), 1523-1544, doi:http://dx.doi.org/10.1016/j.csr.2003.08.004.

Floor, G. H., R. Clough, M. C. Lohan, S. J. Ussher, P. J. Worsfold, and C. R. Quétel (2015), Combined uncertainty estimation for the determination of the dissolved iron amount content in seawater using flow injection with chemiluminescence detection, *Limnology and Oceanography: Methods*, *13*(12), 673-686, doi:10.1002/lom3.10057.

Forryan, A., A. P. Martin, M. A. Srokosz, E. E. Popova, S. C. Painter, and M. C. Stinchcombe (2012), Turbulent nutrient fluxes in the Iceland Basin, *Deep Sea Research Part I: Oceanographic Research Papers*, *63*, 20-35, doi:http://doi.org/10.1016/j.dsr.2011.12.006.

Friedl, G., C. Dinkel, and B. Wehrli (1998), Benthic fluxes of nutrients in the northwestern Black Sea, *Marine Chemistry*, *62*(1–2), 77-88, doi:http://dx.doi.org/10.1016/S0304-4203(98)00029-2.

Froelich, P. N., G. P. Klinkhammer, M. L. Bender, N. A. Luedtke, G. R. Heath, D. Cullen, P. Dauphin, D. Hammond, B. Hartman, and V. Maynard (1979), Early oxidation of organic matter in pelagic sediments of the eastern equatorial Atlantic: suboxic diagenesis, *Geochimica et Cosmochimica Acta*, *43*(7), 1075-1090, doi:http://dx.doi.org/10.1016/0016-7037(79)90095-4.

Gaiero, D. M., J. L. Probst, P. J. Depetris, S. M. Bidart, and L. Leleyter (2003), Iron and other transition metals in Patagonian riverborne and windborne materials:

References

---

geochemical control and transport to the southern South Atlantic Ocean, *Geochimica et Cosmochimica Acta*, *67*(19), 3603-3623, doi:https://doi.org/10.1016/S0016-7037(03)00211-4.

Gao, Y., Y. Kaufman, D. Tanre, D. Kolber, and P. Falkowski (2001), Seasonal distributions of aeolian iron fluxes to the global ocean, *Geophysical Research Letters*, *28*(1), 29-32.

Garcia-Solsona, E., J. Garcia-Orellana, P. Masqué, and H. Dulaiova (2008), Uncertainties associated with ^{223}Ra and ^{224}Ra measurements in water via a Delayed Coincidence Counter (RaDeCC), *Marine Chemistry*, *109*(3), 198-219.

Garcia, H. E., R. A. Locarnini, T. P. Boyer, J. I. Antonov, O.K. Baranova, M.M. Zweng, J.R. Reagan, and D. R. Johnson (2014), World Ocean Atlas 2013 Dissolved Inorganic Nutrients (phosphate, nitrate, silicate), edited by S. Levitus and A. Mishonov, p. 25, NOAA Atlas NESDIS

Garcia, V. M. T., C. A. E. Garcia, M. M. Mata, R. C. Pollery, A. R. Piola, S. R. Signorini, C. R. McClain, and M. D. Iglesias-Rodriguez (2008), Environmental factors controlling the phytoplankton blooms at the Patagonia shelf-break in spring, *Deep Sea Research Part I: Oceanographic Research Papers*, *55*(9), 1150-1166, doi:https://doi.org/10.1016/j.dsr.2008.04.011.

Giering, S. L., S. Steigenberger, E. P. Achterberg, R. Sanders, and D. J. Mayor (2012), Elevated iron to nitrogen recycling by mesozooplankton in the Northeast Atlantic Ocean, *Geophysical Research Letters*, *39*(12).

References

Gledhill, M., E. P. Achterberg, K. Li, K. N. Mohamed, and M. J. Rijkenberg (2015), Influence of ocean acidification on the complexation of iron and copper by organic ligands in estuarine waters, *Marine Chemistry*, *177*, 421-433.

Gledhill, M., and K. N. Buck (2012), The organic complexation of iron in the marine environment: a review, *Frontiers in microbiology*, *3*, doi:10.3389/fmicb.2012.00069.

Gledhill, M., P. McCormack, S. Ussher, E. P. Achterberg, R. F. C. Mantoura, and P. J. Worsfold (2004), Production of siderophore type chelates by mixed bacterioplankton populations in nutrient enriched seawater incubations, *Marine Chemistry*, *88*(1), 75-83.

Gledhill, M., and C. M. G. van den Berg (1994), Determination of complexation of iron(III) with natural organic complexing ligands in seawater using cathodic stripping voltammetry, *Marine Chemistry*, *47*(1), 41-54, doi:http://dx.doi.org/10.1016/0304-4203(94)90012-4.

Gordon, R. M., J. H. Martin, and G. A. Knauer (1982), Iron in north-east Pacific waters, *Nature*, *299*(5884), 611-612.

Gowen, R., R. Raine, M. Dickey-Collas, and M. White (1998), Plankton distributions in relation to physical oceanographic features on the southern Malin Shelf, August 1996, *ICES Journal of Marine Science: Journal du Conseil*, *55*(6), 1095-1111.

Gran, H. H. (1932), Phytoplankton. Methods and problems, *Journal du Conseil*, *7*(3), 343-358.

Grantham, B., and P. Tett (1993), The nutrient status of the Clyde Sea in winter, *Estuarine, Coastal and Shelf Science*, *36*(5), 449-462.

References

Haber, F., and J. Weiss (1934), The catalytic decomposition of hydrogen peroxide by iron salts, _Proceedings of the Royal Society of London. Series A, Mathematical and Physical Sciences_, _147_(861), 332-351.

Hadfield, M. G., and J. Sharples (1996), Modelling mixed layer depth and plankton biomass off the west coast of South Island, New Zealand, _Journal of Marine Systems_, _8_(1), 1-29, doi:http://dx.doi.org/10.1016/0924-7963(95)00045-3.

Harris, P. T., M. Macmillan-Lawler, J. Rupp, and E. K. Baker (2014), Geomorphology of the oceans, _Marine Geology_, _352_, 4-24, doi:http://dx.doi.org/10.1016/j.margeo.2014.01.011.

Hatta, M., C. I. Measures, J. Wu, S. Roshan, J. N. Fitzsimmons, P. Sedwick, and P. Morton (2015), An overview of dissolved Fe and Mn distributions during the 2010–2011 U.S. GEOTRACES north Atlantic cruises: GEOTRACES GA03, _Deep Sea Research Part II: Topical Studies in Oceanography_, _116_, 117-129, doi:http://dx.doi.org/10.1016/j.dsr2.2014.07.005.

Henson, S. A., R. Sanders, C. Holeton, and J. T. Allen (2006), Timing of nutrient depletion, diatom dominance and a lower-boundary estimate of export production for Irminger Basin, North Atlantic, _Marine Ecology Progress Series_, _313_, 73-84.

Hickman, A. E., P. M. Holligan, C. M. Moore, J. Sharples, V. Krivtsov, and M. R. Palmer (2009), Distribution and chromatic adaptation of phytoplankton within a shelf sea thermocline, _Limnology and Oceanography_, _54_(2), 525-536, doi:10.4319/lo.2009.54.2.0525.

References

Hickman, A. E., C. M. Moore, J. Sharples, M. I. Lucas, G. H. Tilstone, V. Krivtsov, and P. M. Holligan (2012), Primary production and nitrate uptake within the seasonal thermocline of a stratified shelf sea, *Marine Ecology Progress Series*, *463*, 39-57.

Ho, T. Y., A. Quigg, Z. V. Finkel, A. J. Milligan, K. Wyman, P. G. Falkowski, and F. M. Morel (2003), The elemental composition of some marine phytoplankton, *Journal of Phycology*, *39*(6), 1145-1159.

Holl, C. M., A. M. Waite, S. Pesant, P. A. Thompson, and J. P. Montoya (2007), Unicellular diazotrophy as a source of nitrogen to Leeuwin Current coastal eddies, *Deep Sea Research Part II: Topical Studies in Oceanography*, *54*(8–10), 1045-1054, doi:https://doi.org/10.1016/j.dsr2.2007.02.002.

Holliday, N. (2003), Air sea interaction and circulation changes in the northeast Atlantic, *Journal of Geophysical Research: Oceans*, *108*(C8).

Holliday, P. N., R. T. Pollard, J. F. Read, and H. Leach (2000), Water mass properties and fluxes in the Rockall Trough, 1975–1998, *Deep Sea Research Part I: Oceanographic Research Papers*, *47*(7), 1303-1332, doi:https://doi.org/10.1016/S0967-0637(99)00109-0.

Holligan, P. M., and S. B. Groom (1986), Phytoplankton distributions along the shelf break, *Proceedings of the Royal Society of Edinburgh. Section B. Biological Sciences*, *88*, 239-263, doi:10.1017/S0269727000004589.

Holm-Hansen, O., C. J. Lorenzen, R. W. Holmes, and J. D. Strickland (1965), Fluorometric determination of chlorophyll, *Journal du Conseil*, *30*(1), 3-15.

References

Holt, J., S. Wakelin, and J. Huthnance (2009), Down-welling circulation of the northwest European continental shelf: A driving mechanism for the continental shelf carbon pump, *Geophysical Research Letters*, *36*(14), doi:10.1029/2009GL038997.

Holt, J., S. Wakelin, J. Lowe, and J. Tinker (2010), The potential impacts of climate change on the hydrography of the northwest European continental shelf, *Progress in Oceanography*, *86*(3–4), 361-379, doi:http://doi.org/10.1016/j.pocean.2010.05.003.

Homoky, W. B., D. J. Hembury, L. E. Hepburn, R. A. Mills, P. J. Statham, G. R. Fones, and M. R. Palmer (2011), Iron and manganese diagenesis in deep sea volcanogenic sediments and the origins of pore water colloids, *Geochimica et Cosmochimica Acta*, *75*(17), 5032-5048, doi:http://dx.doi.org/10.1016/j.gca.2011.06.019.

Homoky, W. B., S. G. John, T. M. Conway, and R. A. Mills (2013), Distinct iron isotopic signatures and supply from marine sediment dissolution, *Nature communications*, *4*, doi:10.1038/ncomms3143.

Homoky, W. B., S. Severmann, J. McManus, W. M. Berelson, T. E. Riedel, P. J. Statham, and R. A. Mills (2012), Dissolved oxygen and suspended particles regulate the benthic flux of iron from continental margins, *Marine Chemistry*, *134*, 59-70.

Honeyman, B. D., and P. H. Santschi (1991), Coupling adsorption and particle aggregation: laboratory studies of" colloidal pumping" using iron-59-labeled hematite, *Environmental science & technology*, *25*(10), 1739-1747.

Hong, H., and D. R. Kester (1986), Redox state of iron in the offshore waters of Peru, *Limnol. Oceanogr*, *31*(3), 512-524.

Hopkinson, B. M., and K. A. Barbeau (2008), Interactive influences of iron and light limitation on phytoplankton at subsurface chlorophyll maxima in the eastern North Pacific, *Limnology and Oceanography*, *53*(4), 1303-1318, doi:10.4319/lo.2008.53.4.1303.

Hopwood, M. J., S. Bacon, K. Arendt, D. P. Connelly, and P. J. Statham (2015), Glacial meltwater from Greenland is not likely to be an important source of Fe to the North Atlantic, *Biogeochemistry*, *124*(1), 1-11, doi:10.1007/s10533-015-0091-6.

Hopwood, M. J., A. J. Birchill, M. Gledhill, A. Milne, and E. P. Achterberg (2017), A 4 method comparison for the measurement of Fe(II) at nanomolar concentrations in coastal seawater, *Frontiers in Chemistry*.

Humphreys., M. P., E. P. Achterberg., M. Z. H. Chowdhury., A. M. Griffiths., S. E. Hartman., J. E. Hopkins., T. Hull., C. Kivimäe., A. Smilenova., J. Wihsgott., E. M. S. Woodward., and C. M. Moore. (in prep), Mechanisms for a nutrient-conserving carbon pump in a seasonally stratified, temperate continental shelf sea, *Progress in Oceanography*.

Hurst, M. P., A. M. Aguilar-Islas, and K. W. Bruland (2010), Iron in the southeastern Bering Sea: elevated leachable particulate Fe in shelf bottom waters as an important source for surface waters, *Continental Shelf Research*, *30*(5), 467-480.

Hurst, M. P., and K. W. Bruland (2007), An investigation into the exchange of iron and zinc between soluble, colloidal, and particulate size-fractions in shelf waters using low-abundance isotopes as tracers in shipboard incubation experiments, *Marine Chemistry*, *103*(3–4), 211-226, doi:https://doi.org/10.1016/j.marchem.2006.07.001.

References

___

Hutchins, D. A., and K. W. Bruland (1998), Iron-limited diatom growth and Si:N uptake ratios in a coastal upwelling regime, *Nature*, *393*(6685), 561-564.

Huthnance, J. M., H. Coelho, C. R. Griffiths, P. J. Knight, A. P. Rees, B. Sinha, A. Vangriesheim, M. White, and P. G. Chatwin (2001), Physical structures, advection and mixing in the region of Goban spur, *Deep Sea Research Part II: Topical Studies in Oceanography*, *48*(14–15), 2979-3021, doi:http://dx.doi.org/10.1016/S0967-0645(01)00030-3.

Huthnance, J. M., J. T. Holt, and S. L. Wakelin (2009), Deep ocean exchange with west-European shelf seas, *Ocean Sci.*, *5*(4), 621-634, doi:10.5194/os-5-621-2009.

Hydes, D., M. Aoyama, A. Aminot, K. Bakker, S. Becker, S. Coverly, A. Daniel, A. Dickson, O. Grosso, and R. Kerouel (2010), Determination of dissolved nutrients (N, P, Si) in seawater with high precision and inter-comparability using gas-segmented continuous flow analysers, *The GO-SHIP Repeat Hydrography Manual: a collection of expert reports and guidelines; IOCCP report No.14, ICPO publication series No. 134, version 1*.

Hydes, D., R. Gowen, N. Holliday, T. Shammon, and D. Mills (2004a), External and internal control of winter concentrations of nutrients (N, P and Si) in north-west European shelf seas, *Estuarine, Coastal and Shelf Science*, *59*(1), 151-161.

Hydes, D. J., R. J. Gowen, N. P. Holliday, T. Shammon, and D. Mills (2004b), External and internal control of winter concentrations of nutrients (N, P and Si) in north-west European shelf seas, *Estuarine, Coastal and Shelf Science*, *59*(1), 151-161, doi:http://dx.doi.org/10.1016/j.ecss.2003.08.004.

References

Ibisanmi, E., S. G. Sander, P. Boyd, A. R. Bowie, and K. A. Hunter (2011), Vertical distributions of iron-(III) complexing ligands in the Southern Ocean, *Deep Sea Research Part II: Topical Studies in Oceanography*, *58*(21–22), 2113-2125, doi:http://dx.doi.org/10.1016/j.dsr2.2011.05.028.

Inall, M., P. Gillibrand, C. Griffiths, N. MacDougal, and K. Blackwell (2009), On the oceanographic variability of the North-West European Shelf to the West of Scotland, *Journal of Marine Systems*, *77*(3), 210-226.

Jefferies, D., A. Preston, and A. Steele (1973), Distribution of caesium-137 in British coastal waters, *Marine Pollution Bulletin*, *4*(8), 118-122.

Jiann, K.-T., P. H. Santschi, and B. J. Presley (2013), Relationships Between Geochemical Parameters (pH, DOC, SPM, EDTA Concentrations) and Trace Metal (Cd, Co, Cu, Fe, Mn, Ni, Pb, Zn) Concentrations in River Waters of Texas (USA), *Aquatic Geochemistry*, *19*(2), 173-193.

Jickells, T. D., Z. S. An, K. K. Andersen, A. R. Baker, G. Bergametti, N. Brooks, J. J. Cao, P. Boyd, R. A. Duce, K. A. Hunter, H. Kawahata, N. Kubilay, J. laRoche, P. S. Liss, N. Mahowald, J. M. Prospero, A. J. Ridgwell, I. Tegen, and R. Torres (2005), Global Iron Connections Between Desert Dust, Ocean Biogeochemistry, and Climate, *Science*, *308*(5718), 67-71, doi:10.1126/science.1105959.

John, S. G., J. Mendez, J. Moffett, and J. Adkins (2012), The flux of iron and iron isotopes from San Pedro Basin sediments, *Geochimica et Cosmochimica Acta*, *93*, 14-29, doi:http://dx.doi.org/10.1016/j.gca.2012.06.003.

References

Johnson, C., M. Inall, and S. Häkkinen (2013), Declining nutrient concentrations in the northeast Atlantic as a result of a weakening Subpolar Gyre, *Deep Sea Research Part I: Oceanographic Research Papers*, *82*, 95-107.

Johnson, K. S., F. P. Chavez, and G. E. Friederich (1999), Continental-shelf sediment as a primary source of iron for coastal phytoplankton, *Nature*, *398*(6729), 697-700.

Johnson, K. S., R. M. Gordon, and K. H. Coale (1997), What controls dissolved iron concentrations in the world ocean?, *Marine Chemistry*, *57*(3), 137-161.

Johnson, Z. I., R. Shyam, A. E. Ritchie, C. Mioni, V. P. Lance, J. W. Murray, and E. R. Zinser (2010), The effect of iron-and light-limitation on phytoplankton communities of deep chlorophyll maxima of the western Pacific Ocean, *Journal of Marine Research*, *68*(2), 283-308.

Jones, K., and R. Gowen (1990), Influence of stratification and irradiance regime on summer phytoplankton composition in coastal and shelf seas of the British Isles, *Estuarine, Coastal and Shelf Science*, *30*(6), 557-567.

Kämpf, J., M. Doubell, D. Griffin, R. L. Matthews, and T. M. Ward (2004), Evidence of a large seasonal coastal upwelling system along the southern shelf of Australia, *Geophysical Research Letters*, *31*(9), n/a-n/a, doi:10.1029/2003GL019221.

Kieber, R. J., K. Williams, J. D. Willey, S. Skrabal, and G. B. Avery Jr (2001), Iron speciation in coastal rainwater: concentration and deposition to seawater, *Marine Chemistry*, *73*(2), 83-95, doi:http://dx.doi.org/10.1016/S0304-4203(00)00097-9.

References

King, A. L., and K. Barbeau (2007), Evidence for phytoplankton iron limitation in the southern California Current System, *Marine Ecology Progress Series*, *342*, 91-103.

King, D. W., H. A. Lounsbury, and F. J. Millero (1995), Rates and Mechanism of Fe(II) Oxidation at Nanomolar Total Iron Concentrations, *Environmental Science & Technology*, *29*(3), 818-824, doi:10.1021/es00003a033.

Kirkwood, D. (1996), *Nutrients: Practical notes on their determination in sea water*, International Council for the Exploration of the Sea.

Klar, J., W. B. Homoky, P. J. Statham, A. J. Birchill, E. Harris, E. M. S. Woodward, B. Silburn, M. Cooper, R. H. James, and D. P. Connelly (2017), Stability of dissolved and soluble Fe (II) in shelf sediment pore waters and release to an oxic water column, *Biogeochemistry*, doi:10.1007/s10533-017-0309-x.

Klopf, L. L., and T. A. Nieman (1983), Effect of iron(II), cobalt(II), copper(II), and manganese(II) on the chemiluminescence of luminol in the absence of hydrogen peroxide, *Analytical Chemistry*, *55*(7), 1080-1083, doi:10.1021/ac00258a023.

Klunder, M., P. Laan, R. Middag, H. De Baar, and J. Van Ooijen (2011), Dissolved iron in the Southern Ocean (Atlantic sector), *Deep Sea Research Part II: Topical Studies in Oceanography*, *58*(25), 2678-2694.

Klunder, M. B., D. Bauch, P. Laan, H. Baar, S. Heuven, and S. Ober (2012), Dissolved iron in the Arctic shelf seas and surface waters of the central Arctic Ocean: Impact of Arctic river water and ice‐melt, *Journal of Geophysical Research: Oceans (1978‐2012)*, *117*(C1).

References

Laës, A., S. Blain, P. Laan, E. P. Achterberg, G. Sarthou, and H. J. W. de Baar (2003), Deep dissolved iron profiles in the eastern North Atlantic in relation to water masses, *Geophysical Research Letters*, *30*(17), 1902, doi:10.1029/2003GL017902.

Laes, A., S. Blain, P. Laan, S. Ussher, E. P. Achterberg, P. Treguer, and H. De Baar (2007), Sources and transport of dissolved iron and manganese along the continental margin of the Bay of Biscay, *Biogeosciences*, *4*(2), 181-194.

Lam, P. J., and J. K. B. Bishop (2008), The continental margin is a key source of iron to the HNLC North Pacific Ocean, *Geophysical Research Letters*, *35*(7), doi:10.1029/2008GL033294.

Lam, P. J., J. K. B. Bishop, C. C. Henning, M. A. Marcus, G. A. Waychunas, and I. Y. Fung (2006), Wintertime phytoplankton bloom in the subarctic Pacific supported by continental margin iron, *Global Biogeochemical Cycles*, *20*(1), doi:10.1029/2005GB002557.

Lam, P. J., B. S. Twining, C. Jeandel, A. Roychoudhury, J. A. Resing, P. H. Santschi, and R. F. Anderson (2015), Methods for analyzing the concentration and speciation of major and trace elements in marine particles, *Progress in Oceanography*, *133*, 32-42, doi:https://doi.org/10.1016/j.pocean.2015.01.005.

Landing, W. M., C. Haraldsson, and N. Paxeus (1986), Vinyl polymer agglomerate based transition metal cation-chelating ion-exchange resin containing the 8-hydroxyquinoline functional group, *Analytical Chemistry*, *58*(14), 3031-3035, doi:10.1021/ac00127a029.

References

Landry, M., J. Constantinou, M. Latasa, S. Brown, R. Bidigare, and M. Ondrusek (2000), Biological response to iron fertilization in the eastern equatorial Pacific (IronEx II). III. Dynamics of phytoplankton growth and microzooplankton grazing, *Marine Ecology Progress Series*, *201*(57-72), 453.

Lannuzel, D., J. de Jong, V. Schoemann, A. Trevena, J.-L. Tison, and L. Chou (2006), Development of a sampling and flow injection analysis technique for iron determination in the sea ice environment, *Analytica chimica acta*, *556*(2), 476-483.

Larsson, U., S. Hajdu, J. Walve, and R. Elmgren (2001), Baltic Sea nitrogen fixation estimated from the summer increase in upper mixed layer total nitrogen, *Limnology and Oceanography*, *46*(4), 811-820, doi:10.4319/lo.2001.46.4.0811.

Lentz, S., K. Shearman, S. Anderson, A. Plueddemann, and J. Edson (2003), Evolution of stratification over the New England shelf during the Coastal Mixing and Optics study, August 1996–June 1997, *Journal of Geophysical Research: Oceans*, *108*(C1), doi:10.1029/2001JC001121.

Lis, H., Y. Shaked, C. Kranzler, N. Keren, and F. M. M. Morel (2015), Iron bioavailability to phytoplankton: an empirical approach, *ISME J*, *9*(4), 1003-1013, doi:10.1038/ismej.2014.199.

Liu, S. M., J. Zhang, S. Z. Chen, H. T. Chen, G. H. Hong, H. Wei, and Q. M. Wu (2003), Inventory of nutrient compounds in the Yellow Sea, *Continental Shelf Research*, *23*(11–13), 1161-1174, doi:https://doi.org/10.1016/S0278-4343(03)00089-X.

References

Liu, X., and F. J. Millero (2002), The solubility of iron in seawater, *Marine Chemistry*, *77*(1), 43-54.

Lohan, M. C., A. M. Aguilar-Islas, R. P. Franks, and K. W. Bruland (2005), Determination of iron and copper in seawater at pH 1.7 with a new commercially available chelating resin, NTA Superflow, *Analytica Chimica Acta*, *530*(1), 121-129, doi:http://dx.doi.org/10.1016/j.aca.2004.09.005.

Lohan, M. C., and K. W. Bruland (2008), Elevated Fe (II) and dissolved Fe in hypoxic shelf waters off Oregon and Washington: An enhanced source of iron to coastal upwelling regimes, *Environmental science & technology*, *42*(17), 6462-6468.

Lohse, L., W. Helder, E. Epping, and W. Balzer (1998), Recycling of organic matter along a shelf-slope transect across the NW European Continental Margin (Goban Spur), *Progress in Oceanography*, *42*(1), 77-110.

Loscher, B. M., H. J. W. De Baar, J. T. M. De Jong, C. Veth, and F. Dehairs (1997), The distribution of Fe in the antarctic circumpolar current, *Deep Sea Research Part II: Topical Studies in Oceanography*, *44*(1), 143-187, doi:http://dx.doi.org/10.1016/S0967-0645(96)00101-4.

Louanchi, F., and R. G. Najjar (2000), A global monthly climatology of phosphate, nitrate, and silicate in the upper ocean: Spring-summer export production and shallow remineralization, *Global Biogeochemical Cycles*, *14*(3), 957-977, doi:10.1029/1999GB001215.

References

Lourey, M. J., J. R. Dunn, and J. Waring (2006), A mixed-layer nutrient climatology of Leeuwin Current and Western Australian shelf waters: Seasonal nutrient dynamics and biomass, *Journal of Marine Systems*, *59*(1), 25-51, doi:http://dx.doi.org/10.1016/j.jmarsys.2005.10.001.

Lucas, J. S., S. Marc, and V. Marlies (1999), Nutrient control of cyanobacterial blooms in the Baltic Sea, *Aquatic Microbial Ecology*, *18*(2), 165-173.

Mackey, K. R., A. F. Post, M. R. McIlvin, G. A. Cutter, S. G. John, and M. A. Saito (2015), Divergent responses of Atlantic coastal and oceanic Synechococcus to iron limitation, *Proceedings of the National Academy of Sciences*, *112*(32), 9944-9949.

Magnusson, B., T. Näykk, H. Hovind, and M. Krysell (2012), Handbook for calculation of measurement uncertainty in environmental laboratories (NT TR 537 - Edition 3.1)*Rep.*

Mahowald, N. M., A. R. Baker, G. Bergametti, N. Brooks, R. A. Duce, T. D. Jickells, N. Kubilay, J. M. Prospero, and I. Tegen (2005), Atmospheric global dust cycle and iron inputs to the ocean, *Global biogeochemical cycles*, *19*(4).

Marsay, C. M., P. N. Sedwick, M. S. Dinniman, P. M. Barrett, S. L. Mack, and D. J. McGillicuddy (2014), Estimating the benthic efflux of dissolved iron on the Ross Sea continental shelf, *Geophysical Research Letters*, *41*(21), 7576-7583, doi:10.1002/2014GL061684.

Martin, J. H. (1990), Glacial-interglacial CO_2 change: The iron hypothesis, *Paleoceanography*, *5*(1), 1-13.

References

Martin, J. H., K. H. Coale, K. S. Johnson, S. E. Fitzwater, R. M. Gordon, S. J. Tanner, C. N. Hunter, V. A. Elrod, J. L. Nowicki, T. L. Coley, R. T. Barber, S. Lindley, A. J. Watson, K. Van Scoy, C. S. Law, M. I. Liddicoat, R. Ling, T. Stanton, J. Stockel, C. Collins, A. Anderson, R. Bidigare, M. Ondrusek, M. Latasa, F. J. Millero, K. Lee, W. Yao, J. Z. Zhang, G. Friederich, C. Sakamoto, F. Chavez, K. Buck, Z. Kolber, R. Greene, P. Falkowski, S. W. Chisholm, F. Hoge, R. Swift, J. Yungel, S. Turner, P. Nightingale, A. Hatton, P. Liss, and N. W. Tindale (1994), Testing the iron hypothesis in ecosystems of the equatorial Pacific Ocean, *Nature*, *371*(6493), 123-129.

Martin, J. H., and S. E. Fitzwater (1988), Iron deficiency limits phytoplankton growth in the north-east Pacific subarctic, *Nature*, *331*, 341-343, doi:10.1038/331341a0.

Martin, J. H., S. E. Fitzwater, R. Michael Gordon, C. N. Hunter, and S. J. Tanner (1993), Iron, primary production and carbon-nitrogen flux studies during the JGOFS North Atlantic bloom experiment, *Deep Sea Research Part II: Topical Studies in Oceanography*, *40*(1), 115-134, doi:http://dx.doi.org/10.1016/0967-0645(93)90009-C.

McCave, I. N. (1971), Wave effectiveness at the sea bed and its relationship to bed-forms and deposition of mud, *Journal of Sedimentary Research*, *41*(1), 89-96, doi:10.1306/74d721f3-2b21-11d7-8648000102c1865d.

McCave, I. N., I. R. Hall, A. N. Antia, L. Chou, F. Dehairs, R. S. Lampitt, L. Thomsen, T. C. E. van Weering, and R. Wollast (2001), Distribution, composition and flux of particulate material over the European margin at 47°–50°N, *Deep Sea Research Part II: Topical*

Studies in Oceanography, *48*(14–15), 3107-3139, doi:http://dx.doi.org/10.1016/S0967-0645(01)00034-0.

McCubbin, D., K. S. Leonard, J. Brown, P. J. Kershaw, R. A. Bonfield, and T. Peak (2002), Further studies of the distribution of technetium-99 and caesium-137 in UK and European coastal waters, *Continental Shelf Research*, *22*(10), 1417-1445.

McGillicuddy, D. J., P. N. Sedwick, M. Dinniman, K. R. Arrigo, T. S. Bibby, B. J. Greenan, E. E. Hofmann, J. M. Klinck, W. O. Smith, and S. Mack (2015), Iron supply and demand in an Antarctic shelf ecosystem, *Geophysical Research Letters*, *42*(19), 8088-8097.

McKay, W. A., M. S. Baxter, D. J. Ellett, and D. T. Meldrum (1986), Radiocaesium and circulation patterns west of Scotland, *Journal of Environmental Radioactivity*, *4*(3), 205-232, doi:http://dx.doi.org/10.1016/0265-931X(86)90011-1.

McLennan, S. M. (2001), Relationships between the trace element composition of sedimentary rocks and upper continental crust, *Geochemistry, Geophysics, Geosystems*, *2*(4).

Measures, C. I., W. M. Landing, M. T. Brown, and C. S. Buck (2008), High-resolution Al and Fe data from the Atlantic Ocean CLIVAR-CO_2 Repeat Hydrography A16N transect: Extensive linkages between atmospheric dust and upper ocean geochemistry, *Global Biogeochemical Cycles*, *22*(1), doi:10.1029/2007GB003042.

Measures, C. I., and S. Vink (2001), Dissolved Fe in the upper waters of the Pacific sector of the Southern Ocean, *Deep Sea Research Part II: Topical Studies in*

Oceanography, *48*(19–20), 3913-3941, doi:http://dx.doi.org/10.1016/S0967-0645(01)00074-1.

Menard, H. W., and S. M. Smith (1966), Hypsometry of ocean basin provinces, *Journal of Geophysical Research*, *71*(18), 4305-4325, doi:10.1029/JZ071i018p04305.

Merényi, G., J. Lind, and T. E. Eriksen (1990), Luminol chemiluminescence: Chemistry, excitation, emitter, *Journal of Bioluminescence and Chemiluminescence*, *5*(1), 53-56, doi:10.1002/bio.1170050111.

Mikuška, P., and Z. Večeřa (2003), Simultaneous determination of nitrite and nitrate in water by chemiluminescent flow-injection analysis, *Analytica Chimica Acta*, *495*(1), 225-232.

Millero, F. J., and S. Sotolongo (1989), The oxidation of Fe (II) with H_2O_2 in seawater, *Geochimica et Cosmochimica Acta*, *53*(8), 1867-1873.

Millero, F. J., S. Sotolongo, and M. Izaguirre (1987), The oxidation kinetics of Fe(II) in seawater, *Geochimica et Cosmochimica Acta*, *51*(4), 793-801, doi:http://dx.doi.org/10.1016/0016-7037(87)90093-7.

Milne, A., M. S. Davey, P. J. Worsfold, E. P. Achterberg, and A. R. Taylor (2009), Real-time detection of reactive oxygen species generation by marine phytoplankton using flow injection-chemiluminescence, *Limnology and Oceanography: Methods*, *7*, 706-715.

Milne, A., W. Landing, M. Bizimis, and P. Morton (2010), Determination of Mn, Fe, Co, Ni, Cu, Zn, Cd and Pb in seawater using high resolution magnetic sector inductively

References

---

coupled mass spectrometry (HR-ICP-MS), *Analytica Chimica Acta*, *665*(2), 200-207, doi:http://dx.doi.org/10.1016/j.aca.2010.03.027.

Milne, A., C. Schlosser, B. D. Wake, E. P. Achterberg, R. Chance, A. Baker, A. Forryan, and M. C. Lohan (2017), Particulate phases are key in controlling dissolved iron concentrations in the (sub)-tropical North Atlantic, *Geophysical Research Letters*, *44*(5), 2377-2387, doi:10.1002/2016GL072314.

Moore, C., M. Mills, K. Arrigo, I. Berman-Frank, L. Bopp, P. Boyd, E. Galbraith, R. J. Geider, C. Guieu, and S. Jaccard (2013a), Processes and patterns of oceanic nutrient limitation, *Nature Geoscience*, *6*(9), 701-710.

Moore, C. M., M. M. Mills, A. Milne, R. Langlois, E. P. Achterberg, K. Lochte, R. J. Geider, and J. La Roche (2006), Iron limits primary productivity during spring bloom development in the central North Atlantic, *Global Change Biology*, *12*(4), 626-634, doi:10.1111/j.1365-2486.2006.01122.x.

Moore, J., and O. Braucher (2008), Sedimentary and mineral dust sources of dissolved iron to the world ocean, *Biogeosciences*, *5*(3), 631-656, doi:10.5194/bg-5-631-2008.

Moore, J. K., K. Lindsay, S. C. Doney, M. C. Long, and K. Misumi (2013b), Marine ecosystem dynamics and biogeochemical cycling in the Community Earth System Model [CESM1 (BGC)]: Comparison of the 1990s with the 2090s under the RCP4. 5 and RCP8. 5 scenarios, *Journal of Climate*, *26*(23), 9291-9312.

Moore, W. S. (2008), Fifteen years experience in measuring ^{224}Ra and ^{223}Ra by delayed-coincidence counting, *Marine Chemistry*, *109*(3), 188-197.

References

Moore, W. S., and R. Arnold (1996), Measurement of ^{223}Ra and ^{224}Ra in coastal waters using a delayed coincidence counter, _J. Geophys. Res_, _101_(C1), 1321-1329.

Moran, B. S., and K. O. Buesseler (1993), Size-fractionated ^{234}Th in continental shelf waters off New England: Implications for the role of colloids in oceanic trace metal scavenging, _Journal of Marine Research_, _51_(4), 893-922.

Muller-Karger, F. E., R. Varela, R. Thunell, R. Luerssen, C. Hu, and J. J. Walsh (2005), The importance of continental margins in the global carbon cycle, _Geophysical Research Letters_, _32_(1), doi:10.1029/2004GL021346.

Muller, F., A. Tappin, P. Statham, J. Burton, and D. Hydes (1994), Trace-metal fronts in waters of the Celtic Sea, _Oceanologica acta_, _17_(4), 383-396.

National Geophysical Data Center, N. N. U. S. D. o. C. (1995), TerrainBase, Global 5 Arc-minute Ocean Depth and Land Elevation from the US National Geophysical Data Center (NGDC), edited, Research Data Archive at the National Center for Atmospheric Research, Computational and Information Systems Laboratory, Boulder, CO.

Nédélec, F., P. J. Statham, and M. Mowlem (2007), Processes influencing dissolved iron distributions below the surface at the Atlantic Ocean–Celtic Sea shelf edge, _Marine Chemistry_, _104_(3), 156-170.

Nielsdóttir, M. C., C. M. Moore, R. Sanders, D. J. Hinz, and E. P. Achterberg (2009), Iron limitation of the postbloom phytoplankton communities in the Iceland Basin, _Global Biogeochemical Cycles_, _23_(3).

References

Nishioka, J., T. Ono, H. Saito, T. Nakatsuka, S. Takeda, T. Yoshimura, K. Suzuki, K. Kuma, S. Nakabayashi, and D. Tsumune (2007), Iron supply to the western subarctic Pacific: Importance of iron export from the Sea of Okhotsk, *Journal of Geophysical Research: Oceans (1978–2012)*, *112*(C10).

Noble, A. E., C. H. Lamborg, D. C. Ohnemus, P. J. Lam, T. J. Goepfert, C. I. Measures, C. H. Frame, K. L. Casciotti, G. R. DiTullio, J. Jennings, and M. A. Saito (2012), Basin-scale inputs of cobalt, iron, and manganese from the Benguela-Angola front to the South Atlantic Ocean, *Limnology and Oceanography*, *57*(4), 989-1010, doi:10.4319/lo.2012.57.4.0989.

Nodwell, L. M., and N. M. Price (2001), Direct use of inorganic colloidal iron by marine mixotrophic phytoplankton, *Limnology and Oceanography*, *46*(4), 765-777, doi:10.4319/lo.2001.46.4.0765.

Noffke, A., C. Hensen, S. Sommer, F. Scholz, L. Bohlen, T. Mosch, M. Graco, and K. Wallmann (2012), Benthic iron and phosphorus fluxes across the Peruvian oxygen minimum zone, *Limnology and Oceanography*, *57*(3), 851.

Nowicki, J. L., K. S. Johnson, K. H. Coale, V. A. Elrod, and S. H. Lieberman (1994), Determination of Zinc in Seawater Using Flow Injection Analysis with Fluorometric Detection, *Analytical Chemistry*, *66*(17), 2732-2738, doi:10.1021/ac00089a021.

O'Sullivan, D. W., A. K. Hanson Jr, and D. R. Kester (1995), Stopped flow luminol chemiluminescence determination of Fe (II) and reducible iron in seawater at subnanomolar levels, *Marine Chemistry*, *49*(1), 65-77.

References

Obata, H., H. Karatani, and E. Nakayama (1993), Automated determination of iron in seawater by chelating resin concentration and chemiluminescence detection, *Analytical Chemistry*, *65*(11), 1524-1528, doi:10.1021/ac00059a007.

Ohnemus, D. C., M. E. Auro, R. M. Sherrell, M. Lagerstrom, P. L. Morton, B. S. Twining, S. Rauschenberg, and P. J. Lam (2014), Laboratory intercomparison of marine particulate digestions including Piranha: a novel chemical method for dissolution of polyethersulfone filters, *Limnol. Oceanogr. Meth.*, *12*, 530-547, doi:10.4319/lom.2014.12.530.

Öztürk, M., P. L. Croot, S. Bertilsson, K. Abrahamsson, B. Karlson, R. David, A. Fransson, and E. Sakshaug (2004), Iron enrichment and photoreduction of iron under UV and PAR in the presence of hydroxycarboxylic acid: implications for phytoplankton growth in the Southern Ocean, *Deep Sea Research Part II: Topical Studies in Oceanography*, *51*(22–24), 2841-2856, doi:http://dx.doi.org/10.1016/j.dsr2.2000.10.001.

Painter, S., S. Henson, A. Forryan, S. Steigenberger, J. Klar, M. Stinchcombe, N. Rogan, A. Baker, E. P. Achterberg, and C. Moore (2014), An assessment of the vertical diffusive flux of iron and other nutrients to the surface waters of the subpolar North Atlantic Ocean, *Biogeosciences*, *11*(8), 2113.

Painter, S. C., S. E. Hartman, C. Kivimäe, L. A. Salt, N. M. Clargo, Y. Bozec, C. J. Daniels, S. C. Jones, V. S. Hemsley, and L. R. Munns (2016), Carbon exchange between a shelf sea and the ocean: The Hebrides Shelf, west of Scotland, *Journal of Geophysical Research: Oceans*, *121*(7), 4522-4544.

References

Painter, S. C., S. E. Hartman, C. Kivimäe, L. A. Salt, N. M. Clargo, C. J. Daniels, Y. Bozec, L. Munns, S. Allen, V. S. Hemsley, G. Moschonas, and K. Davidson (submitted), The elemental stoichiometry (C, Si, N, P) of the Hebrides Shelf and its role in carbon export, *Progress in Oceanography*.

Palmer, M. R. (2016), OMG Kz glider data, edited.

Palmer, M. R., M. E. Inall, and J. Sharples (2013), The physical oceanography of Jones Bank: A mixing hotspot in the Celtic Sea, *Progress in Oceanography*, *117*, 9-24.

Parkinson, C. L., and A. J. Gratz (1983), On the seasonal sea ice cover of the Sea of Okhotsk, *Journal of Geophysical Research: Oceans*, *88*(C5), 2793-2802, doi:10.1029/JC088iC05p02793.

Patey, M. D., M. J. Rijkenberg, P. J. Statham, M. C. Stinchcombe, E. P. Achterberg, and M. Mowlem (2008), Determination of nitrate and phosphate in seawater at nanomolar concentrations, *TrAC Trends in Analytical Chemistry*, *27*(2), 169-182.

Pauly, D., V. Christensen, S. Guenette, T. J. Pitcher, U. R. Sumaila, C. J. Walters, R. Watson, and D. Zeller (2002), Towards sustainability in world fisheries, *Nature*, *418*(6898), 689-695.

Petit, J.-R., J. Jouzel, D. Raynaud, N. Barkov, J.-M. Barnola, I. Basile, M. Bender, J. Chappellaz, M. Davis, and G. Delaygue (1999), Climate and atmospheric history of the past 420,000 years from the Vostok ice core, Antarctica, *Nature*, *399*(6735), 429-436.

Pingree, R., P. Holligan, and R. Head (1977), Survival of dinoflagellate blooms in the western English Channel, *Nature*, *265*, 266-269, doi:10.1038/265266a0.

References

Pingree, R., P. Holligan, G. Mardell, and R. Head (1976), The influence of physical stability on spring, summer and autumn phytoplankton blooms in the Celtic Sea, *Journal of the Marine Biological Association of the United Kingdom*, *56*(04), 845-873.

Pingree, R., and B. Le Cann (1990), Structure, strength and seasonality of the slope currents in the Bay of Biscay region, *Journal of the Marine Biological Association of the United Kingdom*, *70*(04), 857-885.

Pingree, R., and A. New (1989), Downward propagation of internal tidal energy into the Bay of Biscay, *Deep Sea Research Part A. Oceanographic Research Papers*, *36*(5), 735-758.

Pingree, R., and L. Pennycuick (1975), Transfer of heat, fresh water and nutrients through the seasonal thermocline, *Journal of the Marine Biological Association of the United Kingdom*, *55*(02), 261-274.

Pingree, R., B. Sinha, and C. Griffiths (1999), Seasonality of the European slope current (Goban Spur) and ocean margin exchange, *Continental Shelf Research*, *19*(7), 929-975.

Pingree, R. D. (1973), A COMPONENT OF LABRADOR SEA WATER IN THE BAY OF BISCAY, *Limnology and Oceanography*, *18*(5), 711-718, doi:10.4319/lo.1973.18.5.0711.

Pingree, R. D. (1975), The advance and retreat of the thermocline on the continental shelf, *Journal of the Marine Biological Association of the United Kingdom*, *55*(04), 965-974, doi:doi:10.1017/S0025315400017859.

References

Pingree, R. D. (1984), Some Applications of Remote Sensing to Studies in the Bay of Biscay, Celtic Sea and English Channel, in *Elsevier Oceanography Series*, edited by C. J. N. Jacques, pp. 287-315, Elsevier, doi:http://dx.doi.org/10.1016/S0422-9894(08)70617-2.

Pingree, R. D., and B. Le Cann (1989), Celtic and Armorican slope and shelf residual currents, *Progress in Oceanography*, *23*(4), 303-338, doi:http://dx.doi.org/10.1016/0079-6611(89)90003-7.

Pingree, R. D., G. T. Mardell, and A. L. New (1986), Propagation of internal tides from the upper slopes of the Bay of Biscay, *Nature*, *321*(6066), 154-158.

Pollard, R. T., I. Salter, R. J. Sanders, M. I. Lucas, C. M. Moore, R. A. Mills, P. J. Statham, J. T. Allen, A. R. Baker, D. C. E. Bakker, M. A. Charette, S. Fielding, G. R. Fones, M. French, A. E. Hickman, R. J. Holland, J. A. Hughes, T. D. Jickells, R. S. Lampitt, P. J. Morris, F. H. Nedelec, M. Nielsdottir, H. Planquette, E. E. Popova, A. J. Poulton, J. F. Read, S. Seeyave, T. Smith, M. Stinchcombe, S. Taylor, S. Thomalla, H. J. Venables, R. Williamson, and M. V. Zubkov (2009), Southern Ocean deep-water carbon export enhanced by natural iron fertilization, *Nature*, *457*(7229), 577-580, doi:http://www.nature.com/nature/journal/v457/n7229/suppinfo/nature07716_S1.html.

Poulton, S., and R. Raiswell (2002), The low-temperature geochemical cycle of iron: from continental fluxes to marine sediment deposition, *American Journal of Science*, *302*(9), 774-805.

<u>*References*</u>

Radic, A., F. Lacan, and J. W. Murray (2011), Iron isotopes in the seawater of the equatorial Pacific Ocean: New constraints for the oceanic iron cycle, *Earth and Planetary Science Letters*, *306*(1), 1-10.

Raiswell, R., L. Benning, L. Davidson, and M. Tranter (2008), Nanoparticulate bioavailable iron minerals in icebergs and glaciers, *Mineralogical Magazine*, *72*(1), 345-348.

Redfield, A. C. (1958), The biological control of chemical factors in the environment, *American scientist*, *46*(3), 230A-221.

Resing, J. A., P. N. Sedwick, C. R. German, W. J. Jenkins, J. W. Moffett, B. M. Sohst, and A. Tagliabue (2015), Basin-scale transport of hydrothermal dissolved metals across the South Pacific Ocean, *Nature*, *523*(7559), 200-203, doi:10.1038/nature14577.

Revels, B. N., D. C. Ohnemus, P. J. Lam, T. M. Conway, and S. G. John (2015), The isotopic signature and distribution of particulate iron in the North Atlantic Ocean, *Deep Sea Research Part II: Topical Studies in Oceanography*, *116*, 321-331, doi:http://dx.doi.org/10.1016/j.dsr2.2014.12.004.

Rich, H. W., and F. M. Morel (1990), Availability of well defined iron colloids to the marine diatom Thalassiosira weissflogii, *Limnology and Oceanography*, *35*(3), 652-662.

Richardson, A. J., and D. S. Schoeman (2004), Climate Impact on Plankton Ecosystems in the Northeast Atlantic, *Science*, *305*(5690), 1609-1612, doi:10.1126/science.1100958.

References

Rijkenberg, M. J., R. Middag, P. Laan, L. J. Gerringa, H. M. van Aken, V. Schoemann, J. T. de Jong, and H. J. de Baar (2014), The distribution of dissolved iron in the West Atlantic Ocean, *PLoS One*, *9*(6), e101323.

Rijkenberg, M. J. A., C. F. Powell, M. Dall'Osto, M. C. Nielsdottir, M. D. Patey, P. G. Hill, A. R. Baker, T. D. Jickells, R. M. Harrison, and E. P. Achterberg (2008), Changes in iron speciation following a Saharan dust event in the tropical North Atlantic Ocean, *Marine Chemistry*, *110*(1–2), 56-67, doi:http://dx.doi.org/10.1016/j.marchem.2008.02.006.

Rippeth, T. P., and K. J. Jones (1997), The seasonal cycle of nitrate in the Clyde Sea, *Journal of Marine Systems*, *12*(1), 299-310, doi:http://dx.doi.org/10.1016/S0924-7963(96)00104-2.

Rippeth, T. P., P. Wiles, M. R. Palmer, J. Sharples, and J. Tweddle (2009), The diapcynal nutrient flux and shear-induced diapcynal mixing in the seasonally stratified western Irish Sea, *Continental Shelf Research*, *29*(13), 1580-1587.

Romero, S. I., A. R. Piola, M. Charo, and C. A. E. Garcia (2006), Chlorophyll-a variability off Patagonia based on SeaWiFS data, *Journal of Geophysical Research: Oceans*, *111*(C5), n/a-n/a, doi:10.1029/2005JC003244.

Rose, A. L., and T. D. Waite (2001), Chemiluminescence of Luminol in the Presence of Iron(II) and Oxygen: Oxidation Mechanism and Implications for Its Analytical Use, *Analytical Chemistry*, *73*(24), 5909-5920, doi:10.1021/ac015547q.

References

Rose, A. L., and T. D. Waite (2002), Kinetic model for Fe (II) oxidation in seawater in the absence and presence of natural organic matter, *Environmental science & technology*, *36*(3), 433-444.

Rubin, M., I. Berman-Frank, and Y. Shaked (2011), Dust-and mineral-iron utilization by the marine dinitrogen-fixer Trichodesmium, *Nature Geoscience*, *4*(8), 529-534.

Rudnick, R. L., and S. Gao (2003), 3.01 - Composition of the Continental Crust A2 - Holland, Heinrich D, in *Treatise on Geochemistry*, edited by K. K. Turekian, pp. 1-64, Pergamon, Oxford, doi:http://dx.doi.org/10.1016/B0-08-043751-6/03016-4.

Rue, E. L., and K. W. Bruland (1995), Complexation of iron(III) by natural organic ligands in the Central North Pacific as determined by a new competitive ligand equilibration/adsorptive cathodic stripping voltammetric method, *Marine Chemistry*, *50*(1–4), 117-138, doi:http://dx.doi.org/10.1016/0304-4203(95)00031-L.

Ryan-Keogh, T. J., A. I. Macey, M. C. Nielsdóttir, M. I. Lucas, S. S. Steigenberger, M. C. Stinchcombe, E. P. Achterberg, T. S. Bibby, and C. M. Moore (2013), Spatial and temporal development of phytoplankton iron stress in relation to bloom dynamics in the high-latitude North Atlantic Ocean, *Limnology and oceanography*, *58*(2), 533-545.

Sanders, R., L. Brown, S. Henson, and M. Lucas (2005), New production in the Irminger Basin during 2002, *Journal of Marine Systems*, *55*(3–4), 291-310, doi:http://doi.org/10.1016/j.jmarsys.2004.09.002.

Santana-Casiano, J. M., M. González-Dávila, and F. J. Millero (2005), Oxidation of nanomolar levels of Fe (II) with oxygen in natural waters, *Environmental science & technology*, *39*(7), 2073-2079.

Santschi, P., P. Höhener, G. Benoit, and M. Buchholtz-ten Brink (1990), Chemical processes at the sediment-water interface, *Marine Chemistry*, *30*(0), 269-315, doi:http://dx.doi.org/10.1016/0304-4203(90)90076-O.

Sarthou, G., A. R. Baker, S. Blain, E. P. Achterberg, M. Boye, A. R. Bowie, P. Croot, P. Laan, H. J. W. de Baar, T. D. Jickells, and P. J. Worsfold (2003), Atmospheric iron deposition and sea-surface dissolved iron concentrations in the eastern Atlantic Ocean, *Deep Sea Research Part I: Oceanographic Research Papers*, *50*(10–11), 1339-1352, doi:http://dx.doi.org/10.1016/S0967-0637(03)00126-2.

Sarthou, G., E. Bucciarelli, F. Chever, S. Hansard, J. Planchon, S. Speich, M. González-Dávila, and J. M. Santana-Casiano (2011), Labile Fe (II) concentrations in the Atlantic sector of the Southern Ocean along a transect from the subtropical domain to the Weddell Sea Gyre.

Schmidt, K., C. Schlosser, A. Atkinson, S. Fielding, H. J. Venables, C. M. Waluda, and E. P. Achterberg (2016), Zooplankton gut passage mobilizes lithogenic iron for ocean productivity, *Current Biology*, *26*(19), 2667-2673.

Sedwick, P., B. Sohst, S. Ussher, and A. Bowie (2015), A zonal picture of the water column distribution of dissolved iron (II) during the US GEOTRACES North Atlantic transect cruise (GEOTRACES GA03), *Deep Sea Research Part II: Topical Studies in Oceanography*, *116*, 166-175.

Sedwick, P. N., A. R. Bowie, and T. W. Trull (2008), Dissolved iron in the Australian

sector of the Southern Ocean (CLIVAR SR3 section): Meridional and seasonal trends,

Deep Sea Research Part I: Oceanographic Research Papers, *55*(8), 911-925,

doi:https://doi.org/10.1016/j.dsr.2008.03.011.

Sedwick, P. N., and G. R. DiTullio (1997), Regulation of algal blooms in Antarctic shelf

waters by the release of iron from melting sea ice, *Gephysics Research Letters*, *24*(20).

Sedwick, P. N., G. R. DiTullio, and D. J. Mackey (2000), Iron and manganese in the Ross

Sea, Antarctica: Seasonal iron limitation in Antarctic shelf waters, *Journal of

Geophysical Research: Oceans (1978–2012)*, *105*(C5), 11321-11336.

Sedwick, P. N., C. M. Marsay, B. M. Sohst, A. M. Aguilar Islas, M. Lohan, M. C. Long, K.

R. Arrigo, R. B. Dunbar, M. A. Saito, and W. O. Smith (2011), Early season depletion of

dissolved iron in the Ross Sea polynya: Implications for iron dynamics on the Antarctic

continental shelf, *Journal of Geophysical Research: Oceans*, *116*(19), doi:

10.1029/2010jc006553.

Severmann, S., C. Johnson, B. Beard, C. German, H. Edmonds, H. Chiba, and D. Green

(2004), The effect of plume processes on the Fe isotope composition of hydrothermally

derived Fe in the deep ocean as inferred from the Rainbow vent site, Mid-Atlantic

Ridge, 36 14′ N, *Earth and Planetary Science Letters*, *225*(1), 63-76.

Severmann, S., J. McManus, W. M. Berelson, and D. E. Hammond (2010), The

continental shelf benthic iron flux and its isotope composition, *Geochimica et

Cosmochimica Acta*, *74*(14), 3984-4004.

References

___

Shaked, Y., and H. Lis (2012), Disassembling iron availability to phytoplankton, *Environmental Bioinorganic Chemistry of Aquatic Microbial Organisms*, 3-123, doi:10.3389/fmicb.2012.00123.

Sharples, J., C. M. Moore, A. E. Hickman, P. M. Holligan, J. F. Tweddle, M. R. Palmer, and J. H. Simpson (2009), Internal tidal mixing as a control on continental margin ecosystems, *Geophysical Research Letters*, *36*(23), doi:10.1029/2009GL040683.

Sharples, J., M. C. Moore, T. P. Rippeth, P. M. Holligan, D. J. Hydes, N. R. Fisher, and J. H. Simpson (2001), Phytoplankton distribution and survival in the thermocline, *Limnology and Oceanography*, *46*(3), 486-496.

Sharples, J., J. F. Tweddle, J. Mattias Green, M. R. Palmer, Y.-N. Kim, A. E. Hickman, P. M. Holligan, C. Moore, T. P. Rippeth, and J. H. Simpson (2007), Spring-neap modulation of internal tide mixing and vertical nitrate fluxes at a shelf edge in summer, *Limnology and Oceanography*, *52*(5), 1735-1747.

Shelley, R. U., B. Zachhuber, P. N. Sedwick, P. J. Worsfold, and M. C. Lohan (2010), Determination of total dissolved cobalt in UV-irradiated seawater using flow injection with chemiluminescence detection, *Limnology and Oceanography: Methods*, *8*(7), 352-362, doi:10.4319/lom.2010.8.352.

Sholkovitz, E. R., P. N. Sedwick, T. M. Church, A. R. Baker, and C. F. Powell (2012), Fractional solubility of aerosol iron: Synthesis of a global-scale data set, *Geochimica et Cosmochimica Acta*, *89*, 173-189, doi:http://dx.doi.org/10.1016/j.gca.2012.04.022.

References

Siemering, B., E. Bresnan, S. C. Painter, C. J. Daniels, M. Inall, and K. Davidson (2016),

Phytoplankton Distribution in Relation to Environmental Drivers on the North West

European Shelf Sea, *PloS one*, *11*(10), e0164482.

Sieracki, M. E., P. G. Verity, and D. K. Stoecker (1993), Plankton community response to

sequential silicate and nitrate depletion during the 1989 North Atlantic spring bloom,

Deep Sea Research Part II: Topical Studies in Oceanography, *40*(1), 213-225,

doi:http://dx.doi.org/10.1016/0967-0645(93)90014-E.

Simpson, J., and D. Bowers (1984), The role of tidal stirring in controlling the seasonal

heat cycle in shelf seas, paper presented at Annales Geophysicae, Gauthier-Villars.

Simpson, J., and J. Hunter (1974), Fronts in the Irish sea, *Nature*, *250*, 404-406.

Simpson, J. H., and A. E. Hill (1986), The Scottish Coastal Current, in *The Role of*

Freshwater Outflow in Coastal Marine Ecosystems, edited by S. Skreslet, pp. 295-308,

Springer Berlin Heidelberg, Berlin, Heidelberg, doi:10.1007/978-3-642-70886-2_21.

Simpson, J. H., and R. R. McCandliss (2013), "The Ekman Drain": a conduit to the deep

ocean for shelf material, *Ocean Dynamics*, *63*(9), 1063-1072, doi:10.1007/s10236-013-

0644-y.

Simpson, J. H., and J. Sharples (2012), *Introduction to the physical and biological*

oceanography of shelf seas, Cambridge University Press.

Souza, A. J., J. H. Simpson, M. Harikrishnan, and J. Malarkey (2001), Flow structure and

seasonalityin the Hebridean slope current, *Oceanologica Acta*, *24, Supplement 1*, 63-

76, doi:http://doi.org/10.1016/S0399-1784(00)01103-8.

Srokosz, M., J. Robinson, H. McGrain, E. Popova, and A. Yool (2015), Could the Madagascar bloom be fertilized by Madagascan iron?, *Journal of Geophysical Research: Oceans*, *120*(8), 5790-5803.

Stallard, R., and J. Edmond (1983), Geochemistry of the Amazon: 2. The influence of geology and weathering environment on the dissolved load, *Journal of Geophysical Research: Oceans*, *88*(C14), 9671-9688.

Statham, P. J., and V. Hart (2005), Dissolved iron in the Cretan Sea (eastern Mediterranean), *Limnology and Oceanography*, *50*(4), 1142-1148, doi:10.4319/lo.2005.50.4.1142.

Staubwasser, M., R. Schoenberg, F. v. Blanckenburg, S. Krüger, and C. Pohl (2013), Isotope fractionation between dissolved and suspended particulate Fe in the oxic and anoxic water column of the Baltic Sea, *Biogeosciences*, *10*(1), 233-245.

Strzepek, R., M. Maldonado, J. Higgins, J. Hall, K. Safi, S. Wilhelm, and P. Boyd (2005), Spinning the "Ferrous Wheel": The importance of the microbial community in an iron budget during the FeCycle experiment, *Global biogeochemical cycles*, *19*(4), doi:10.1029/2005GB002490.

Strzepek, R., and N. Price (2000), Influence of irradiance and temperature on the iron content of the marine diatom Thalassiosira weissflogii (Bacillariophyceae), *Marine Ecology Progress Series*, *206*, 107-117.

Stumm, W., and J. Morgan (1996), *aquatic chemistry chemical equlibria and rates in natural waters*, 3rd ed., Wiley & Sons, Canada.

References

Sulzberger, B., D. Suter, C. Siffert, S. Banwart, and W. Stumm (1989), Dissolution of fe(III)(hydr)oxides in natural waters; laboratory assessment on the kinetics controlled by surface coordination, *Marine Chemistry*, *28*(1), 127-144, doi:http://dx.doi.org/10.1016/0304-4203(89)90191-6.

Sun, Y., and T. Torgersen (1998), The effects of water content and Mn-fiber surface conditions on [224]Ra measurement by [220]Rn emanation, *Marine Chemistry*, *62*(3), 299-306.

Sunda, W. G., J. Buffke, and H. P. Van Leeuwen (2001), Bioavailability and Bioaccumulation of Iron in the Sea, in *The Biogeochemistry of Iron in Seawater*, edited by D. R. Turner and K. A. Hunter, pp. 41-84, John Wiley & Sons,Ltd, Chichester.

Sunda, W. G., and S. A. Huntsman (1995), Iron uptake and growth limitation in oceanic and coastal phytoplankton, *Marine Chemistry*, *50*(1), 189-206, doi:http://dx.doi.org/10.1016/0304-4203(95)00035-P.

Sunda, W. G., and S. A. Huntsman (1997), Interrelated influence of iron, light and cell size on marine phytoplankton growth, *Nature*, *390*(6658), 389-392.

Sverdrup, H. U. (1953), On Conditions for the Vernal Blooming of Phytoplankton, *Journal du Conseil*, *18*(3), 287-295, doi:10.1093/icesjms/18.3.287.

Tagliabue, A., O. Aumont, and L. Bopp (2014a), The impact of different external sources of iron on the global carbon cycle, *Geophysical Research Letters*, 2013GL059059, doi:10.1002/2013GL059059.

References

Tagliabue, A., O. Aumont, R. DeAth, J. P. Dunne, S. Dutkiewicz, E. Galbraith, K. Misumi, J. K. Moore, A. Ridgwell, and E. Sherman (2015), How well do global ocean biogeochemistry models simulate dissolved iron distributions?, *Global Biogeochemical Cycles*.

Tagliabue, A., L. Bopp, J.-C. Dutay, A. R. Bowie, F. Chever, P. Jean-Baptiste, E. Bucciarelli, D. Lannuzel, T. Remenyi, and G. Sarthou (2010), Hydrothermal contribution to the oceanic dissolved iron inventory, *Nature Geoscience*, *3*(4), 252-256.

Tagliabue, A., A. R. Bowie, P. W. Boyd, K. N. Buck, K. S. Johnson, and M. A. Saito (2017), The integral role of iron in ocean biogeochemistry, *Nature*, *543*(7643), 51-59, doi:10.1038/nature21058.

Tagliabue, A., J.-B. Sallée, A. R. Bowie, M. Lévy, S. Swart, and P. Boyd (2014b), Surface-water iron supplies in the Southern Ocean sustained by deep winter mixing, *Nature Geoscience*, *7*(4), 314-320.

Takahashi, T., S. C. Sutherland, C. Sweeney, A. Poisson, N. Metzl, B. Tilbrook, N. Bates, R. Wanninkhof, R. A. Feely, C. Sabine, J. Olafsson, and Y. Nojiri (2002), Global sea–air CO_2 flux based on climatological surface ocean pCO_2, and seasonal biological and temperature effects, *Deep Sea Research Part II: Topical Studies in Oceanography*, *49*(9–10), 1601-1622, doi:http://dx.doi.org/10.1016/S0967-0645(02)00003-6.

Takeda, S. (1998), Influence of iron availability on nutrient consumption ratio of diatoms in oceanic waters, *Nature*, *393*(6687), 774-777.

References

Tarran, G., A. E. Hickman, A. Poulton, C. Widdicombe, A. Rees, J. Fox, and L. Munns (in prep), European Shelf Sea plankton community; abundance, seasonality and succession in the Celtic Sea, *In prep for Progress in Oceanography*.

Tett, P., L. Gilpin, H. Svendsen, C. P. Erlandsson, U. Larsson, S. Kratzer, E. Fouilland, C. Janzen, J.-Y. Lee, C. Grenz, A. Newton, J. G. Ferreira, T. Fernandes, and S. Scory (2003a), Eutrophication and some European waters of restricted exchange, *Continental Shelf Research*, *23*(17–19), 1635-1671, doi:http://doi.org/10.1016/j.csr.2003.06.013.

Tett, P., D. Hydes, and R. Sanders (2003b), Influence of nutrient biogeochemistry on the ecology of northwest European shelf seas, in *Biogeochemistry of Marine Systems*, edited by K. Black and G. Shimmield, pp. 293-363, Blackwell Publishings, Oxford.

Thomas, H., Y. Bozec, K. Elkalay, and H. J. W. de Baar (2004), Enhanced Open Ocean Storage of CO_2 from Shelf Sea Pumping, *Science*, *304*(5673), 1005-1008, doi:10.1126/science.1095491.

Townsend, D. W., and N. R. Pettigrew (1997), Nitrogen limitation of secondary production on Georges Bank, *Journal of Plankton Research*, *19*(2), 221-235.

Tsuda, A., S. Takeda, H. Saito, J. Nishioka, Y. Nojiri, I. Kudo, H. Kiyosawa, A. Shiomoto, K. Imai, T. Ono, A. Shimamoto, D. Tsumune, T. Yoshimura, T. Aono, A. Hinuma, M. Kinugasa, K. Suzuki, Y. Sohrin, Y. Noiri, H. Tani, Y. Deguchi, N. Tsurushima, H. Ogawa, K. Fukami, K. Kuma, and T. Saino (2003), A Mesoscale Iron Enrichment in the Western Subarctic Pacific Induces a Large Centric Diatom Bloom, *Science*, *300*(5621), 958-961, doi:10.1126/science.1082000.

References

Twining, B. S., and S. B. Baines (2013), The trace metal composition of marine phytoplankton, *Annual review of marine science*, *5*, 191-215.

Tyrrell, T., A. Merico, J. Waniek, C. Wong, N. Metzl, and F. Whitney (2005), Effect of seafloor depth on phytoplankton blooms in high nitrate, low chlorophyll (HNLC) regions, *Journal of Geophysical Research: Biogeosciences (2005–2012)*, *110*(G2).

Ussher, S. (2005), Determination of dissolved iron speciation in the North East Atlantic Ocean by flow injection chemiluminesence, 197 pp, University of Plymouth, Plymouth.

Ussher, S. J., E. P. Achterberg, C. Powell, A. R. Baker, T. D. Jickells, R. Torres, and P. J. Worsfold (2013), Impact of atmospheric deposition on the contrasting iron biogeochemistry of the North and South Atlantic Ocean, *Global Biogeochemical Cycles*, *27*(4), 1096-1107.

Ussher, S. J., E. P. Achterberg, G. Sarthou, P. Laan, H. J. W. de Baar, and P. J. Worsfold (2010), Distribution of size fractionated dissolved iron in the Canary Basin, *Marine Environmental Research*, *70*(1), 46-55, doi:http://dx.doi.org/10.1016/j.marenvres.2010.03.001.

Ussher, S. J., E. P. Achterberg, and P. J. Worsfold (2004), Marine biogeochemistry of iron, *Environmental Chemistry*, *1*(2), 67-80.

Ussher, S. J., A. Milne, W. M. Landing, K. Attiq-ur-Rehman, M. J. M. Séguret, T. Holland, E. P. Achterberg, A. Nabi, and P. J. Worsfold (2009), Investigation of iron(III) reduction and trace metal interferences in the determination of dissolved iron in seawater using

References

---

flow injection with luminol chemiluminescence detection, *Analytica Chimica Acta*, *652*(1–2), 259-265, doi:http://dx.doi.org/10.1016/j.aca.2009.06.011.

Ussher, S. J., P. J. Worsfold, E. P. Achterberg, A. Laës, S. Blain, P. Laan, and H. J. De Baar (2007), Distribution and redox speciation of dissolved iron on the European continental margin, *Limnology and Oceanography: Methods*, *52*(6), 2530-2539.

van Aken, H. M. (2000), The hydrography of the mid-latitude northeast Atlantic Ocean: I: The deep water masses, *Deep Sea Research Part I: Oceanographic Research Papers*, *47*(5), 757-788, doi:http://dx.doi.org/10.1016/S0967-0637(99)00092-8.

Van Der Merwe, P., A. Bowie, F. Quéroué, L. Armand, S. Blain, F. Chever, D. Davies, F. Dehairs, F. Planchon, and G. Sarthou (2015), Sourcing the iron in the naturally fertilised bloom around the Kerguelen Plateau: particulate trace metal dynamics, *Biogeosciences*, *12*(3), 739-755.

van Weering, T. C. E., I. R. Hall, H. C. de Stigter, I. N. McCave, and L. Thomsen (1998), Recent sediments, sediment accumulation and carbon burial at Goban Spur, N.W. European Continental Margin (47–50°N), *Progress in Oceanography*, *42*(1–4), 5-35, doi:http://dx.doi.org/10.1016/S0079-6611(98)00026-3.

Vaughan, N., and T. Lenton (2011), A review of climate geoengineering proposals, *Climatic Change*, *109*(3-4), 745-790, doi:10.1007/s10584-011-0027-7.

Wang, J. H. (1955), On the Detailed Mechanism of a New Type of Catalase-like Action, *Journal of the American Chemical Society*, *77*(18), 4715-4719, doi:10.1021/ja01623a007.

References

Wang, S., D. Bailey, K. Lindsay, J. K. Moore, and M. Holland (2014), Impact of sea ice on the marine iron cycle and phytoplankton productivity, edited, doi:10.5194/bg-11-4713-2014.

Warnken, K. W., G. A. Gill, L. L. Griffin, and P. H. Santschi (2001), Sediment-water exchange of Mn, Fe, Ni and Zn in Galveston Bay, Texas, *Marine Chemistry*, *73*(3), 215-231.

Warnken, K. W., D. Tang, G. A. Gill, and P. H. Santschi (2000), Performance optimization of a commercially available iminodiacetate resin for the determination of Mn, Ni, Cu, Cd and Pb by on-line preconcentration inductively coupled plasma-mass spectrometry, *Analytica Chimica Acta*, *423*(2), 265-276, doi:http://dx.doi.org/10.1016/S0003-2670(00)01137-5.

Watson, A. J., D. C. E. Bakker, A. J. Ridgwell, P. Boyd, and C. S. Law (2000), Effect of iron supply on Southern Ocean CO_2 uptake and implications for glacial atmospheric CO_2, *Nature*, *407*(6805), 730-733, doi:http://www.nature.com/nature/journal/v407/n6805/suppinfo/407730a0_S1.html.

Wedepohl, H. K. (1995), The composition of the continental crust, *Geochimica et Cosmochimica Acta*, *59*(7), 1217-1232.

Wells, M. L. (2002), Marine colloids and trace metals, *Biogeochemistry of marine dissolved organic matter*, 367-404.

Wells, M. L., and E. D. Goldberg (1993), Colloid aggregation in seawater, *Marine Chemistry*, *41*(4), 353-358, doi:http://dx.doi.org/10.1016/0304-4203(93)90267-R.

Wells, M. L., and E. D. Goldberg (1994), The distribution of colloids in the North Atlantic and Southern Oceans, *Limnology and Oceanography*, *39*(2), 286-302, doi:10.4319/lo.1994.39.2.0286.

Wells, M. L., and L. M. Mayer (1991a), The phttoconversion of colloidal iron oxyhydroxides in seawater, *Deep Sea Research Part A. Oceanographic Research Papers*, *38*(11), 1379-1395, doi:http://dx.doi.org/10.1016/0198-0149(91)90012-5.

Wells, M. L., and L. M. Mayer (1991b), Variations in the chemical lability of iron in estuarine, coastal and shelf waters and its implications for phytoplankton, *Marine Chemistry*, *32*(2), 195-210, doi:http://dx.doi.org/10.1016/0304-4203(91)90038-X.

Wells, M. L., L. M. Mayer, O. F. X. Donard, M. M. de Souza Sierra, and S. G. Ackelson (1991), The photolysis of colloidal iron in the oceans, *Nature*, *353*(6341), 248-250.

Wells, M. L., G. J. Smith, and K. Bruland (2000), The distribution of colloidal and particulate bioactive metals in Narragansett Bay, RI, *Marine Chemistry*, *71*(1), 143-163.

White, E. H., and M. M. Bursey (1964), Chemiluminescence of LUminol and Related Hydrazides: The Light Emission Step, *Journal of the American Chemical Society*, *86*(5), 941-942, doi:10.1021/ja01059a051.

Wihsgott, J. U., J. Sharples, J. E. Hopkins, E. M. S. Woodward, N. Greenwood, T. Hull, and D. B. Sivyer (in prep), Investigating the autumn bloom's significance withing the seasonal cycle of primary production in a temperate shelf sea.

References

Williams, C., J. Sharples, M. Green, C. Mahaffey, and T. Rippeth (2013a), The maintenance of the subsurface chlorophyll maximum in the stratified western Irish Sea, *Limnology and Oceanography: Fluids and Environments*, *3*(1), 61-73.

Williams, C., J. Sharples, C. Mahaffey, and T. Rippeth (2013b), Wind driven nutrient pulses to the subsurface chlorophyll maximum in seasonally stratified shelf seas, *Geophysical Research Letters*, *40*(20), 5467-5472.

Williams, C. A. J., Palmer, M. , C. Mahaffey, and C. Davis (in prep), How does the motion in the ocean breathe life into shelf seas? An autonomous study of vertical mixing and ventilation.

Williams, R. J. P., and J. J. R. Frausto da Silva (2006), *The Chemistry of Evolution The Development of our Ecosystem*, Elsevier, Netherlands.

Windom, H. L., W. S. Moore, L. F. H. Niencheski, and R. A. Jahnke (2006), Submarine groundwater discharge: A large, previously unrecognized source of dissolved iron to the South Atlantic Ocean, *Marine Chemistry*, *102*(3–4), 252-266, doi:http://dx.doi.org/10.1016/j.marchem.2006.06.016.

Worsfold, P. J., R. Clough, M. C. Lohan, P. Monbet, P. S. Ellis, C. R. Quétel, G. H. Floor, and I. D. McKelvie (2013), Flow injection analysis as a tool for enhancing oceanographic nutrient measurements—A review, *Analytica chimica acta*, *803*, 15-40.

Wu, J., and G. W. Luther (1994), Size-fractionated iron concentrations in the water column of the western North Atlantic Ocean, *Limnology and Oceanography*, *39*(5), 1119-1129.

References

Wyatt, N. (2013), The biogeochemistry of iron, zinc and cobalt in the Atlantic Ocean: The Atlantic meridional transect and the UK GEOTRACES sections, 269 pp, University of Plymouth, Plymouth.

Yin, J., Z. Jiang, G. Chang, and B. Hu (2005), Simultaneous on-line preconcentration and determination of trace metals in environmental samples by flow injection combined with inductively coupled plasma mass spectrometry using a nanometer-sized alumina packed micro-column, _Analytica Chimica Acta_, _540_(2), 333-339, doi:http://dx.doi.org/10.1016/j.aca.2005.03.045.

Yool, A., E. Popova, and T. Anderson (2013), MEDUSA-2.0: an intermediate complexity biogeochemical model of the marine carbon cycle for climate change and ocean acidification studies, _Geoscientific Model Development_, _6_(5), 1767-1811.

Yoshida, M., K. Kuma, S. Iwade, Y. Isoda, H. Takata, and M. Yamada (2006), Effect of aging time on the availability of freshly precipitated ferric hydroxide to coastal marine diatoms, _Marine Biology_, _149_(2), 379-392.

Zaragosi, S., G. A. Auffret, J. C. Faugères, T. Garlan, C. Pujol, and E. Cortijo (2000), Physiography and recent sediment distribution of the Celtic Deep-Sea Fan, Bay of Biscay, _Marine Geology_, _169_(1–2), 207-237, doi:http://dx.doi.org/10.1016/S0025-3227(00)00054-2.

Appendices

Appendix A- Figures of merit

Figures of merit for the analyses of total sFe, dFe and TdFe by FI-CL (Table A1).

Table A1- Figures of merit for the determination of low iron concentrations.

BATS= Surface seawater from the Bermuda Atlantic Time Series, 40 S SW= surface seawater from 40° S Atlantic, Celtic Sea= surface seawater from the Celtic Sea.

LOD= limit of detection, 3 SD of blank or calibration seawater with no added Fe i.e the lowest concentration calibrant.

a and b refer to coefficients when the calibration curve was quadratic ($y=ax^2+bx(+c)$), using calibration procedure described above c is 0. m refers to coefficient when the calibration curve was linear ($y=mx+c$).

A range of internal quality control materials were used, initially the seawater used to condition the system was used, then a 0.2-0.4nM addition standard (A.S), however, these varied daily. Therefore, several internal standards were used depending on desired concentration, C.S & C.S #1 ≈1.1 nM, CS #3 ≈ 50 nM and CS #4 ≈ 8 nM Fe. Where n/a appears these days were method development days and so an internal standard was not run.

* indicates suspect poor data quality and samples reanalysed at a later date.
[1] new luminol reagent, associated with decreased sensitivity.
[2] attempted to run an internal standard but it contained a lower concentration of Fe than expected

Date	Calibration Water	Range (nM)	a	b	m	r^2	LOD (nM)	Blank (nM)	RSD (%) of check standard *(n)*	Check Standard	Load time (s)	Luminol (mM)
7.7.14	BATS	LOD-2	0.3738	1.7802		1.000	0.018	0.000	4.8 (*6*)	0.80nM	60	0.25
9.7.14	BATS	LOD-3	0.0946	1.2175		1.000	0.043	0.000	1.4 (*4*)	0.19nM	60	0.25
10.7.14	BATS	LOD-3	0.1592	0.9862		0.999	0.014	0.000	15.0 (*6*)	0.11nM	60	0.25

Date	Location	LOD										
11.7.14	BATS	LOD-3	0.1820	0.8315		0.999	0.010	0.014	0.0 (*3*)	0.08nM	60	0.25
13.7.14	BATS	LOD-2	0.2453	0.7184		0.999	0.039	0.000	6.2 (*3*)	1.28nM	60	0.25
20.1.15	40 S SW	LOD-2.4	0.1509	0.8844		0.997	0.012	0.039	n/a	n/a	60	0.25
23.1.15	Celtic Sea	LOD-4	0.2337	1.5145		0.999	0.034	0.084	Check		60	0.25
25.1.15	Celtic Sea	LOD-4	0.1818	1.5161		1.000	0.008	0.063	check		60	0.25
27.1.15	Celtic Sea	LOD-3	0.2471	1.2744		1.000	0.034	0.046	7.6 (*4*)	0.2-0.4nM A.S	60	0.25
5.2.15	Celtic Sea	LOD-2	0.3271	1.1213		0.998	0.039	0.057	8.5 (*4*)	0.2-0.4nM A.S	60	0.25
7.2.15	Celtic Sea	LOD-2	0.2835	1.2011		0.997	0.010	0.000	6.6 (*4*)	0.2-0.4nM A.S	60	0.25
10.2.15	Celtic Sea	LOD-1.5	0.3713	1.1013		1.000	0.021	0.000	3.3 (*4*)	0.2-0.4nM A.S	60	0.25
11.2.15	Celtic Sea	LOD-2	0.1874	1.2425		1.000	0.010	0.000	9.9 (*3*)	0.2-0.4nM A.S	60	0.25
13.2.15	Celtic Sea	LOD-2	0.4211	0.9256		0.999	0.028	0.000	7.0 (*3*)	0.2-0.4nM A.S	60	0.25
20.2.15	Celtic Sea	LOD-2	0.4668	1.1764		0.999	0.028	0.000	check	0.2-0.4nM A.S	60	0.25
25.2.15	Celtic Sea	LOD-2	0.5193	0.9286		0.999	0.023	0.000	5.5 (*3*)	0.2-0.4nM A.S	60	0.25
3.3.15	Celtic Sea	LOD-2	0.2601	1.5133		0.999	0.047	0.000	3.2 (*4*)	0.2-0.4nM A.S	60	0.25
4.3.15	Celtic Sea	LOD-2	0.3657	0.773		0.997	0.018	0.000	13.8 (*4*)	0.2-0.4nM A.S	60	0.25
6.03.15	Celtic Sea	LOD-2	0.4107	0.8718		1.000	0.017	0.000	9.3 (*5*)	0.2-0.4nM A.S	60	0.25
9.03.15	Celtic Sea	LOD-4	0.2021	1.0996		0.999	0.020	0.000	8.5 (*4*)	0.2-0.4nM A.S	60	0.25
10.03.15	Celtic Sea	LOD-2	0.2557	1.3009		1.000	0.015	0.000	13.2 (*4*)	0.2-0.4nM A.S	60	0.25
7.05.15	Celtic Sea	LOD-4	0.1743	1.5586		0.998	0.039	0.000	17.4 (*3*)	0.2-0.4nM A.S	60	0.25
11.05.15	Celtic Sea	LOD-2	0.4024	1.0915		0.991	0.013	0.000	6.0 (*4*)	0.2-0.4nM A.S	60	0.25
12.05.15	Celtic Sea	LOD-2	0.3778	1.0021		0.999	0.028	0.000	7.2 (*4*)	0.2-0.4nM A.S	60	0.25
14.05.15	Celtic Sea	LOD-4	0.2237	1.1253		0.999	0.026	0.000	10.1 (*4*)	0.2-0.4nM A.S	60	0.25
18.05.15	Celtic Sea	LOD-4	0.223	1.5645		1.000	0.021	0.000	17.4 (*4*)	0.2-0.4nM A.S	60	0.25
19.05.15	Celtic Sea	LOD-2	0.3253	1.0212		0.998	0.032	0.000	16.1 (*5*)	0.2-0.4nM A.S	60	0.25
22.05.15	Celtic Sea	LOD-2	0.3163	0.9049		0.999	0.028	0.000	8.7 (*4*)	0.2-0.4nM A.S	60	0.25
9.06.15	Celtic Sea	LOD-2	0.5257	1.5801		0.999	0.012	0.000	9.1 (*4*)	C.S	60	0.25
12.06.15	Celtic Sea	LOD-2	0.3213	0.7102		0.999	0.069	0.000	3.1 (*4*)	C.S	60	0.25

8.09.15	Celtic Sea	LOD-2	0.1761	0.7713		0.998	0.087	0.219[*]	5.6 (*3*)	C.S	60	0.25
10.09.15	Celtic Sea	LOD-2	0.2704	1.3285		0.999	0.032	0.000	2.6 (*4*)	C.S	60	0.25
14.09.15	Celtic Sea	LOD-2	0.2704	1.5428		0.998	0.014	0.000	6.2 (*9*)	C.S	60	0.25
17.09.15	Celtic Sea	LOD-2	0.2559	1.7006		0.998	0.037	0.000	4.8 (*6*)	C.S	60	0.25
21.09.15	Celtic Sea	LOD-2	0.2203	1.777		1.000	0.015	0.000	1.4 (*6*)	C.S	60	0.25
25.09.15	Celtic Sea	LOD-4	0.0905	2.1131		0.999	0.029	0.000	6.0 (*5*)	C.S	60	0.25
26.09.15	Celtic Sea	LOD-2	0.3469	0.9858		0.999	0.044	0.000	3.8 (*4*)	C.S	60	0.25
28.09.15	Celtic Sea	LOD-2	0.1836	1.3419		0.999	0.014	0.000	5.0 (*7*)	C.S	60	0.25
6.10.15	Celtic Sea	LOD-2	0.3646	2.0694		0.999	0.023	0.000	4.3 (*6*)	C.S #1	60	0.25
8.10.15	Celtic Sea	LOD-2	0.2279	1.3578		0.999	0.059	0.000	4.7 (*5*)	C.S #1	60	0.25
13.10.15	Celtic Sea	LOD-2	0.0605	1.1017		1.000	0.017	0.000	6.7 (*3*)	C.S #1	60	0.25
2.11.15	Celtic Sea	LOD-2	0.632	1.8907		1.000	0.021	0.000	2.7 (*6*)	C.S #1	60	0.25
3.11.15	Celtic Sea	LOD-2	0.5318	1.5325		0.999	0.027	0.000	4.2 (*5*)	C.S #1	60	0.25
4.11.15	Celtic Sea	LOD-2	0.2034	0.8824		0.998	0.068	0.000	4.1 (*4*)	C.S #1	60	0.25
11.11.15	Celtic Sea	LOD-2	0.1633	1.1511		1.000	0.012	0.000	check	C.S #1	60	0.25
6.4.16	Celtic Sea	LOD-3	0.0896	0.2023[1]		0.999	0.230	0.000	7.4 (*5*)	C.S #1	60	0.25
18.4.16	Celtic Sea	LOD-2	0.0668	0.3149[1]		0.998	0.045	0.000	4.3 (*5*)	C.S #1	60	0.25
19.4.16	Celtic Sea	LOD-4	0.0615	0.3326[1]		0.996	0.042	0.000	4.1 (*5*)	C.S #1	60	0.25
29.4.16	Celtic Sea	LOD-2	0.2825	0.6738[1]		1.000	0.021	0.000	3.0 (*5*)	C.S #1	60	0.25
2.5.16	Celtic Sea	10-100			0.0486	0.998	0.80	0.000	[2]		20	0.25
10.5.16	Celtic Sea	10-100			0.4720	1.000	0.70	0.000	5.1	C.S #3	20	0.25
16.5.16	Celtic Sea	10-100			0.382	1.000	2.30	0.000	n/a	n/a	20	0.25
16.5.16	Celtic Sea	10-150			0.01160	0.999	0.60	0.000	n/a	n/a	20	0.083
8.6.16	Celtic Sea	10-200			0.00936	1.000	0.80	0.000	n/a	n/a	20	0.083
9.6.16	Celtic Sea	10-200			0.01180	0.999	0.90	0.000	6.6 (*6*)	C.S #3	20	0.083
13.6.16	Celtic Sea	10-200			0.01260	1.000	1.50	0.000	6.4 (*6*)	C.S #3	20	0.083
17.6.16	Celtic Sea	10-200			0.00880	0.998	2.00	0.000	6.5 (*6*)	C.S #3	20	0.083

19.6.16	Celtic Sea	10-200			0.00930	0.998	0.60	0.000	2.5 (*3*)	C.S #3	20	0.083
21.6.16	Celtic Sea	LOD-20	0.0061	0.2865		0.999	0.050	0.000	2.4 (*6*)	C.S #4	30	0.25
23.6.16	Celtic Sea	LOD-20	0.0037	0.2988		1.000	0.064	0.000	5.1 (*6*)	C.S #4	30	0.25

Appendix B- In house quality control materials

Concentrations determined during the analysis of in house quality control material (Table B1).

Table B1- The concentrations determined of the in house reference materials. 40 S SW= surface seawater from 40° S Atlantic filtered through a 0.2 µm filter, two bottles used and analysis overlapped to check consistency. CS and CS #1 were Celtic Sea samples that had been filtered through a 0.2 µm filter. CS #3 and CS #4 were unfiltered Celtic Sea samples.

Date	40 S SW Bottle 1 Conc (nM)	±	40 S SW Bottle 2 Conc (nM)	±	CS Conc (nM)	±	CS #1 Conc (nM)	±	CS #3 Conc (nM)	±	CS #4 Conc (nM)	±
20.1.15	0.28	0.017										
23.1.15	0.20	0.014										
25.1.15	0.14	0.003			0.98	0.008						
27.1.15	0.21	0.008			1.08	0.003						
5.2.15	0.19	0.002			1.04	0.002						
7.2.15	0.21	0.015			1.05	0.044						
10.2.15	0.25	0.005			1.09	0.008						
11.2.15	0.19	0.010			1.05	0.004						
13.2.15	0.30	0.022			1.11	0.005						
20.2.15	0.29	0.015			1.16	0.006						

Date								
25.2.15	0.30	0.003			1.19	0.022		
03.3.15	0.25	0.007	0.22	0.010	1.13	0.025		
04.3.15	0.30	0.010			1.12	0.042		
06.03.15	0.26	0.015	0.26	0.029	1.35	0.006		
09.03.15	0.19	0.022	0.18	0.016	1.07	0.042		
10.03.15	0.20	0.004	0.19	0.008	1.09	0.050		
07.05.15			0.23	0.010	0.95	0.060		
11.05.15			0.25	0.012	1.20	0.039		
12.05.15			0.28	0.010	1.11	0.023		
14.05.15			0.19	0.007	1.13	0.011		
18.05.15			0.26	0.013	1.18	0.003		
19.05.15			0.24	0.022	1.15	0.007		
22.05.15			0.26	0.029	1.08	0.018		
09.06.15			0.25	0.025	1.11	0.028		
12.06.15			0.21	0.011	1.14	0.025		
08.09.15			0.15	0.007	1.20	0.043		
10.09.15			0.21	0.000	1.15	0.062		
14.09.15			0.22	0.030	1.17	0.036		
17.09.15			0.20	0.010	1.16	0.024	1.09	0.023
21.09.15			0.21	0.004	1.16	0.001	1.17	0.072
25.09.15			0.19	0.017	0.98	0.017	1.03	0.016
26.09.15			0.20	0.018	1.24	0.023	1.14	0.095
28.09.15			0.17	0.008	1.14	0.002	1.14	0.101
06.10.15			0.22	0.010			1.11	0.021
08.10.15			0.30	0.022			1.05	0.052
13.10.15			0.24	0.007			1.07	0.023

Date										
02.11.15	0.25	0.005			1.31	0.202				
03.11.15	0.25	0.003			1.16	0.019				
04.11.15	0.30	0.043			1.20	0.014				
11.11.15	0.19	0.018			1.11	0.000				
6.4.16	0.38	0.061			1.16	0.013				
18.4.16	0.29	0.016			1.22	0.024				
19.4.16	0.29	0.015			1.17	0.156				
29.4.16	0.29	0.004			1.26	0.052				
2.5.16										
10.5.16							48.0	2.2		
16.5.16							50.0	0.6		
16.5.16							51.5	0.4		
8.6.16							46.7	1.3		
9.6.16							49.7	2.2		
13.06.16							48.1	1.6		
17.6.16							48.9	0.3	8.1	0.0
19.6.16							47.1	0.5	9.6	0.3
21.6.16					1.31	0.01			8.2	0.3
23.6.16					1.00	0.01			8.5	0.5
4.7.16					1.04	0.01			7.9	0.0
7.7.16							50.9	1.5		
8.7.16							52.0	1.1		
12.7.16							49.9	0.2		
13.7.16							52.4	0.0		
14.7.16							49.9	1.7		
22.7.16							53.2	0.8		

23.7.16						1.36	0.07			8.2	0.3
25.7.16						1.06	0.02			8.2	0.3
28.7.16								53.5	0.3		
Mean	**0.24**		**0.24**		**1.12**	**1.15**		**50.1**		**8.36**	
± (1 SD)	**0.05**		**0.04**		**0.08**	**0.10**		**2.1**		**0.57**	

Appendix C- Nordtest estimation of analytical uncertainty

The calculation used to estimate the relative analytical uncertainty using the Nordtest approach.

Main equation: $u_c = \sqrt{u(R_w)^2 + u(bias)^2}$

u_c= combined standard uncertainty (approximates to the 68% confidence interval)
$u(R_w)$= uncertainty estimate of within lab reproducibility (random effects)
$u(bias)$= uncertainty estimate of possible laboratory and procedural bias (systematic

effects)

Table C1 includes all the data used to carry out the Nordtest estimation of analytical uncertainty.

Table C1- Data uses to calculate the Nordtest estimation of analytical uncertainty.

	D1	D2	CS	CS#1	GSC
Mean (nM)	0.69	0.96	1.12	1.15	1.49
SD (nM)	0.03	0.10	0.08	0.08	0.14
RSD (%)	4	11	7	7	10
N	4	14	31	18	12
Consensus concentration (nM)	0.69	0.956			
Consensus SD (nM)	0.04	0.024			
RSD (%)	5.8	2.5			

u(R_w)

This was estimated using the pooled relative standard deviation of results from the analysis of SAFe D1 and D2 consensus material and the analysis of in house quality control materials CS and CS#1.

The pooled relative standard deviation:

S pooled= √((n1-1)RSD1^2+(n2-1)RSDs2^2)+(nk-1)RSDk^2/(n-k)

k= number of series
RSD= within group relative standard deviation
n= number of measurements

Using the above equation and data u(R_w) was estimated to be 7.8 %.

u(*bias*)

This accounts for possible relative bias. This is calculated using the root mean square of the relative bias between D1 and D2 consensus concentrations and concentrations determined in this work and the uncertainty of the consensus material used.

$u(bias) = \sqrt{RMS_{bias}^2 + u(Cref)^2}$

$RMS_{bias} = \sqrt{\sum (bias\_rel_i)^2/n}$

> $Bias\_rel_i = (Clab_i - Cconsensus_i)/Cconsensus_i$
>
> $Clab_i$ = concentration determined in this work
> $Cconsensus_i$ = consensus concentration
> n= number of consensus material
> This was estimated to be 0.7%.

$u(Cref) = \sqrt{\sum u(Cref)_i^2/n}$

> $u(Cref)$ = relative standard deviation of the consensus concentrations
> n= number of consensus materials
> This was estimated to be 4.5%

Using the above equation u(*bias*) was estimated to be 4.5%.

$u_c = \sqrt{u(R_w)^2 + u(bias)^2}$

Using the values calculated for $u(R_w)$ and u(*bias*) the combined standard uncertainty was estimated at 9.5%.

Appendix D- Comparison of different analysts

As part of the supervisory process, the data generated by Nora Hartner was subjected to quality control procedure. Firstly, analyses of consensus materials were conducted to confirm the accuracy of the analytical procedure conducted by N. Hartner (Table D1). Following this a depth profile was re-analysed to demonstrate data comparability between two analysts (Fig. D1), during this analysis N. Hartner was not aware of the concentrations previously determined by A. Birchill. The results demonstrate that variability between users was within the combined analytical uncertainty (section 2.3.4). In addition to confirming comparability, the results

demonstrated that samples were stable for a period of two years. Moreover, during 6 months of analyses, the concentration of Fe in internal quality control materials was determined daily by N. Hartner. This allowed an estimation of the combined uncertainty following the Nordtest approach, which resulted in an estimate of the expanded uncertainty of 7.8% for the concentration range 0.69-1.59 nM. This compares well to the estimation of 9.5% reported in section 2.3.4.

Table D1- Concentration of consensus materials determined by N.Hartner and associated consensus concentrations

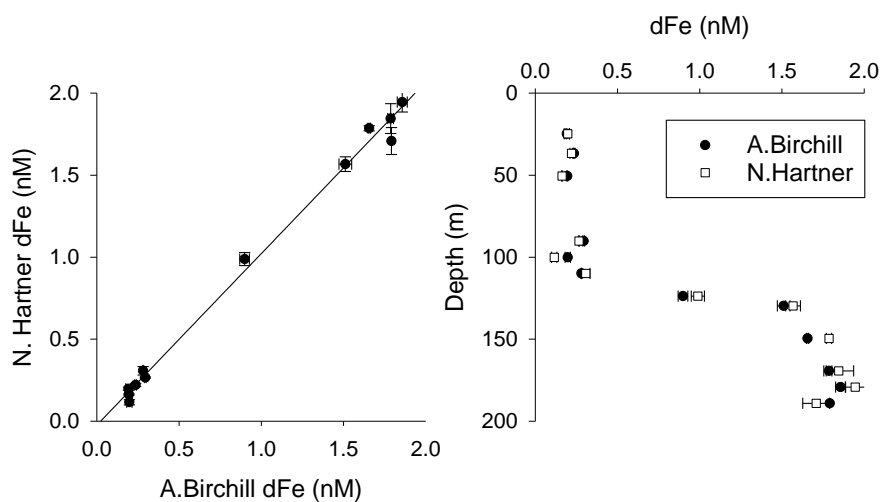|	Consensus (nM)	± (nM)	Determined (nM)	± (nM)
SAFe S	0.10	0.03	0.095	0.008
SAFe D1	0.69	0.05	0.687	0.04
SAFe D2	0.946	0.05	0.956	0.024

Figure D1- A comparison of dissolved iron concentrations determined for station C4, Hebridean shelf. Sample analysis was carried out by A. Birchill in December 2015 and N. Hartner in February 2017. **Left-** Scatter plot comparison (r^2=0.99, y= 1.05x − 0.02). **Right-** Comparison of depth profiles.